

---

[All ETDs from UAB](#)

[UAB Theses & Dissertations](#)

---

2023

## Streptococcus Mutans Biofilm Inhibiting Small Molecules with Anticariogenic Activity

Parmanand Ahirwar  
*University Of Alabama At Birmingham*

Follow this and additional works at: <https://digitalcommons.library.uab.edu/etd-collection>

 Part of the [Arts and Humanities Commons](#)

---

### Recommended Citation

Ahirwar, Parmanand, "Streptococcus Mutans Biofilm Inhibiting Small Molecules with Anticariogenic Activity" (2023). *All ETDs from UAB*. 453.  
<https://digitalcommons.library.uab.edu/etd-collection/453>

This content has been accepted for inclusion by an authorized administrator of the UAB Digital Commons, and is provided as a free open access item. All inquiries regarding this item or the UAB Digital Commons should be directed to the [UAB Libraries Office of Scholarly Communication](#).

*STREPTOCOCCUS MUTANS* BIOFILM INHIBITING SMALL MOLECULES WITH  
ANTICARIOGENIC ACTIVITY

by

PARMANAND AHIRWAR

SADANANDAN E. VELU, COMMITTEE CHAIR  
CHAMPION DEIVANAYAGAM  
EUGENIA KHARLAMPIEVA  
JESSICA SCOFFIELD  
GAYAN WIJERATNE

A DISSERTATION

Submitted to the graduate faculty of The University of Alabama at Birmingham,  
in partial fulfillment of the requirement for the degree of  
Doctor of Philosophy

BIRMINGHAM, ALABAMA

2023



*STREPTOCOCCUS MUTANS* BIOFILM INHIBITING SMALL MOLECULES WITH  
ANTICARIOGENIC ACTIVITY

PARMANAND AHIRWAR

CHEMISTRY

**ABSTRACT**

Dental caries, a highly prevalent disease, is characterized by the erosion of the tooth surface. This disease is caused by the oral bacteria living in complex communities called biofilms. *Streptococcus mutans*, among the various pathogenic bacterial species inhabiting the oral cavity, is considered to be the major etiological agent for dental caries. This bacterium forms robust biofilms capable of producing significant amounts of acid, leading to the demineralization of hydroxyapatite in the tooth enamel and subsequent erosion over time. Biofilm penetration into the dentin and pulp causes severe pain, while the entry of the bacteria into the bloodstream can result in severe complications, including sepsis and potential fatality.

*S. mutans* adhere to the tooth surface and attach to other bacteria in the oral cavity using sucrose-dependent and sucrose-independent adhesion mechanisms. In the sucrose-independent mechanism, the bacteria utilize surface proteins such as antigen I/II, to recognize and bind to salivary agglutinin (SAG) proteins present in the salivary pellicle of the tooth surface. In the sucrose-dependent mechanism, *S. mutans* employs a set of surface-secreted proteins called glucosyltransferases (Gtfs). These enzymes catalyze the synthesis of glucose oligomers called glucans, which have the ability to bind to the bacterial cell surface through another set of surface proteins known as glucan binding proteins (GBP). Glucans also contribute to the formation of an exopolysaccharide matrix, providing architectural support to the biofilms and acting as a nutrient reservoir for the bacteria within the biofilm. This enables the bacteria to form three-dimensional, robust, and tenacious biofilms. Consequently, Gtfs are considered as targets for the therapeutic development against dental caries. Saliva employs buffering mechanisms to maintain a healthy physiological pH of 7.0 - 7.5 and prevent dental erosion, but this system fails when acidogenic bacteria such as *S. mutans* produce excessive amounts of acid. Under cariogenic conditions, the lactic acid produced by pathogenic bacteria shifts the balance of oral pH to lower than 5.5 causing the demineralization of tooth.

The work described in this Ph. D. thesis focuses on the design and development of selective inhibitors of *S. mutans* biofilm formation while preserving the planktonic growth of oral commensal bacterial flora. Optimized lead biofilm inhibitors with *in vitro* and *in vivo* anticariogenic activity were identified through structure-based drug design and lead optimization studies. The optimized lead compound **HA5** was then encapsulated into pH-responsive hydrogel to generate hydrogel-encapsulated biofilm inhibitor (**HEBI**) for the

pH-responsive drug delivery. The *in vitro* and *in vivo* evaluation of anticariogenic activity of **HEBI** is also presented. Overall, the data presented in this thesis suggests that the biofilm-specific therapy using *S. mutans* biofilm inhibitors or **HEBI** reported here is a viable approach for prevention and treatment of dental caries while preserving the oral microbiome.

**Keywords:** dental caries, biofilm, *Streptococcus mutans*, glucosyltransferases, pH-responsive hydrogel, on-demand drug delivery, and targeted therapeutics.

## **DEDICATION**

Dedicated to the ever-nurturing soil of Bharat and my ever-sacrificing parents  
who gave me the zeal to struggle, succeed and stay grounded.

## **ACKNOWLEDGEMENTS**

Being a Ph. D. student at the University of Alabama at Birmingham has been a rich experience of absolute pleasure and learning which expanded the horizons of my life. I owe this to following group of people:

First and foremost, I extend my deepest appreciation to my advisor and the Chair of my graduate committee, Dr. Sadanandan E. Velu whose unwavering support, expert knowledge, and insightful guidance have been instrumental in shaping the direction of this research. His mentorship has not only challenged me to excel but also nurtured my academic growth. I am truly fortunate to have had the opportunity to work under Dr. Velu's supervision.

I would like to extend my thanks to my graduate committee members, Dr. Champion Deivanayagam, Dr. Eugenia Kharlampieva, Dr. Jessica Scoffield, and Dr. Gayan Wijeratne for their valuable feedback, constructive criticism, and guidance throughout this research endeavor. Their expertise and input have significantly enriched the quality of my research as a Ph. D. student. I am grateful for their time, dedication, and commitment to academic excellence.

I am grateful for the collaboration and contributions from Dr. Hui Wu, Dr. Suzanne Michalek, Dr. Eugenia Kharlampieva, and Dr. Champion Deivanayagam. Their expertise, suggestions, and support have played a vital role in the successful completion of this



research project. The collective effort and shared knowledge have undoubtedly been pivotal in the experiments, science, and quality of this research.

I would like to express my sincere appreciation to my family and friends for their unwavering support, love, and encouragement throughout this academic journey. Their understanding, patience, and motivation have been a constant source of strength, and I am deeply grateful for their presence in my life.

I can never forget members of Velu group who have been wonderful colleagues and a constant support during my Ph. D. In particular, I am grateful to Edwin M. Rojas for constantly lifting me during the downfalls and encouraging me to realize my potential; B. Owen Garret for being an absolutely good friend and engaging in knowledgeable intriguing discussions ranging from personal to global topics; Piyasuda Pukkanasut for being a source of inspiration in her dedication and organization of work; Frank Saunders for being an understanding colleague with perfect untiring productivity as another source of inspiration. I also want to thank all the undergraduate research students who worked in Velu lab, especially the students who worked with me, Anna Law, Bradley Thigpen, and Whitney Sharer for their contributions and cheerful presence.

I am indebted to the University of Alabama at Birmingham for providing me with a conducive research environment and resources necessary to carry out this study. Additionally, I would like to acknowledge the financial support provided by the National Institute of Health, which has made this research possible and partially supported my salary.

Finally, I extend my heartfelt appreciation to all those who have helped me during my time at the University of Alabama at Birmingham, USA and contributed to the

completion of this dissertation. Their support, guidance, and encouragement have been vital to my success, and I am truly grateful for their contributions.

## TABLE OF CONTENTS

	<i>Page</i>
ABSTRACT.....	iii
DEDICATION.....	vi
ACKNOWLEDGEMENTS.....	vii
LIST OF TABLES.....	xv
LIST OF FIGURES .....	xvi
LIST OF ABBREVIATIONS USED .....	xviii
INTRODUCTION .....	1
ORAL MICROBIOTA AND BIOFILMS.....	1
Bacterial colonization in the oral cavity.....	2
Extracellular polysaccharides .....	3
Oral commensal bacteria .....	3
<i>STREPTOCOCCUS MUTANS</i> AND ITS PATHOGENESIS .....	4
<i>S. mutans</i> ' virulence factors .....	4
Adhesion mechanisms of <i>S. mutans</i> .....	5
<i>S. mutans</i> in other diseases.....	7
GLUCOSYLTRANSFERASES AND GLUCAN PRODUCTION.....	8
Functional domains of <i>S. mutans</i> glucosyltransferases .....	8
Production of soluble and insoluble glucans by Gtfs .....	9
Mechanism of action of Gtfs.....	9
DEMINERALIZATION AND REMINERALIZATION PROCESSES .....	10
Tooth structure and its hydroxyapatite surface.....	10

Stephan's curve and critical pH.....	12
Role of saliva in oral health.....	13
CURRENT METHODS OF CARIES MANAGEMENT .....	14
Oral hygiene: regular brushing, flossing, and cleaning.....	15
Mouthwashes.....	15
Fluoride treatment.....	17
Gtf inhibitors .....	18
NANOMATERIALS IN ANTI-CARIES RESEARCH.....	20
OVERVIEW OF THIS WORK.....	21
CHAPTER 1: DESIGN AND SYNTHESIS OF A SMALL MOLECULE LIBRARY OF AURONES TO INHIBIT <i>STREPTOCOCCUS MUTANS</i> GLUCOSYLTRANSFERASES AND BIOFILM .....	23
ABSTRACT.....	24
INTRODUCTION .....	25
RESULTS AND DISCUSSION .....	32
Lipinski properties of the aurone analogs.....	34
Determination of solubility of aurones.....	36
CONCLUSIONS .....	39
EXPERIMENTAL SECTION .....	40
General considerations.....	40
General procedure for synthesis of chalcones ( <b>3a-f</b> ).....	41
General procedure for synthesis of methoxy aurones ( <b>MA1-6</b> ) .....	44
General procedure for synthesis of hydroxy aurones ( <b>HA2-6</b> ).....	46
Determination of solubility .....	48
ACKNOWLEDGEMENTS.....	48
REFERENCES .....	50
CHAPTER 2: EVALUATION OF AURONES FOR THEIR INHIBITORY ACTIVITIES AGAINST <i>S. MUTANS</i> BIOFILM AND	

GLUCOSYLTRANSFERASES <i>IN VITRO</i> AND ANTICARIOGENIC ACTIVITY <i>IN VIVO</i> .....	58
ABSTRACT.....	59
INTRODUCTION .....	60
RESULTS AND DISCUSSION .....	63
Inhibition of <i>S. mutans</i> planktonic growth.....	63
Screening of <b>3a-f</b> , <b>MA1-6</b> and <b>HA2-6</b> against <i>S. mutans</i> biofilms.....	64
Inhibition of commensal streptococci biofilms .....	68
<b>HA5</b> inhibits UA159 biofilms, glucan production and eDNA levels .....	69
<b>HA5</b> inhibits glucan production by <i>S. mutans</i> Gtfs in a dose dependent manner .....	71
<b>HA5</b> does not affect growth of commensal streptococci.....	71
<b>HA6</b> inhibits UA159 biofilms, glucan production and eDNA.....	72
Effect of <b>HA6</b> on commensal species growth .....	73
<b>HA5</b> and <b>HA6</b> bind to GtfB in OctetRed experiments .....	73
Structural studies on <b>HA5</b> in the catalytic domain of GtfB.....	74
Co-crystal structure of <b>HA5</b> with GtfB .....	76
<b>HA5</b> and <b>HA6</b> reduce caries score <i>in vivo</i> .....	78
CONCLUSIONS .....	80
EXPERIMENTAL SECTION .....	81
General considerations.....	81
Biofilm inhibition assays.....	82
Gtf inhibition determined by glucan quantification assays.....	82
<i>S. mutans</i> and commensal <i>S. gordonii</i> and <i>S. sanguinis</i> growth assays.....	83
Rat model of dental caries .....	83
OctetRed binding assay .....	85
ACKNOWLEDGEMENTS .....	85
IACUC APPROVAL .....	86

REFERENCES .....	87
CHAPTER 3: PH-RESPONSIVE DELIVERY OF BIOFILM INHIBITOR HA5 TO ABROGATE <i>STREPTOCOCCUS MUTANS</i> CARIOGENIC BIOFILMS.....	92
ABSTRACT.....	93
INTRODUCTION .....	94
RESULTS AND DISCUSSION .....	97
Synthesis and characterization of <b>HA5</b> .....	97
Hydrogels encapsulated biofilm inhibitor ( <b>HEBI</b> ) .....	100
Encapsulation of <b>HA5</b> in (PMAA) <sub>5</sub> hydrogel microparticles. ....	101
Inhibition of <i>S. mutans</i> and commensal species biofilms by <b>HEBI</b> .....	102
<b>HEBI</b> is not bactericidal to pathogenic and commensal streptococci.....	104
Reduction of <i>S. mutans</i> virulence <i>in vivo</i> by <b>HEBI</b> .....	105
CONCLUSIONS .....	107
EXPERIMENTAL SECTION .....	108
General considerations.....	108
Synthesis of 1-(2-Hydroxyphenyl)-3-(2',4',5'-trimethoxyphenyl)prop-2- en-1-one ( <b>3e</b> ) .....	110
Synthesis of 2-[(2',4',5'-Trimethoxyphenyl)methylidene]-2,3-dihydro-1- benzofuran-3-one ( <b>MA5</b> ) .....	110
Synthesis of 2-[(2',4',5'-Trihydroxyphenyl)methylidene]-2,3-dihydro-1- benzofuran-3-one ( <b>HA5</b> ) .....	111
<i>S. mutans</i> and commensal species planktonic growth assays.....	112
Hydroxyapatite disc assay .....	112
Synthesis of porous cubic manganese oxide microparticle templates .....	113
Synthesis of cubical hydrogel microparticles .....	113
Rat model of dental caries used in the evaluation of <b>HEBI</b> .....	114
ACKNOWLEDGEMENTS .....	116
IRB AND IACUC APPROVALS .....	116

REFERENCES .....	117
CONCLUSIONS .....	122
CHAPTER 1: DESIGN AND SYNTHESIS OF A SMALL MOLECULE LIBRARY AURONES TO INHIBIT <i>STREPTOCOCCUS MUTANS</i> GLUCOSYLTRANSFERASES AND BIOFILM. ....	125
CHAPTER 2: EVALUATION OF AURONES FOR THEIR INHIBITORY ACTIVITIES AGAINST <i>S. MUTANS</i> BIOFILM AND GLUCOSYLTRANSFERASES <i>IN VITRO</i> AND ANTICARIOGENIC ACTIVITY <i>IN VIVO</i> . ....	126
CHAPTER 3: PH-RESPONSIVE DELIVERY OF BIOFILM INHIBITORS TO ABROGATE <i>S. MUTANS</i> CARIOGENIC BIOFILMS. ....	127
FUTURE DIRECTIONS .....	129
GENERAL REFERENCES.....	131
APPENDIX: <sup>1</sup> H AND <sup>13</sup> C SPECTRA, AND HPLC TRACES OF CHALCONES, METHOXYAURONES AND HYDROXYAURONES .....	142

## LIST OF TABLES

Table 1.1: Physicochemical properties of aurones calculated using SwissADME.....	35
Table 1.2: Structure, yield, melting point, and the solubility of the synthesized aurones.....	38
Table 2.1: Biofilm inhibition profiles of <b>3a-f</b> , <b>MA1-6</b> , and <b>HA2-6</b> .....	67
Table 2.2: Data collection and refinement statistics for GtfB in complex with HA5. ....	75
Table 2.3: Effect of <b>HA5</b> or <b>HA6</b> treatment on <i>S. mutans</i> -induced buccal caries.....	79
Table 2.4: Effect of <b>HA5</b> or <b>HA6</b> treatment on <i>S. mutans</i> -induced sulcal caries. ....	79
Table 2.5: Effect of <b>HA5</b> or <b>HA6</b> treatment on <i>S. mutans</i> -induced proximal caries.....	80
Table 2.6: Effect of <b>HA5</b> or <b>HA6</b> treatment on <i>S. mutans</i> CFU and the body weight of the treated animals. ....	80
Table 3.1: Effect of <b>HEBI</b> treatment on <i>S. mutans</i> UA159 induced buccal caries.....	106
Table 3.2: Effect of <b>HEBI</b> treatment on <i>S. mutans</i> UA159 induced sulcal caries.....	106
Table 3.3: Effect of <b>HEBI</b> treatment on <i>S. mutans</i> UA159 induced proximal caries.....	107
Table 3.4: Effect of <b>HEBI</b> treatment on <i>S. mutans</i> UA159 CFU and the body weight of the animals. ....	107



## LIST OF FIGURES

Figure 0.1: Virulence factors of <i>S. mutans</i> : two mechanisms of adhesion, acidogenesis.....	6
Figure 0.2: Structure of tooth: enamel, dentin, and pulp.. .....	12
Figure 0.3: A) Stephan's curve, pH around tooth surface drops following sugar intake but in disease conditions, it goes below critical pH causing tooth erosion over time. B) Due to lactic acid production, pH drops below critical in case of plaque.....	13
Figure 0.4: Common ingredients in mouthwashes.....	17
Figure 0.5: Currently known Gtf inhibitors .....	19
Figure 1.1: A) Structures of indigoid and hemiindigoids derived from indigo, B) Aurone scaffold, C) A few commonly occurring aurone natural products.....	28
Figure 1.2: Biosynthetic pathway for aurones. ....	29
Figure 1.3: Approaches used in the laboratory synthesis of aurones.....	30
Figure 1.4: Chemical structures, solubility, and bioactivity of inhibitors <b>G43</b> and <b>IIC5</b> . ....	31
Figure 1.5: Aurone library of small molecules. ....	32
Figure 1.6: A) <b>G43</b> co-crystal structure with GtfB, B) Docking models of aurones with GtfB aligning with <b>G43</b> crystal structure. ....	33
Figure 1.7: Synthesis of methoxyaurones and hydroxyaurones.....	34
Figure 1.8: A) UV spectra for methoxy aurones, B) UV spectra for hydroxy aurones, C) Solubility calibration curves for methoxy aurones, D) solubility calibration curves for hydroxy aurones. ....	37
Figure 2.1: Chalcones ( <b>3a-f</b> ) methoxyaurones ( <b>MA1-6</b> ) and hydroxyaurones ( <b>HA2-6</b> ).....	62
Figure 2.2: Planktonic growth inhibitory activities of chalcones ( <b>3a-f</b> ), methoxyaurones ( <b>MA1-6</b> ), and hydroxyaurones ( <b>HA2-6</b> ).. .....	64

Figure 2.3: Biofilm inhibitory activities of chalcones ( <b>3a-f</b> ), methoxyaurones ( <b>MA1-6</b> ) and hydroxyaurones ( <b>HA2-6</b> )..	65
Figure 2.4: Inhibitory activities of hydroxyaurones ( <b>HA2-6</b> ) and methoxyaurones ( <b>MA1-6</b> ) against commensal biofilms. ....	69
Figure 2.5: Biofilm inhibitory activities of compound <b>HA5</b> ..	70
Figure 2.6: Biofilm inhibitory activities of compound <b>HA6</b> . ....	72
Figure 2.7: OctetRed binding of A) <b>HA5</b> and B) <b>HA6</b> with GtfB protein from <i>S. mutans</i> . ....	74
Figure 2.8: A) High resolution X-ray co-crystal structure (PDB ID: 8FG8) of the inhibitor <b>HA5</b> with the catalytic domain of GtfB..	78
Figure 3.1: Chemical structure, solubility, and bioactivities of <b>HA5</b> . ....	96
Figure 3.2: Synthesis of <b>HA5</b> .....	98
Figure 3.3: HPLC trace of <b>HA5</b> showing 99.64 % purity .....	100
Figure 3.4: A) Optical images of empty (PMAA) <sub>5</sub> hydrogel microparticles. B) <b>HA5</b> -loaded hydrogel <b>HEBI</b> and HA5 in methanol (insert B). C) Atomic Force Microscopy (AFM) topography images of a tooth surface with height of 280 nm. D) AFM image after (PMAA) <sub>5</sub> hydrogel adsorption, cubical hydrogel particles are clearly seen adhering to the tooth surface. E) Amplitude error image of empty (PMAA) <sub>5</sub> hydrogels dried on the surface of a tooth. Scan size is 20 $\mu\text{m}^2$ in both images, the height (z)-scale is 1.7 $\mu\text{m}$ . ....	102
Figure 3.5: A) <i>S. mutans</i> , B) <i>S. gordonii</i> , and C) <i>S. sanguinis</i> biofilm inhibition by <b>HA5</b> and <b>HEBI</b> .....	103
Figure 3.6: A) <i>S. mutans</i> , B) <i>S. gordonii</i> , and C) <i>S. sanguinis</i> growth inhibition by <b>HA5</b> and <b>HEBI</b> .....	104

## LIST OF ABBREVIATIONS USED

ADME	Absorption, distribution, metabolism, excretion
AFM	Atomic force microscopy
ANOVA	Analysis of variance
BAP	Blood agar plate
BLI	Biolayer Interferometry
CDM	Chemically defined medium
CFU	Colony forming units
DMSO	Dimethyl sulfoxide
eDNA	Extracellular deoxyribonucleic acid
EI	Electron impact
EPS	Exopolysaccharides
GBP	Glucan binding proteins
Gtfs	Glucosyltransferases
HA	Hydroxyapatite
HCl	Hydrochloric acid
HEBI	Hydrogel encapsulated biofilm inhibitor
HPLC	High performance liquid chromatography
HRMS	High resolution mass spectrum

LbL	Layer by layer
MP	Melting point
MS	Mitis salivarius (agar)
NMR	Nuclear magnetic resonance
OD	Optical density
PBS	Phosphate buffered saline
PMAA	Poly(methacrylic acid)
PVPON	Poly(N-vinylpyrrolidone)
SAG	Salivary agglutinin
SAR	Structure-activity relationship
THB	Todd-Hewitt broth
TLC	Thin layer chromatography
TMS	Tetramethylsilane
UV	Ultraviolet

## **INTRODUCTION**

Dental caries or tooth decay is a common oral disease characterized by the demineralization and destruction of tooth structures. The word ‘caries’ means ‘rotten’ in Latin.<sup>1</sup> It is a highly prevalent disease worldwide, as indicated by a recent study published in The Lancet that examined the global burden of various diseases.<sup>2</sup> In the United States, approximately 90 % of people have experienced dental caries, and about 25 % of these cases remain untreated.<sup>3</sup> Although often categorized as a lifestyle-related disease, dental caries presents a significant challenge due to its potential consequences such as tooth loss, infections, and, in severe cases, even sepsis leading to death.<sup>4,5</sup>

Dental caries progresses through different stages. It starts with the formation of a small area of decay on the enamel, which progresses to involve the underlying dentin and, if left untreated, it could even reach the pulp.<sup>6,7</sup> The history of dental caries dates back to centuries, with evidence found in ancient human remains.<sup>8</sup> From then to now, the advancement in science and technology has contributed to better understanding and management of tooth decay.

## **ORAL MICROBIOTA AND BIOFILMS**

The oral cavity harbors a diverse range of microbial organisms. The oral cavity contains a diverse range of microbial species, with approximately 700 prokaryotic species

identified so far. These species can be categorized into 185 genera and further grouped into 12 phyla. A significant portion of these species, around 54 %, have been officially named and classified taxonomically. Additionally, 14 % of the species have been cultivated but have not yet received official names, while the remaining 32 % are known only as uncultivated phylotypes. The identified phyla within the oral microbiota encompass Firmicutes, Fusobacteria, Proteobacteria, Actinobacteria, Bacteroidetes, Chlamydiae, Chloroflexi, Spirochaetes, Synergistetes, Saccharibacteria, and Gracilibacteria.<sup>9</sup>

### **Bacterial colonization in the oral cavity**

The bacterial colonization of the oral cavity is initiated shortly after birth, with early detection of bacteria such as *Staphylococcus epidermidis* and other *Streptococci*.<sup>10</sup> Subsequent growths of dental structures and modifications in nutrition provide favorable conditions for the colonization of additional bacterial species, resulting in the development of a diverse and intricate oral microbiome.<sup>11</sup> The presence of this well-balanced microbiome, in combination with an intact immune response, plays a crucial role in preserving a non-inflammatory state in the periodontium of individuals.<sup>12</sup> Gram-positive facultative anaerobic cocci and rods, including species like *Streptococcus* and *Actinomyces*, serve as the initial colonizers of teeth, playing a critical role in the formation of dental biofilms. These primary colonizers create a foundation upon which other bacterial species adhere through the process of coaggregation.<sup>13</sup>

Bacteria in the mouth often form organized colonies known as biofilms. Dental biofilm, also referred to as dental plaque, is an intricate community composed of diverse bacterial species.<sup>17</sup> These biofilms possess a three-dimensional organization wherein microorganisms are arranged and enveloped by an extracellular matrix.<sup>18</sup> The distinctive

properties and pathogenicity of biofilms arise from their structural features, exopolysaccharide composition, physiological heterogeneity, and quorum sensing abilities.

<sup>19</sup> Within biofilms, bacteria manifest diverse physiological states and engage in intercellular communication facilitated by quorum sensing, a mechanism that involves gene expression regulation in response to cell density. <sup>20</sup> Moreover, biofilms exhibit heightened resistance to antibiotics in comparison to freely suspended planktonic bacteria due to factors such as reduced growth rates, upregulation of defense mechanisms, and the protective nature of the extracellular matrix. <sup>18, 21</sup>

### **Extracellular polysaccharides**

The extracellular matrix (ECM) of the bacteria within biofilms comprises of a complex amalgamation of organic and inorganic materials. Polysaccharides, proteins, glycoproteins, lipids, as well as calcium, phosphorus, potassium, sodium, and fluoride, contribute to the overall composition and functionality of the matrix. Among these constituents, extracellular polysaccharides (EPS) play a pivotal role in providing structural integrity, protecting against harmful attacks, and acting as a reservoir for essential ions that support the growth and survival of the bacteria within the biofilm community. Understanding the intricate dynamics of the ECM is crucial for unraveling the complexities of biofilm formation and developing targeted strategies for inhibiting oral biofilm. <sup>18, 21</sup>

### **Oral commensal bacteria**

Certain bacterial species in the human oral cavity have a beneficial role of preventing the formation of cariogenic biofilms. *S. oralis*, *S. sanguinis*, and *S. gordonii* have been observed in higher proportions in plaque obtained from healthy tooth surfaces.

<sup>22</sup> *S. sanguinis*, a predominant commensal species in the oral microbiota present in saliva

and dental plaque, is commonly associated with tooth surfaces that are free of caries.<sup>23</sup> Studies proposed that the ratio of *S. mutans* to *S. sanguinis* could serve as an indicator of caries risk.<sup>24</sup> Investigations show that *S. sanguinis* may exert an antagonistic effect against the colonization of *S. mutans*, potentially influencing the outcomes of caries.<sup>25</sup> *S. gordonii*, *S. parasanguis*, *S. rattus*, and *S. sanguinis* are additional species that contribute to the oral health by maintaining pH homeostasis through the production of alkali, thus aiding in the prevention of tooth erosion.<sup>26</sup>

### ***STREPTOCOCCUS MUTANS* AND ITS PATHOGENESIS**

The search for the etiology of dental caries began in the early 20<sup>th</sup> century, leading to the discovery of a specific bacterium consistently present in carious lesions. In 1924, J. Clarke from the Institute of Pathology and Research at St. Mary's Hospital in London identified a distinct bacterium in carious lesions with high acidogenic properties. He named this species *Streptococcus mutans*, speculating that it might be a mutant form of the already known oral commensal streptococci.<sup>27</sup> Clarke's observation of this peculiar bacterium marked an important milestone in understanding the role of bacteria in dental caries. Since Clarke's initial discovery, extensive research has been conducted to elucidate the virulence factors, mechanisms of acid production, and pathogenicity of *S. mutans*. This bacterium has been recognized as the key contributor to dental caries and remains a focal point of studies aimed at caries prevention and treatment strategies.<sup>28, 29</sup>

#### ***S. mutans*' virulence factors**

*S. mutans* possesses three major virulence factors that contribute to its pathogenicity in dental caries. Firstly, it produces EPS, which plays a crucial role in the



formation of tenacious biofilms.<sup>30, 31</sup> The biofilms provide protection and enhance the adherence of *S. mutans* to tooth surfaces, facilitating its colonization and survival.<sup>32</sup> Secondly, *S. mutans* exhibits high acidogenicity, meaning it can produce significant amounts of lactic acid by metabolizing dietary sugars. This acid production leads to a decrease in the pH of the oral environment, contributing to the demineralization of tooth enamel and the development of caries. Lastly, *S. mutans* has an exceptional ability to survive and thrive in highly acidic conditions, a characteristic known as high acidity.<sup>33-35</sup> This enables *S. mutans* to persist in the acidic environment it creates through its own acidogenic activity, further promoting the progression of dental caries. Understanding these virulence factors is crucial for developing effective strategies to prevent and manage dental caries by targeting the specific mechanisms employed by *S. mutans* in pathogenesis of dental caries.<sup>33</sup>

#### **Adhesion mechanisms of *S. mutans***

*S. mutans*, the primary etiological agent of dental caries, employs two main mechanisms for adhesion to tooth surfaces and to other bacterial species: 1) a sucrose-dependent mechanism and 2) a sucrose-independent mechanism. In the sucrose-independent mechanism, *S. mutans* utilizes its surface proteins, including antigen I/II, to interact with salivary agglutinin (SAG) proteins present in the tooth pellicle.<sup>36-38</sup> This interaction facilitates the attachment of *S. mutans* to the tooth surface, enabling subsequent colonization and biofilm development. In the sucrose-dependent mechanism, *S. mutans* utilizes a class of secreted proteins called glucosyltransferases (Gtfs) to synthesize oligomers of glucose known as glucans.<sup>39, 40</sup>

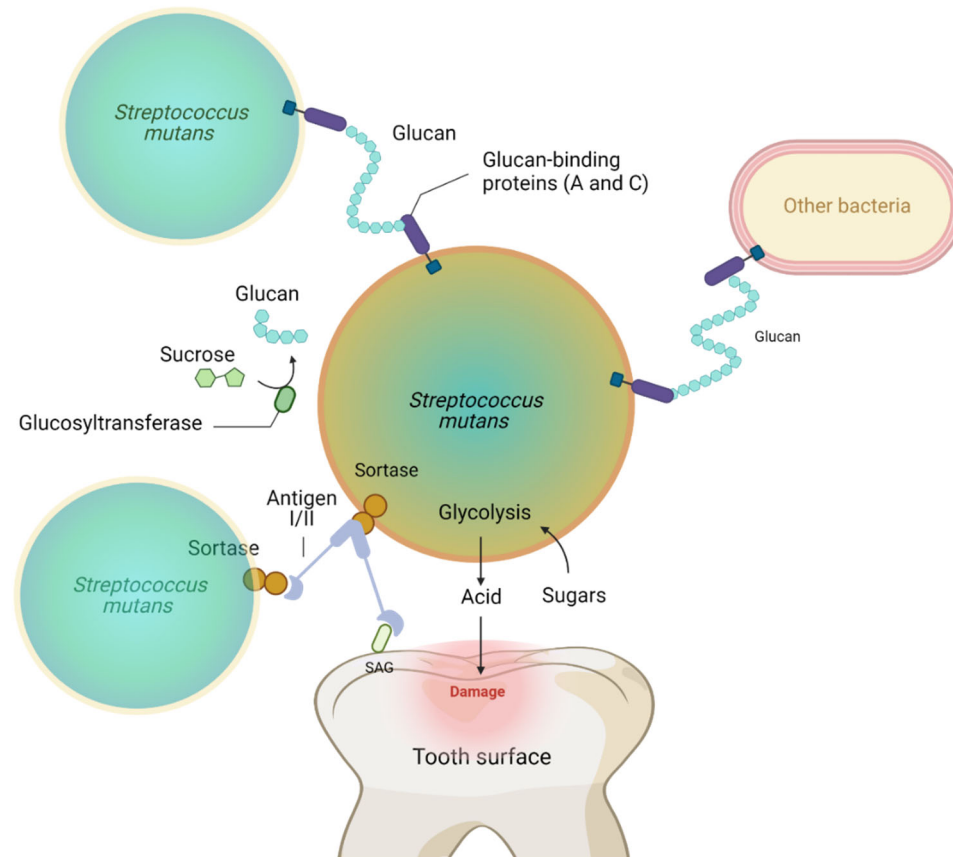


**Figure 0.1** Virulence factors of *S. mutans*: two mechanisms of adhesion, acidogenesis. The image was created with BioRender.com with permission for academic publications (agreement number: AT25J487LO).

The EPS act as adhesive molecules by binding to surface proteins called glucan binding proteins (GBP) present on *S. mutans* and other bacterial species. The binding of glucans to GBP enables the formation of intricate three-dimensional bacterial colonies known as biofilms. Furthermore, glucans contribute to the structural integrity and tenacity of the biofilm, imparting resistance against mechanical forces and host defense mechanisms.<sup>31, 41, 42</sup> Within the biofilms, *S. mutans* metabolizes dietary sugars, particularly sucrose, to produce lactic acid as a metabolic byproduct. The accumulation of lactic acid in the local microenvironment lowers the pH, leading to the demineralization of tooth surfaces and subsequent tooth erosion, which is the characteristic feature of dental caries.

### ***S. mutans* in other diseases**

*S. mutans* has also been frequently detected in cardiovascular specimens, indicating its ability to enter the bloodstream and potentially colonize heart valves.<sup>43</sup> This raises concerns about the involvement of *S. mutans* in the development of heart diseases such as infective endocarditis (IE),<sup>44</sup> a serious condition characterized by the infection and inflammation of the heart valves.<sup>45</sup> The formation of biofilms by *S. mutans* on cardiac valves is believed to play a significant role in the pathogenesis of IE.<sup>46-48</sup> In the case of IE, the biofilm formation on heart valves can lead to the formation of vegetations, which are aggregates of bacteria, host factors, and extracellular material. These vegetations not only cause damage to the valve tissue but also serve as a reservoir for bacteria, leading to persistent infection and increased risk of complications such as congestive heart failure.<sup>46</sup> One of the virulence factors associated with *S. mutans* is the production of glucosyltransferases (Gtfs), which play a crucial role in biofilm formation. Gtfs are responsible for synthesizing glucans, which are extracellular polysaccharides that act as adhesive molecules, facilitating bacterial attachment to surfaces.<sup>31</sup> In addition to their glucan synthesis, Gtfs have been found to have immunomodulatory effects.<sup>49, 50</sup> Studies have shown that Gtfs can induce the production of interleukin-6 from monocytes, triggering an inflammatory response.<sup>49</sup> This inflammation contributes to the pathogenesis of IE, further exacerbating the damage to heart valves. The current treatment for IE uses a combination of antibiotics and surgical procedures.<sup>51, 52</sup> However, the management of IE remains challenging, and the use of antibiotics alone may not effectively eradicate biofilms formed by *S. mutans*. The development of biofilm inhibitors specifically targeting *S. mutans* could be a promising approach to complement the current treatment of IE. These

inhibitors aim to disrupt the formation and stability of biofilms, preventing the colonization of heart valves by *S. mutans* and reducing the risk of complications.

## GLUCOSYLTRANSFERASES AND GLUCAN PRODUCTION

### Functional domains of *S. mutans* glucosyltransferases

*S. mutans* Gtfs are a group of proteins responsible for the synthesis of extracellular glucan polysaccharides promoting bacterial adhesion and formation of robust biofilms.<sup>31, 53</sup> Research focused on the structure-functional relationship of Gtfs in *S. mutans* and *S. sobrinus* has provided valuable insights into the specific domains and amino acid residues involved in their enzymatic activities.<sup>54</sup> These Gtfs possess distinct regions that contribute to their overall functionality.<sup>55</sup> For instance, the C-terminal glucan-binding domain (GBD) consists of a series of homologous direct repeat segments spanning approximately 510 residues.<sup>56</sup> This domain plays a critical role in the synthesis of glucans, but it does not contribute to sucrase activity.<sup>57</sup> On the other hand, the N-terminal catalytic domain, which encompasses about 900 amino acids, is responsible for binding and hydrolyzing sucrose.<sup>58</sup> The N-terminal catalytic domain exhibits a high level of conservation among Gtfs and contains two active sites that have been identified through biochemical and genetic analyses. The first active site, composed of nine residues including a catalytic aspartic acid, has been observed in the stabilized glucosyl-enzyme complex. Site-directed mutagenesis studies have confirmed the significant role of this aspartic acid residue in sucrase activity within Gtfs.<sup>59</sup> Additionally, an adjacent region known as Gtf-P1, consisting of 19 amino acids, has been identified as the second active site.<sup>60, 61</sup> Further mutagenesis investigations

have revealed the essential nature of two aspartic acid residues within Gtf-P1 for sucrose activity, although their specific functions may differ between GtfB and GtfC.<sup>62</sup>

### **Production of soluble and insoluble glucans by Gtfs**

Within most strains of *S. mutans*, three distinct gtf genes are present, each expressing different glucosyltransferase enzymes. Specifically, the genes *gtfB* and *gtfD* are responsible for producing the GtfB (162 kDa) and GtfD (155 kDa) enzymes, respectively. These enzymes play a role in synthesizing water-insoluble glucans with  $\alpha_{1,3}$  linkages and water-soluble glucans with  $\alpha_{1,6}$  linkages, respectively.<sup>63,64</sup> On the other hand, the *gtfC* gene encodes for the GtfC (149 kDa) enzyme, which has the ability to synthesize both water-insoluble and soluble glucans.<sup>54,65</sup> The synthesis of insoluble glucans by *S. mutans* GtfB and GtfC make them crucial for bacterial colonization, biofilm formation and subsequent cariogenesis. The water-insoluble glucans contribute to the formation of dental plaque and the adherence of *S. mutans* to tooth surfaces. Given the importance of these Gtfs in the cariogenic process, the inhibition of *S. mutans* Gtfs using small-molecules<sup>66-69</sup> has emerged as a potential strategy for the prevention and treatment of dental caries. By targeting the catalytic activity of *S. mutans* Gtfs using specific inhibitors, it is possible to disrupt the synthesis of glucans, thereby hindering bacterial colonization and reducing the risk of dental caries.

### **Mechanism of action of Gtfs**

The precise mechanism of glucan formation is not fully understood, although a proposed model<sup>70, 71</sup> suggests the involvement of specific residues, namely Asp477, Asp588, and Glu515, in the oligomerization process. According to this model, the process begins with the initial binding of sucrose to the catalytic domain of Gtf, where the aspartic

acid residue Asp477 attacks the glycosidic carbon, forming a covalent bond with the glucosyl unit and releasing the fructose unit. Glu515, a glutamate residue, aids in this process by providing a proton. The glucosyl unit remains covalently bonded to Asp477, which is stabilized by another aspartic acid residue, Asp588. This cleaves the sucrose into glucose and fructose. Subsequently, another sucrose unit binds to the enzyme, and its hydroxy group loses a proton with the help of Glu515, generating an activated oxygen with negative charge capable of nucleophilically attacking the glucosyl-enzyme complex, ultimately forming glucan.<sup>71</sup>

## **DEMINERALIZATION AND REMINERALIZATION PROCESSES**

The processes of demineralization and remineralization play crucial roles in the pathogenesis of dental caries. The delicate equilibrium between these two processes is highly sensitive to changes in pH in the oral cavity and a disturbance in this balance by increasing the acidity leads to the development of dental caries. Saliva, along with certain commensal bacteria, assists in maintaining the pH levels within an optimal range following sugar consumption. However, in the presence of a significantly higher population of acidogenic bacteria observed in dental caries, the regulation of pH becomes challenging, ultimately resulting in a net progression of tooth demineralization over time.<sup>72</sup>

### **Tooth structure and its hydroxyapatite surface**

A tooth is a complex anatomical structure composed of various components that work together to support its function.<sup>73, 74</sup> The crown, which is the visible part of the tooth, is situated above the gum line and is covered by a protective layer called enamel. Enamel is a hard and mineralized substance that primarily consists of hydroxyapatite crystals. With

chemical formula  $\text{Ca}_{10}(\text{PO}_4)_6(\text{OH})_2$ , hydroxyapatite is an inorganic compound composed of calcium, phosphate, and hydroxide ions.<sup>75</sup> These ions combine to form hexagonal structures within the enamel, giving it its exceptional hardness and durability.<sup>76</sup> Beneath the enamel lies dentin, a calcified tissue that constitutes the majority of the tooth's structure. Dentin is less mineralized than enamel, still provides support and strength to the tooth. It contains microscopic channels called dentinal tubules, which house nerve fibers that make the tooth sensitive to external stimuli such as temperature and pressure. Dentin is formed by specialized cells called odontoblasts that reside in the innermost part of the tooth, known as the pulp.<sup>77</sup> The pulp is located within the central core of the tooth and contains blood vessels, nerves, and connective tissue. It provides nourishment to the tooth and facilitates sensory functions. The pulp also houses odontoblasts, which are responsible for the continuous formation of dentin throughout the lifespan of the tooth.<sup>78</sup> Covering the root portion of the tooth is a layer called cementum. Cementum is a hard connective tissue that helps anchor the tooth to the surrounding jawbone through the periodontal ligament. The periodontal ligament is a fibrous structure that connects the cementum to the alveolar bone, which is the specialized bone tissue that surrounds and supports the tooth within its socket.

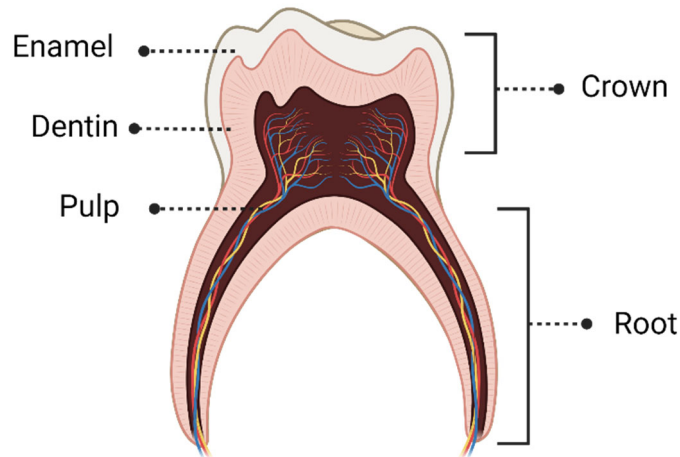


**Figure 0.2.** Structure of tooth: enamel, dentin, and pulp. The image was created with BioRender.com with permission for academic publications (agreement number: UO25JB4CBX).

### Stephan's curve and critical pH

In a healthy state, the hard crystalline hydroxyapatite mineral present in enamel maintains a dynamic equilibrium of ions dissolved in saliva. This equilibrium involves a constant process of demineralization, where enamel hydroxyapatite dissolves into saliva and converts into an ionic form.<sup>72</sup> However, the dissolved ions are recaptured by the enamel surface and reform into crystalline structures, a process known as remineralization.<sup>72</sup> In healthy conditions, demineralization and remineralization are balanced. The balance between demineralization and remineralization is sensitive to pH levels, with lower pH values favoring demineralization. When sugar is consumed, the pH around the tooth surface decreases due to its metabolization by microorganisms (Stephan's curve, Figure 0.3A).<sup>79</sup> However, this drop in pH is eventually normalized to physiological conditions with the assistance of salivary buffers and alkali production by commensal streptococci bacteria.<sup>26, 80</sup> In disease conditions, the buffer systems fail to reestablish the physiological pH due to continuous production of lactic acid by pathogenic bacteria and their



disproportionate growth, which is a result of their exceptional acid tolerance.<sup>12</sup> Consequently, the pH drops below a critical point where demineralization exceeds remineralization (Figure 0.3B). Over time, this leads to overall tooth decay.<sup>81</sup>

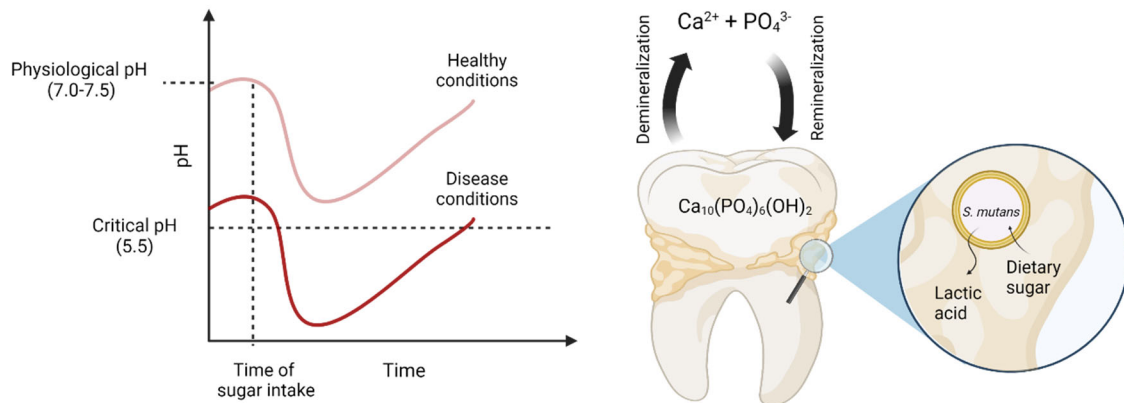


**Figure 0.3. A)** Stephan's curve<sup>79</sup>, pH around tooth surface drops following sugar intake but in disease conditions, it drops below critical pH causing tooth erosion over time. **B)** Due to lactic acid production, pH drops below critical in case of plaque. This causes imbalance of demineralization and remineralization in favor of demineralization. The image was created with BioRender.com with permission for academic publications (agreement number: JN25K6XKNK).

## Role of saliva in oral health

Saliva plays a crucial role in maintaining oral health by performing various functions. It can be categorized into five major categories: lubrication and protection, buffering action and clearance, maintenance of tooth integrity, antibacterial activity, and taste and digestion. As a protective coating, saliva lubricates and safeguards oral tissues from irritants such as enzymes, chemicals, and desiccation.<sup>80</sup> Mucins, complex protein molecules present in saliva, are responsible for its lubricating properties.<sup>82</sup> They have low solubility, high viscosity, elasticity, and adhesiveness, benefiting various intraoral contacts and functions like mastication, speech, and swallowing. Mucins also have antibacterial

properties, selectively modulating the adhesion of microorganisms to oral surfaces and aiding in the control of bacterial colonization.<sup>83</sup> Saliva acts as a buffer through components like bicarbonate, phosphate, urea, and amphoteric proteins and enzymes. Bicarbonate is the most important buffering system, neutralizing acids and generating ammonia. The pH of plaque, influenced by salivary buffering, affects the progression of caries.<sup>84, 85</sup> Saliva also contributes to remineralization and demineralization of teeth. It helps replace lost minerals and forms a fluorapatite-like coating on enamel, making it more resistant to caries.<sup>86</sup> Saliva's antibacterial activity is achieved through immunologic and nonimmunologic agents, including immunoglobulins, proteins, mucins, peptides, and enzymes, which protect teeth and mucosal surfaces.<sup>87</sup> Finally, saliva enhances taste perception, aids in the initial breakdown of starch and fat digestion and lubricates the food bolus for swallowing. Artificial saliva substitutes can provide lubrication but cannot match the full range of benefits offered by natural saliva.<sup>88</sup>

## **CURRENT METHODS OF CARIES MANAGEMENT**

Caries management focuses on promoting a healthy lifestyle rather than a cariogenic one. To achieve a caries balance, certain pathological factors such as frequent sugar consumption, insufficient fluoride exposure, poor oral hygiene, and salivary dysfunctions need to be minimized through lifestyle changes or clinical interventions.<sup>7</sup> In this section, we will discuss some of the current methods used for preventing dental caries and assess their effectiveness.

**Oral hygiene: regular brushing, flossing, and cleaning**

Frequent brushing is indeed a crucial component of maintaining oral hygiene and is one of the most common methods for preventing dental caries. It helps mechanically remove initial bacterial colonization and trapped food particles from the irregular surfaces of the teeth. However, it is important to note that a toothbrush may not reach all the corners and interdental spaces effectively, which is why it is recommended to combine brushing with flossing. Flossing complements brushing by removing plaque and food debris from areas that are difficult to reach with a toothbrush, such as between the teeth and along the gumline. By incorporating flossing into your oral hygiene routine, you can improve your chances of thoroughly cleaning your teeth and reducing the risk of caries. While brushing and flossing are essential practices, it is important to recognize that they require frequent repetition to be effective. Even after regular repetition, bacteria in the mouth can quickly re-colonize tooth surface, with complex communities that adhere and are more resistant to mechanical removal.<sup>89,90</sup>

**Mouthwashes**

Mouthwashes contain a variety of ingredients, including chlorhexidine, cetylpyridinium chloride, sodium fluoride, stannous fluoride, stannous chloride, zinc oxide, zinc chloride, and herbal extracts such as licorice and curcumin (Figure 0.4). Chlorhexidine is an effective antiseptic agent widely used in dentistry. It has bacteriostatic and bactericidal effects, targeting various bacteria, yeasts, and viruses.<sup>91</sup> Chlorhexidine binds to bacterial membranes, causing cell damage and inhibiting bacterial growth.<sup>92,93</sup> It is available in different formulations such as rinses, gels, sprays, varnishes, toothpastes, and mouthwashes. However, long-term use of chlorhexidine may cause temporary taste alteration and tooth pigmentation.<sup>94,95</sup> Chlorhexidine also has antibacterial effects on

periodontal pathogens associated with peri-implantitis and improves clinical outcomes of implant-supported restorations. New formulations and combinations of chlorhexidine with fluoride or anti-biofilm peptides showed promising results in reducing plaque, preventing caries, and enhancing antimicrobial efficacy.<sup>96</sup> Additionally, innovative approaches like low-intensity direct current and nanotechnology are being explored to enhance chlorhexidine's effectiveness against oral biofilms. However, the use of chlorhexidine may impact the oral microbiome by promoting an acidic environment and altering bacterial composition.<sup>97</sup> There is also a concern about potential resistance to chlorhexidine in oral bacteria, which requires further investigation.<sup>98</sup>

Cetylpyridinium chloride is an antimicrobial compound found in mouthwashes that effectively kills bacteria, yeast, and certain viruses. When used alongside brushing of teeth, cetylpyridinium chloride mouth rinses reduce plaque and gingival inflammation. Recent studies highlight the potential of cetylpyridinium chloride containing mouthwashes in maintaining oral health, preventing gingivitis, and reducing the adhesion and biofilm formation of harmful bacteria. New formulations combining cetylpyridinium chloride with other compounds, such as hyaluronic acid and tranexamic acid, have demonstrated promising results in preventing plaque accumulation and alleviating gingival bleeding. Additionally, cetylpyridinium chloride chewing gum and mouthwash have shown potential for maintaining oral hygiene and reducing biofilm viability.<sup>99, 100</sup>

The use of herbs and plant extracts in oral hygiene products has increased due to the rise of multidrug resistant pathogens and the demand for safe and effective alternatives. Licorice and curcumin are two natural products extensively studied for their potential in dental and oral care. Licorice exhibits antimicrobial, anti-inflammatory, and

immunoregulatory effects, making it beneficial for oral diseases like dental caries and gingivitis. Licorice extracts and ingredients have shown antiadhesive and anti-inflammatory effects against oral pathogens.<sup>101</sup> Curcumin, derived from turmeric, has diverse therapeutic properties and has been found effective in treating oral diseases such as gingivitis, periodontitis, and oral cancer. Curcumin mouthwashes have shown comparable efficacy to chlorhexidine mouthwashes in reducing plaque and gingivitis.<sup>102</sup> Both licorice and curcumin are considered safe for use, but high doses of licorice can have adverse effects.

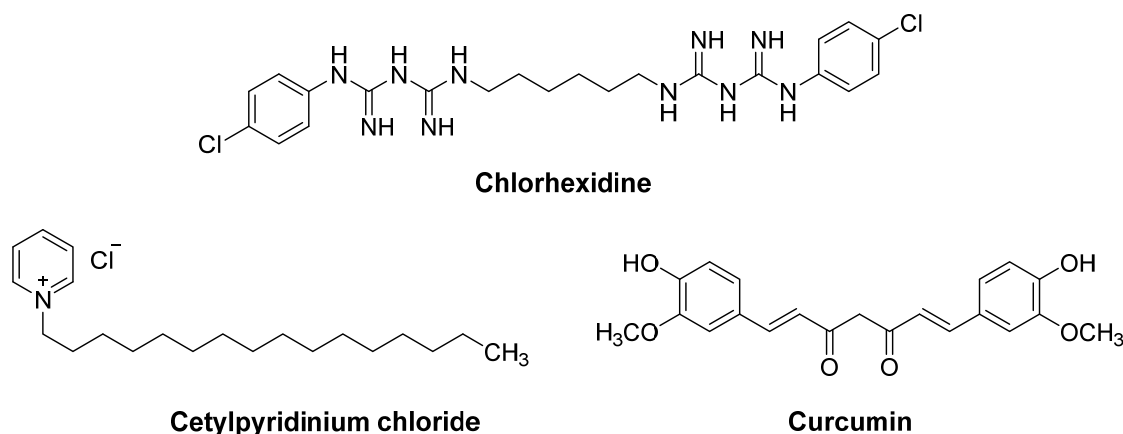


**Figure 0.4.** Common ingredients in mouthwashes

### Fluoride treatment

Fluoride is commonly used in drinking water and oral hygiene products, and it plays a significant role in promoting oral health.<sup>103, 104</sup> It acts as a catalyst for the process of remineralization, aiding in the formation of a more caries-resistant substance called fluorapatite.<sup>105</sup> Fluorapatite is more resistant to cariogenic biofilms compared to the natural hydroxyapatite found in teeth.<sup>106</sup> However, it is important to note that prolonged exposure to high levels of fluoride can lead to a condition called fluorosis, which affects dental and skeletal tissues.<sup>107, 108</sup> Dental fluorosis is characterized by the appearance of white spots

on the teeth and an increased susceptibility to enamel fracture. In severe cases, it can result in brown discoloration and enamel pitting. Skeletal fluorosis, on the other hand, affects the bones, making them extra hardened and more prone to fractures.<sup>109</sup> Moreover, excessive doses of fluoride have been associated with neurotoxicity, particularly in areas with high levels of naturally occurring fluoride in the water.<sup>110</sup> While fluoride has proven to be beneficial in preventing dental caries, its effectiveness is not without limitations.

### **Gtf inhibitors**

Teas such as black, green, and oolong contain polyphenols which show biofilm inhibitory activities. Compounds like theaflavin, (-)-epigallocatechin gallate, and (-)-epicatechin gallate exhibit anticaries activities by inhibiting Gtfs (Figure 0.5). Theaflavin, for example, showed 50 % inhibition of purified GtfB at a concentration of 10  $\mu$ M.<sup>111</sup> Similarly, epigallocatechin gallate demonstrated 28 % GtfB inhibition at 546  $\mu$ M while 23 % inhibition at 566  $\mu$ M was observed for (-)-epicatechin gallate.<sup>112, 113</sup> However, these polyphenols also have antimicrobial effects on *S. mutans* and affect acid production, indicating multiple targeted pathways. In addition to polyphenols derived from tea extracts, flavonoids such as procyanidin, myricetin, kaempferol, and apigenin (Figure 0.5) have demonstrated inhibitory effects on Gtfs at concentrations ranging from high micromolar to millimolar levels.<sup>114-123</sup> Moreover, certain inorganic salts, including  $\text{Fe}^{3+}$ ,  $\text{Zn}^{2+}$ ,  $\text{Fe}^{2+}$ , and  $\text{Cu}^{2+}$ , have exhibited activity against Gtfs.<sup>124</sup> Additionally, several small-molecules, such as acarbose and oxazole 5H6 (Figure 0.5), have been reported as inhibitors of Gtfs.<sup>125, 126</sup> Recently, maltose-derived acylhydrazones A2H2 and A2H8 have been reported to inhibit Gtfs at 500  $\mu$ M.<sup>127</sup> Sulfated vizantin (Figure 0.5) is another recently reported Gtf inhibitor with *S. mutans* biofilm inhibitory activity.<sup>128</sup>

Despite the numerous natural and synthetic Gtf inhibitors reported in the literature, their activity has generally been low. Furthermore, the demonstration of *in vivo* anticariogenic activity for these inhibitors is limited. Given the availability of the crystal structures of GtfB and GtfC,<sup>70</sup> the proteins responsible for insoluble glucan synthesis, it is imperative that structure-based drug design can be used to develop synthetic small molecule inhibitors of Gtfs with potential *in vitro* and *in vivo* anticariogenic activity.

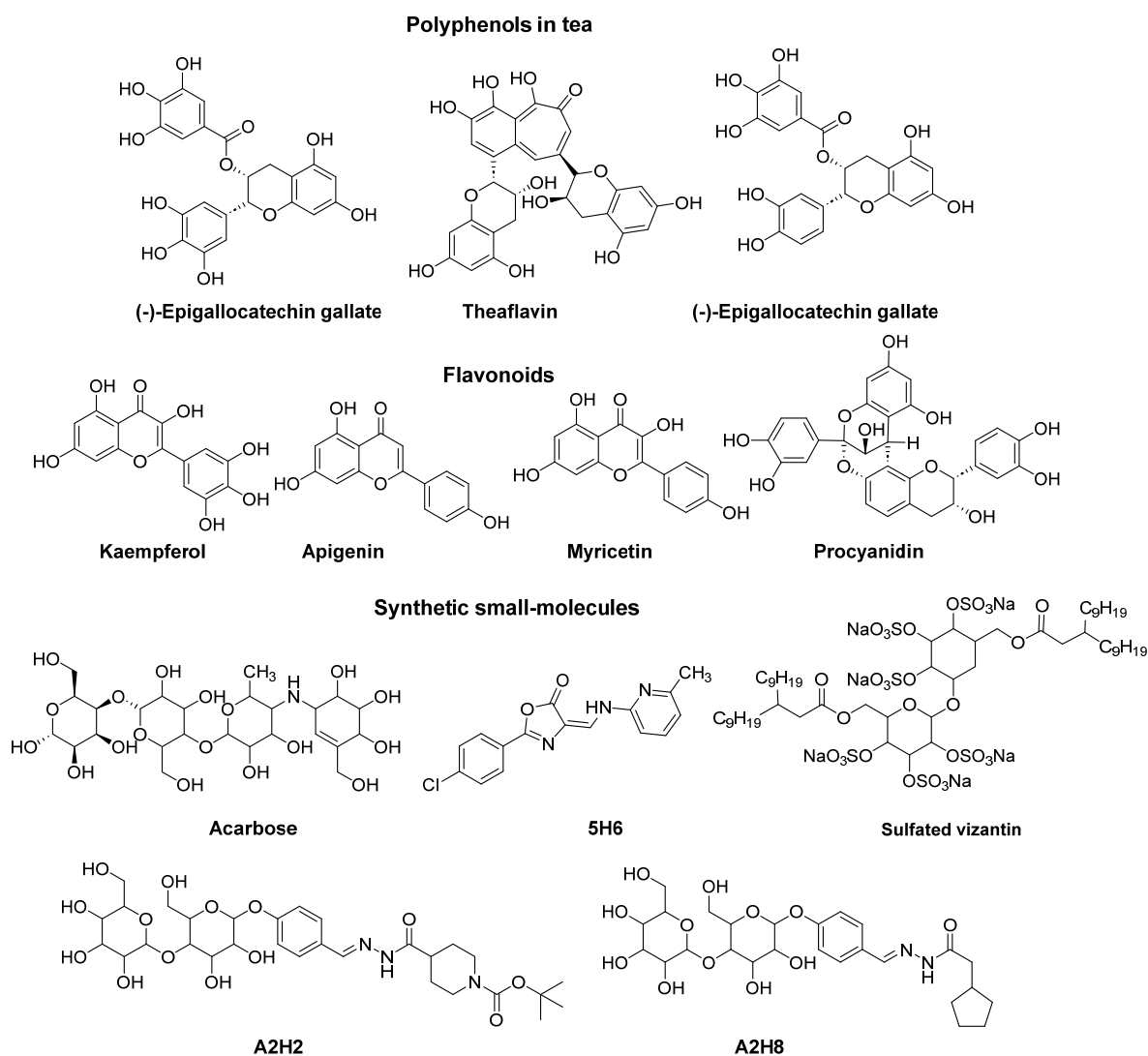


**Figure 0.5.** Currently known Gtf inhibitors

## NANOMATERIALS IN ANTI-CARIES RESEARCH

In recent years, there has been a growing interest in the development of antibacterial nanomaterials for potential applications in anti-caries research. Various nanomaterials have been investigated for their effectiveness in preventing dental caries and inhibiting cariogenic biofilms. For instance, silver nanoparticles have been studied for their ability to prevent dental caries.<sup>129</sup> Co-loaded nanoparticles containing farnesol and myricetin have also shown promise in inhibiting biofilm formation.<sup>130</sup> pH-responsive materials have been explored as carriers for delivering farnesol,<sup>131, 132</sup> while porous silicon microparticles have been utilized to mitigate cariogenic biofilms.<sup>133</sup> Additionally, ferumoxylol nanoparticles,<sup>134, 135</sup> poly(ethylenimine),<sup>136</sup> and chitosan nanoparticles<sup>137</sup> have exhibited strong antibacterial activity against *S. mutans*.

Furthermore, researchers have explored various nano systems for the controlled release of anti-caries drugs. These include,<sup>138, 139</sup> liposome,<sup>140</sup> halloysite nano-tube,<sup>141</sup> polyamidoamine<sup>142</sup> and dextran-coated Iron oxide nanoparticles (also known as nanozymes).<sup>143</sup> Despite the flurry of studies in this area, none of these agents have been translated for clinical use due to either modest *in vivo* efficacy or lack of sufficient evidence supporting their effectiveness. It is important to note that nanomaterials for encapsulation and pH-responsive delivery of dental drugs holds significant potential for combating dental caries because of low pH conditions around dental plaque.



## OVERVIEW OF THIS WORK

This study focuses on the design, synthesis, evaluation, and targeted delivery of small-molecule dental biofilm inhibitors specifically targeting *S. mutans* Gtfs. We have developed a new class of small molecules that exhibit selectivity towards *S. mutans* biofilm formation while not affecting the growth of planktonic bacteria, including the pathogenic *S. mutans* and commensal streptococci such as *S. sanguinis* and *S. gordonii*. To enable the controlled release, the lead inhibitors were encapsulated in a pH-responsive hydrogel to generate hydrogel-encapsulated biofilm inhibitors (**HEBI**) and its anti-carries activity has been demonstrated by *in vitro* and *in vivo* experiments.

Chapter 1 of this thesis delves into the comprehensive design of novel aurone compounds as potential inhibitors of *S. mutans* biofilm formation. Our previous studies have shown promising results with small molecule inhibitors, but their limited water solubility hindered their successful encapsulation into pH-responsive hydrogel material for the controlled and targeted delivery. To overcome this challenge, we modified the structure of the lead compound by substituting the benzothiophene ring system with an aurone ring system, removing nitro and amide groups and adding polar functional groups. All designed compounds were computationally docked in the GtfB active site to examine the binding interactions. All analogs were synthesized and characterized, and their solubilities were determined experimentally.

Chapter 2 entails the evaluation of the newly designed aurones for their anti-virulence activity *in vitro* and *in vivo*. The selective inhibitory activity of these molecules towards *S. mutans* biofilms vs growth was carefully investigated by conducting planktonic

growth and biofilm assays. In addition, the effect of compounds on the planktonic growth of two representative commensal streptococci, *S. gordonii* and *S. sanguinis* were evaluated. Additionally, the binding profiles of the lead inhibitors **HA5** and **HA6** to GtfB was determined through biolayer interferometry experiments and their inhibitory activities against Gtf-mediated glucan formation were assessed using enzymatic assays. To provide definitive evidence of the binding interactions, the lead inhibitor **HA5**, which demonstrated the most potent inhibitory activity among the tested aurones, was co-crystallized with the catalytic domain of GtfB and its interactions within the GtfB binding site was determined at a molecular level.

Chapter 3 focuses on the development of efficient encapsulation methods and pH-responsive delivery systems for the lead compound, **HA5**. A pH-responsive polymeric material, namely hydrogel, was employed for the encapsulation of **HA5**. The hydrogel encapsulated biofilm inhibitor (**HEBI**) was carefully evaluated for its selective inhibition of *S. mutans* biofilms while minimizing the impact on the growth of planktonic *S. mutans* as well as commensal species such as *S. gordonii* and *S. sanguinis*. Moreover, the efficacy of **HEBI** was assessed using *S. mutans* induced experimental rat model of dental caries to demonstrate its ability to release **HA5** and *in vivo* anticaries activity.

Through these comprehensive investigations, this work aims to provide valuable insights into the design, synthesis, evaluation, and targeted delivery of aurone-based small molecule biofilm inhibitors, ultimately contributing to the development of novel strategies for combating *S. mutans* biofilm-associated diseases such as dental caries and promoting oral health.

CHAPTER 1: DESIGN AND SYNTHESIS OF A SMALL MOLECULE LIBRARY OF  
AURONES TO INHIBIT *STREPTOCOCCUS MUTANS*  
GLUCOSYLTRANSFERASES AND BIOFILM

by

PARMANAND AHIRWAR, BHAVITAVYA NIJAMPATNAM, EDWIN M. ROJAS,  
PIYASUDA PUKKANASUT, AND SADANANDAN E. VELU

## ABSTRACT

We recently developed two small molecules, **III**C5 and **G**43, as selective dental biofilm inhibitors which preserve the oral microbiota. Our attempts to encapsulate these compounds into a pH responsive hydrogel for pH-triggered delivery were not successful due to their poor water solubilities (10 - 25  $\mu\text{g/mL}$ ). We designed and synthesized analogs of **III**C5 to improve solubility, retain biofilm inhibitory activities, and to facilitate encapsulation into pH-responsive hydrogel microparticles. The newly designed analogs belong to a class of compounds called aurones, which is a natural product scaffold that occurs abundantly in flowers, fruits, seeds, and other parts of plants. Eleven analogs of **III**C5 were synthesized following a synthetic route similar to their biosynthesis. Prior to their syntheses, all aurones were docked in the *S. mutans* GtfB active site to ensure that their binding was similar to **G**43 observed in its co-crystal structure with GtfB. Physicochemical properties of the designed aurones calculated/predicted using SwissADME. Six methoxyaurones and five hydroxyaurones were synthesized and their solubilities were determined using UV-Vis spectroscopy. In general, hydroxyaurones were found to be more soluble than the methoxyaurones and a trend of increasing solubility was observed with the increase in the number of hydroxy groups on the phenyl ring. Hydroxyaurones **HA**5 and **HA**6 were found to be the most soluble analogs with solubilities 120.09  $\mu\text{g/mL}$  and 90.77  $\mu\text{g/mL}$ , respectively.

## INTRODUCTION

Most tooth and gum related diseases are associated with bacterial infections. Among these, dental caries (tooth decay) is a ubiquitous disease that affects the vast majority of the human population. It is a multifactorial disease that causes localized destruction of susceptible dental tissues.<sup>1</sup> Dental caries is identified as the most prevalent disease worldwide in a recent Lancet study of global burden of 328 major diseases.<sup>2</sup> Despite its general classification as a 'life-style-related' disease, dental caries poses a significant challenge as it results in tooth loss, infection, and in some cases, even death by sepsis.<sup>3,4</sup>

Dental caries occurs due to the colonization of tooth surfaces by oral bacteria.<sup>3</sup> These bacterial colonies called biofilms consist of more than 700 bacterial species. The formation of biofilms is often initiated by harmless commensal bacterial species that reside in oral cavity, such as *Streptococcus gordonii* and *Streptococcus sanguinis*.<sup>5-7</sup> As the disease develops, the number of pathogenic bacteria in the biofilms increases disproportionately. One such pathogenic species, *Streptococcus mutans*, is considered to be the most important etiological agent for dental caries due to its ability to form robust and reoccurring biofilms and adaptability at lower pH.<sup>8,9</sup> Inside the biofilms, bacteria produce lactic acid as a metabolic byproduct which causes erosion of tooth enamel.<sup>10</sup> *S. mutans* employs two main mechanisms for adhesion: 1) a sucrose-dependent mechanism and 2) a sucrose-independent mechanism. In the sucrose-dependent mechanism, *S. mutans* utilizes its extracellular proteins called glucosyltransferases (Gtfs) to produce sticky glucans, which enables bacterial cohesion and the formation of biofilm structures.<sup>11,12</sup> Furthermore, the glucans provide structural integrity to the biofilm, thereby contributing to

its robust and persistent nature.<sup>13, 14</sup> In the sucrose-independent mechanism, *S. mutans* uses its surface proteins, such as antigen I/II, to interact with salivary agglutinin (SAG) proteins on the tooth pellicle to facilitate attachment to the tooth surface.<sup>15-17</sup>

In the sucrose-dependent process, *S. mutans* glucosyltransferases (Gtfs) produce oligomers of glucose known as glucans, which play a key role in biofilm and the subsequent cariogenesis.<sup>18, 19</sup> There are three types of Gtfs classified based on their ability to produce different types of glucans. The enzyme GtfB encoded by *gtfB* gene produces water insoluble glucans.<sup>20</sup> The enzyme GtfC encoded by *gtfC* gene is responsible for the production of both soluble and insoluble glucans.<sup>21</sup> The enzyme GtfD encoded by *gtfD* gene is responsible for the production of water-soluble glucans.<sup>22</sup> These glucans act as linkers between bacteria by binding to, glucan binding proteins (GBP) to form strong three-dimensional bacterial colonies.<sup>23</sup> Therefore, Gtfs are attractive targets for the design and development of biofilm inhibitors. As Gtf inhibitors do not affect the growth bacteria, Gtf inhibition is an excellent strategy to specifically inhibit bacterial biofilm while preserving oral microbiota.

Currently, diverse methods are used to prevent and treat dental caries. Brushing teeth is the most common way to tackle the challenges of dental caries, but requires frequent repetition as the plaque reoccurs rapidly.<sup>24, 25</sup> Another method commonly employed for the treatment of dental caries is the use of fluoride in community water and toothpastes. But it doesn't prevent biofilm formation, rather it helps in the remineralization process of the tooth surfaces.<sup>26</sup> Yet another common treatment is the use of mouthwashes containing broad-spectrum antibacterial agents. However, antibacterial agents lack selectivity towards biofilm inhibition and inhibit the growth of both pathogenic and

commensal species alike.<sup>27, 28</sup> Other than these approaches, several antimicrobial agents have been recently discovered to be effective against biofilms. However, they all have selectivity problems similar to the antibacterial agents used in mouthwashes.<sup>29,30</sup> It is, thus, necessary to develop non-bactericidal anti-biofilm agents as the effective therapies of dental caries.

Recent studies from our lab aimed at developing selective small molecule inhibitors of *S. mutans* biofilm, have resulted in the identification of two potent lead compounds **G43** and **IIIC5**.<sup>31-34</sup> The goal of the present study is to improve the solubility of the most active biofilm inhibitor **IIIC5** by designing and synthesizing a library of new analogs and to identify leads suitable for the nanomaterial encapsulation and subsequent drug-delivery studies. Our rational design of analogs to improve the solubility of **IIIC5** resulted in a group of compounds that belongs to the class of aurones.

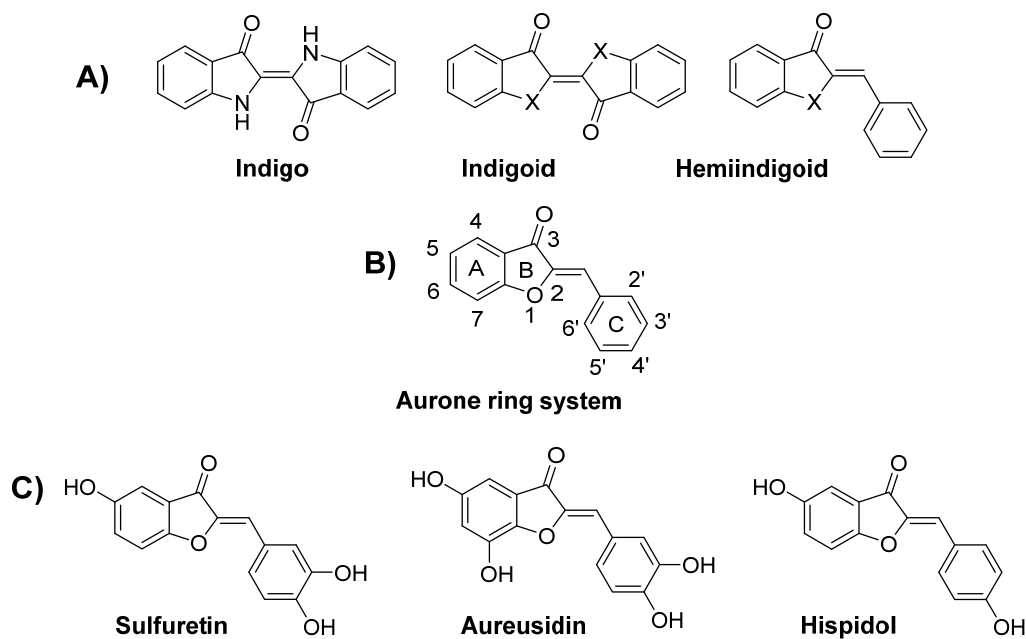


**Figure 1.1.** A) Structures of indigoid and hemiindigoids derived from indigo, B) Aurone scaffold, C) A few commonly occurring aurone natural products.

Aurones are a class of natural products that belong to the hemiindigoid family with an ‘indigoid structure’ connected to the ‘stilbene segment’ through a double bond (Figure 1.1). They were first reported in the early 1940s by Geissman and Heaton.<sup>35, 36</sup> The term ‘aurone’ derived from Latin word *aurum* which means gold, was coined by Bate-Smith and Geissman in 1951 inspired by their bright golden colors.<sup>37</sup> A common aurone ‘aureusidin’ is a natural product found in *Antirrhinum majus* or garden snapdragon flowers.<sup>38, 39</sup> Apart from flowers aurones are found abundantly in heartwoods, seeds, leaves, fruits, and roots of various plant species.<sup>40</sup>

Biosynthesis of aurones, as studied in the plant species *Antirrhinum majus* and *Coreopsis grandiflora* is outlined in Figure 1.1. The biosynthesis involves the formation of chalcones from p-coumaroyl-CoA and malonyl-CoA, catalyzed by the enzyme chalcone synthase. The chalcones thus formed are converted to aurones by other enzymes such as



aurone synthase and polyphenol oxidase. Hydroxy groups are added to the aurone rings either before or after the cyclization. (Figure 1.2).<sup>41-43</sup> Alternatively, as in case of hispidol biosynthesis, peroxidase enzymes mtPRX1 and mtPRX2 are responsible for the conversion of chalcones to aurones.<sup>44</sup>

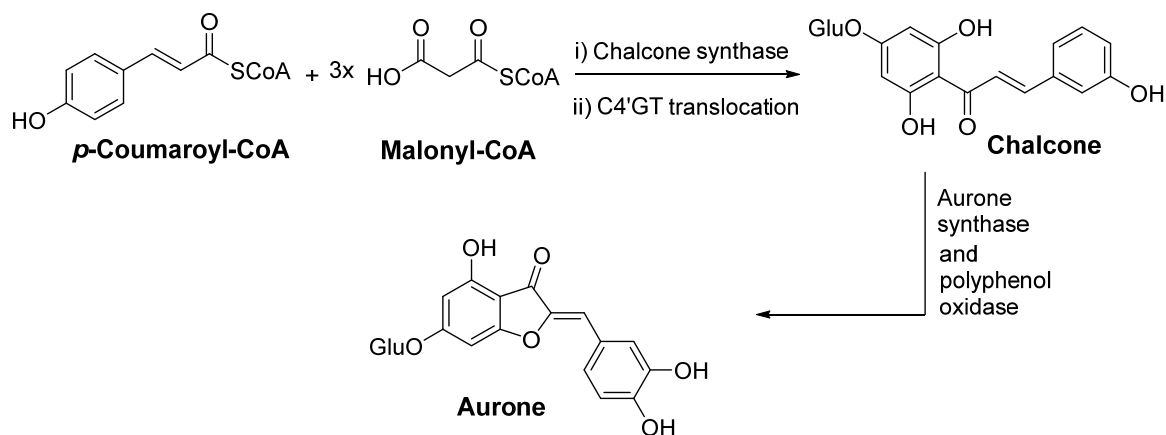


**Figure 1.2.** Biosynthetic pathway for aurones.

Several synthetic pathways have been employed in the laboratory synthesis of aurones as shown in Figure 1.3. For example, aurones have been synthesized by the condensation of benzofuranones with arylaldehydes in the presence of alumina or acetic acid or potassium hydroxide.<sup>45</sup> Another method used is an “on-water” strategy to make aurones from similar starting materials.<sup>46</sup> Alternatively, aurones have been synthesized by the cyclization of chalcones using mercuric acetate<sup>47, 48</sup> or gold (I) halides<sup>49</sup> have also been reported.<sup>47, 48</sup>

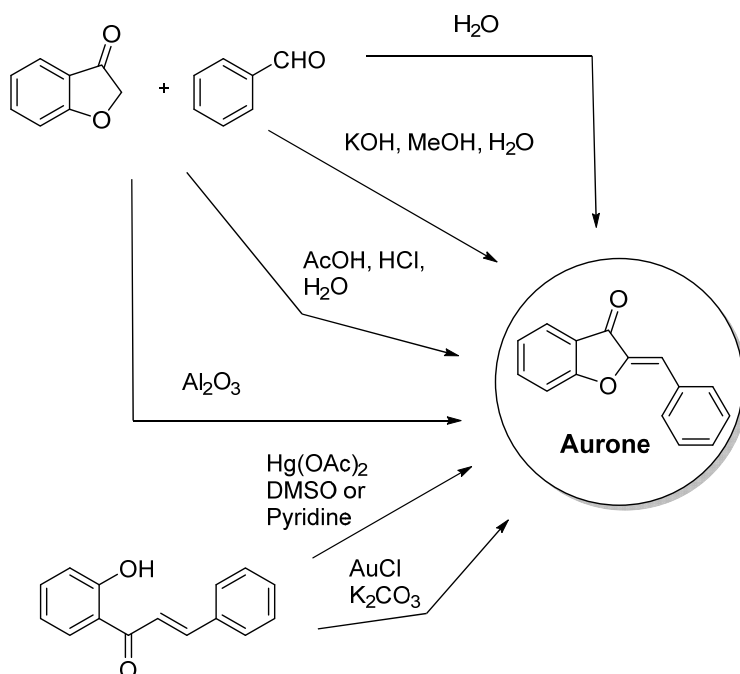


**Figure 1.3.** Approaches used in the laboratory synthesis of aurones.

Aurones have been proven to be a promising chemical scaffold for medicinal applications.<sup>50</sup> Anticancer activities of aurones by inhibition of tubulin polymerization<sup>51, 52</sup>, poly(ADP-ribose)polymerase,<sup>53</sup> tyrosinase,<sup>54, 55</sup> and proto-oncogene serine/threonine-protein kinases,<sup>56, 57</sup> have been reported. Aurones have also been found to exhibit neurochemical,<sup>58</sup> anti-inflammatory,<sup>59, 60</sup> antioxidant,<sup>61</sup> antidiabetic,<sup>62, 63</sup> and antiadipogenic<sup>64, 65</sup> activities. Apart from these, a wide range of anti-infective activities including antibacterial,<sup>66, 67</sup> antifungal,<sup>68, 69</sup> antiparasitic,<sup>70, 71</sup> and antiviral<sup>72, 73</sup> properties have been reported for aurones.

Our lab has recently developed a potent biofilm inhibitor, **G43**, with selective biofilm inhibitory activity without affecting the planktonic growth of *S. mutans* and oral commensal bacteria at its biofilm-inhibiting doses.<sup>34</sup> **G43** inhibited Gtfs in a zymogram assay with an IC<sub>50</sub> value of ~10  $\mu$ M. In biolayer interferometry experiments **G43** showed

binding affinity to GtfB ( $K_D = 3.6 \mu\text{M}$ ).<sup>34</sup> We have evaluated the bactericidal activities of **G43** against two commensal oral bacterial species, *S. sanguinis* and *S. gordonii*, along with *S. mutans* and demonstrated that growth inhibition was minimal at 200  $\mu\text{M}$ , which is a much higher concentration than its biofilm  $\text{IC}_{50}$  concentration. Structure-activity relationship (SAR) studies on **G43** led to the discovery of several more active inhibitors, such as **IIIC5**.<sup>74</sup>

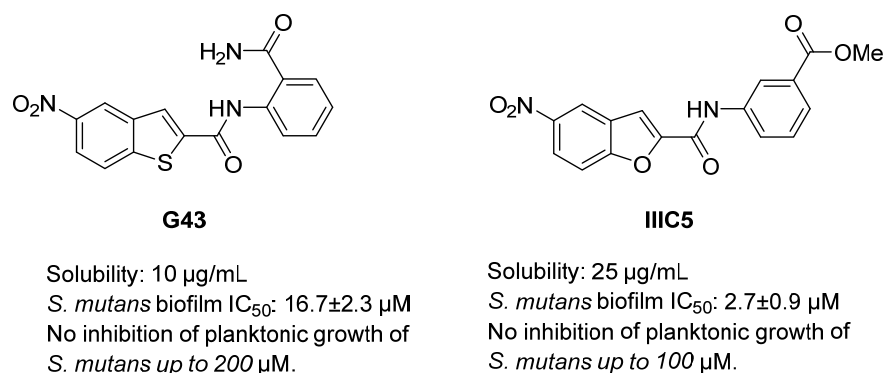


**Figure 1.4.** Chemical structures, solubility, and bioactivity of inhibitors **G43** and **IIIC5**.

Inhibitor **IIIC5** exhibited excellent selectivity towards biofilm inhibition with an  $\text{IC}_{50}$  value of 2.7  $\mu\text{M}$  with no inhibition of commensal growth at 100  $\mu\text{M}$ . *in vivo* anticaries activity of one of these inhibitors, **G43** has also been reported in this publication.<sup>31</sup> A 4-week treatment of *S. mutans* UA159 infected gnotobiotic rats with 100  $\mu\text{M}$  **G43** resulted in a significant reduction in buccal, sulcal, and proximal dental caries scores compared to control groups. The rats treated with **G43** did not experience any weight loss over the course of the study in comparison with the control group, suggesting that it is non-toxic. The bacterial colonization appears to be unaffected in **G43** treated rats.<sup>31</sup>

## RESULTS AND DISCUSSION

Our initial efforts to prepare pH-responsive hydrogel encapsulated biofilm inhibitors using **G43** or **IIC5** did not yield the expected results due to the low solubility (10-25  $\mu\text{g/mL}$ ) of these inhibitors. Therefore, efforts were made to modify the structure of **IIC5** to improve its solubility. Specifically, analogs of **IIC5** were prepared by substituting the benzofuran ring with a structurally similar aurone ring, removing the nitro, amide, and ester groups, and by introducing multiple hydrophilic OMe or OH groups on the phenyl ring. This study resulted in the identification of several new aurone derivatives (**MA1-6** and **HA2-6**, Figure 1.5), of which the hydroxyaurones (**HA2-6**) were found to have the desired solubility required for the hydrogel encapsulation while maintaining the potency and selectivity of biofilm inhibition.

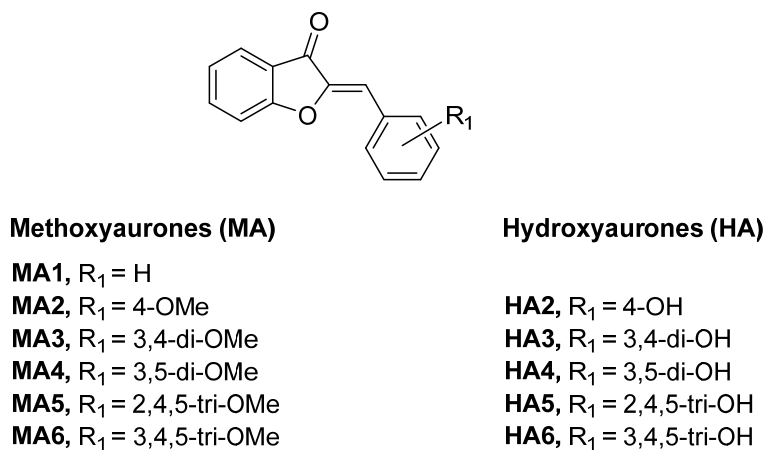


**Figure 1.5.** Aurone library of small molecules.

All designed aurone analogs were docked in the GtfB active site using SeeSAR and compared with the co-crystal structure of **GtfB** + **G43** to elucidate their predicted binding interactions with the catalytic residues in the site (Figure 1.6). It was observed that all the

aurones occupied the same binding pocket as **G43** with similar orientations and interacted with critical active site amino acid residues, suggesting that the designed aurone derivatives have potential to demonstrate similar Gtf inhibition activity as **G43**.

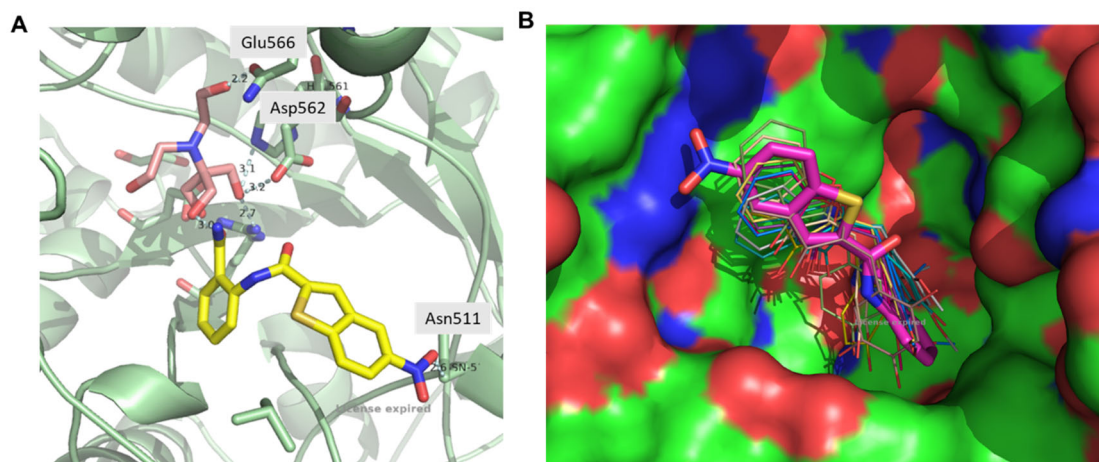


**Figure 1.6. A)** **G43** co-crystal structure with GtfB, **B)** Docking models of aurones with GtfB aligning with **G43** crystal structure.

Aurones is a class of organic compounds that is gaining interest in medicinal chemistry due to their biological activities and presence in natural products.<sup>75</sup> Biosynthetically, aurones are derived from chalcones.<sup>76</sup> Therefore, we took a biomimetic synthetic approach (Figure 1.7) to generate the proposed library of aurones (Figure 1.5), which includes one aurone derivative with an unsubstituted phenyl ring (**MA1**), five methoxy substituted aurones (**MA2-6**) and five hydroxy substituted aurones (**HA2-6**). These aurones were prepared from 2-hydroxychalcones (**3a-f**), which in turn were prepared by the Claisen-Schmidt aldol condensation<sup>77</sup> of the benzaldehydes (**2a-f**) and 2-hydroxyacetophenone (**1**) in the presence of KOH in ethanol in 37-90 % yield. Cyclization of chalcones (**3a-f**) in the presence of Hg(OAc)<sub>2</sub> in anhydrous pyridine afforded the aurones (**MA1-6**) in 79-100 % yield. Methyl groups in methoxyaurones (**MA2-6**) were then

removed by treatment with BBr<sub>3</sub> in anhydrous CH<sub>2</sub>Cl<sub>2</sub> to afford the hydroxyaurones (**HA2-6**) in 80-86 % yield.

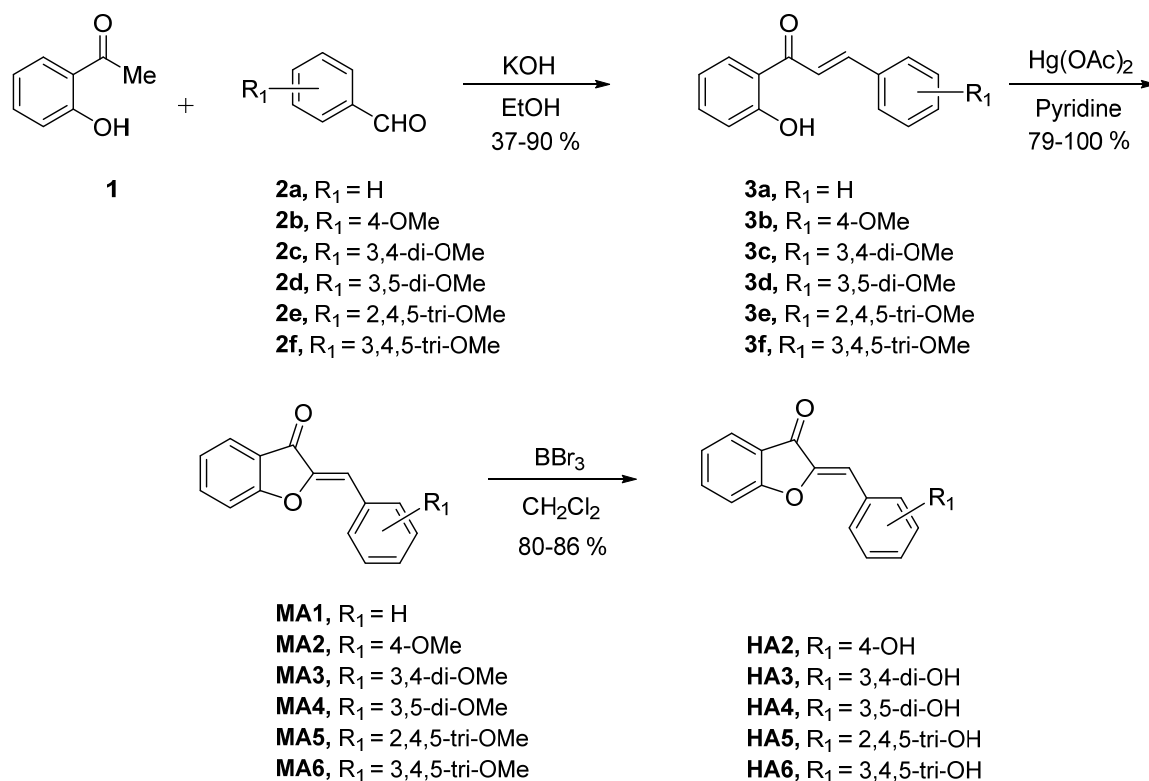


**Figure 1.7.** Synthesis of methoxyaurones and hydroxyaurones

### Lipinski properties of the aurone analogs

Furthermore, the aurones were examined for Lipinski's rule of 5, computationally predicted water solubility and lipophilicity based on LogP<sub>o/w</sub> (Table 1.1) using SwissADME<sup>78</sup>. According to Lipinski's rule of 5, for a molecule to be drug-like, it should not contain more than 5 hydrogen bond (H-bond) donor atoms, 10 H-bond acceptors, its molecular weight must not exceed 500 and log P must be less than 5.<sup>79</sup> All the methoxy and hydroxy aurones satisfy all the Lipinski's drug likeness criteria, hence SwissADME returned 0 violations.

**Table 1.1.** Physicochemical properties of aurones calculated using SwissADME

Compd No	MW	H-bond acceptors	H-bond donors	LogP
MA1	222.24	2	0	3.11
MA2	252.26	3	0	3.09
MA3	282.29	4	0	3.07
MA4	282.29	4	0	3.11
MA5	312.32	5	0	3.05
MA6	312.32	5	0	3.05
HA2	238.24	3	1	2.69
HA3	254.24	4	2	2.31
HA4	254.24	4	2	2.28
HA5	270.24	5	3	1.91
HA6	270.24	5	3	1.95

*MW = molecular weight; LogP = average lipophilicity of 5 logP<sub>o/w</sub> predictions*

Lipophilicity<sup>80</sup> and water solubility<sup>81-83</sup> are important properties of a molecule which are used to assess membrane permeability, ease of handling and formulation, potency, selectivity, and promiscuity of a potential drug molecule. LogP is a classical descriptor for lipophilicity, which is defined as the partition coefficient between n-octanol and water. SwissADME calculates a consensus logP (Table 1.1) which is average of 5 logP<sub>o/w</sub> predictions; iLOGP, XLOGP3, MLOGP and SILICOS-IT.<sup>84-88</sup> As expected, hydroxyaurones were seen to be less lipophilic than methoxyaurones due to the presence of more hydrophilic ‘OH’ groups. For methoxyaurones, lipophilicity decreases with increase in methoxy groups; similarly, for hydroxyaurones, a greater number of hydroxy groups adversely affected lipophilicity as evident from logP values. Water solubility trend is inversely related to lipophilicity based on logP values i.e., lower the logP value, higher the solubility of a compound. The trend among methoxy and hydroxy aurones are as

expected, i.e., water solubility increases with the increase in methoxy or hydroxy groups in methoxy and hydroxy aurones respectively. Therefore, hydroxyaurones are expected to be more soluble than methoxyaurones, with **HA5** and **HA6** being the most soluble compounds out of the aurone library. Despite having several methods for prediction of solubility,<sup>89-91</sup> it's difficult to accurately predict the solubility, necessitating the experimental determination of solubilities of the synthesized compounds.

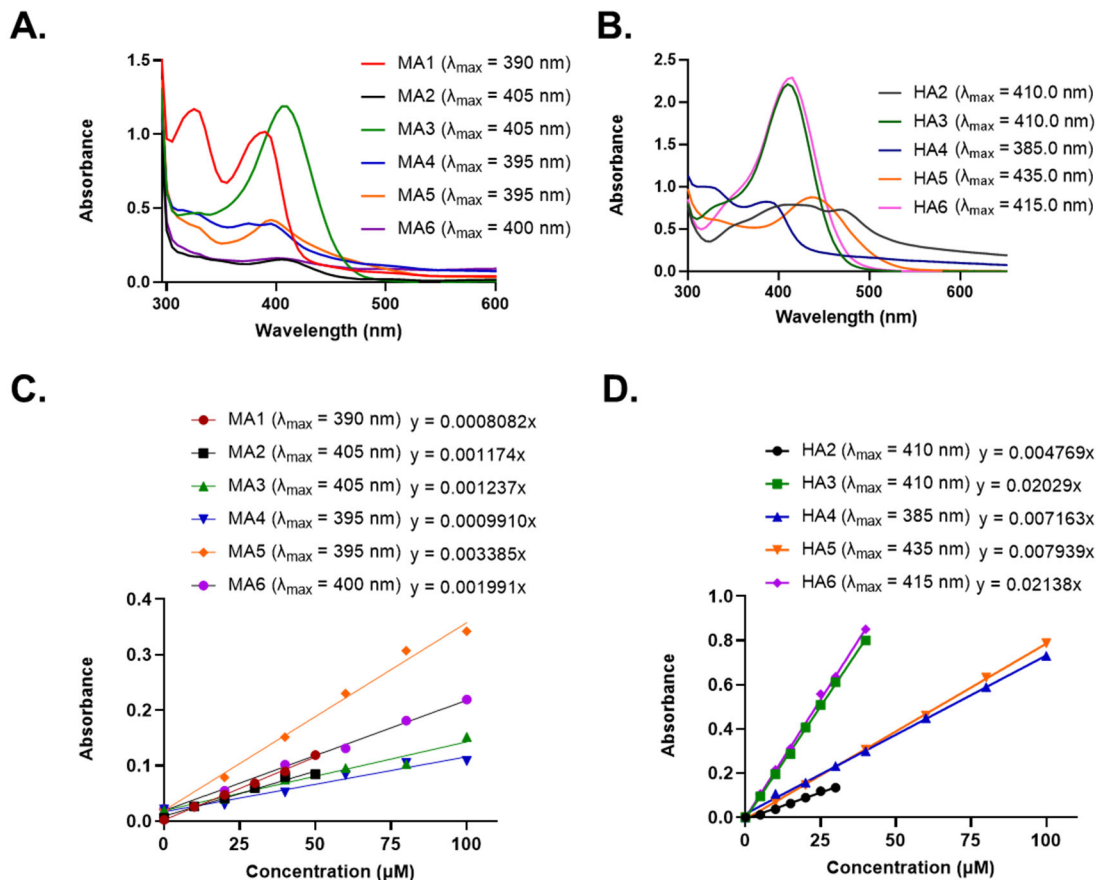
### Determination of solubility of aurones

. Thus, the solubilities of methoxyaurones, **MA1-6** and hydroxyaurones **HA2-6** were determined using a UV-Vis spectroscopy method reported in the literature.<sup>92</sup> Using UV-Vis spectroscopy,  $\lambda_{\text{max}}$  for each compound was determined by scanning across a range of wavelengths followed by the generation of calibration curves using serial dilutions (Figure 1.4).

These calibration curves were used to determine solubility from saturated solutions of methoxy and hydroxy aurones (Table 1.2). As expected, the majority of aurone derivatives had better solubility than the lead compound **IIIC5** (25  $\mu\text{g/mL}$ ).<sup>31</sup> Among the aurones, hydroxyaurones were found to be more soluble than methoxyaurones and a trend of increasing solubility was observed with the increase in the number of hydroxy groups on the phenyl ring. Hydroxyaurone, **HA5** possessing a 2,4,5-trihydroxyphenyl ring, was found to be the most soluble analog, with a solubility of 120.09  $\mu\text{g/mL}$ . A close analog, **HA6**, with a 3,4,5-trihydroxyphenyl ring had the next highest solubility (90.77  $\mu\text{g/mL}$ ). The monohydroxyphenyl analog, **HA2**, showed the lowest solubility (18.93  $\mu\text{g/mL}$ ) among the hydroxyaurones. Methoxyaurones displayed a similar trend of increase in solubility with the increase in number of methoxy groups. The least soluble methoxyaurone was

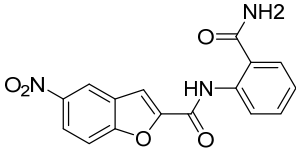
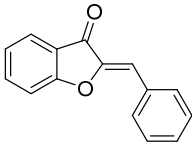
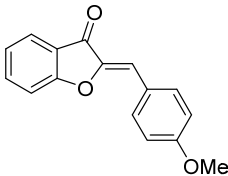
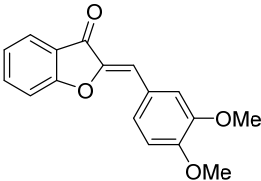
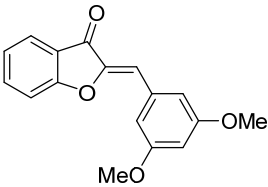
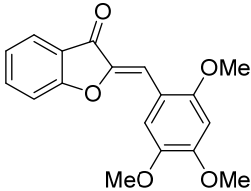
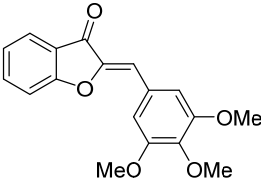


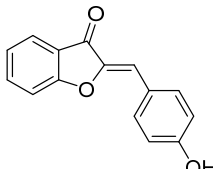
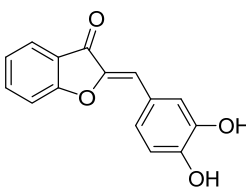
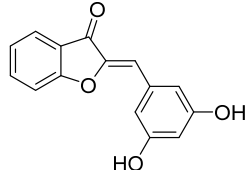
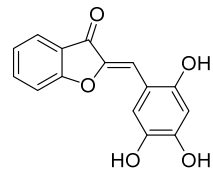
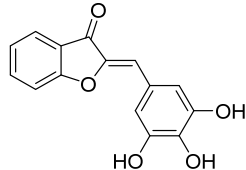
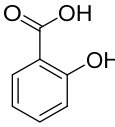
found to be the monomethoxy analog, **MA2** with the solubility of 16.23  $\mu\text{g/mL}$ . Trimethoxy aurone analogs **MA5** and **MA6** were found to be the most soluble methoxyaurone analogs with the solubilities of 42.36  $\mu\text{g/mL}$  and 44.68  $\mu\text{g/mL}$ , respectively. The only exception to this trend was the 3,5-dimethoxy analog, **MA4**, which showed a lower solubility of 18.97  $\mu\text{g/mL}$  compared to 3,4-dimethoxy analog **MA3** (36.26  $\mu\text{g/mL}$ ). The aurone analogs that displayed lower solubilities than **IIIC5**<sup>31</sup> are **MA1**, **MA2**, **MA4** and **HA2**.



**Figure 1.8.** A) UV spectra for methoxyaurones, B) UV spectra for hydroxyaurones, C) Solubility calibration curves for methoxyaurones, D) Solubility calibration curves for hydroxyaurones.

**Table 1.2.** Structure, yield, melting point, and the solubility of the synthesized aurones.

Compd No	Structure	Yield (%)	MP (°C)	Solubility (µg/mL)
G43		NA	250 <sup>a</sup>	10 ± 0.00
MA1		78.8	110-111	8.51 ± 2.00
MA2		92.5	140-142	16.23 ± 0.41
MA3		100.0	157-159	36.26 ± 1.56
MA4		89.0	157-160	18.97 ± 2.33
MA5		99.0	240-242	42.36 ± 2.86
MA6		89.0	182-183	44.68 ± 0.87

HA2		89.8	264-266	18.93 ± 1.41
HA3		92.0	231-233	81.56 ± 2.90
HA4		80.0	250 <sup>a</sup>	76.50 ± 0.57
HA5		83.0	191-193	120.09 ± 1.73
HA6		86.0	256 <sup>a</sup>	90.77 ± 0.48
SA		NA	NA	1880 ± 30

<sup>a</sup>Decomposed, SA = Salicylic acid, *Salicylic acid with previously reported solubility*<sup>93</sup> as 2180 µg/mL was taken as a control for these experiments. UV-Vis spectroscopy method was used to determine the solubility of all aurones in water with 1 % DMSO. Each experiment was repeated three times and solubilities are reported as mean ± standard deviation

## CONCLUSIONS

In conclusion, we designed and synthesized analogs of a previously identified lead biofilm inhibitor, **IIIC5** to improve solubility, retain inhibitory activities, and to facilitate encapsulation into pH-responsive hydrogel microparticles. The newly designed analogs

belong to a class of natural products called aurones. The design of new analogs was supported by docking analysis and physicochemical property calculations/predictions using SwissADME. Eleven aurone analogs of **IIIC5** were synthesized following a synthetic route similar to the biosynthesis of aurones and the solubility of the newly synthesized aurones were determined using standard UV-Vis spectroscopic methods. Among the aurone analogs, hydroxyaurones were found to be more soluble than methoxyaurones and a trend of increasing solubility was observed with the increase in the number of hydroxy groups on the phenyl ring. Hydroxyaurones **HA5** and **HA6** were found to be the most soluble analogs identified, with solubilities of 120.09  $\mu\text{g/mL}$  and 90.77 $\mu\text{g/mL}$ , respectively.

## EXPERIMENTAL SECTION

### General considerations

$^1\text{H}$ -NMR and  $^{13}\text{C}$ -NMR spectra were recorded on Bruker Avance Neo 400 and Avance II 700 spectrometers using TMS or appropriate solvent signals as internal standards. The chemical shift values are given in parts per million (ppm) relative to the internal standard used and the coupling constants ( $J$ ) are given in hertz (Hz). High resolution mass spectra (HRMS) were recorded using Waters AutoSpec-Ultima<sup>TM</sup> NT magnetic sector mass spectrometer with an electron impact (EI) ionization source. The mass analyzer is an electric-magnetic-electric (EBE) sector (a double focusing sector). Anhydrous solvents used for reactions were purchased in Sure-Seal<sup>TM</sup> bottles from MilliporeSigma chemical company. Other chemical reagents were purchased from MilliporeSigma or Fisher chemical companies and used as received. Reactions were

monitored with thin layer chromatography (TLC), which were performed on silica gel plates with fluorescent indicator (Silicycle, silica gel, UV254, 25  $\mu$ m plates). The TLC spots were observed under UV light at wavelengths of 254 nm and 365 nm. The reaction mixtures were purified by column chromatography using Si gel (32-63 $\mu$ m) from Dynamic Absorbent, Inc. Melting points were determined on a Mel-Temp II melting point apparatus and are uncorrected. All tested compounds have  $\geq 95$  % purity, as determined by HPLC. HPLC traces were obtained using Shimadzu SPD-M20A. Solubilities of compounds were determined by UV-Vis spectroscopy method using Agilent Cary 60 UV-Vis spectrophotometer. HPLC analysis of the final compounds were conducted using Kinetex 5  $\mu$ m C18 100 Å, LC Column 150 x 4.6 mm, compound concentration = 3 mM; 20  $\mu$ L injection; solvent: mobile phase buffer; Conditions: 60 % MeCN / 40 % H<sub>2</sub>O / 0.1 % Formic acid (isocratic), HPLC method 0-10 min. Signals were analyzed using a 254 nm UV detector. A chromatogram of Mobile Phase Buffer (20  $\mu$ L) was obtained for comparison. SeeSAR 10.1.0 was used to generate docking model of compounds with the GtfB protein crystal structure. ADME properties were calculated computationally using SwissADME. Solubility data was plotted using GraphPad Prism 9.5.1.

### **General procedure for synthesis of chalcones (3a-f)**

To a solution of the 2-hydroxyacetophenone **1** (1 mmol) and benzaldehyde **2a** (1 mmol) in EtOH (10 mL), an aqueous solution of KOH (40 %, 1 mL) was added, and the reaction mixture was stirred at room temperature for 12 h. TLC examination (30 % EtOAc in hexanes) indicated the completion of the reaction. The reaction mixture was then poured over crushed ice and acidified to pH 2 using 1.0 N HCl. The precipitate formed was filtered, washed with copious amounts of water, and dried to obtain the crude product, which was

purified on column chromatography over Si gel using 10 % EtOAc in hexanes as eluent to afford clean chalcones **3a-f**. All chalcone products were characterized by  $^1\text{H}$  NMR,  $^{13}\text{C}$  NMR and HRMS.

**1-(2-Hydroxyphenyl)-3-phenyl-2-propen-1-one (3a):** 61.9 % yield, yellow solid; mp. 89-90 °C;  $^1\text{H}$  NMR (700 MHz,  $\text{CDCl}_3$ )  $\delta$ : 12.84 (s, 1H), 7.94-7.92 (m, 2H), 7.68-7.66 (m, 3H), 7.52-7.49 (m, 1H), 7.45 (t, 3H,  $J = 3.1$  Hz), 7.04 (d, 1H,  $J = 8.5$  Hz), 6.95 (t, 1H,  $J = 7.6$  Hz);  $^{13}\text{C}$  NMR (700 MHz,  $\text{CDCl}_3$ )  $\delta$ : 193.7, 163.6, 145.5, 136.4, 134.6, 130.9, 129.7, 129.0, 128.7, 120.1, 120.0, 118.9, 118.6; HRMS  $[\text{M}-\text{H}]^-$  calculated for  $\text{C}_{15}\text{H}_{12}\text{O}_2$  223.0759, found 223.0763.

**1-(2-Hydroxyphenyl)-3-(4'-methoxyphenyl)-2-propen-1-one (3b):** 36.5 % yield, yellow solid; mp. 93-95 °C;  $^1\text{H}$  NMR (700 MHz,  $\text{CDCl}_3$ )  $\delta$ : 12.96 (s, 1H), 7.93-7.89 (m, 2H), 7.63 (d, 2H,  $J = 8.6$  Hz), 7.54 (d, 1H,  $J = 15.4$  Hz), 7.49 (t, 1H,  $J = 7.7$  Hz), 7.02 (d, 1H,  $J = 8.3$  Hz), 6.96-6.93 (m, 3H), 3.86 (s, 3H);  $^{13}\text{C}$  NMR (700 MHz,  $\text{CDCl}_3$ )  $\delta$ : 193.7, 163.6, 162.0, 145.4, 136.2, 130.6, 129.5, 127.3, 120.1, 118.8, 118.6, 117.6, 114.5, 55.5; HRMS  $[\text{M}+\text{H}]^+$  calculated for  $\text{C}_{16}\text{H}_{14}\text{O}_3$  255.1021, found 255.1014.

**3-(3',4'-Dimethoxyphenyl)-1-(2-hydroxyphenyl)prop-2-en-1-one (3c):** 53.0 % yield, yellow solid; mp. 115-117 °C;  $^1\text{H}$  NMR (400 MHz,  $\text{CDCl}_3$ )  $\delta$ : 12.94 (s, 1H), 7.94 (dd, 1H,  $J = 8.1, 1.6$  Hz), 7.89 (d, 1H,  $J = 15.4$  Hz), 7.53 (d, 1H,  $J = 15.4$  Hz), 7.52-7.47 (m, 1H), 7.29-7.26 (m, 1H), 7.18 (d, 1H), 7.03 (dd, 1H,  $J = 8.3$  Hz), 6.97-6.91 (m, 2H), 3.97 (s, 3H), 3.95 (s, 3H);  $^{13}\text{C}$  NMR (700 MHz,  $\text{CDCl}_3$ )  $\delta$ : 193.6, 163.6, 151.9, 149.4, 145.8, 136.3, 129.6, 127.7, 123.7, 120.2, 118.8, 118.7, 117.8, 111.2, 110.3, 56.1 (2); HRMS  $[\text{M}-\text{H}]^+$  calculated for  $\text{C}_{17}\text{H}_{16}\text{O}_4$  283.0970, found 283.0969.

**3-(3',5'-Dimethoxyphenyl)-1-(2-hydroxyphenyl)prop-2-en-1-one (3d):** 78.0 % yield, yellow solid; mp. 107-109 °C <sup>1</sup>H NMR (700 MHz, CDCl<sub>3</sub>) δ: 12.80 (s, 1H), 7.90 (d, 1H, *J* = 7.7 Hz), 7.81 (d, 1H, *J* = 15.4 Hz), 7.58 (d, 1H, *J* = 15.4 Hz), 7.49 (t, 1H, *J* = 8.4 Hz), 7.02 (d, 1H, *J* = 8.4 Hz), 6.93 (t, 1H, *J* = 7.7 Hz), 6.77 (d, 2H, *J* = 1.4 Hz), 6.56 (t, 1H, *J* = 1.4 Hz), 3.83 (s, 6H) ; <sup>13</sup>C NMR (700 MHz, CDCl<sub>3</sub>) δ: 193.6, 163.5, 161.0, 145.4, 136.4, 136.4, 129.6, 120.5, 119.9, 118.8, 118.6, 106.5, 103.0, 55.4; HRMS [M-H]<sup>+</sup> calculated for C<sub>17</sub>H<sub>16</sub>O<sub>4</sub> 283.0970, found 283.0969.

**1-(2-Hydroxyphenyl)-3-(2',4',5'-trimethoxyphenyl)prop-2-en-1-one (3e):** 90.0 % yield, orange solid; mp. 135-137 °C; <sup>1</sup>H NMR (700 MHz, CDCl<sub>3</sub>) δ: 13.08 (s, 1H), 8.21 (d, 1H, *J* = 15.4 Hz), 7.91 (dd, 1H, *J* = 7.7, 7.0 Hz), 7.60 (d, 1H, *J* = 15.4 Hz), 7.46 (dd, 1H, *J* = 8.4, 7.0 Hz), 6.99 (d, 1H, *J* = 8.3 Hz), 6.92 (t, 1H, *J* = 7.9 Hz), 6.5 (s, 1H), 3.94 (s, 3H), 3.92 (s, 3H), 3.90 (s, 3H) ; <sup>13</sup>C NMR (700 MHz, CDCl<sub>3</sub>) δ: 194.0, 163.5, 155.1, 152.9, 143.2, 140.9, 135.8, 129.5, 120.2, 118.6, 118.4, 117.7, 115.1, 111.7, 96.6, 56.5, 56.2, 56.0; HRMS calculated for C<sub>18</sub>H<sub>18</sub>O<sub>5</sub> 314.1154, found 314.1151.

**1-(2-Hydroxyphenyl)-3-(3',4',5'-trimethoxyphenyl)prop-2-en-1-one (3f):** 85.4 % yield, yellow solid; mp. 155-157 °C; <sup>1</sup>H NMR (700 MHz, CDCl<sub>3</sub>) δ: 12.86 (s, 1H), 7.92 (d, 1H, *J* = 7.9 Hz), 7.83 (d, 1H, *J* = 15.3 Hz), 7.53 (d, 1H, *J* = 15.3 Hz), 7.49 (t, 1H, *J* = 7.7 Hz), 7.02 (d, 1H, *J* = 8.2 Hz), 6.94 (t, 1H, *J* = 7.5 Hz), 6.87 (s, 2H), 3.93 (s, 6H), 3.91 (s, 3H) ; <sup>13</sup>C NMR (700 MHz, CDCl<sub>3</sub>) δ: 193.5, 163.6, 153.5, 145.6, 140.8, 136.4, 130.0, 129.6, 120.0, 119.2, 118.8, 118.6, 105.9, 61.0, 56.2; HRMS [M-H]<sup>+</sup> calculated for C<sub>18</sub>H<sub>18</sub>O<sub>5</sub> 313.1076, found 313.1082.

### General procedure for synthesis of methoxyaurones (MA1-6)

Chalcones **3a-f** (0.6 mmol) was added to a homogeneous solution of Hg(OAc)<sub>2</sub> (0.221 g, 0.7 mmol) in anhydrous pyridine (20 mL) and the reaction mixture was heated at 110 °C for 12 h. The completion of the reaction was marked by the consumption of starting material and formation of a single product as visualized by TLC (50 % EtOAc in hexanes). The reaction mixture was then quenched with ice and acidified to the pH of 2 by adding 1.0 N HCl. It was extracted in EtOAc (4 × 50 mL), and the combined extract was washed with water (2 × 50 mL), brine (1 × 50 mL), and dried over anhydrous Na<sub>2</sub>SO<sub>4</sub>. The drying agent was filtered off and the filtrate was concentrated *in vacuo* to obtain pure solid products **MA1-6**. All products were characterized by <sup>1</sup>H NMR, <sup>13</sup>C NMR and HRMS as follows.

**2-(Phenylmethylidene)-2,3-dihydro-1-benzofuran-3-one (MA1):** 78.8 % yield, off-white or beige solid; mp. 110-111 °C; <sup>1</sup>H NMR (400 MHz, CDCl<sub>3</sub>) δ: 7.92 (d, 2H, *J* = 7.5 Hz), 7.81 (d, 1H, *J* = 8.4 Hz), 7.66-7.64 (m, 1H), 7.46 (t, 2H, *J* = 7.8 Hz), 7.42-7.40 (m, 1H), 7.34 (d, 1H, *J* = 8.4 Hz), 7.22 (t, 1H, *J* = 7.4 Hz), 6.90 (s, 1H); <sup>13</sup>C NMR (700 MHz, CDCl<sub>3</sub>) δ: 184.8, 166.2, 146.9, 136.9, 132.3, 131.6, 129.9, 128.9, 124.7, 123.5, 121.6, 113.1, 113.0; HRMS [M-H]<sup>+</sup> calculated for C<sub>15</sub>H<sub>10</sub>O<sub>2</sub> 221.0603, found 221.0596.

**2-[(4'-Methoxyphenyl)methylidene]-2,3-dihydro-1-benzofuran-3-one (MA2):** 92.5 % yield, yellow solid; mp. 140-142 °C; <sup>1</sup>H NMR (700 MHz, CDCl<sub>3</sub>) δ: 7.88 (d, 2H, *J* = 8.8 Hz), 7.79 (d, 1H, *J* = 7.6 Hz), 7.64-7.62 (m, 1H), 7.31 (d, 1H, *J* = 8.3 Hz), 7.20 (t, 1H, *J* = 7.5 Hz), 6.97 (d, 2H, *J* = 8.8 Hz), 6.88 (s, 1H), 3.86 (s, 3H); <sup>13</sup>C NMR (700 MHz, CDCl<sub>3</sub>) δ: 184.5, 165.8, 161.1, 145.9, 136.5, 133.4, 125.0, 124.5, 123.3, 121.9, 114.5, 113.4, 112.9, 55.4; HRMS [M-H]<sup>+</sup> calculated for C<sub>16</sub>H<sub>12</sub>O<sub>3</sub> 251.0708, found 251.0701.



**2-[(3',4'-Dimethoxyphenyl)methylidene]-2,3-dihydro-1-benzofuran-3-one**

**(MA3):** quantitative yield, yellow solid; mp. 157-159 °C; <sup>1</sup>H NMR (700 MHz, CDCl<sub>3</sub>) δ: 7.81 (d, 1H, *J* = 7.5 Hz), 7.66-7.63 (m, 1H), 7.54 (d, 1H, *J* = 1.7 Hz), 7.50 (dd, 1H, *J* = 8.4, 1.7 Hz), 7.31 (d, 1H, *J* = 8.3 Hz), 7.22 (t, 1H, *J* = 7.4 Hz), 6.95 (d, 1H, *J* = 8.3 Hz), 6.87 (s, 1H), 3.98 (s, 3H), 3.95 (s, 3H); <sup>13</sup>C NMR (700 MHz, CDCl<sub>3</sub>) δ: 184.5, 165.8, 150.9, 149.1, 146.0, 136.6, 126.1, 125.3, 124.6, 123.4, 122.0, 113.8, 113.7, 112.9, 111.3, 56.0 (2). HRMS [M-H]<sup>-</sup> calculated for C<sub>17</sub>H<sub>14</sub>O<sub>4</sub> 281.0814, found 281.0805.

**2-[(3',5'-Dimethoxyphenyl)methylidene]-2,3-dihydro-1-benzofuran-3-one**

**(MA4):** 89.0 % yield, yellow solid; mp. 157-160 °C; <sup>1</sup>H NMR (400 MHz, CDCl<sub>3</sub>) δ: 7.78 (d, 1H *J* = 7.2 Hz), 7.66-7.62 (m, 1H), 7.30 (d, 1H, *J* = 8.3 Hz), 7.20 (t, 1H, *J* = 7.5 Hz), 7.07 (s, 1H), 7.06 (s, 1H), 6.79 (s, 1H), 6.51 (t, 1H, *J* = 2.2 Hz), 3.84 (s, 6H); <sup>13</sup>C NMR (400 MHz, CDCl<sub>3</sub>) δ: 184.8, 166.2, 160.9, 147.1, 137.1, 133.9, 124.8, 123.6, 121.7, 113.1, 113.0, 109.6, 102.4, 55.6; HRMS [M+H]<sup>+</sup> calculated for C<sub>17</sub>H<sub>14</sub>O<sub>4</sub> 283.0970, found 283.0979.

**2-[(2',4',5'-Trimethoxyphenyl)methylidene]-2,3-dihydro-1-benzofuran-3-one**

**(MA5):** 99.0 % yield, yellow solid; mp. 240-242 °C; <sup>1</sup>H NMR (700 MHz, CDCl<sub>3</sub>) δ: 7.91 (s, 1H), 7.80 (dd, 1H, *J* = 7.6, 7.0 Hz), 7.63-7.61 (m, 1H), 7.46 (s, 1H), 7.28 (d, 1H, *J* = 8.2 Hz), 7.20 (t, 1H, *J* = 7.6 Hz), 6.51 (s, 1H), 3.96 (s, 3H), 3.95 (s, 3H), 3.90 (s, 3H); <sup>13</sup>C NMR (700 MHz, CDCl<sub>3</sub>) δ: 184.3, 165.4, 155.3, 152.4, 145.7, 143.2, 136.2, 124.5, 123.2, 122.2, 114.5, 113.1, 112.8, 108.0, 96.3, 56.6, 56.4, 56.0; HRMS calculated for C<sub>18</sub>H<sub>16</sub>O<sub>5</sub> 312.0998, found 312.0998.

**2-[(3',4',5'-Trimethoxyphenyl)methylidene]-2,3-dihydro-1-benzofuran-3-one**

**(MA6):** 89.0 %, yellow solid; mp. 182-183 °C; <sup>1</sup>H NMR (700 MHz, CDCl<sub>3</sub>) δ: 7.82 (d,

1H,  $J = 7.2$  Hz), 7.68-7.63 (m, 1H), 7.31 (d, 1H,  $J = 8.3$  Hz), 7.24 (t, 1H,  $J = 7.4$  Hz), 7.19 (s, 2H), 6.84 (s, 1H), 3.95 (s, 6H), 3.93 (s, 3H);  $^{13}\text{C}$  NMR (700 MHz,  $\text{CDCl}_3$ )  $\delta$ : 184.5, 165.9, 153.3, 146.4, 140.1, 136.8, 127.7, 124.7, 123.5, 121.7, 113.4, 112.9, 108.9, 61.0, 56.2; HRMS  $[\text{M}+\text{H}]^+$  calculated for  $\text{C}_{18}\text{H}_{16}\text{O}_5$  313.1076, found 313.1082

### General procedure for synthesis of hydroxyaurones (HA2-6)

The methoxyaurone **MA2-6** (0.25 mmol, 1.0 eq) was dissolved in anhydrous  $\text{CH}_2\text{Cl}_2$  (15 mL) and cooled down to 0 °C.  $\text{BBr}_3$  (1 mmol, 4.0 eq) was added slowly to the reaction mixture under  $\text{N}_2$  atmosphere and stirred. The reaction mixture was allowed to attain room temperature and stirring continued for 12 h. TLC examination (50 % EtOAc in hexanes) revealed the completion of the reaction. The reaction mixture was then cooled to 0 °C and carefully quenched with slow drop-wise addition of water until the excess  $\text{BBr}_3$  reacted completely. The precipitated solid product was filtered, washed with water, and dried over  $\text{CaCl}_2$  in a vacuum desiccator. The crude product thus obtained was purified by column chromatography over Si gel using 10 % MeOH in  $\text{CH}_2\text{Cl}_2$  to afford pure hydroxyaurones **HA2-6**. All hydroxyaurones were characterized by  $^1\text{H}$  NMR,  $^{13}\text{C}$  NMR and HRMS.

#### 2-[(4'-Hydroxyphenyl)methylidene]-2,3-dihydro-1-benzofuran-3-one (HA2):

89.8% yield, yellow solid; mp. 264-266 °C;  $^1\text{H}$  NMR (700 MHz,  $\text{DMSO}-d_6$ )  $\delta$ : 10.23 (s, 1H), 7.88 (d, 2H,  $J = 8.4$  Hz), 7.79-7.77 (m, 2H), 7.54 (d, 1H,  $J = 8.6$  Hz), 7.30 (t, 1H,  $J = 7.4$  Hz), 6.91 (d, 3H,  $J = 8.8$  Hz);  $^{13}\text{C}$  NMR (700 MHz,  $\text{DMSO}-d_6$ )  $\delta$ : 183.2, 165.0, 159.8, 144.7, 137.2, 133.8, 124.1, 123.7, 122.9, 121.3, 116.2, 113.5, 113.2; HRMS  $[\text{M}+\text{H}]^+$  calculated for  $\text{C}_{15}\text{H}_{10}\text{O}_3$  239.0708, found 239.0718.

**2-[(3',4'-Dihydroxyphenyl)methylidene]-2,3-dihydro-1-benzofuran-3-one**

**(HA3):** 92.0 % yield, yellow solid; mp. 231-233 °C; <sup>1</sup>H NMR (400 MHz, DMSO-d<sub>6</sub>) δ: 9.82 (bs, 1H), 9.34 (bs, 1H), 7.80-7.76 (m, 2H), 7.53-7.50 (m, 2H), 7.34-7.28 (m, 2H), 6.86 (d, 1H), 6.82 (s, 1H); <sup>13</sup>C NMR (700 MHz, DMSO-d<sub>6</sub>) δ: 183.1, 165.0, 148.6, 145.7, 144.7, 137.1, 125.2, 124.1, 123.7, 123.3, 121.4, 118.3 (d), 116.1 (d), 114.0 (d), 113.0; HRMS [M+H]<sup>+</sup> calculated for C<sub>15</sub>H<sub>10</sub>O<sub>4</sub> 255.0657, found 255.0660.

**2-[(3',5'-Dihydroxyphenyl)methylidene]-2,3-dihydro-1-benzofuran-3-one**

**(HA4):** 80.0 % yield, grey solid; decomposed at 250 °C; <sup>1</sup>H NMR (700 MHz, DMSO- d<sub>6</sub>) δ: 7.79 (t, 2H, *J* = 7.4 Hz), 7.50 (d, 1H, *J* = 8.6 Hz), 7.30 (t, 1H, *J* = 7.3 Hz), 6.88 (d, 2H, *J* = 2.3 Hz), 6.73 (s, 1H), 6.36 (t, 1H, *J* = 2.0 Hz) ; <sup>13</sup>C NMR (700 MHz, DMSO-d<sub>6</sub>) δ: 183.7, 165.4, 158.7, 146.2, 137.8, 133.2, 124.4, 124.0, 121.0, 113.1, 113.1, 109.7, 105.0; HRMS [M-H]<sup>-</sup> calculated for C<sub>15</sub>H<sub>10</sub>O<sub>4</sub> 253.0501, found 253.0513.

**2-[(2',4',5'-Trihydroxyphenyl)methylidene]-2,3-dihydro-1-benzofuran-3-one**

**(HA5):** 83.0 % yield, red solid; mp. 191-193 °C; <sup>1</sup>H NMR (400 MHz, Acetone-d<sub>6</sub>) δ: 8.94 (s, 1H), 8.71 (s, 1H), 7.97 (s, 1H), 7.85 (s, 1H), 7.71-7.76 (m, 2H), 7.43 (d, 1H, *J* = 8.2 Hz), 7.40 (s, 1H), 7.28 (t, 1H, *J* = 7.4 Hz), 6.57 (s, 1H); <sup>13</sup>C NMR (400 MHz, Acetone-d<sub>6</sub>) δ: 183.9, 166.1, 153.8, 150.7, 145.6, 139.7, 137.2, 124.7, 124.1, 123.0, 117.7, 113.7, 111.6, 108.9, 103.7; HRMS calculated for C<sub>15</sub>H<sub>10</sub>O<sub>5</sub> 270.0528, found 270.0529.

**2-[(3',4',5'-Trihydroxyphenyl)methylidene]-2,3-dihydro-1-benzofuran-3-one**

**(HA6):** 86.0 % yield, greenish-yellow solid; decomposed at 256 °C; <sup>1</sup>H NMR (700 MHz, DMSO- d<sub>6</sub>) δ: 9.28 (s, 2H), 9.05 (s, 1H), 7.78-7.76 (m, 2H), 7.48 (d, 1H, *J* = 8.5 Hz), 7.28 (dd, 1H, *J* = 14.8, 7.3 Hz), 7.03 (s, 2H), 6.72 (s, 1H) ; <sup>13</sup>C NMR (700 MHz, DMSO-d<sub>6</sub>) δ:

183.0, 164.9, 146.2, 144.8, 137.1, 137.0, 124.2, 123.7, 122.0, 121.4, 114.5, 113.0, 111.3;  
HRMS [M-H]<sup>-</sup> calculated for C<sub>15</sub>H<sub>10</sub>O<sub>5</sub> 269.0450, found 269.0445.

### **Determination of solubility**

Solubility of aurone library was determined using reported spectroscopic method<sup>92</sup>. First,  $\lambda_{\text{max}}$  for each aurone compounds was determined by obtaining UV-Vis spectrum across wavelengths 200-800 nm at 100  $\mu\text{M}$  concentration in 1 % DMSO-water. To obtain calibration curves, several dilutions of each compound were made in 1 % DMSO-water and absorbances at their  $\lambda_{\text{max}}$  were read using Agilent Cary 60 UV-Vis spectrophotometer. Absorbance versus concentration plots produced equation of solubility calibration curves for each aurone which were used to determine concentrations of saturated solutions. Saturated solutions were prepared by dissolving the compound in water containing 1 % DMSO and vortexing for 10 minutes and centrifuging out any undissolved compound at 6500 rpm, the saturated supernatant were used for the solubility measurements. From absorbances of these saturated solutions, solubility was determined using solubility calibration curve equations. In some cases, dilution factors were used for the saturated solutions to keep the concentration within the range of calibration curve to maintain accuracy. Experiments were repeated in triplicate for each compound and standard deviations were reported.

### **ACKNOWLEDGEMENTS**

The research work described in this chapter was supported by the NIH grants R21CA22649 (Velu), R21DE028349 (Velu), R03DE025058 (Velu), and University of Alabama at Birmingham Microbiome Center Pilot Grant (Velu). Graduate student

Teaching Assistantship (Ahirwar) from the Department of Chemistry, University of Alabama at Birmingham is highly appreciated.

## REFERENCES

- (1) Marsh, P. D. Dental Plaque as a Microbial Biofilm. *Caries Res.* **2004**, 38 (3), 204-211
- (2) Vos, T.; Allen, C.; Arora, M.; Barber, R. M.; Bhutta, Z. A.; Brown, A.; Carter, A.; Casey, D. C.; Charlson, F. J.; Chen, A. Z.; et al. Global, regional, and national incidence, prevalence, and years lived with disability for 310 diseases and injuries, 1990-2015: a systematic analysis for the Global Burden of Disease Study 2015. *Lancet* **2016**, 388 (10053), 1545-1602
- (3) Hamada, S.; Slade, H. D. Biology, immunology, and cariogenicity of *Streptococcus mutans*. *Microbiol. Rev.* **1980**, 44 (2), 331-384
- (4) Kim, J. K.; Baker, L. A.; Davarian, S.; Crimmins, E. Oral health problems and mortality. *J. Dent. Sci.* **2013**, 8 (2), 115-120
- (5) Kuramitsu, H. K.; He, X. S.; Lux, R.; Anderson, M. H.; Shi, W. Y. Interspecies interactions within oral microbial communities. *Microbiol. Mol. Biol. Rev.* **2007**, 71 (4), 653-670
- (6) Kolenbrander, P. E.; Palmer, R. J.; Periasamy, S.; Jakubovics, N. S. Oral multispecies biofilm development and the key role of cell-cell distance. *Nat. Rev. Microbiol.* **2010**, 8 (7), 471-480
- (7) Kolenbrander, P. E.; Andersen, R. N.; Blehert, D. S.; Egland, P. G.; Foster, J. S.; Palmer, R. J., Jr. Communication among oral bacteria. *Microbiol. Mol. Biol. Rev.* **2002**, 66 (3), 486-505, table of contents
- (8) Loesche, W. J. Role of *Streptococcus mutans* in human dental decay. *Microbiol. Rev.* **1986**, 50 (4), 353-380
- (9) Quivey, R. G., Jr.; Kuhnert, W. L.; Hahn, K. Adaptation of oral streptococci to low pH. *Adv. Microb. Physiol.* **2000**, 42, 239-274
- (10) Moore, B. W.; Carter, W. J.; Dunn, J. K.; Fosdick, L. S. The Formation of Lactic Acid in Dental Plaques: I. Caries-Active Individuals. *J. Dent. Res.* **1956**, 35 (5), 778-785
- (11) Matsumoto-Nakano, M. Role of *Streptococcus mutans* surface proteins for biofilm formation. *Jpn. Dent. Sci. Rev.* **2018**, 54 (1), 22-29
- (12) Tamesada, M.; Kawabata, S.; Fujiwara, T.; Hamada, S. Synergistic effects of streptococcal glucosyltransferases on adhesive biofilm formation. *J. Dent. Res.* **2004**, 83 (11), 874-879
- (13) Koo, H.; Xiao, J.; Klein, M.; Jeon, J. Exopolysaccharides produced by *Streptococcus mutans* glucosyltransferases modulate the establishment of microcolonies within multispecies biofilms. *Am. Soc. Microbiol.* 2010.

- (14) Xiao, J.; Koo, H. Structural organization and dynamics of exopolysaccharide matrix and microcolonies formation by *Streptococcus mutans* in biofilms. *J. Appl. Microbiol.* **2010**, *108* (6), 2103-2113
- (15) Larson, M. R.; Rajashankar, K. R.; Crowley, P. J.; Kelly, C.; Mitchell, T. J.; Brady, L. J.; Deivanayagam, C. Crystal structure of the C-terminal region of *Streptococcus mutans* antigen I/II and characterization of salivary agglutinin adherence domains. *J. Biol. Chem.* **2011**, *286* (24), 21657-21666
- (16) Jakubovics, N. S.; Strömberg, N.; van Dolleweerd, C. J.; Kelly, C. G.; Jenkinson, H. F. Differential binding specificities of oral streptococcal antigen I/II family adhesins for human or bacterial ligands. *Mol. Microbiol.* **2005**, *55* (5), 1591-1605
- (17) Brady, L. J.; Maddocks, S. E.; Larson, M. R.; Forsgren, N.; Persson, K.; Deivanayagam, C. C.; Jenkinson, H. F. The changing faces of *Streptococcus* antigen I/II polypeptide family adhesins. *Mol. Microbiol.* **2010**, *77* (2), 276-286
- (18) Yamashita, Y.; Bowen, W. H.; Burne, R. A.; Kuramitsu, H. K. Role of the *Streptococcus mutans* gtf genes in caries induction in the specific-pathogen-free rat model. *Infect. Immun.* **1993**, *61* (9), 3811-3817
- (19) Ooshima, T.; Matsumura, M.; Hoshino, T.; Kawabata, S.; Sobue, S.; Fujiwara, T. Contributions of three glycosyltransferases to sucrose-dependent adherence of *Streptococcus mutans*. *J. Dent. Res.* **2001**, *80* (7), 1672-1677
- (20) Aoki, H.; Shiroza, T.; Hayakawa, M.; Sato, S.; Kuramitsu, H. K. Cloning of a *Streptococcus mutans* glucosyltransferase gene coding for insoluble glucan synthesis. *Infect. Immun.* **1986**, *53* (3), 587-594
- (21) Hanada, N.; Kuramitsu, H. K. Isolation and characterization of the *Streptococcus mutans* gtfC gene, coding for synthesis of both soluble and insoluble glucans. *Infect. Immun.* **1988**, *56* (8), 1999-2005
- (22) Hanada, N.; Kuramitsu, H. K. Isolation and characterization of the *Streptococcus mutans* gtfD gene, coding for primer-dependent soluble glucan synthesis. *Infect. Immun.* **1989**, *57* (7), 2079-2085
- (23) Banas, J. A.; Vickerman, M. M. Glucan-binding proteins of the oral streptococci. *Crit. Rev. Oral. Biol. Med.* **2003**, *14* (2), 89-99
- (24) Overman, P. R. Biofilm: a new view of plaque. *J. Contemp. Dent. Pract.* **2000**, *1* (3), 18-29
- (25) Melo, P.; Fine, C.; Malone, S.; Taylor, S. Impact of the Brush Day & Night Programme on Well-Being, Plaque, and Dental Caries in Children. *Int. Dent. J.* **2021**, *71*, S15-S30
- (26) Horst, J. A.; Tanzer, J. M.; Milgrom, P. M. Fluorides and Other Preventive Strategies for Tooth Decay. *Dent. Clin. N. Am.* **2018**, *62* (2), 207-234

- (27) Walsh, T.; Oliveira-Neto, J. M.; Moore, D. Chlorhexidine treatment for the prevention of dental caries in children and adolescents. *Cochrane Database Syst. Rev.* **2015**, (4), Cd008457
- (28) Yang, S.-J.; Han, S.-H.; Lee, A.-R.; Jun, J.-H.; Son, M.-W.; Oh, S.-H.; Kim, J.; Paik, S.-Y. Evaluation of antimicrobial effects of commercial mouthwashes utilized in South Korea. *BMB Rep.* **2015**, 48 (1), 42-47
- (29) Ferrazzano, G. F.; Amato, I.; Ingenito, A.; De Natale, A.; Pollio, A. Anti-cariogenic effects of polyphenols from plant stimulant beverages (cocoa, coffee, tea). *Fitoterapia* **2009**, 80 (5), 255-262
- (30) Tang, Z. S.; Zhu, M.; Liu, Z. Susceptibility of *Streptococcus mutans* biofilm to antimicrobial agents. *Zhonghua Kou. Qiang. Yi Xue. Za Zhi* **2006**, 41 (5), 266-268
- (31) Nijampatnam, B.; Ahirwar, P.; Pukkanasut, P.; Womack, H.; Casals, L.; Zhang, H.; Cai, X.; Michalek, S. M.; Wu, H.; Velu, S. E. Discovery of Potent Inhibitors of *Streptococcus mutans* Biofilm with Antivirulence Activity. *ACS Med. Chem. Lett.* **2021**, 12 (1), 48-55
- (32) Nijampatnam, B.; Casals, L.; Zheng, R.; Wu, H.; Velu, S. E. Hydroxychalcone inhibitors of *Streptococcus mutans* glucosyl transferases and biofilms as potential anticaries agents. *Bioorg. Med. Chem. Lett.* **2016**, 26 (15), 3508-3513
- (33) Nijampatnam, B.; Zhang, H.; Cai, X.; Michalek, S. M.; Wu, H.; Velu, S. E. Inhibition of *Streptococcus mutans* Biofilms by the Natural Stilbene Piceatannol Through the Inhibition of Glucosyltransferases. *ACS Omega* **2018**, 3 (7), 8378-8385
- (34) Zhang, Q.; Nijampatnam, B.; Hua, Z.; Nguyen, T.; Zou, J.; Cai, X.; Michalek, S. M.; Velu, S. E.; Wu, H. Structure-Based Discovery of Small Molecule Inhibitors of Cariogenic Virulence. *Sci. Rep.* **2017**, 7 (1), 5974
- (35) Geissman, T. A.; Heaton, C. D. Anthochlor Pigments. IV. The Pigments of *Coreopsis grandiflora*, Nutt. I. *Journal of the American Chemical Society* **1943**, 65 (4), 677-683
- (36) Geissman, T. A. Anthochlor Pigments. The Pigment of *Coreopsis Douglasii*. *Journal of the American Chemical Society* **1941**, 63 (3), 656-658
- (37) Bate-Smith, E. C.; Geissman, T. A. Benzalcoumaranones. *Nature* **1951**, 167 (4252), 688-688
- (38) Asen, S.; Norris, K. H.; Stewart, R. N. Copigmentation of aurone and flavone from petals of *Antirrhinum majus*. *Phytochem.* **1972**, 11 (9), 2739-2741
- (39) Schwarz-Sommer, Z.; Davies, B.; Hudson, A. An everlasting pioneer: the story of *Antirrhinum* research. *Nat. Rev. Genet.* **2003**, 4 (8), 657-666
- (40) Boucherle, B.; Peuchmaur, M.; Boumendjel, A.; Haudecoeur, R. Occurrences, biosynthesis and properties of aurones as high-end evolutionary products. *Phytochem.* **2017**, 142, 92-111



- (41) Kaintz, C.; Molitor, C.; Thill, J.; Kampatsikas, I.; Michael, C.; Halbwirth, H.; Rompel, A. Cloning and functional expression in *E. coli* of a polyphenol oxidase transcript from *Coreopsis grandiflora* involved in aurone formation. *Febs Lett.* **2014**, 588 (18), 3417-3426
- (42) Nakayama, T.; Yonekura-Sakakibara, K.; Sato, T.; Kikuchi, S.; Fukui, Y.; Fukuchi-Mizutani, M.; Ueda, T.; Nakao, M.; Tanaka, Y.; Kusumi, T. Aureusidin synthase: a polyphenol oxidase homolog responsible for flower coloration. *Science* **2000**, 290 (5494), 1163-1166
- (43) Nakayama, T.; Sato, T.; Fukui, Y.; Yonekura-Sakakibara, K.; Hayashi, H.; Tanaka, Y.; Kusumi, T.; Nishino, T. Specificity analysis and mechanism of aurone synthesis catalyzed by aureusidin synthase, a polyphenol oxidase homolog responsible for flower coloration. *FEBS lett.* **2001**, 499 (1-2), 107-111
- (44) Farag, M. A.; Deavours, B. E.; de Fátima, Â.; Naoumkina, M.; Dixon, R. A.; Sumner, L. W. Integrated metabolite and transcript profiling identify a biosynthetic mechanism for hispidol in *Medicago truncatula* cell cultures. *Plant Physiol.* **2009**, 151 (3), 1096-1113
- (45) Varma, R. S.; Varma, M. Alumina-mediated condensation. A simple synthesis of aurones. *Tetrahedron Lett.* **1992**, 33 (40), 5937-5940
- (46) Venkateswarlu, S.; Murty, G. N.; Satyanarayana, M. "On water" synthesis of aurones: first synthesis of 4,5,3',4',5'-pentamethoxy-6-hydroxyaurone from *Smilax riparia*. *ARKIVOC* **2017**, 2017 (4), 303-314
- (47) Narsinghani, T.; Sharma, M. C.; Bhargav, S. Synthesis, docking studies and antioxidant activity of some chalcone and aurone derivatives. *Med. Chem. Res.* **2013**, 22 (9), 4059-4068
- (48) Regenass, P.; Abboud, D.; Daubeuf, F.; Lehalle, C.; Gizzi, P.; Riché, S.; Hachet-Haas, M.; Rohmer, F.; Gasparik, V.; Boeglin, D.; et al. Discovery of a Locally and Orally Active CXCL12 Neutraligand (LIT-927) with Anti-inflammatory Effect in a Murine Model of Allergic Airway Hypereosinophilia. *J. Med. Chem.* **2018**, 61 (17), 7671-7686
- (49) Harkat, H.; Blanc, A.; Weibel, J.-M.; Pale, P. Versatile and Expeditious Synthesis of Aurones via AuI-Catalyzed Cyclization. *J. Org. Chem.* **2008**, 73 (4), 1620-1623
- (50) Lazinski, L. M.; Royal, G.; Robin, M.; Maresca, M.; Haudecoeur, R. Bioactive Aurones, Indanones, and Other Hemiindigoid Scaffolds: Medicinal Chemistry and Photopharmacology Perspectives. *J. Med. Chem.* **2022**, 65 (19), 12594-12625
- (51) Kaur, R.; Kaur, G.; Gill, R. K.; Soni, R.; Bariwal, J. Recent developments in tubulin polymerization inhibitors: An overview. *Eur. J. Med. Chem.* **2014**, 87, 89-124
- (52) Lewin, G.; Aubert, G.; Thoret, S.; Dubois, J.; Cresteil, T. Influence of the skeleton on the cytotoxicity of flavonoids. *Bioorg. Med. Chem.* **2012**, 20 (3), 1231-1239
- (53) Patel, M. R.; Bhatt, A.; Steffen, J. D.; Chergui, A.; Murai, J.; Pommier, Y.; Pascal, J. M.; Trombetta, L. D.; Fronczek, F. R.; Talele, T. T. Discovery and Structure–

- Activity Relationship of Novel 2, 3-Dihydrobenzofuran-7-carboxamide and 2, 3-Dihydrobenzofuran-3 (2 H)-one-7-carboxamide Derivatives as Poly (ADP-ribose) polymerase-1 Inhibitors. *J. Med. Chem.* **2014**, 57 (13), 5579-5601
- (54) Radhakrishnan, S.; Shimmon, R.; Conn, C.; Baker, A. Inhibitory kinetics of novel 2, 3-dihydro-1H-inden-1-one chalcone-like derivatives on mushroom tyrosinase. *Bioorg. Med. Chem.* **2015**, 25 (23), 5495-5499
- (55) Choi, H.; Ryu, I. Y.; Choi, I.; Ullah, S.; Jung, H. J.; Park, Y.; Hwang, Y.; Jeong, Y.; Hong, S.; Chun, P. Identification of (Z)-2-benzylidene-dihydroimidazothiazolone derivatives as tyrosinase inhibitors: Anti-melanogenic effects and in silico studies. *Computational and Structural Biotechnology Journal* **2022**, 20, 899-912
- (56) Tsuganezawa, K.; Watanabe, H.; Parker, L.; Yuki, H.; Taruya, S.; Nakagawa, Y.; Kamei, D.; Mori, M.; Ogawa, N.; Tomabechei, Y. A novel Pim-1 kinase inhibitor targeting residues that bind the substrate peptide. *J. Mol. Biol.* **2012**, 417 (3), 240-252
- (57) Parker, L. J.; Watanabe, H.; Tsuganezawa, K.; Tomabechei, Y.; Handa, N.; Shirouzu, M.; Yuki, H.; Honma, T.; Ogawa, N.; Nagano, T. Flexibility of the P-loop of Pim-1 kinase: observation of a novel conformation induced by interaction with an inhibitor. *Acta Crystallogr. F: Struct. Biol.* **2012**, 68 (8), 860-866
- (58) Qhobosheane, M. A.; Beteck, R. M.; Baratte, B.; Robert, T.; Ruchaud, S.; Bach, S.; Legoabe, L. J. Exploration of 7-azaindole-coumaranone hybrids and their analogues as protein kinase inhibitors. *Chem. Biol. Interact.* **2021**, 343, 109478
- (59) Park, H. S.; Nelson, D. E.; Taylor, Z. E.; Hayes, J. B.; Cunningham, K. D.; Arivett, B. A.; Ghosh, R.; Wolf, L. C.; Taylor, K. M.; Farone, M. B. Suppression of LPS-induced NF- $\kappa$ B activity in macrophages by the synthetic aurone, (Z)-2-((5-(hydroxymethyl) furan-2-yl) methylene) benzofuran-3 (2H)-one. *Int. Immun.* **2017**, 43, 116-128
- (60) Ren, J.; Su, D.; Li, L.; Cai, H.; Zhang, M.; Zhai, J.; Li, M.; Wu, X.; Hu, K. Anti-inflammatory effects of Aureusidin in LPS-stimulated RAW264. 7 macrophages via suppressing NF- $\kappa$ B and activating ROS-and MAPKs-dependent Nrf2/HO-1 signaling pathways. *Toxicol. Appl. Pharmacol.* **2020**, 387, 114846
- (61) Chen, Y.; Yang, M.; Wang, Z.-J. (Z)-7, 4'-Dimethoxy-6-hydroxy-aurone-4-O- $\beta$ -glucopyranoside mitigates retinal degeneration in Rd10 mouse model through inhibiting oxidative stress and inflammatory responses. *Cutan. Ocul. Toxicol.* **2020**, 39 (1), 36-42
- (62) Wang, S.; Xu, L.; Lu, Y.-T.; Liu, Y.-F.; Han, B.; Liu, T.; Tang, J.; Li, J.; Wu, J.; Li, J.-Y. Discovery of benzofuran-3 (2H)-one derivatives as novel DRAK2 inhibitors that protect islet  $\beta$ -cells from apoptosis. *Eur. J. Med. Chem.* **2017**, 130, 195-208
- (63) Sun, H.; Ding, W.; Song, X.; Wang, D.; Chen, M.; Wang, K.; Zhang, Y.; Yuan, P.; Ma, Y.; Wang, R. Synthesis of 6-hydroxyaurone analogues and evaluation of their  $\alpha$ -glucosidase inhibitory and glucose consumption-promoting activity: development

- of highly active 5, 6-disubstituted derivatives. *Bioorg. Med. Chem. Lett.* **2017**, *27* (15), 3226-3230
- (64) Lamichhane, R.; Kim, S.-G.; Kang, S.; Lee, K.-H.; Pandeya, P. R.; Jung, H.-J. Exploration of underlying mechanism of anti-adipogenic activity of sulfuretin. *Biol. Pharm. Bull.* **2017**, *40* (9), 1366-1373
  - (65) Roh, K.; Kim, S.; Kang, H.; Ku, J.-M.; Park, K. W.; Lee, S. Sulfuretin has therapeutic activity against acquired lymphedema by reducing adipogenesis. *Pharmacol. Res.* **2017**, *121*, 230-239
  - (66) Ashok, D.; Ziauddin, M.; Lakshmi, B. V.; Sarasija, M. Microwave assisted synthesis of substituted (Z)-2-{[1-phenyl-3-(thiophen-2-yl)-1 H-pyrazol-4-yl] methylene} benzofuran-3 (2 H)-ones and their antimicrobial activity. *Russ. J. Gen. Chem.* **2016**, *86*, 1753-1757
  - (67) Reynolds, R. C.; Ananthan, S.; Faaleolea, E.; Hobrath, J. V.; Kwong, C. D.; Maddox, C.; Rasmussen, L.; Sosa, M. I.; Thammasuvimol, E.; White, E. L. High throughput screening of a library based on kinase inhibitor scaffolds against *Mycobacterium tuberculosis* H37Rv. *Tuberculosis* **2012**, *92* (1), 72-83
  - (68) Sutton, C. L.; Taylor, Z. E.; Farone, M. B.; Handy, S. T. Antifungal activity of substituted aurones. *Bioorg. Med. Chem. Lett.* **2017**, *27* (4), 901-903
  - (69) Fedorova, O.; Jagdmann Jr, G. E.; Adams, R. L.; Yuan, L.; Van Zandt, M. C.; Pyle, A. M. Small molecules that target group II introns are potent antifungal agents. *Nat. Chem. Biol.* **2018**, *14* (12), 1073-1078
  - (70) Sharma, M. C.; Sharma, S.; Sharma, P.; Kumar, A. Pharmacophore and QSAR modeling of some structurally diverse azaaurones derivatives as anti-malarial activity. *Med. Chem. Res.* **2014**, *23*, 181-198
  - (71) Silva Torres, D.; Alves de Oliveira, B.; Souza d Silveira, L.; Paulo da Silva, M.; Rodrigues Duraes Pereira, V.; Moraes, J.; Rubia Costa Couri, M.; Fortini Grenfell e Queiroz, R.; Martins Parreiras, P.; Roberto Silva, M. Synthetic aurones: New features for *Schistosoma mansoni* therapy. *Chem. Biodivers.* **2021**, *18* (11), e2100439
  - (72) Chintakrindi, A. S.; Gohil, D. J.; Chowdhary, A. S.; Kanyalkar, M. A. Design, synthesis and biological evaluation of substituted flavones and aurones as potential anti-influenza agents. *Bioorg. Med. Chem.* **2020**, *28* (1), 115191
  - (73) Meguellati, A.; Ahmed-Belkacem, A.; Nurisso, A.; Yi, W.; Brillet, R.; Berqouch, N.; Chavoutier, L.; Fortuné, A.; Pawlotsky, J.-M.; Boumendjel, A. New pseudodimeric aurones as palm pocket inhibitors of Hepatitis C virus RNA-dependent RNA polymerase. *Eur. J. Med. Chem.* **2016**, *115*, 217-229
  - (74) Nijampatnam, B.; Ahirwar, P.; Pukkanasut, P.; Womack, H.; Casals, L.; Zhang, H.; Cai, X.; Michalek, S. M.; Wu, H.; Velu, S. E. Discovery of Potent Inhibitors of *Streptococcus mutans* Biofilm with Antivirulence Activity. *ACS Med. Chem. Lett.* **2021**, *12* (1), 48-55

- (75) Lawrence, N. J.; Rennison, D.; McGown, A. T.; Hadfield, J. A. The Total Synthesis of an Aurone Isolated from *Uvaria hamiltonii*: Aurones and Flavones as Anticancer Agents. *Bioorg. Med. Chem. Lett.* **2003**, *13* (21), 3759-3763
- (76) Ono, E.; Fukuchi-Mizutani, M.; Nakamura, N.; Fukui, Y.; Yonekura-Sakakibara, K.; Yamaguchi, M.; Nakayama, T.; Tanaka, T.; Kusumi, T.; Tanaka, Y. Yellow Flowers Generated by Expression of the Aurone Biosynthetic Pathway. *Proc. Natl. Acad. Sci.* **2006**, *103* (29), 11075-11080
- (77) Balsera, B.; Mulet, J.; Fernández-Carvajal, A.; Torre-Martínez, R. d. I.; Ferrer-Montiel, A.; Hernández-Jiménez, J. G.; Estévez-Herrera, J.; Borges, R.; Freitas, A. E.; López, M. G.; et al. Chalcones as Positive Allosteric Modulators of  $\alpha 7$  Nicotinic Acetylcholine Receptors: A New Target for a Privileged Structure. *Eur. J. Med. Chem.* **2014**, *86*, 724-739
- (78) Daina, A.; Michielin, O.; Zoete, V. SwissADME: a free web tool to evaluate pharmacokinetics, drug-likeness and medicinal chemistry friendliness of small molecules. *Sci. Rep.* **2017**, *7* (1), 42717
- (79) Lipinski, C. A.; Lombardo, F.; Dominy, B. W.; Feeney, P. J. Experimental and computational approaches to estimate solubility and permeability in drug discovery and development. *Adv. Drug Deliv. Rev.* **2001**, *46* (1), 3-26
- (80) Arnott, J. A.; Planey, S. L. The influence of lipophilicity in drug discovery and design. *Expert Opin. Drug Discov.* **2012**, *7* (10), 863-875
- (81) Savjani, K. T.; Gajjar, A. K.; Savjani, J. K. Drug solubility: importance and enhancement techniques. *ISRN Pharm.* **2012**, *2012*, 195727
- (82) Ottaviani, G.; Gosling, D. J.; Patissier, C.; Rodde, S.; Zhou, L.; Faller, B. What is modulating solubility in simulated intestinal fluids? *Eur. J. Pharm. Sci.* **2010**, *41* (3-4), 452-457
- (83) Ritchie, T. J.; Macdonald, S. J. F.; Peace, S.; Pickett, S. D.; Luscombe, C. N. Increasing small molecule drug developability in sub-optimal chemical space. *Med. Chem. Comm.* **2013**, *4* (4), 673-680
- (84) Daina, A.; Michielin, O.; Zoete, V. iLOGP: a simple, robust, and efficient description of n-octanol/water partition coefficient for drug design using the GB/SA approach. *J. Chem. Inf. Model.* **2014**, *54* (12), 3284-3301
- (85) Cheng, T.; Zhao, Y.; Li, X.; Lin, F.; Xu, Y.; Zhang, X.; Li, Y.; Wang, R.; Lai, L. Computation of Octanol–Water Partition Coefficients by Guiding an Additive Model with Knowledge. *J. Chem. Inf.* **2007**, *47* (6), 2140-2148
- (86) Wildman, S. A.; Crippen, G. M. Prediction of Physicochemical Parameters by Atomic Contributions. *J. Chem. Inf. Comput.* **1999**, *39* (5), 868-873
- (87) Moriguchi, I.; Hirano, S.; Liu, Q.; Nakagome, I.; Matsushita, Y. Simple Method of Calculating Octanol/Water Partition Coefficient. *Chem. Pharm. Bull.* **1992**, *40* (1), 127-130

- (88) Moriguchi, I.; Hirono, S.; Nakagome, I.; Hirano, H. Comparison of Reliability of log P Values for Drugs Calculated by Several Methods. *Chem. Pharm. Bull.* **1994**, *42* (4), 976-978
- (89) Ali, J.; Camilleri, P.; Brown, M. B.; Hutt, A. J.; Kirton, S. B. Revisiting the general solubility equation: in silico prediction of aqueous solubility incorporating the effect of topographical polar surface area. *J. Chem. Inf. Model.* **2012**, *52* (2), 420-428
- (90) Delaney, J. S. ESOL: Estimating Aqueous Solubility Directly from Molecular Structure. *J. Chem. Inf. Comput.* **2004**, *44* (3), 1000-1005
- (91) Yalkowsky, S. H.; Valvani, S. C. Solubility and partitioning I: Solubility of nonelectrolytes in water. *J. Pharm. Sci.* **1980**, *69* (8), 912-922
- (92) Stieger, N.; Liebenberg, W.; Wessels, J. C. UV spectrophotometric method for the identification and solubility determination of nevirapine. *Pharmazie* **2009**, *64* (10), 690-691
- (93) Mota, F. L.; Queimada, A. J.; Pinho, S. P.; Macedo, E. A. Aqueous Solubility of Some Natural Phenolic Compounds. *Ind. Eng. Chem. Res.* **2008**, *47* (15), 5182-5189

CHAPTER 2: EVALUATION OF AURONES FOR THEIR INHIBITORY  
ACTIVITIES AGAINST *S. MUTANS* BIOFILM AND  
GLUCOSYLTRANSFERASES *IN VITRO* AND ANTICARIOGENIC ACTIVITY  
*IN VIVO*

by

PARMANAND AHIRWAR, NORBERT SCHORMANN, CHAMPION  
DEIVANAYAGAM, GREGORY J. HARBER, SUZANNE M. MICHALEK, AND  
SADANANDAN E. VELU.

## ABSTRACT

The optimized lead compounds, **HA5** and **HA6** inhibited *S. mutans* biofilm with IC<sub>50</sub> values 6.42  $\mu$ M and of 18.92  $\mu$ M, respectively. **HA5** and **HA6** inhibited *S. mutans* Gtfs with IC<sub>50</sub> values 10.56  $\mu$ M and of 8.90  $\mu$ M, respectively. These compounds did not affect the growth of oral commensal species *S. gordonii* and *S. sanguinis* up to 15-fold higher concentration than their biofilm inhibition IC<sub>50</sub> values. Fluorescence microscopy imaging of biofilms, glucans and eDNA confirmed the ability of **HA5** and **HA6** to inhibit biofilms. The co-crystal structure of **HA5** with the GtfB catalytic domain resolved at 2.35 Å resolution revealed the interactions of **HA5** with a Ca<sup>2+</sup> ion and critical amino acid residues within the active site. The ability of **HA5** to inhibit *S. mutans* Gtfs and to reduce glucan production has also been demonstrated. Finally, treatment of *S. mutans* UA159 infected rats with 100  $\mu$ M of **HA5** and **HA6** for 4 weeks resulted in significant reduction in buccal, sulcal, and proximal dental caries scores compared to untreated infected rats. The compound treatments did not affect the bacterial colonization significantly in these *in vivo* studies. Moreover, the rats treated with the compound **HA5** or **HA6** did not experience any weight loss over the course of the study in comparison with the control group, suggesting that the compounds are non-toxic. Overall, the results of this study suggest that the compounds **HA5** and **HA6** selectively target *S. mutans* ' virulence factors; Gtfs and Gtf-mediated biofilm formation, rather than a simple inhibition of bacterial growth, are very effective in inhibiting dental caries *in vivo*.

## INTRODUCTION

Originating from Latin, the word 'caries' means "rot" or "decay". Dental caries, also referred to as tooth decay or cavities, is a widespread disease that results in the deterioration of tooth structures.<sup>1, 2</sup> This condition is considered to be one of the most prevalent chronic diseases globally, affecting individuals across all age groups.<sup>3-5</sup> Tooth decay is attributed to the presence of microorganisms in the oral cavity, forming colonies on the tooth surface known as biofilms.<sup>6, 7</sup> These biofilms, also known as dental plaque, play intricate roles in the adhesion of bacteria to the tooth surface and among themselves.<sup>2</sup> There are more than 700 bacterial species living in mouth<sup>8</sup> among which *S. mutans* is widely acknowledged as the predominant etiological agent for the pathogenesis of dental caries.<sup>9</sup> This bacterium is commonly present in the oral cavity and is renowned for its ability to form tenacious biofilms which ferment dietary sugars resulting in the production of acidic metabolites. The ensuing acidogenicity and acidity contribute to the demineralization of tooth enamel. Extensive research in this area has demonstrated the significant role played by *S. mutans* in the formation of dental biofilms and in the progression of tooth decay.<sup>10, 11</sup>

*S. mutans* employs two main mechanisms for its adhesion to tooth surface: 1) sucrose-dependent and 2) sucrose-independent. In the sucrose-independent mechanism, *S. mutans* utilizes its surface proteins such as antigen I/II to interact with salivary agglutinin (SAG) proteins present in the tooth pellicle for the adherence.<sup>12-14</sup> In the sucrose-dependent mechanism, *S. mutans* utilizes a class of proteins called glucosyltransferases (Gtfs) to synthesize glucose oligomers called glucans.<sup>15, 16</sup> The glucans act as a sticky substance, allowing the bacteria to adhere to one another and to form three-dimensional bacterial



colonies. Additionally, the glucans provide structural support to biofilm, contributing to its tenacious nature.<sup>17, 18</sup>

There are three kinds of glucosyltransferases in *S. mutans*, namely, GtfB, GtfC and GtfD encoded by genes *gtfB*, *gtfC*, and *gtfD*, respectively. GtfB predominantly synthesizes water insoluble glucans. GtfD synthesizes water soluble glucans while GtfC is capable of producing both soluble and insoluble glucans.<sup>17, 19-21</sup> Each of the Gtfs contains two functional domains: an N-terminal catalytic domain and a C-terminal glucan binding domain. The catalytic domain binds and hydrolyses sucrose while glucan binding domain is utilized as an acceptor and plays a critical role in determining the nature of glucans synthesized by a particular Gtf.<sup>22-24</sup>

Current methods for the treatment of dental caries have severe limitations. The conventional oral hygiene practices, such as brushing and mouthwashes, are not highly effective due to rapid re-colonization of the bacteria.<sup>25</sup> Fluoride sealants and varnishes are commonly used to prevent dental caries in children.<sup>26, 27</sup> While there is a general consensus on the safety of fluoride treatments,<sup>28, 29</sup> their high fluoride content (1-5 %) and potential neurotoxic effects is a concern.<sup>30</sup> The antimicrobial agents used in mouthwashes such as chlorhexidine, xylitol, silver diamine fluoride and delmopinol lack selectivity, affecting both pathogenic and commensal beneficial species alike giving rise to undesired side effects such as vomiting, diarrhea, addiction, or teeth discoloration.<sup>31</sup> In addition, the biofilm nature of cariogenic bacteria makes them resistant to traditional anti-microbial treatments.<sup>32</sup> A few preventive and therapeutic strategies are under investigation by targeting different virulent determinants of *S. mutans*.<sup>33-35</sup> However, currently known small molecules that possess antibacterial and antibiofilm properties are randomly

identified inhibitors that lack selectivity towards pathogenic biofilms, and the *in vivo* applications of these inhibitors are unclear.<sup>36</sup>

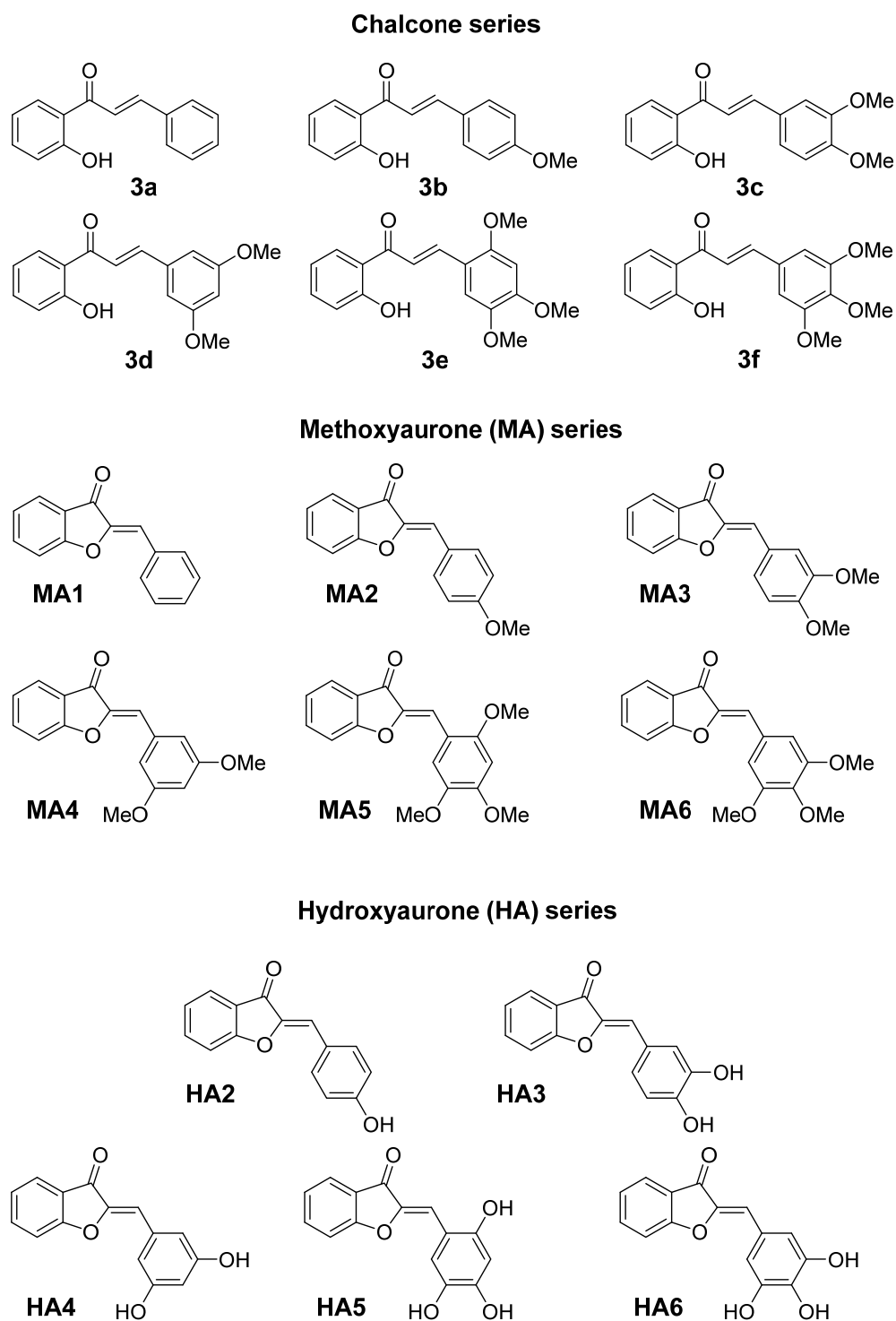


**Figure 2.1.** Chalcones (**3a-f**) methoxyaurones (**MA1-6**) and hydroxyaurones (**HA2-6**).

The previous chapter of this thesis described the design and synthesis of a library of aurones (Figure 2.1), which inhibited of *S. mutans* Gtfs and biofilm at low micromolar concentrations and possessed improved solubility required for biological evaluations and encapsulation studies. In this chapter, we present the *in vitro* and *in vivo* evaluations of this library of compounds and the identification of a lead compound suitable for the encapsulation studies. The structures of the aurones (**MA1-6** and **HA2-6**) and the synthetic intermediate chalcones (**3a-f**) used in this evaluation are presented in Figure 2.1.

## RESULTS AND DISCUSSION

### Inhibition of *S. mutans* planktonic growth

As one of our goals is to identify molecules that are non-toxic to planktonic cells, we first examined the effect of the compounds **3a-e**, **MA1-6** and **HA2-6** at a single concentration of 50  $\mu$ M on the planktonic growth of *S. mutans*.<sup>37</sup> No significant inhibition of planktonic growth was observed between the control group and treated groups for all chalcone derivatives, **3a-f** (Figure 2.2A). Methoxyaurones **MA2-6** were found to be slightly more bactericidal than the chalcones showing 25-40 % planktonic growth inhibition (Figure 2.2B). The aurone analog with unsubstituted phenyl ring (**MA1**) showed the highest bactericidal activity, with 80 % inhibition of the planktonic growth. Some of the hydroxyaurones were more bactericidal than chalcones and methoxyaurones with **HA2**, **HA3** and **HA4** showing 60 %, 40 % and 30 % inhibition, respectively. Two hydroxyaurones, **HA5** and **HA6**, did not inhibit the planktonic growth of *S. mutans* at 50  $\mu$ M and appeared to be promising lead compounds (Figure 2.2C) for further evaluation.

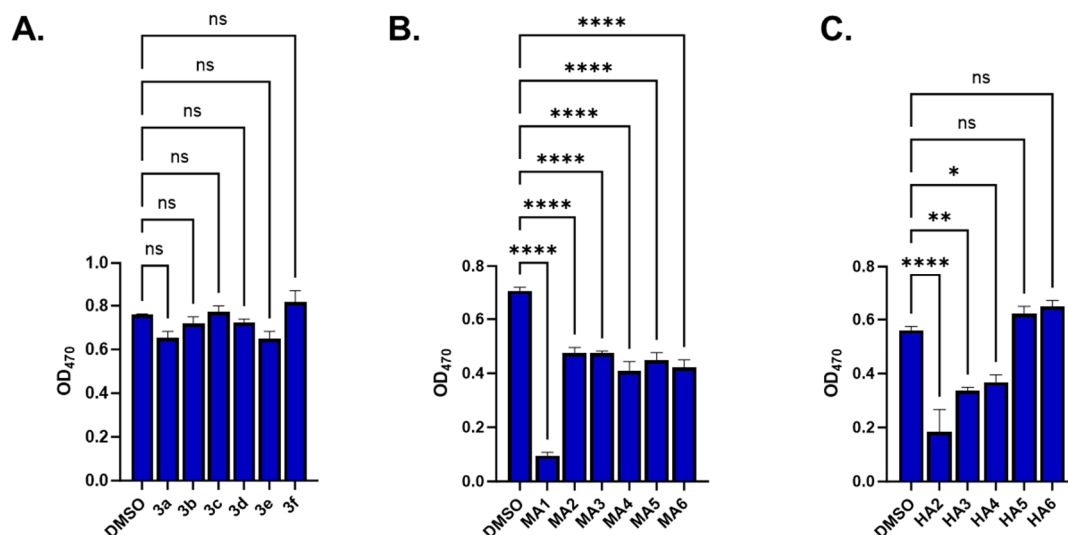


**Figure 2.2.** Planktonic growth inhibitory activities of chalcones (**3a-f**), methoxyaurones (**MA1-6**), and hydroxyaurones (**HA2-6**). **A)** *S. mutans* UA159 were co-incubated with 50  $\mu$ M of chalcones **3a-f** and the planktonic growth was measured at OD<sub>470</sub>. **B)** *S. mutans* UA159 were co-incubated with 50  $\mu$ M of methoxyaurones, **MA1-6** and the planktonic growth was measured at OD<sub>470</sub>. **C)** *S. mutans* UA159 were co-incubated with 50  $\mu$ M of hydroxyaurones, **HA2-6** and the planktonic growth was measured at OD<sub>470</sub>. Each experiment was repeated three times with triplicate microwells for each compound. Statistical significance was tested with one-way ANOVA.  $p = 0.0190$  for **A** and  $p < 0.0001$  for **B** and **C**.

### Screening of **3a-f**, **MA1-6** and **HA2-6** against *S. mutans* biofilms

Initial screening of compounds **3a-f**, **MA1-6** and **HA2-6** in an *S. mutans* biofilm assay was carried out at a single treatment dose of 50  $\mu$ M. Members of all three series of compounds were effective in inhibiting biofilms with hydroxyaurones exhibiting the most pronounced activity compared to methoxyaurones and chalcones (Figure 2.3). More importantly, all compounds showed varying degrees of selectivity towards inhibition of biofilm as opposed to growth. Chalcones, **3a-f** were generally less active compared to the aurones (Figure 2.3A). The most active chalcone derivative, **3f**, exhibited 40 % biofilm inhibition and no growth inhibition at 50  $\mu$ M. The most potent methoxyaurone, **MA5**, exhibited 60 % biofilm inhibition (Figure 2.3B). However, this compound also inhibited 30 % of planktonic growth at 50  $\mu$ M making it a less selective biofilm inhibitor. The other

methoxyaurones, **MA1**, **MA2**, **MA4** and **MA6** were relatively less active displaying only 20-40 % biofilm inhibition, while **MA3** was inactive at this dose. Overall, hydroxyaurones were better biofilm inhibitors than chalcones and methoxyaurones with derivatives, **HA2**, **HA5** and **HA6** showing more than 95 % inhibition and **HA3** showing about 80 % inhibition of biofilms (Figure 2.3C). Among the most active hydroxyaurones, 4-hydroxyanalog, **HA2** inhibited bacterial growth by 70 % at the treated dose, making it a less selective biofilm inhibitor (Figure 2.2C). The 3,5-dihydroxyaurone analog, **HA4** did not show significant biofilm inhibition. The 2,4,5-trihydroxy and 3,4,5-trihydroxy analogs, **HA5** and **HA6**, respectively were found to be the most active hydroxyaurones with more than 95 % biofilm inhibition and no effect on the planktonic growth at 50  $\mu$ M, making them the most active and selective biofilm inhibitors from this screening (Figure 2.3C).

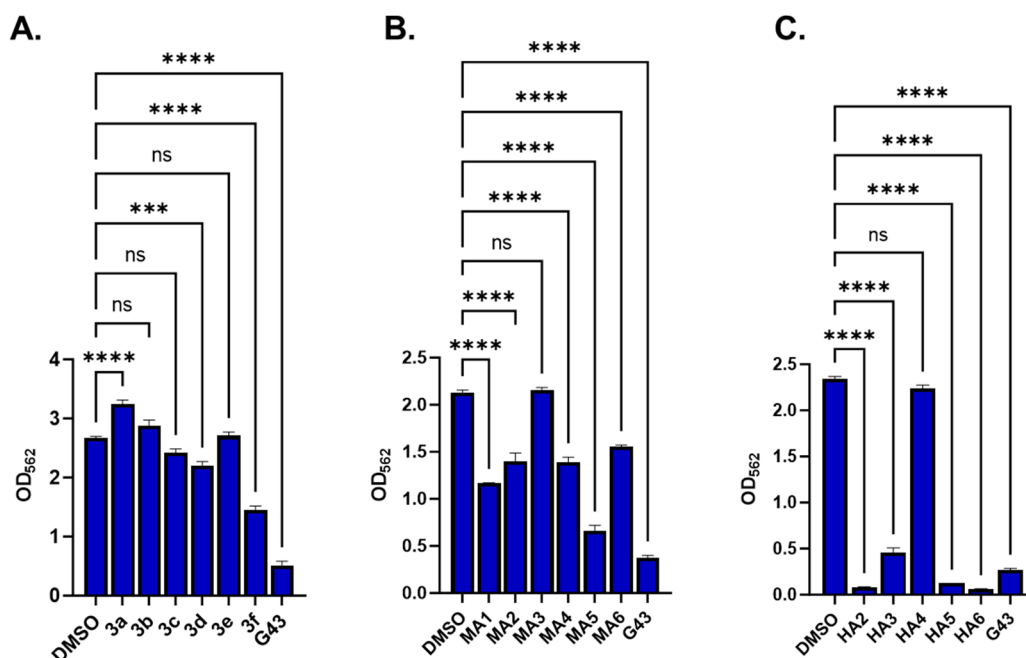


**Figure 2.3.** Biofilm inhibitory activities of chalcones (**3a-f**), methoxyaurones (**MA1-6**) and hydroxyaurones (**HA2-6**). **A)** *S. mutans* UA159 were co-incubated with 50  $\mu$ M of chalcones **3a-f** and biofilm formation was measured at OD<sub>562</sub> using the crystal violet protocol. **B)** *S. mutans* UA159 were co-incubated with 50  $\mu$ M of methoxyaurones, **MA1-6** and biofilm formation was measured at OD<sub>562</sub> using the crystal violet protocol. **C)** *S. mutans* UA159 were co-incubated with 50  $\mu$ M of

hydroxyaurones **HA2-6** and biofilm formation was measured at OD<sub>562</sub> using the crystal violet protocol. Each experiment was repeated three times with triplicate microwells for each compound. Statistical significance was tested with one-way ANOVA.  $p < 0.0001$ .

Considering the potential of methoxyaurones and hydroxyaurones for further development, their biofilm inhibitory activities were further characterized in serial dilutions and IC<sub>50</sub> values were determined. The hydroxyaurones were found to have lower IC<sub>50</sub> values compared to the corresponding methoxyaurones (Table 2.1). Among methoxyaurones, 3,4-dimethoxyaurone, **MA3** was found to be the most active analog with an IC<sub>50</sub> value of 49.40  $\mu$ M. The 2,4,5-trimethoxyaurone, **MA5** had a similar IC<sub>50</sub> value of 52.81  $\mu$ M and the 4-methoxyaurone, **MA2** had an IC<sub>50</sub> value of 107.80 while 3,4-dimethoxy- and 3,4,5-trimethoxy- aurones were inactive. Interestingly, the unsubstituted aurone, **MA1** was more potent than all methoxyaurones with an IC<sub>50</sub> value of 33.61  $\mu$ M. However, **MA1** also displayed about 80 % inhibition of *S. mutans* growth at 50  $\mu$ M, suggesting that its observed biofilm inhibition may be arising from its bactericidal activity.

Two of the hydroxyaurones, 2,4,5-trihydroxyaurone (**HA5**) and 3,4,5-trihydroxyaurone (**HA6**) were found to be the most active derivatives with IC<sub>50</sub> values of 6.42  $\mu$ M and 18.92  $\mu$ M respectively. The 3,4-dihydroxyaurone, **HA3** and 3,5-dihydroxyaurone, **HA4** were found to be less active with IC<sub>50</sub> values of 30.67  $\mu$ M and 94.22  $\mu$ M, respectively. Among these, **HA4** with no OH at the 4-position, was less active than **HA3** with an OH group at 4-position. Interestingly, the monohydroxy analog, **HA2** with an OH group at 4-position was found to be more active than the dihydroxyaurones, **HA3** and **HA4**. It should be noted that both of our most active analogs, **HA5** and **HA6**, also contained an OH group at the 4-position, indicating the importance of the 4-OH group for the biofilm inhibitory activities of hydroxyaurones. This observation is further

supported by our co-crystal structure of **HA5** + **GtfB** complex, showing that the two oxygen atoms at the 4,5-position of the 2,4,5-trihydroxyphenyl moiety interacted with the key amino acid residues in the active site through the coordination with a conserved  $\text{Ca}^{2+}$  ion (Figure 2.8). Of all the aurone analogs synthesized, 2,4,5-trihydroxyaurone **HA5** (Figure 2.5B) was selected as our lead compound for further analysis and encapsulation studies based on its potent biofilm inhibition, lack of growth inhibition and improved solubility.

**Table 2.1.** Biofilm inhibition profiles of **3a-f**, **MA1-6**, and **HA2-6**

Compd No	R <sub>2</sub> Group	R <sub>1</sub> Group	Biofilm IC <sub>50</sub> <sup>a</sup> (μM)
IIIC5 <sup>38</sup>		NA	2.70 ± 0.09
<b>3a</b>		H	>300 <sup>b</sup>
<b>3b</b>		4-OMe	>300 <sup>b</sup>
<b>3c</b>		3,4-di-OMe	>300 <sup>b</sup>
<b>3d</b>		3,5-di-OMe	>300 <sup>b</sup>
<b>3e</b>		2,4,5-tri-OMe	>300 <sup>b</sup>
<b>3f</b>		3,4,5-tri-OMe	180.80 ± 0.65
<b>MA1</b>		H	33.61 ± 0.53
<b>MA2</b>		4-OMe	107.80 ± 0.65
<b>MA3</b>		3,4-di-OMe	49.40 ± 4.79
<b>MA4</b>		3,5-di-OMe	>300 <sup>b</sup>
<b>MA5</b>		2,4,5-tri-OMe	52.81 ± 7.42
<b>MA6</b>		3,4,5-tri-OMe	>300 <sup>b</sup>
<b>HA2</b>		4-OH	18.79 ± 2.36
<b>HA3</b>		3,4-di-OH	30.67 ± 2.28
<b>HA4</b>		3,5-di-OH	94.22 ± 2.18
<b>HA5</b>		2,4,5-tri-OH	6.42 ± 0.61
<b>HA6</b>		3,4,5-tri-OH	18.92 ± 0.39
<b>G43</b> <sup>39</sup>	NA	NA	6.28 ± 0.58

*a)* *S. mutans* UA159 were co-incubated with the compounds at various concentrations and biofilm formation was measured at OD<sub>562</sub> using an established crystal violet protocol<sup>37</sup>. IC<sub>50</sub> values represent the means ± standard error in mean (SEM) from three independent experiments; *b)* Highest concentration tested.

### **Inhibition of commensal streptococci biofilms**

Since hydroxyaurones series (**HA2-6**) was the most active biofilm inhibitors compared to chalcones and methoxyaurones, their selectivity toward *S. mutans* biofilm formation over the biofilms of other species were determined. For this, we evaluated the effects of these compounds on the biofilm formation by two oral commensal Streptococci bacteria: *S. gordonii* and *S. sanguinis*, at 50  $\mu$ M concentration. **HA2-6** inhibited *S. gordonii* biofilm formation by 40-50 % (Figure 2.4A) and *S. sanguinis* biofilm formation by 30-40 % (Figure 2.4B). However, these effects were less pronounced than their effects on *S. mutans* biofilm. For example, compounds **HA5** and **HA6** displayed about 95 % inhibition of *S. mutans* biofilm at 50  $\mu$ M (Figure 2.3C). These effects were also comparable to the control Gtf inhibitor **G43** reported from our lab previously<sup>38</sup>. Overall, this data suggests that hydroxyaurones have a high degree of selectivity towards inhibiting pathogenic biofilms compared to commensal biofilms.



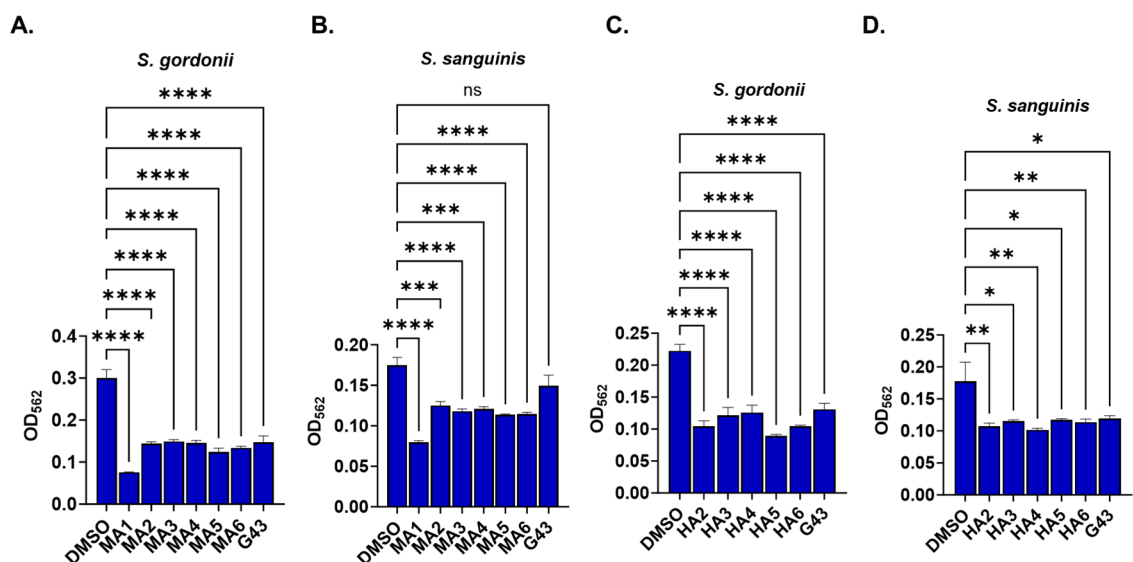


**Figure 2.4.** Inhibitory activities of hydroxyaurones (**HA2-6**) and methoxyaurones (**MA1-6**) against commensal biofilms. **A)** & **C)** *S. gordonii* DL1 were co-incubated with 50  $\mu$ M of methoxyaurones **MA1-6**, hydroxyaurones, **HA2-6** or **G43** and biofilm formation was measured at OD<sub>562</sub> using the crystal violet protocol. **B)** & **D)** *S. sanguinis* SK36 were co-incubated with 50  $\mu$ M of methoxyaurones **MA1-6**, hydroxyaurones, **HA2-6** or **G43** and biofilm formation was measured at OD<sub>562</sub> using the crystal violet protocol. Each experiment was repeated three times with triplicate microwells for each compound. Statistical significance was tested with one-way ANOVA.  $p < 0.0001$  for **A**, **B** and **C**.  $p = 0.0080$  for **D**

### **HA5 inhibits UA159 biofilms, glucan production and eDNA levels**

The antibiofilm activities of the most active and selective analog **HA5** were further investigated by fluorescence microscopy imaging. Compound **HA5** displayed a dose-dependent inhibition of *S. mutans* biofilm as shown in Figure 2.5A. Staining of bacterial cells within biofilms with Syto-9 showed significant reduction in biofilms at 10  $\mu$ M of **HA5** and a complete inhibition at 50  $\mu$ M of **HA5** (Figure 2.5C, Panel-I).

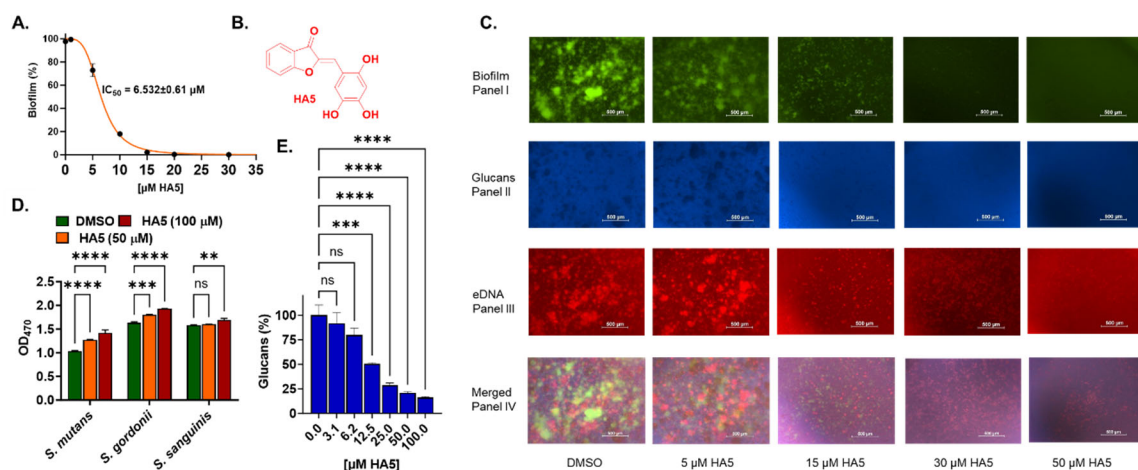


**Figure 2.5.** Biofilm inhibitory activities of compound **HA5**. **A)** *S. mutans* UA159 were co-incubated with **HA5** at various concentrations and biofilm formation was measured at OD<sub>562</sub> using the crystal violet protocol. **B)** Chemical structure of **HA5**. **C)** Representative fluorescence microscopy images of UA159 biofilms after 16 h of treatment with various concentrations of **HA5**. Bacterial cells were stained with Syto-9 (green, panel I); glucans were stained with Cascade Blue–dextran conjugated dye (blue, panel II); eDNA was stained with propidium iodide (red, panel III) and a merged image of all three staining images (panel IV). **D)** *S. mutans* UA159, *S. gordonii* DL1 and *S. sanguinis* SK36 were co-incubated with **HA5** at 50  $\mu$ M and 100  $\mu$ M and their growth were measured at OD<sub>470</sub>. **E)** Gtfs precipitated from *S. mutans* culture were co-incubated with **HA5** at various concentrations and the glucan production was quantified using cascade blue staining and subsequent image processing with ImageJ. Each of the biofilm, glucan and growth assays were conducted in triplicate and statistical significance was tested with one-way ANOVA.  $p < 0.0001$ .

The presence of glucans, which were stained with Cascade Blue-dextran conjugated dye, was significantly reduced at 10  $\mu$ M of **HA5** and no glucan formation was evident at 50  $\mu$ M of **HA5** (Figure 5C, Panel II). In addition, propidium iodide was used to determine the presence of extracellular DNA (eDNA) in *S. mutans* biofilms. Again, there was a noticeable reduction of eDNA at 10  $\mu$ M of **HA5** and almost complete absence of eDNA at 50  $\mu$ M of **HA5** (Figure 2.5C, Panel III). These findings reaffirm that **HA5** inhibited *S. mutans* biofilms by preventing the synthesis of glucans and minimizing the presence of eDNA, two integral biofilm matrix elements crucial for *S. mutans* biofilm formation.

### **HA5 inhibits glucan production by *S. mutans* Gtfs in a dose dependent manner**

The interspecies co-adherence between *S. mutans* and other microorganisms in the oral cavity is critical for biofilm formation and cariogenicity. Though the mechanisms of such adhesions and co-aggregations are not fully elucidated, it is believed that the extracellular polysaccharide (EPS) matrix of *S. mutans* has an important role in this process.<sup>40-42</sup> It is reported that glucans synthesized by Gtfs when incorporated into the tooth pellicle to provide enhanced binding sites for other microorganisms to form stable and persistent microcolonies, which provides mechanical stability to the EPS matrix.<sup>42, 43</sup> Therefore, Gtf inhibition assays were performed to assess the ability of **HA5** to inhibit the Gtfs and glucan production using a reported procedure and an IC<sub>50</sub> value was calculated.<sup>44, 45</sup> Compound **HA5** exhibited dose dependent inhibition of glucan production by Gtfs with an IC<sub>50</sub> value of 10.56  $\mu$ M (Figure 2.5E). These findings reinforce the biofilm inhibitory activity of **HA5** and confirm that the compound inhibits biofilm formation by inhibiting glucans production by *S. mutans* Gtfs.

### **HA5 does not affect growth of commensal streptococci**

To determine if compound **HA5** selectively inhibits *S. mutans* biofilms over the growth of *S. mutans* and oral commensal species, the effects of **HA5** on the growth of two representative commensal oral streptococci, *S. sanguinis*, and *S. gordonii* along with *S. mutans* at 50  $\mu$ M and 100  $\mu$ M doses, were evaluated. As shown in Figure 2.5D, compound **HA5** did not inhibit the growth of the two commensals compared to the control group at these doses that are much higher than its biofilm IC<sub>50</sub> value of 6.42  $\mu$ M. Similarly, the compound did not inhibit *S. mutans* growth at these doses, suggesting that **HA5** selectively inhibited *S. mutans* biofilms without affecting its growth as well as the growth of both commensal species, *S. gordonii* and *S. sanguinis* (Figure 2.5D).

## HA6 inhibits UA159 biofilms, glucan production and eDNA

Like **HA5**, compound **HA6** was also found to be inhibiting *S. mutans* biofilm selectively in dose dependent manner with IC<sub>50</sub> value of 18.92  $\mu$ M (Figure 2.6A). **HA6** was also seen to be inhibiting Gtfs enzymatically with IC<sub>50</sub> = 8.90  $\mu$ M (Figure 2.6B). Fluorescence microscope images of *S. mutans* bacteria cells in biofilm stained by Syto-9 fluorescent probe show that the biofilm reduces significantly at 15  $\mu$ M and completely disappears at 50  $\mu$ M concentrations of **HA6** (Figure 2.6C, Panel I). The extracellular glucans stained with the Cascade Blue-dextran conjugated dye were produced in significantly less amount at 15  $\mu$ M and reduced to zero at 50  $\mu$ M of **HA6** (Figure 2.6C, Panel II). Similar trends were seen in case of eDNA stained with propidium iodide (Figure 2.6C, Panel III). This confirms the fact that **HA6**, similar to **HA5** inhibits *S. mutans* biofilm by inhibiting production of extracellular polysaccharides in a dose dependent manner.

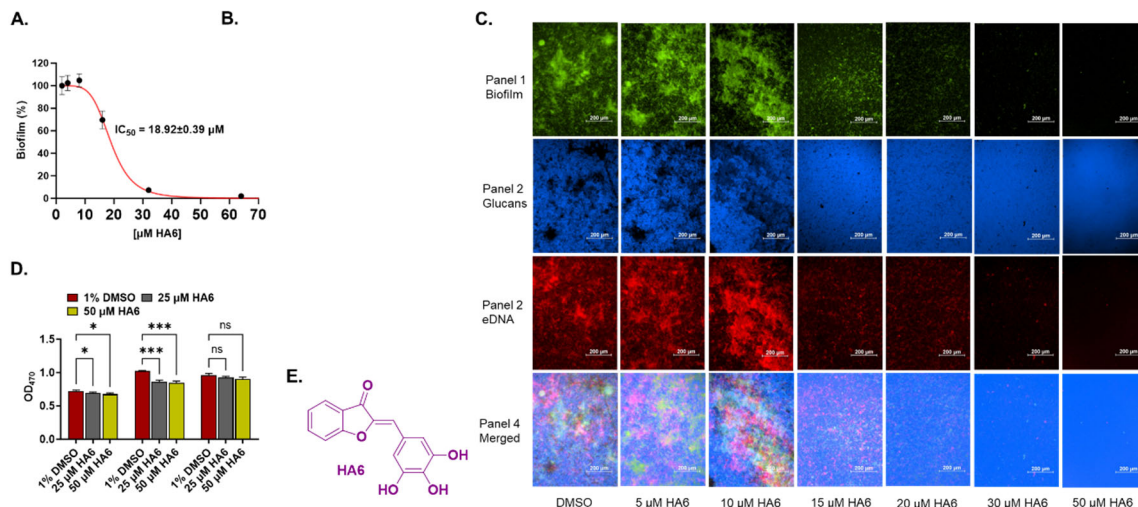


**Figure 2.6.** Biofilm inhibitory activities of compound **HA6**. **A)** *S. mutans* UA159 were co-incubated with **HA6** at various concentrations and biofilm formation was measured at OD<sub>562</sub> using the crystal violet protocol. **B)** Gtfs precipitated from *S. mutans* culture were co-incubated with **HA6** at various concentrations and the glucan production was quantified using cascade blue staining and subsequent image processing with ImageJ. **C)** Representative fluorescence microscopy images of UA159 biofilms after 16 h of treatment with various concentrations of **HA6**. Bacterial cells were stained with Syto-9 (green, panel I); glucans were stained with Cascade Blue–dextran conjugated dye (blue, panel II); eDNA was stained with propidium iodide (red, panel III) and a merged image of all three staining images (panel IV). **D)** *S. mutans* UA159, *S. gordonii* DL1 and *S. sanguinis*

SK36 were co-incubated with **HA6** at 25  $\mu$ M and 50  $\mu$ M and their growth were measured at OD<sub>470</sub>. **E)** Chemical structure of **HA6**. Each of the biofilm, glucan and growth assays were conducted in triplicate and statistical significance was tested with one-way ANOV.  $P < 0.0001$ .

### Effect of HA6 on commensal species growth

The effects of **HA6** on the growth of two representative commensal oral streptococci, *S. sanguinis*, and *S. gordonii*, along with *S. mutans* at 50  $\mu$ M dose were evaluated. As shown in Figure 2.6 D, compound **HA6** did not inhibit the growth of both commensals compared to the control group at these doses that are much higher than its biofilm IC<sub>50</sub> value of 18.92  $\mu$ M. Similarly, the compound did not inhibit *S. mutans* growth at these doses, suggesting that similar to **HA5**, compound **HA6** also selectively inhibited *S. mutans* biofilms without affecting its growth as well as the growth of the commensal species.

### HA5 and HA6 bind to GtfB in OctetRed experiments

Biolayer Interferometry (BLI) is a sensitive technique to detect the drug-target engagement.<sup>46</sup> It utilizes change in refractive index when a protein is adsorbed at the sensor. In this technique, protein is first allowed to bind to the sensor surface followed by binding of ligand (drug) to the protein. This drug-protein association is detected as shift in wavelength. Similar shift can be detected when protein ligand complex is dissociated after rinsing with buffer.<sup>47, 48</sup> The BLI binding studies of **HA5** and **HA6** using OctetRed96 instrument showed that both drugs are able to bind to GtfB with dissociation constant,  $K_D$  values of 0.595  $\mu$ M and 0.248  $\mu$ M respectively (Figure 2.7A-B). The results of this study are consistent with the results of the glucan inhibition assay (Figures 2.5E and 2.6B).

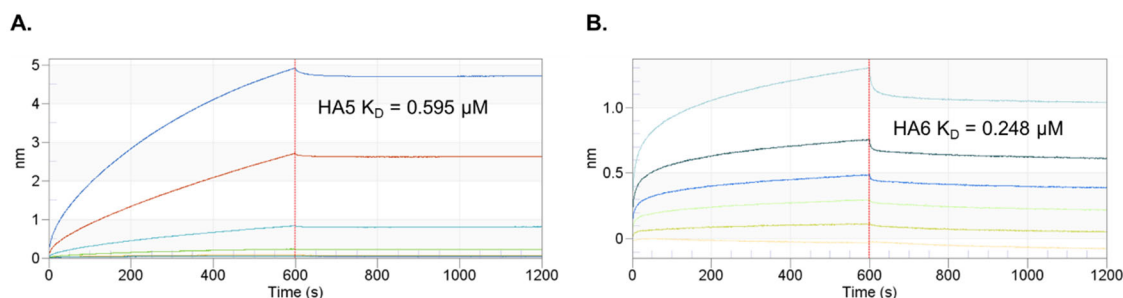


**Figure 2.7:** OctetRed binding of **A) HA5** and **B) HA6** with GtfB protein from *S. mutans*. The binding kinetics of **HA5** and **HA6** with GtfB were examined using the Octet® Red96 system (ForteBio, Menlo Park, CA) in phosphate buffer and the dissociation constants  $K_D$  were determined. The proteins were immobilized on a dip-and-read Anti-Penta-HIS (HIS1K) Biosensor, which contains a highly specific Penta-His antibody from Qiagen. The ForteBio Octet analysis software (ForteBio, Menlo Park, CA) was employed to generate sensorgrams and ensure the accuracy of the analysis.

### Structural studies on HA5 in the catalytic domain of GtfB

Apo crystals of GtfB were obtained in the Index (Hampton Research) A3 crystallization condition using the hanging drop vapor diffusion technique produced reliably large enough (0.1-0.2 mm) tetragonal crystals for GtfB. Apo crystals of GtfB were soaked with **HA5** for 5-10 mins (final concentration 1-2 mM; 20 mM stock solution of compound **HA5** in H<sub>2</sub>O). The GtfB structure complexed with **HA5** diffracted to a resolution of 2.35 Å. Diffraction data for the inhibitor structure were collected at 100 K using the hybrid pixel DECTRIS Eiger 16m detector at the SERCAT 22-ID beamline in the Advanced Photon Source (APS), Chicago. For cryoprotection of GtfB crystals 20 % ethylene glycol was added to the crystallization buffer. The collected data were processed using XDS<sup>49, 50</sup> for initial indexing, merging, and scaling, and were followed by optimization using Aimless<sup>51</sup> in CCP4.<sup>52</sup> The data collection statistics are shown in Table 2.2. The structure for GtfB was solved by molecular replacement using Phaser with a model for GtfB generated by the SWISS-MODEL web server based on the catalytic domain of GtfC (3AIE). Refinement was performed using a combination of Refmac5<sup>53</sup> in CCP4<sup>52</sup>

and Phenix<sup>54, 55</sup>. MOGUL (CSD release) restraints for compound **HA5** were based on the CCDC small molecule database and obtained from the Grade web server. Compound **HA5** is unknown to PDB, and therefore, was sketched in ChemAxon and the resulting SMILES notation provided the initial input. Coot was used for all model building<sup>56</sup> and figures were created with PyMOL (Version 2.5.0, Schrödinger, LLC). Validation of the model quality was performed using Phenix and the wwPDB validation service. The ligand was validated using the same set of MOGUL restraints described above. The conserved Ca<sup>2+</sup> site in the structure of GtfB was verified with the CheckMyMetal web server. The protein structure has been deposited in PDB. Final refinement statistics are presented in Table 2.2.

**Table 2.2:** Data collection and refinement statistics for GtfB in complex with **HA5**.

<i>Data collection</i>	
Space Group	P4 <sub>3</sub> 22
Unit cell parameters [Å]	a = b = 150.46, c = 304.95
Resolution [Å]	87.25 - 2.35 (2.39 - 2.35)
Unique reflections	142674 (7062)
Completeness [%]	98.5 (99.2)
Multiplicity	7.4 (7.2)
R <sub>merge</sub> [%]	19.1 (210.7)
R <sub>pim</sub> [%]	6.5 (71.2)
CC <sub>1/2</sub> (2.39 – 2.35Å)	0.350
CC* (2.39 - 2.35Å)	0.720
I/σ(I)	8.1 (1.1)
<i>Refinement</i>	
Resolution [Å]	73.04 - 2.35 (2.41 - 2.35)
No. of reflections	139861 (10356)
Completeness [%]	96.1 (97.6)
R <sub>work</sub> [%]	20.5 (33.6)
R <sub>free</sub> [%]	23.3 (35.5)
Wilson B [Å <sup>2</sup> ]	48.0
<i>Average B-factors [Å<sup>2</sup>]</i>	
Overall	57.9 (13785 atoms)
Protein, Ca <sup>2+</sup> , HA5, BTB	57.8 (13091 atoms), 55.9 (3 ions), 83.7 (40 atoms), 73.9 (28 atoms)

SO <sub>4</sub> <sup>2-</sup> , Waters	97.7 (125 atoms), 47.2 (503 atoms)
Rmsd bonds [Å]	0.013
Rmsd angles [°]	1.74
CC (Fo-Fc)	0.95
Ramachandran [%]	95.9 favored (outliers 0.7)
Clash score	3.76
Molprobability score	1.44

---

### Co-crystal structure of HA5 with GtfB

To define the underlying mechanism of **HA5**'s ability to inhibit Gtfs and biofilm, a high-resolution co-crystal structure of **HA5** with the catalytic domain of GtfB was resolved. The analysis of **GtfB/HA5** co-crystal structure revealed that the inhibitor **HA5** was crystallized along with Bis-Tris (BTB), a chemical component of the buffer used in the crystallization studies (Figure 2.8A-B). Inhibitor **HA5** was found to adopt a classic  $\pi$ - $\pi$  stacking interaction with Trp491 residue in the GtfB active site (Figure 2.8C). In the structure only water-mediated hydrogen bonds are observed for **HA5**, which differs from the reported *in silico* docking results with the inhibitor **G43**, which highlighted hydrogen bond interactions of **G43** with the three active site residues Asp451, Glu489 and Asp562.

<sup>38</sup> In the crystal structure of **HA5**, the inhibitor makes only hydrophobic contact with these residues (Figure 2.8C). For the sucrose to undergo the invertase activity, the glucose molecule will nest within the -1 subsite, which consists of residues Arg449, Asp451, Glu489, His561, Asp562 and Tyr890. The fructose interacts with the +1 subsite which consists of residues Tyr404, Leu407 and Trp491. These nomenclatures were adopted for sugar binding sites for glycosylhydrolases.<sup>57</sup> The inhibitor **HA5** in this crystal structure binds to subsites +1 and +2 which include residues Asn511, Arg514, and Asp567. **HA5** makes hydrophobic interactions with a total of 15 interface residues in these two subsites. 50 % of its solvent accessible surface area is buried in the protein-ligand interactions. In



chain B of GtfB, two oxygen atoms at the 4,5-position of the 2,4,5-trihydroxyphenyl moiety of the inhibitor **HA5** coordinated with a conserved  $\text{Ca}^{2+}$  ion and extends its interaction with Asp451 and Glu489 (Figure 2.8C). The 4-OH group on the benzene ring of **HA5** interacts with Tyr404. In chain A of GtfB, the 2,4,5-trihydroxyphenyl moiety is rotated around the methyldene atom with respect to the benzofuran ring system allowing a hydrogen bond with BTB buffer molecule (buffer of the crystallization condition) within the active site. The result of finding BTB in the GtfB active site is not surprising since Tris as an ethanolamine derivative has been previously reported as a competitive inhibitor of GtfB.<sup>58</sup> Binding of the BTB in this structure occurs in -1 subsite and overlaps with proposed binding of the glucosyl moiety of sucrose. The BTB molecule provides 11 hydrogen bonds to protein residues within the active site.

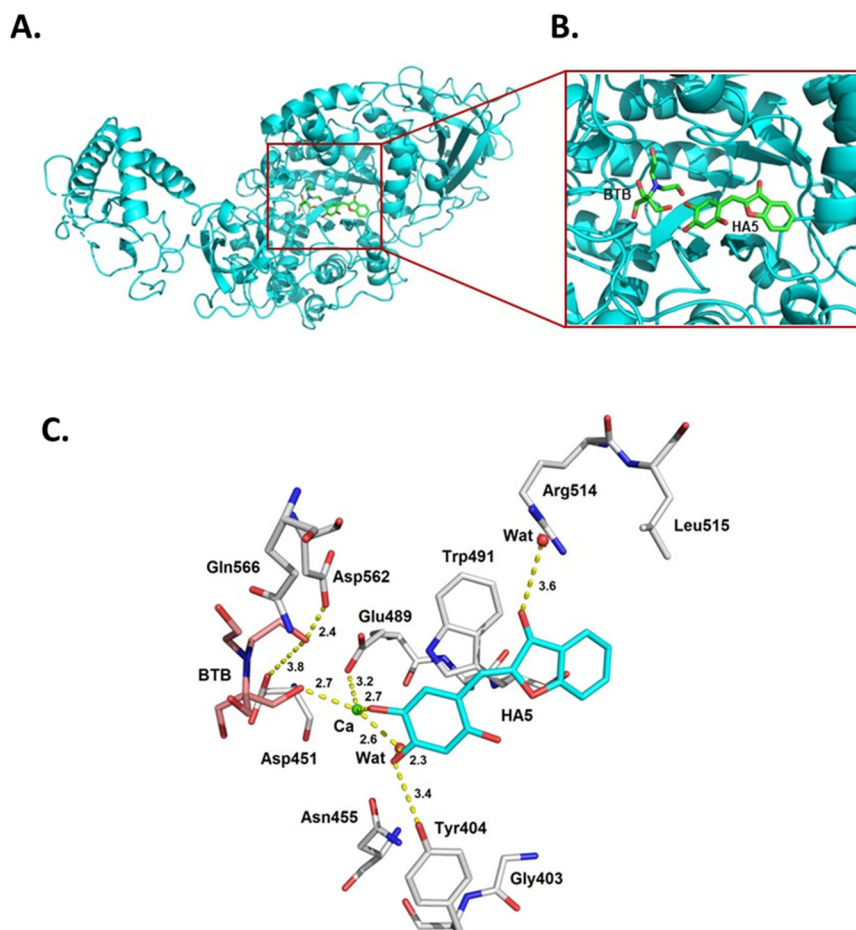


**Figure 2.8:** A) High resolution X-ray co-crystal structure (PDB ID: 8FG8) of the inhibitor **HA5** with the catalytic domain of GtfB. Inhibitor **HA5** and BTB are displayed as green sticks. B) Expansion of the GtfB binding site showing the binding mode of **HA5**. C) Key active site interactions of **HA5** with active site residues (grey sticks) along with its H-bond interactions with water (Wat) molecules and calcium (Ca<sup>2+</sup>) ion depicted as yellow dotted lines. Inhibitor **HA5** is depicted as light blue sticks and BTB is depicted as lavender sticks.

### **HA5 and HA6 reduce caries score *in vivo***

The potential effects of compound **HA5** and **HA6** on the virulence of *S. mutans* were investigated using a well-established gnotobiotic rat model of dental caries.<sup>59, 60</sup> To serve as a negative control, a group receiving only the vehicle and infection was included. All the experimental and control groups of rats were colonized with *S. mutans* UA159. Following a 4-week treatment with 100 µM of either **HA5** or **HA6** in *S. mutans* UA159 infected gnotobiotic rats, a notable reduction in buccal, sulcal and proximal caries scores

was observed compared to the control groups (Tables 2.3-2.5). We were unable to record the effect of the treatment on Dentinal moderate (Dm) and Dentinal extensive (Dx) scores in the proximal area as there were no significant proximal dentinal lesions for the control and treated groups. At the end of the study, the animals were euthanized, and their mandibles were extracted for microbiological analysis of plaque samples on MS agar plates and BAP. The presence of **HA5** or **HA6** did not significantly affect bacterial colonization when compared to the control group (Table 2.6). Furthermore, the rats treated with **HA5** or **HA6** did not experience any weight loss throughout the study, suggesting their non-toxic nature (Table 2.6).

**Table 2.3:** Effect of **HA5** or **HA6** treatment on *S. mutans* UA159 induced buccal caries.

Treatment Group	Buccal Mean Caries Scores ( $\pm$ SEM)			
	E	Ds	Dm	Dx
<b>UA159 infected and untreated</b>	13.2 $\pm$ 0.4	9.2 $\pm$ 0.6	6.2 $\pm$ 0.7	3.6 $\pm$ 0.4
<b>HA5 treated (100 <math>\mu</math>M)</b>	7.8 $\pm$ 0.4	6.6 $\pm$ 0.5	3.6 $\pm$ 0.4	2.2 $\pm$ 0.7
<b>HA6 treated (100 <math>\mu</math>M)</b>	8.2 $\pm$ 0.7	6.8 $\pm$ 0.5	4.0 $\pm$ 0.7	1.2 $\pm$ 0.5
<b>NaF treated (250 ppm)</b>	6.2 $\pm$ 0.9	3.2 $\pm$ 0.9	1.6 $\pm$ 0.5	0.4 $\pm$ 0.2

*Enamel (E); Dentinal slight (Ds); Dentinal moderate (Dm); Dentinal extensive (Dx)*

**Table 2.4:** Effect of **HA5** or **HA6** treatment on *S. mutans* UA159 induced sulcal caries.

Treatment Group	Sulcal Mean Caries Scores ( $\pm$ SEM)			
	E	Ds	Dm	Dx
<b>UA159 infected and untreated</b>	25.8 $\pm$ 1.2	18.8 $\pm$ 1.3	12.8 $\pm$ 0.7	6.6 $\pm$ 0.3
<b>HA5 treated (100 <math>\mu</math>M)</b>	16.4 $\pm$ 2.2	11.2 $\pm$ 0.6	4.6 $\pm$ 0.2	1.0 $\pm$ 0.3
<b>HA6 treated (100 <math>\mu</math>M)</b>	14.6 $\pm$ 0.9	11.2 $\pm$ 0.7	6.4 $\pm$ 0.4	1.6 $\pm$ 0.4
<b>NaF treated (250 ppm)</b>	15.2 $\pm$ 0.7	10.4 $\pm$ 0.5	5.4 $\pm$ 0.4	1.6 $\pm$ 0.5

*Enamel (E); Dentinal slight (Ds); Dentinal moderate (Dm); Dentinal extensive (Dx)*

**Table 2.5:** Effect of **HA5** or **HA6** treatment on *S. mutans* UA159 induced proximal caries.

Treatment Group	Proximal Mean Caries Scores ( $\pm$ SEM)	
	E	Ds
<b>UA159 infected and untreated</b>	8.0 $\pm$ 0.0	5.8 $\pm$ 0.7
<b>HA5 treated (100 <math>\mu</math>M)</b>	1.0 $\pm$ 0.3	0.0 $\pm$ 0.0
<b>HA6 treated (100 <math>\mu</math>M)</b>	1.2 $\pm$ 0.8	0.0 $\pm$ 0.0
<b>NaF treated (250 ppm)</b>	0.0 $\pm$ 0.0	0.0 $\pm$ 0.0

*Enamel (E); Dentinal slight (Ds); Dentinal moderate (Dm); Dentinal extensive (Dx); Dentinal moderate (Dm) and Dentinal extensive (Dx) scores are not included as there were no significant proximal dentinal lesions for the control and treated groups in this study.*

**Table 2.6:** Effect of **HA5** or **HA6** treatment on *S. mutans* UA159 CFU and the body weight of the treated animals.

Treatment Group	CFU/mL ( $\times 10^5$ )		Animals	
	MS	BAP	Weight (g)	Number
<b>UA159 infected and untreated</b>	2.3 $\pm$ 1.2	3.3 $\pm$ 2.0	161 $\pm$ 12	5
<b>HA5 treated (100 <math>\mu</math>M)</b>	2.2 $\pm$ 0.8	3.9 $\pm$ 1.4	156 $\pm$ 16	5
<b>HA6 treated (100 <math>\mu</math>M)</b>	1.3 $\pm$ 0.4	1.9 $\pm$ 0.5	165 $\pm$ 13	5
<b>NaF treated (250 ppm)</b>	1.6 $\pm$ 0.6	2.8 $\pm$ 0.7	145 $\pm$ 12	5

*Mitis-Salivarius agar (MS); Blood agar plate (BAP)*

## CONCLUSIONS

In conclusion, we have developed novel small-molecule inhibitors of *S. mutans* glucosyltransferases as selective biofilm inhibitors that do not affect the growth of oral commensal bacteria. The optimized lead compounds, **HA5** or **HA6** inhibited *S. mutans* biofilm with an  $IC_{50}$  values of 6.42  $\mu$ M and of 18.92  $\mu$ M respectively. **HA5** or **HA6** inhibited *S. mutans* Gtfs with an  $IC_{50}$  values of 10.56  $\mu$ M and of 8.90  $\mu$ M respectively. These compounds did not affect the growth of oral commensal species *S. gordonii* and *S. sanguinis* up to 15-fold higher concentration than its biofilm inhibition  $IC_{50}$  value.

Fluorescence microscopy imaging of biofilms, glucans and eDNA confirmed the ability of **HA5** and **HA6** to inhibit biofilms. The co-crystal structure of **HA5** with GtfB catalytic domain determined at 2.35 Å resolution revealed the interactions of **HA5** with a Ca<sup>2+</sup> ion and critical amino acid residues within the active site. The ability of **HA5** to inhibit *S. mutans* Gtfs and to reduce glucan production has also been demonstrated. Finally, treatment of *S. mutans* infected rats with 100 µM of **HA5** or **HA6** for 4 weeks resulted in a significant reduction in buccal, sulcal, and proximal dental caries compared to untreated, infected rats without affecting the bacterial colonization significantly. Moreover, the rats treated with the compound **HA5** or **HA6** did not experience any weight loss over the course of the study in comparison with the control group, suggesting that they are non-toxic. These results of this study suggest that the compound **HA5** and **HA6** selectively target *S. mutans* virulence factors; Gtfs and Gtf- mediated biofilm formation, rather than a simple inhibition of bacterial growth and are very effective in inhibiting dental caries *in vivo*.

## EXPERIMENTAL SECTION

### General considerations

The bacterial strains, *S. mutans* UA159, *S. gordonii* DL1, and *S. sanguinis* SK36 were inoculated statically at 37 °C under 5 % CO<sub>2</sub> in Todd Hewitt Broth (THB) for 24 h. The cultures were then diluted with fresh THB (1:5) and reinoculated until optical density at 470 nm (OD<sub>470</sub>) reached 1. The optical density was read using BioTek 800TS microplate reader at 470 nm for bacterial growth and 562 nm for biofilm stained with crystal violet. Data was plotted in Graphpad Prism 9.5.1.

### **Biofilm inhibition assays**

Biofilm inhibition assays were performed in polystyrene microtiter 96 well plates. Stock solutions were prepared in chemically defined medium (CDM, JRH Biosciences, Lenexa, KS) with 1 % sucrose, 1 % bacteria cultures and various concentrations of the small molecule inhibitors to examine their activity against biofilm formation as described<sup>61, 62</sup>. These stocks were assayed in 96 well plates in triplicate and incubated at 37 °C and 5 % CO<sub>2</sub> for 16 h. After reading optical density for bacterial growth, the plate was gently carefully washed with water, dried, and stained with crystal violet, and then gently rinsed again with deionized water leaving the stained biofilm at the bottom of the wells. Biofilms were dissolved in 200 µL of 30 % acetic acid and absorbance at 562 nm was used read to determine biofilm biomass. Each assay was carried out at least in triplicate. Biofilm inhibitory concentration (IC<sub>50</sub>) of the compounds were determined by serial dilutions.

### **Gtf inhibition determined by glucan quantification assays**

Overnight cultures of *S. mutans* UA159 were centrifuged (6500 rpm, 4 °C, 10 min) to remove cells. The supernatant was mixed with ethanol (1:1) and incubated at -80 °C for 1h. The precipitated Gtfs were pelleted using centrifugation and resuspended in chemically defined media (CDM). 10 µL of Gtfs suspended in CDM were assayed on Ibidi slides with varying concentrations of inhibitor, 1 % sucrose, 1 % DMSO and 1 µM Cascade blue dye in CDM. The slides were then incubated at 37 °C with 5 % CO<sub>2</sub> for 16 h after which, the wells of Ibidi slides were gently rinsed with 1x PBS and treated with 1x PBS for fluorescence microscopy imaging. The images obtained were processed in ImageJ to quantify glucans and graphed in GraphPad Prism 9.5.1.

### ***S. mutans* and commensal *S. gordonii* and *S. sanguinis* growth assays**

Effects of compounds on *S. mutans* and commensal bacterial growth were evaluated using the growth assay as described.<sup>61</sup> *S. mutans* UA159, *S. gordonii* DL1, *S. sanguinis* SK36, cultures were grown for 24 h with 5 % CO<sub>2</sub> at 37 °C. These cultures were then reinoculated with fresh THB (1:5) until OD<sub>470</sub> = 1 when the bacteria were ready to be used. Different concentrations of the inhibitor were assayed in chemically defined media (CDM) with 1:100 of the bacteria, 1 % sucrose and 1 % DMSO in 96 well plates. The 96 well plates were incubated with 5 % CO<sub>2</sub> at 37 °C for 16 h. Growth of the bacteria was read after 16 h at OD<sub>470</sub>. Each assay was carried out at least in triplicate.

### **Rat model of dental caries**

*In vivo* studies of colonization and virulence of *S. mutans* were evaluated using a previously reported rat model of dental caries,<sup>63, 64</sup> Offsprings of gnotobiotic Fischer 344 rats used in this experiment were bred and maintained in trexler isolators. Male and female rat pups were removed from isolators at 20 days of age and randomly assigned into 5 treatment groups of 5 rats / group in cages with filter tops. Rats were then infected with *S. mutans* UA159 strain by oral swabbing daily for four consecutive days with a fresh overnight culture of *S. mutans* UA159. Rats were provided with caries promoting Teklad Diet 305 containing 5 % sucrose (Harlan Laboratories, Inc., Indianapolis, IN) and sterile drinking water *ad libitum*. Oral swabs were taken 5 days post-infection and plated on Todd Hewitt (TH) agar plates and incubated at 37 °C in an environment of 5 % CO<sub>2</sub> in the air to confirm colonization. Rats were weighed at weaning and at the termination of the experiment. One-week post-infection, the molars of the rats were treated topically twice daily for 4 weeks with the test compounds using camel-hair brushes. The five treatment groups used in this study were: 1) **HA5** (100 µM); 2) **HA6** (100 µM); 3) 250 ppm NaF

(positive control), and 4) infected untreated group (negative control). Drinking water was withheld for 60 min following each treatment with the compound. Animals were weighed at weaning and at the termination of the experiment. On day 60, the rats were sacrificed using CO<sub>2</sub> followed by cervical dislocation or bilateral thoracotomy. The mandibles were surgically removed and cleaned of excess tissue to assess the level of bacteria present and the extent of caries formation. The right mandibles from each rat were placed in a tube containing phosphate buffer (3 mL), placed on ice and sonicated (10 sec) to release bacteria from the molars. Each sample was serially diluted, plated on blood agar plates (BAP) and mitis-salivarius (MS) agar plates and incubated in an environment of 5 % CO<sub>2</sub> at 37 °C to quantify the level of total bacteria and *S. mutans* present in the plaque. The right and left mandibles from each rat were then placed in 95 % ethanol for 24 h. The mandibles will be cleaned and stained overnight with murexide solution. After drying, the mandibles were sectioned and scored for caries activity using the Keyes method<sup>39</sup>. Caries scores were recorded for the buccal, sulcal and proximal molar surfaces individually so that differences among the surfaces can be distinguished. Statistical significance in the mean caries scores, colony-forming units (CFUs) / mandible and body weights between groups of rats were determined by one-way analysis of variance (ANOVA) with the Tukey-Kramer multiple comparison test using the InStat program (Graphpad Software, San Diego, CA). When determining the statistical significance between the two groups, an unpaired t-test was applied. Differences between groups were considered significant at a *P*-value < 0.05. The methods were carried out in accordance with the relevant guidelines and regulations.



### **OctetRed binding assay**

The binding kinetics of **HA5** and **HA6** with GtfB were examined using the Octet<sup>®</sup> Red96 system (ForteBio, Menlo Park, CA) in phosphate buffer and the rate constants  $k_D$  were determined. The proteins were immobilized on a dip-and-read Anti-Penta-HIS (HIS1K) Biosensor, which contains a highly specific Penta-His antibody from Qiagen. The biosensor, based on fiber optic technology, facilitated the capture of the proteins. To determine the binding affinity, **HA5** and **HA6** were subjected to serial dilutions in phosphate buffer ranging from 100  $\mu$ M to 0  $\mu$ M, with intermediate concentrations of 50, 25, 12.5, 6.25, and 3.125  $\mu$ M. The ForteBio Octet analysis software (ForteBio, Menlo Park, CA) was employed to generate sensorgrams and ensure the accuracy of the analysis.

### **ACKNOWLEDGEMENTS**

The contents described in this chapter were supported by the NIH grants R21CA22649 (Velu), R21DE028349 (Velu), R03DE025058 (Velu), and University of Alabama at Birmingham Microbiome Center Pilot Grant (Velu). We acknowledge Drs. Champion Deivanayagam and Norbert Schormann the department of Biochemistry and Molecular Genetics for the high-resolution X-ray crystallographic data presented in this chapter. We would also like to express our gratitude to Drs. Suzanne M. Michalek and Gregory Harber from the department of Microbiology for the *in vivo* rat model studies presented in this chapter. Graduate student Teaching Assistantship (Ahirwar) from the Department of Chemistry, University of Alabama at Birmingham is greatly appreciated.

## **IACUC APPROVAL**

All *in vivo* experimental protocols were approved by the University of Alabama at Birmingham Institutional Animal Care and Use Committee (Protocol No: IACUC-20047).

## REFERENCES

- (1) Loesche, W. J. Role of *Streptococcus mutans* in human dental decay. *Microbiol. Rev.* **1986**, *50* (4), 353-380
- (2) Marsh, P. D. Dental Plaque as a Microbial Biofilm. *Caries Research* **2004**, *38* (3), 204-211
- (3) Cherian, J. M.; Kurian, N.; Varghese, K. G.; Thomas, H. A. World Health Organization's global oral health status report: Paediatric dentistry in the spotlight. *J. Paediatr. Child. Health.* **2023**,
- (4) Jain, N.; Dutt, U.; Radenkov, I.; Jain, S. WHO's global oral health status report 2022: Actions, discussion and implementation. *Oral Dis.* **2023**,
- (5) Vos, T.; Lim, S. S.; Abbafati, C.; Abbas, K. M.; Abbasi, M.; Abbasifard, M.; Abbasi-Kangevari, M.; Abbastabar, H.; Abd-Allah, F.; Abdelalim, A.; et al. Global burden of 369 diseases and injuries in 204 countries and territories, 1990–2019: a systematic analysis for the Global Burden of Disease Study 2019. *The Lancet* **2020**, *396* (10258), 1204-1222
- (6) Kolenbrander, P. E.; Palmer, R. J.; Periasamy, S.; Jakubovics, N. S. Oral multispecies biofilm development and the key role of cell–cell distance. *Nat. Rev. Microbiol.* **2010**, *8* (7), 471-480
- (7) Kuramitsu, H. K.; He, X. S.; Lux, R.; Anderson, M. H.; Shi, W. Y. Interspecies interactions within oral microbial communities. *Microbiology and Molecular Biology Reviews* **2007**, *71* (4), 653-+
- (8) Aas, J. A.; Paster, B. J.; Stokes, L. N.; Olsen, I.; Dewhirst, F. E. Defining the normal bacterial flora of the oral cavity. *J Clin Microbiol* **2005**, *43* (11), 5721-5732
- (9) Mattos-Graner, R. O.; Klein, M. I.; Smith, D. J. Lessons Learned from Clinical Studies: Roles of Mutans Streptococci in the Pathogenesis of Dental Caries. *Current Oral Health Reports* **2014**, *1* (1), 70-78
- (10) Hamada, S.; Slade, H. D. Biology, immunology, and cariogenicity of *Streptococcus mutans*. *Microbiol Rev* **1980**, *44* (2), 331-384
- (11) Lemos, J. A.; Palmer, S. R.; Zeng, L.; Wen, Z. T.; Kajfasz, J. K.; Freires, I. A.; Abranches, J.; Brady, L. J. The Biology of *Streptococcus mutans*. *Microbiol Spectr* **2019**, *7* (1),
- (12) Brady, L. J.; Maddocks, S. E.; Larson, M. R.; Forsgren, N.; Persson, K.; Deivanayagam, C. C.; Jenkinson, H. F. The changing faces of *Streptococcus* antigen I/II polypeptide family adhesins. *Mol Microbiol* **2010**, *77* (2), 276-286
- (13) Jakubovics, N. S.; Strömberg, N.; van Dolleweerd, C. J.; Kelly, C. G.; Jenkinson, H. F. Differential binding specificities of oral streptococcal antigen I/II family adhesins for human or bacterial ligands. *Mol Microbiol* **2005**, *55* (5), 1591-1605

- (14) Larson, M. R.; Rajashankar, K. R.; Crowley, P. J.; Kelly, C.; Mitchell, T. J.; Brady, L. J.; Deivanayagam, C. Crystal structure of the C-terminal region of *Streptococcus mutans* antigen I/II and characterization of salivary agglutinin adherence domains. *J Biol Chem* **2011**, *286* (24), 21657-21666
- (15) Tamesada, M.; Kawabata, S.; Fujiwara, T.; Hamada, S. Synergistic effects of streptococcal glucosyltransferases on adhesive biofilm formation. *J. Dent. Res.* **2004**, *83* (11), 874-879
- (16) Matsumoto-Nakano, M. Role of *Streptococcus mutans* surface proteins for biofilm formation. *Japanese Dental Science Review* **2018**, *54* (1), 22-29
- (17) Bowen, W. H.; Koo, H. Biology of *Streptococcus mutans*-derived glucosyltransferases: role in extracellular matrix formation of cariogenic biofilms. *Caries Res* **2011**, *45* (1), 69-86
- (18) Xiao, J.; Koo, H. Structural organization and dynamics of exopolysaccharide matrix and microcolonies formation by *Streptococcus mutans* in biofilms. *J. Appl. Microbiol.* **2010**, *108* (6), 2103-2113
- (19) Ooshima, T.; Matsumura, M.; Hoshino, T.; Kawabata, S.; Sobue, S.; Fujiwara, T. Contributions of three glycosyltransferases to sucrose-dependent adherence of *Streptococcus mutans*. *J Dent Res* **2001**, *80* (7), 1672-1677
- (20) Hanada, N.; Kuramitsu, H. K. Isolation and characterization of the *Streptococcus mutans* gtfD gene, coding for primer-dependent soluble glucan synthesis. *Infect Immun* **1989**, *57* (7), 2079-2085
- (21) Aoki, H.; Shiroza, T.; Hayakawa, M.; Sato, S.; Kuramitsu, H. K. Cloning of a *Streptococcus mutans* glucosyltransferase gene coding for insoluble glucan synthesis. *Infect Immun* **1986**, *53* (3), 587-594
- (22) Kato, C.; Nakano, Y.; Lis, M.; Kuramitsu, H. Molecular genetic analysis of the catalytic site of *Streptococcus mutans* glucosyltransferases. *Biochemical and biophysical research communications* **1992**, *189* (2), 1184-1188
- (23) Mooser, G.; Wong, C. Isolation of a glucan-binding domain of glucosyltransferase (1, 6- $\alpha$ -glucan synthase) from *Streptococcus sobrinus*. *Infection and Immunity* **1988**, *56* (4), 880-884
- (24) Wong, C.; Hefta, S.; Paxton, R.; Shively, J.; Mooser, G. Size and subdomain architecture of the glucan-binding domain of sucrose: 3- $\alpha$ -D-glucosyltransferase from *Streptococcus sobrinus*. *Infect. Immun.* **1990**, *58* (7), 2165-2170
- (25) Overman, P. R. Biofilm: a new view of plaque. *J. Contemp. Dent. Pract.* **2000**, *1* (3), 18-29
- (26) Ahovuo-Saloranta, A.; Forss, H.; Walsh, T.; Nordblad, A.; Mäkelä, M.; Worthington, H. V. Pit and fissure sealants for preventing dental decay in permanent teeth. *Cochrane Database Syst. Rev.* **2017**, *7* (7), Cd001830

- (27) Baik, A.; Alamoudi, N.; El-Housseiny, A.; Altuwirqi, A. Fluoride Varnishes for Preventing Occlusal Dental Caries: A Review. *Dent. J.* **2021**, *9* (6), 1-15
- (28) Aoun, A.; Darwiche, F.; Al Hayek, S.; Doumit, J. The Fluoride Debate: The Pros and Cons of Fluoridation. *Prev. Nutr. Food Sci.* **2018**, *23* (3), 171-180
- (29) Duffin, S.; Duffin, M.; Grootveld, M. Revisiting Fluoride in the Twenty-First Century: Safety and Efficacy Considerations. *Front. Oral Health* **2022**, *3*, 873157
- (30) Grandjean, P. Developmental fluoride neurotoxicity: an updated review. *Environ. Health* **2019**, *18* (1), 110
- (31) Oyanagi, T.; Tagami, J.; Matin, K. Potentials of mouthwashes in disinfecting cariogenic bacteria and biofilms leading to inhibition of caries. *Open Dent. J.* **2012**, *6*, 23-30
- (32) Kolenbrander, P. E. Oral microbial communities: biofilms, interactions, and genetic systems. *Annu. Rev. Microbiol.* **2000**, *54*, 413-437
- (33) Ren, Z.; Chen, L.; Li, J.; Li, Y. Inhibition of *Streptococcus mutans* polysaccharide synthesis by molecules targeting glycosyltransferase activity. *J. Oral Microbiol.* **2016**, *8*, 31095
- (34) Ren, Z.; Cui, T.; Zeng, J.; Chen, L.; Zhang, W.; Xu, X.; Cheng, L.; Li, M.; Li, J.; Zhou, X.; et al. Molecule Targeting Glucosyltransferase Inhibits *Streptococcus mutans* Biofilm Formation and Virulence. *Antimicrob. Agents Chemother.* **2015**, *60* (1), 126-135
- (35) Taubman, M. A.; Nash, D. A. The scientific and public-health imperative for a vaccine against dental caries. *Nat. Rev. Immunol.* **2006**, *6* (7), 555-563
- (36) Koo, H.; Jeon, J. G. Naturally occurring molecules as alternative therapeutic agents against cariogenic biofilms. *Adv. Dent. Res.* **2009**, *21* (1), 63-68
- (37) Lemos, J. A.; Abranches, J.; Koo, H.; Marquis, R. E.; Burne, R. A. Protocols to study the physiology of oral biofilms. *Methods Mol. Biol.* **2010**, *666*, 87-102
- (38) Nijampatnam, B.; Ahirwar, P.; Pukkanasut, P.; Womack, H.; Casals, L.; Zhang, H.; Cai, X.; Michalek, S. M.; Wu, H.; Velu, S. E. Discovery of Potent Inhibitors of *Streptococcus mutans* Biofilm with Antivirulence Activity. *ACS Med. Chem. Lett.* **2021**, *12* (1), 48-55
- (39) Zhang, Q.; Nijampatnam, B.; Hua, Z.; Nguyen, T.; Zou, J.; Cai, X.; Michalek, S. M.; Velu, S. E.; Wu, H. Structure-Based Discovery of Small Molecule Inhibitors of Cariogenic Virulence. *Sci. Rep.* **2017**, *7* (1), 5974
- (40) Koo, H.; Falsetta, M. L.; Klein, M. I. The exopolysaccharide matrix: a virulence determinant of cariogenic biofilm. *J. Dent. Res.* **2013**, *92* (12), 1065-1073
- (41) Xiao, J.; Klein, M. I.; Falsetta, M. L.; Lu, B.; Delahunty, C. M.; Yates, J. R., 3rd; Heydorn, A.; Koo, H. The exopolysaccharide matrix modulates the interaction

- between 3D architecture and virulence of a mixed-species oral biofilm. *PLoS Pathog.* **2012**, *8* (4), e1002623
- (42) Koo, H.; Xiao, J.; Klein, M. I.; Jeon, J. G. Exopolysaccharides produced by *Streptococcus mutans* glucosyltransferases modulate the establishment of microcolonies within multispecies biofilms. *J. Bacteriol.* **2010**, *192* (12), 3024-3032
  - (43) Bowen, W. H.; Koo, H. Biology of *Streptococcus mutans*-derived glucosyltransferases: role in extracellular matrix formation of cariogenic biofilms. *Caries Res.* **2011**, *45* (1), 69-86
  - (44) Huffines, J. T.; Scofield, J. A. Disruption of *Streptococcus mutans* and *Candida albicans* synergy by a commensal streptococcus. *Sci. Rep.* **2020**, *10* (1), 19661
  - (45) Huffines, J. T.; Stoner, S. N.; Baty, J. J.; Scofield, J. A. Nitrite Triggers Reprogramming of the Oral Polymicrobial Metabolome by a Commensal *Streptococcus*. *Front. Cell Infect. Microbiol.* **2022**, *12*, 833339
  - (46) Peterson, R. L. Strategies Using Bio-Layer Interferometry Biosensor Technology for Vaccine Research and Development. *Biosens.* **2017**, *7*, 49
  - (47) Barrows, J. K.; Dyke, M. W. Biolayer interferometry for DNA-protein interactions. *PLoS ONE.* **2022**, *17*, e0263322
  - (48) Shah, N. B.; Duncan, T. M. Bio-layer Interferometry for Measuring Kinetics of Protein-protein Interactions and Allosteric Ligand Effects. *J. Vis. Exp.* **2014**, *84*, e51383
  - (49) Kabsch, W. XDS. *Acta Crystallogr. D.* **2010**, *66*, 125-132
  - (50) Kabsch, W. Integration, scaling, space-group assignment and post-refinement. *Acta Crystallogr. D Biol. Crystallogr.* **2010**, *66*, 133-144
  - (51) Evans, P. R. An introduction to data reduction: space-group determination, scaling and intensity statistics. *Acta Crystallogr. D Biol. Crystallogr.* **2011**, *67*, 282-292
  - (52) Winn, M. D.; Ballard, C. C.; Cowtan, K. D.; Dodson, E. J.; Emsley, P.; Evans, P. R.; Keegan, R. M.; Krissinel, E. B.; Leslie, A. G.; McCoy, A.; et al. Overview of the CCP4 suite and current developments. *Acta Crystallogr. D Biol. Crystallogr.* **2011**, *67*, 235-242
  - (53) Murshudov, G. N.; Vagin, A. A.; Dodson, E. J. Refinement of macromolecular structures by the maximum-likelihood method. *Acta Crystallogr. D Biol. Crystallogr.* **1997**, *53*, 240-255
  - (54) Afonine, P. V.; Grosse-Kunstleve, R. W.; Echols, N.; Headd, J. J.; Moriarty, N. W.; Mustyakimov, M.; Terwilliger, T. C.; Urzhumtsev, A.; Zwart, P. H.; Adams, P. D. Towards automated crystallographic structure refinement with phenix.refine. *Acta Crystallogr. D Biol. Crystallogr.* **2012**, *68*, 352-367
  - (55) Liebschner, D.; Afonine, P. V.; Baker, M. L.; Bunkóczi, G.; Chen, V. B.; Croll, T. I.; Hintze, B.; Hung, L. W.; Jain, S.; McCoy, A. J.; et al. Macromolecular structure

determination using X-rays, neutrons and electrons: recent developments in Phenix. *Acta Crystallogr. D Struct. Biol.* **2019**, *75*, 861-877

- (56) Emsley, P.; Lohkamp, B.; Scott, W. G.; Cowtan, K. Features and development of Coot. *Acta Crystallogr. D Biol. Crystallogr.* **2010**, *66*, 486-501
- (57) Davies, G. J.; Wilson, K. S.; Henrissat, B. Nomenclature for sugar-binding subsites in glycosyl hydrolases. *Biochem. J.* **1997**, *321* ( Pt 2) (Pt 2), 557-559
- (58) Zhang, Q.; Ma, Q.; Wang, Y.; Wu, H.; Zou, J. Molecular mechanisms of inhibiting glucosyltransferases for biofilm formation in *Streptococcus mutans*. *Int. J. Oral Sci.* **2021**, *13* (1), 30
- (59) Hazlett, K. R.; Michalek, S. M.; Banas, J. A. Inactivation of the *gbpA* gene of *Streptococcus mutans* increases virulence and promotes in vivo accumulation of recombinations between the glucosyltransferase B and C genes. *Infect. Immun.* **1998**, *66* (5), 2180-2185
- (60) Michalek, S. M.; McGhee, J. R.; Shiota, T.; Devenyns, D. Virulence of *Streptococcus mutans*: cariogenicity of *S. mutans* in adult gnotobiotic rats. *Infect. Immun.* **1977**, *15* (2), 466-471
- (61) Liu, C.; Worthington, R. J.; Melander, C.; Wu, H. A new small molecule specifically inhibits the cariogenic bacterium *Streptococcus mutans* in multispecies biofilms. *Antimicrob. Agents Chemother.* **2011**, *55* (6), 2679-2687
- (62) Zhang, Q.; Nguyen, T.; McMichael, M.; Velu, S. E.; Zou, J.; Zhou, X.; Wu, H. New small-molecule inhibitors of dihydrofolate reductase inhibit *Streptococcus mutans*. *Int. J. Antimicrob. Agents* **2015**, *46* (2), 174-182
- (63) Lynch, D. J.; Michalek, S. M.; Zhu, M.; Drake, D.; Qian, F.; Banas, J. A. Cariogenicity of *Streptococcus mutans* glucan-binding protein deletion mutants. *Oral Health Dent. Manag.* **2013**, *12* (4), 191-199
- (64) Peng, X.; Zhang, Y.; Bai, G.; Zhou, X.; Wu, H. Cyclic di-AMP mediates biofilm formation. *Mol. Microbiol.* **2016**, *99* (5), 945-959
- (65) Keyes, P. H. Dental caries in the molar teeth of rats. II. A method for diagnosing and scoring several types of lesions simultaneously. *J. Dent. Res.* **1958**, *37* (6), 1088-10

CHAPTER 3: PH-RESPONSIVE DELIVERY OF BIOFILM INHIBITOR HA5 TO  
ABROGATE *STREPTOCOCCUS MUTANS* CARIOGENIC BIOFILMS

by

PARMANAND AHIRWAR, VERONIKA KOZLOVSKAYA, DANIEL INMAN,  
MAKSIM DOLMAT, GREGORY J. HARBER, SUZANNE M. MICHALEK,  
EUGENIA KHARLAMPIEVA AND SADANANDAN E. VELU.

Part of this chapter is adapted with permission from *J. Med. Chem.* **2023**, 66, 7909-7925.  
Copyright © 2023, American Chemical Society.



## ABSTRACT

This chapter focuses on the development of novel drug delivery platforms for the pH-responsive delivery of biofilm inhibitors for the prevention and treatment of dental caries. The most active biofilm inhibitor **HA5** identified by the studies from the previous chapters was encapsulated into pH-responsive hydrogel microparticles to form hydrogel encapsulated biofilm inhibitor (**HEBI**). **HEBI** selectively inhibited *S. mutans* biofilms similar to **HA5** without affecting the planktonic growth of the commensal streptococcal species *S. gordonii* and *S. sanguinis*. Treatment of *S. mutans* infected rats with 100  $\mu$ M of **HEBI** for 4 weeks resulted in a significant reduction in buccal, sulcal, and proximal dental caries compared to untreated control group and the results were comparable to 100  $\mu$ M **HA5** treatment. Bacterial colonization was not significantly affected by the treatment with **HEBI**. Moreover, the rats treated with **HEBI** did not experience any weight loss over the course of the study in comparison with the control group, suggesting that **HEBI** is non-toxic. Taken together, our data suggests that **HEBI** can release the biofilm inhibitor **HA5** under the acidic conditions of the caries infected oral cavity and can prevent development of carious lesions similar to **HA5** treatment. Overall, the biofilm-specific therapy using **HEBI** reported here is a viable approach for prevention and treatment of dental caries while preserving the oral microbiome.

## INTRODUCTION

Dental caries is a major health concern in United States as it affects about 90 % of its population. This disease is attributed to the formation of bacterial colonies on tooth surface known as biofilms, which cause the erosion of hydroxyapatite material of the tooth enamel over time. This erosion is caused by the byproducts of sugar metabolism such as lactic acid produced within biofilms.<sup>1</sup> Dental biofilm consists of more than 700 bacterial species.<sup>2, 3</sup> Biofilm formation is initiated by the attachment of commensal *streptococci* such as *S. gordonii* and *S. sanguinis* to the saliva-coated tooth surface, which then engages in developing intra- and inter-species bacterial interactions.<sup>4-6</sup> Under the disease conditions, the delicate balance between commensal and pathogenic members of the plaque bacteria is disturbed, leading to an overgrowth of pathogenic species.<sup>7, 8</sup> *S. mutans* has been implicated as the major etiological agent in the initiation and propagation of this disease.<sup>9</sup> The formation of tenacious biofilms is the hallmark of *S. mutans* induced cariogenesis. Therefore, the studies aimed at developing dental caries treatments should be focused on selective inhibitors of biofilms that do not affect the growth of oral commensal bacteria.

Major virulence factors of *S. mutans* that significantly contribute to its ability to form cariogenic biofilm are its extracellular glucosyltransferases (Gtfs).<sup>10</sup> Most strains of *S. mutans* harbor three distinct *gtf* genes expressing different Gtf activities. The genes *gtfB* codes for GtfB enzyme that synthesizes predominantly water-insoluble glucans,<sup>11, 12</sup> while *gtfC* codes for GtfC that synthesizes both water-insoluble and soluble glucans.<sup>13, 14</sup> The gene *gtfD* codes for GtfD enzyme that synthesizes soluble glucans.<sup>15</sup> Previous gene knockout studies have shown that *S. mutans* GtfB and GtfC are essential for glucan

synthesis, bacterial colonization and cariogenesis.<sup>16</sup> Therefore, small molecules inhibitors of *S. mutans* Gtfs<sup>17-20</sup> have potential application in treating and preventing dental caries.

Many known anti-biofilm agents display undesirable efficacy within the oral cavity due to poor solubility, inability to penetrate biofilms and lack of retention in the locally infected areas.<sup>21</sup> Given these challenges, antibacterial nanomaterials have generated recent interest in anti-caries research due to their potential for drug-delivery applications. Examples of such materials are silver nanoparticles in the prevention of dental caries,<sup>22</sup> farnesol and myricetin co-loaded nanoparticles to inhibit biofilms,<sup>23</sup> pH responsive materials to deliver farnesol,<sup>24, 25</sup> porous silicon microparticles to mitigate cariogenic biofilm<sup>26</sup>, ferumoxytol nanoparticles,<sup>27, 28</sup> poly(ethylenimine)<sup>29</sup> and chitosan nanoparticles<sup>30</sup> with strong antibacterial activity against *S. mutans*. Several nano systems for controlled release of anti-caries drugs have also been explored including mesoporous silica nanoparticle,<sup>31, 32</sup> liposome,<sup>33</sup> halloysite nano-tube,<sup>34</sup> polyamidoamine<sup>35</sup> and dextran-coated Iron oxide nanoparticles (nanozymes).<sup>36</sup> Despite the flurry of these recent studies, none of these agents are translated for clinical use as their *in vivo* efficacies are either modest or not proven.

Since the pH level in the oral cavity is critical for the demineralization of tooth enamel, our efforts were focused on developing a novel drug delivery system with built-in pH-sensitivity for the delivery of biofilm inhibitors as an anti-caries treatment. Under physiological conditions, the human salivary system maintains a healthy pH range of 6.0 - 7.5 in the oral cavity<sup>37, 38</sup> using three buffer systems: 1) bicarbonate, 2) phosphate, and 3) salivary proteins.<sup>39, 40</sup> A salivary pH below 5.5 is potentially harmful to the hard and soft tissues in the oral cavity.<sup>39, 41, 42</sup> Under pathogenic oral conditions, biofilms ferment dietary

carbohydrates to produce acidic byproducts such as lactic acid, which decreases the pH and causes the demineralization of tooth enamel.<sup>43</sup> Therefore, a drug that can specifically inhibit the biofilm delivered into the oral cavity in a pH-responsive manner would be highly desirable.

In the previous chapters, we evaluated the biofilm inhibitory properties of two classes of aurone compounds called methoxyaurones and hydroxyaurones. Additionally, we examined the inhibitory effects of these compounds on the growth of *S. mutans* and commensal streptococcal strains, *S. gordonii* and *S. sanguinis*. Two lead compounds selected based on their activity and selectivity towards pathogenic biofilm inhibition, **HA5** and **HA6** were further investigated for the inhibition of glucan production, GtfB binding using OctetRed96, and the *in vivo* anticariogenic activities in an *S. mutans* induced experimental rat model of dental caries. In these studies, **HA5** consistently showed higher solubility, better biofilm inhibition properties and anticaries activity compared to **HA6** (Figure 3.1), and thus was selected as the candidate for the encapsulation studies.

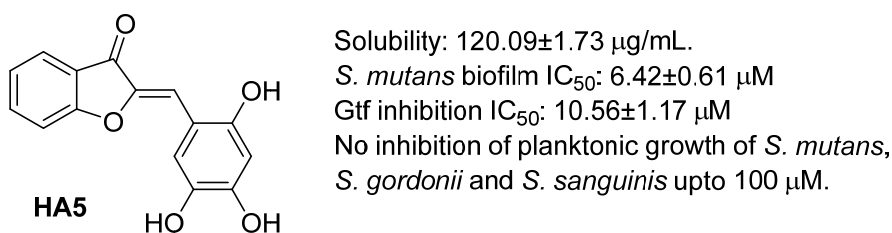


**Figure 3.1:** Chemical structure, solubility, and bioactivities of **HA5**.

## RESULTS AND DISCUSSION

In this chapter, we report the use of pH-responsive hydrogel microparticles to encapsulate **HA5** to produce hydrogel encapsulated biofilm inhibitor called **HEBI**, and its *in vitro* and *in vivo* evaluations to establish its potential to be a dental caries treatment.

### Synthesis and characterization of **HA5**

The synthesis of **HA5** was performed on a larger scale to meet the requirements of its applications in the hydrogel encapsulation and the subsequent *in vivo* studies. Various steps were involved in the synthesis process, leading to the successful production of **HA5** (Figure 3.2). The initial step in the synthesis involved an aldol condensation reaction. Specifically, 2'-hydroxyacetophenone and 2,4,5-trimethoxybenzaldehyde were utilized as the starting materials. The reaction was carried out in the presence of potassium hydroxide as a base. This aldol condensation reaction was highly efficient, resulting in a 90 % yield of the desired product, chalcone **3e**. After obtaining the chalcone **3e**, the next step involved its cyclization. Mercuric acetate was employed for this purpose. Pyridine played a dual role in this reaction, acting as both a base and a solvent. The cyclization of chalcone **3e** proceeded smoothly, leading to the formation of methoxyaurone **MA5** in quantitative yield. Finally, the synthesized methoxyaurone **MA5** underwent demethylation using boron tribromide. This demethylation reaction was crucial to introduce hydroxyl groups, resulting in the formation of the final product, hydroxyaurone **HA5**. The demethylation reaction produced **HA5** as orange-red solid with a yield of 74 %. Figure 3.2 illustrates the sequential transformations and structural changes that occur during the synthesis of **HA5**, highlighting the key intermediates and final product.

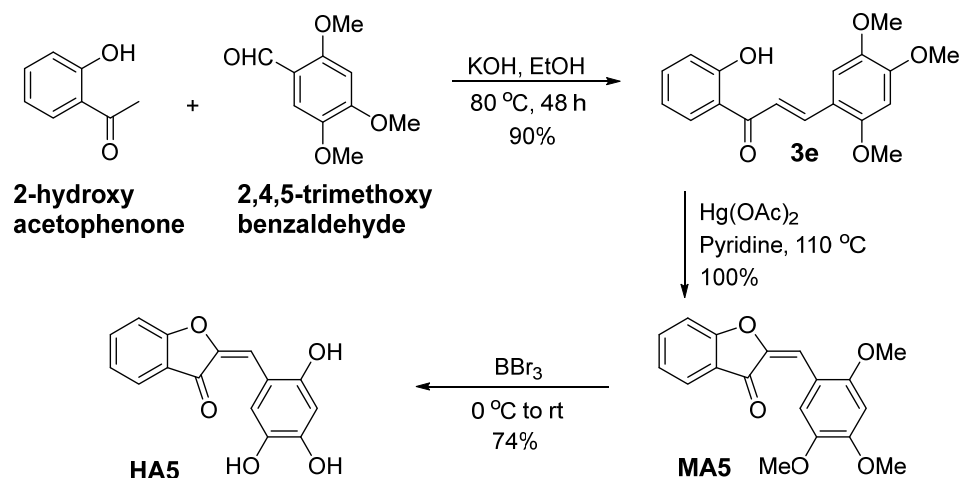


**Figure 3.2:** Synthesis of **HA5**

Following the synthesis of **HA5**, purification was carried out using silica gel column chromatography. This purification technique is commonly employed to separate and purify organic compounds based on their polarity and other physical properties. Silica gel, packed in a column, acts as the stationary phase, while a suitable solvent system is used as the mobile phase. By carefully controlling the elution conditions, impurities can be separated from the target compound. Purified **HA5** underwent a series of analytical techniques to ensure its structural integrity and purity. The first technique employed was  $^1\text{H}$ -NMR (proton nuclear magnetic resonance), which provides valuable information about the chemical environment and connectivity of hydrogen atoms in the compound. The  $^{13}\text{C}$ -NMR (carbon-13 nuclear magnetic resonance) technique was also utilized to gain insights into the carbon atom environments and connectivity in **HA5**. These NMR techniques are powerful tools for structural elucidation and confirmation of organic compounds. Furthermore, high-resolution mass spectrometry (HRMS) was employed to determine the accurate molecular weight of **HA5**. HRMS offers superior mass accuracy, enabling precise

determination of the molecular formula. This technique is particularly useful for confirming the molecular composition and verifying the synthesis of the desired compound. The calculated molecular weight for **HA5**, assuming the molecular formula  $C_{15}H_{10}O_5$ , was found to be 270.0528 atomic mass units (amu) whereas, the experimental measurement from the HRMS analysis yielded a molecular weight of 270.0529 amu. The close agreement between the calculated and found molecular weights demonstrates the successful synthesis and characterization of the compound with confirmed molecular formula.

To assess the purity of the synthesized **HA5**, high-performance liquid chromatography (HPLC) was utilized. HPLC is a widely used technique for separating, quantifying, and evaluating the purity of compounds in a mixture. By comparing the retention time and peak area of the target compound with those of known standards, the purity of **HA5** can be determined. The HPLC traces obtained for **HA5** demonstrated a purity of 99.64 %, indicating a high degree of homogeneity and minimal impurities in the sample. Figure 3.3 was included to provide a visual representation of the HPLC trace, showing the sharp and well-defined peak corresponding to **HA5**. This peak's purity assessment reinforces the suitability of the synthesized **HA5** for further encapsulation and evaluation, ensuring that the compound is of high quality and ready for subsequent studies. The combination of silica gel column chromatography, along with the analytical techniques such as NMR, HRMS, and HPLC, ensures the purification, comprehensive characterization, and assessment of purity of **HA5**. These steps are crucial in guaranteeing the reliability, reproducibility, and suitability of **HA5** for its intended applications in hydrogel encapsulation and subsequent evaluation studies.

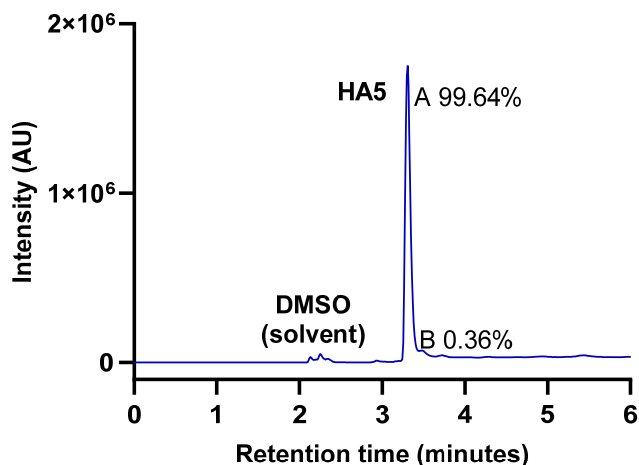


**Figure 3.3:** HPLC trace of **HA5** showing 99.64 % purity

### Hydrogel encapsulated biofilm inhibitor (HEBI)

Hydrophilicity, the ease of chemical modification and structural stability of hydrogel matrices ensure excellent biocompatibility and versatility for its use in biomedical applications. Poly(methacrylic acid) [PMAA] hydrogel is an excellent platform for the pH-triggered drug delivery of the biofilm inhibitors as these respond to varying pH due to the existence of ionizable pendant groups (e.g.  $-\text{COOH}$  and  $-\text{NH}_2$ ) in the network. In previous studies, PMAA hydrogels have been prepared by layer-by-layer (LbL) assembly of hydrogen-bonded polymers of PMAA and poly(N-vinylpyrrolidone) (PVPON). The PMAA and PVPON layers were alternately adsorbed onto surfaces of porous inorganic microparticles of manganese oxide, followed by chemical crosslinking of PMAA with ethylenediamine and dissolution of the manganese oxide template microparticles.<sup>44-46</sup> The nanoscale multilayers of chemically crosslinked PMAA result in the interconnected porous hydrogel structure, which provides excellent drug loading capacity. Besides, the pH-responsiveness of the hydrogel can be easily tuned during particle formation by using pH-



sensitive cross-linkers.<sup>47, 48</sup> We have recently demonstrated the biocompatibility and degradability of hydrogel biomaterial in the delivery of small-molecule drugs.<sup>46</sup>

### **Encapsulation of HA5 in (PMAA)<sub>5</sub> hydrogels microparticles**

Compound **HA5** was encapsulated in the (PMAA)<sub>5</sub> hydrogel cubes through post-loading by soaking the hydrogels in 5 mg/mL solution of **HA5** in methanol for 48 h in the dark to produce hydrogel encapsulated biofilm inhibitor (**HEBI**, Figures 3.4A-B). The free, non-encapsulated **HA5** was removed from particle solution by rinsing with HEPES buffer (pH = 7.4) five times using centrifugation at 5000 rpm for 10 min. The **HA5** quantification was carried out with UV-Vis spectroscopy (NanoDrop One C, ThermoFisher) at  $\lambda = 448$  nm using an **HA5** calibration curve. The drug solution was analyzed before and after the exposure to the hydrogel particles and the differences in the absorbance spectra were used to determine the loading of the drug into the hydrogel network. The loading capacity was found to be  $5.5 \times 10^{-3}$  ng of **HA5** per particle.

To demonstrate the tooth adhesion of (PMAA)<sub>5</sub> hydrogel microparticles, a drop of the hydrogel particle dispersion was placed on the tooth surface and dried at room temperature for 10 min in a Petri dish and morphology of the hydrogels were analyzed using atomic force microscopy (AFM NTEGRA II microscope: NT-MDT) imaging. The AFM silicon probes NSG30 (NT-MDT, resonance frequency 240-440 kHz, force constant 22-100 N m<sup>-1</sup>, tip radii is 10 nm, scan rate is 0.5 Hz) were used for imaging the tooth surfaces in tapping mode before and after hydrogel adhesion. The AFM image shows that the bare tooth surface displays natural topography (Figure 3.4C) with height of 280 nm. After hydrogel addition, the cubical hydrogel particles are seen to adhere to the tooth surface (Figures 3.4D-E). The height of the dried hydrogel cubes was determined using

section profiles, which indicated an average particle height of  $1.3 \pm 0.2 \mu\text{m}$ . The hydrogel cubes decreased in size compared to their size in solution due to the hydrogel shrinkage upon drying.<sup>46</sup>

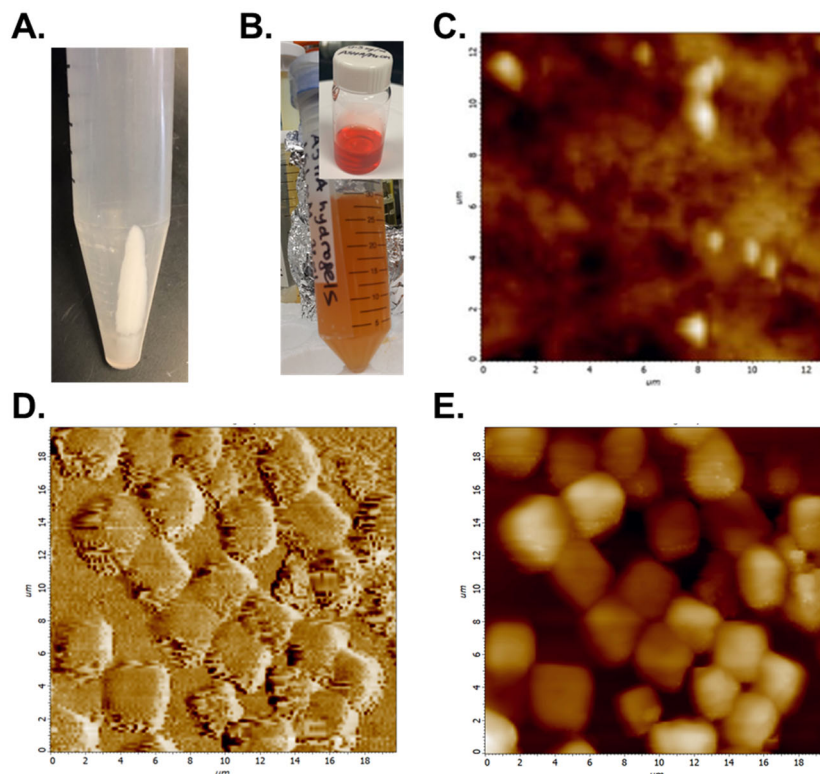


**Figure 3.4:** **A)** Optical images of empty (PMAA)<sub>5</sub> hydrogel microparticles. **B)** HA5-loaded hydrogel HEBI and HA5 in methanol (insert B). **C)** Atomic Force Microscopy (AFM) topography images of a tooth surface with height of 280 nm. **D)** AFM image after (PMAA)<sub>5</sub> hydrogel adsorption, cubical hydrogel particles are clearly seen sticking to the tooth surface. **E)** Amplitude error image of empty (PMAA)<sub>5</sub> hydrogels dried on the surface of a tooth. Scan size is  $20 \mu\text{m}^2$  in both images, the height (z)-scale is  $1.7 \mu\text{m}$ .

### Inhibition of *S. mutans* and commensal species biofilms by HEBI

To assess whether the compound HA5 is released from HEBI at the low pH of biofilm assay conditions and the biofilm inhibitory activity of HA5 is preserved, we employed hydroxyapatite (HA) disc assay. Usually, we use *S. mutans* biofilm inhibition assays using 96 well plates to assess biofilm inhibition activity of an inhibitor, but in case

of hydrogels, these assays could not be used in their original form because hydrogel microparticles tend to settle down during the course of experiment and do not allow bacteria to make biofilms at the bottom of the plate. To address this issue, we used HA discs and allowed the biofilms to be formed on surface of these discs submerged in the wells of the 96 well plate. The biofilms so formed were stained with crystal violet and quantified by dissolving in 30 % acetic acid and reading OD<sub>562</sub>. These experiments were conducted using a single dose of 25  $\mu$ M **HEBI** and 25  $\mu$ M **HA5** side by side. The results of the HA disc assays indicate that both **HA5** and **HEBI** exhibit similar inhibitory effects on *S. mutans* biofilm displaying about 90 % and 85 % inhibition of biofilm respectively (Figure 3.5A). Similar biofilm inhibition evaluations were conducted using the commensal streptococci *S. gordonii* and *S. sanguinis* using a single dose of 25  $\mu$ M **HEBI** and 25  $\mu$ M **HA5** side by side. No significant inhibition of commensal biofilm was observed except in the case of **HA5** against *S. gordonii* biofilm, which was inhibited by 10-20 % (Figure 3.5B-C).

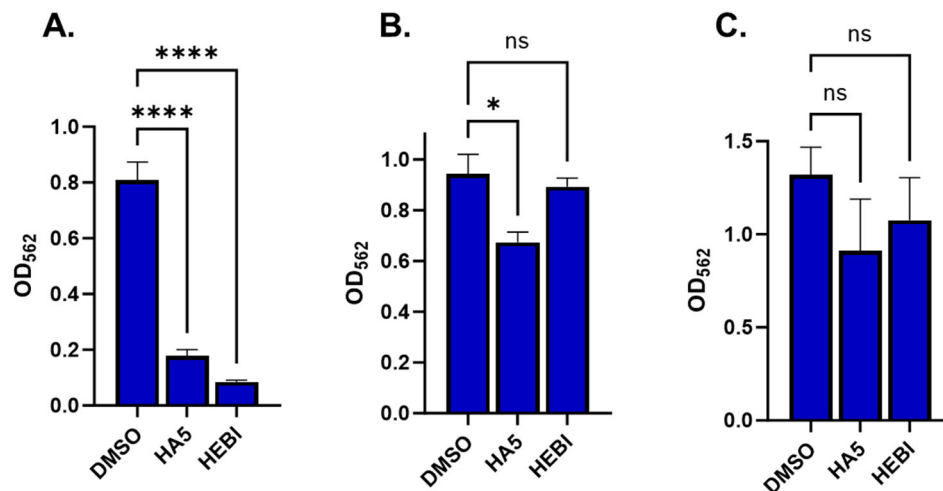


**Figure 3.5:** A) *S. mutans*, B) *S. gordonii*, and C) *S. sanguinis* biofilm inhibition by **HA5** and **HEBI**. 25  $\mu$ M of **HA5** or **HEBI** were co-incubated with *S. mutans*, *S. gordonii* or *S. sanguinis* bacteria

with  $OD_{470} = 1$ , for 16 h at 37 °C, 5 %  $CO_2$ . Biofilms were stained with crystal violet and absorbance was read at 562 nm. Each of the biofilm and growth assays were conducted in triplicate and statistical significance was tested with one-way ANOVA.  $P < 0.0001$  for **A**,  $p = 0.0252$  for **B**,  $p = 0.4773$  for **C**.

### HEBI is not bactericidal to pathogenic and commensal streptococci

Both **HEBI** and **HA5** were assessed at a single concentration of 25  $\mu$ M to determine their impact on the planktonic growth of *S. mutans* as well as the commensal species *S. gordonii* and *S. sanguinis*. Interestingly, no significant inhibition of growth was observed for either **HEBI** or **HA5** when it came to the planktonic growth of pathogenic *S. mutans* bacteria (Figure 3.6A). Similarly, **HEBI** or **HA5** did not show any growth inhibitory effects on the commensal streptococci species *S. gordonii* and *S. sanguinis* (Figures 3.6B-C).

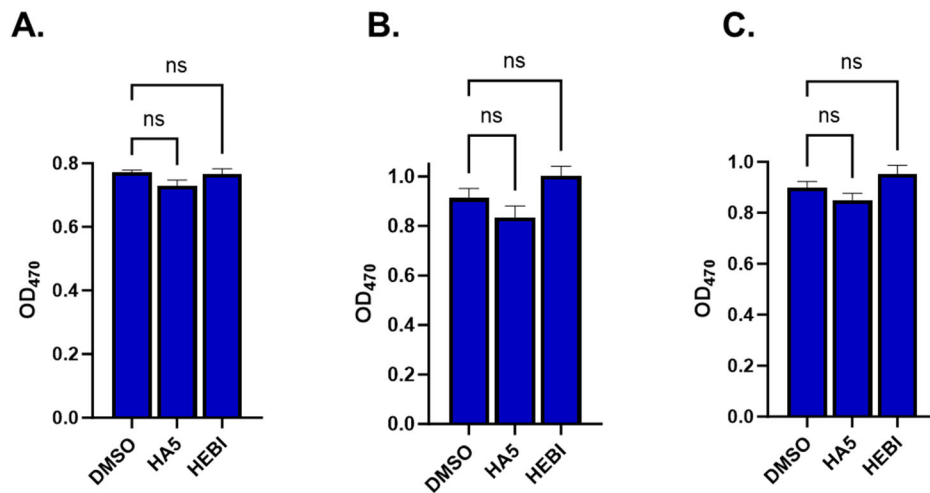


**Figure 3.6:** A) *S. mutans*, B) *S. gordonii*, and C) *S. sanguinis* growth inhibition by **HA5** and **HEBI**. 25  $\mu$ M of **HA5** or **HEBI** were co-incubated with *S. mutans*, *S. gordonii* or *S. sanguinis* bacteria with  $OD_{470} = 1$ , for 16 h at 37 °C, 5 %  $CO_2$ . Growth of bacteria was measured at  $OD_{470}$ .  $P = 0.0957$  for **A**,  $p = 0.7167$  for **B**,  $p = 0.0551$  for **C**.

### Reduction of *S. mutans* virulence *in vivo* by **HEBI**

The effects of **HEBI** on *S. mutans* virulence were evaluated using a well-established experimental rat model of dental caries.<sup>49, 50</sup> Hydrogel microparticles with no drug were used to ensure that the observed anti-virulence activity observed with **HEBI** was not related to the hydrogel material. The standard NaF (250 ppm) was included as a positive control. A (vehicle + infection only) group was included as a negative control. All rats in the experimental groups and control groups were colonized with *S. mutans* UA159. A 4-week treatment of *S. mutans* UA159 infected gnotobiotic rats with 100  $\mu$ M **HEBI** resulted in significant reduction in buccal, sulcal and proximal caries scores compared to control groups. (Tables 3.1-3.3). We were unable to record the effect of the treatment on Dentinal moderate (Dm) and Dentinal extensive (Dx) scores in the proximal area as there were no significant proximal dentinal lesions for the control and treated groups in this study. In comparison, the group treated with hydrogel (no drug) did not show any inhibition compared to the control group suggesting that the hydrogel as such has no antivirulence activity (Tables 3.1-3.3). The observed reduction in caries scores by **HEBI** were similar to **HA5** treatment with **HEBI** displaying slightly better *in vivo* activity, possibly due to the pH-dependent slow release of the drug by **HEBI**. The observed reduction in caries scores by **HEBI** was lower than the 250 ppm NaF treatment. However, it should be noted that the concentration of NaF (250 ppm = 5.95 mM) is about 59-fold higher than **HA5** (100  $\mu$ M). The effect on bacterial colonization was not significant in **HEBI** treated animals when compared to control group, while the bacterial colonization appears to be slightly reduced in unloaded hydrogel treated rats (Table 3.4). Moreover, the **HEBI** treated rats did not experience any weight loss over the course of the study in comparison with the control

group, suggesting that they are non-toxic (Table 3.4). Overall, our data suggest that **HEBI** can release **HA5** in the rat's oral cavity under the acidic conditions of dental caries and the reduction in caries scores produced by **HEBI** is comparable to what was observed for **HA5** treatment alone.

**Table 3.1:** Effect of **HEBI** treatment on *S. mutans* UA159 induced buccal caries.

Treatment Group	Buccal Mean Caries Scores ( $\pm$ SEM)			
	E	Ds	Dm	Dx
<b>UA159 untreated</b>	14.6 $\pm$ 0.2	10.2 $\pm$ 0.4	6.0 $\pm$ 0.0	3.2 $\pm$ 0.5
<b>Hydrogel (no drug)</b>	15.0 $\pm$ 0.3	9.6 $\pm$ 0.8	6.4 $\pm$ 0.7	3.8 $\pm$ 1.1
<b>HEBI (100 <math>\mu</math>M)</b>	7.4 $\pm$ 1.1	5.2 $\pm$ 1.2	2.4 $\pm$ 0.7	1.4 $\pm$ 0.6
<b>HA5 (100 <math>\mu</math>M)</b>	11.0 $\pm$ 0.3	6.0 $\pm$ 0.4	3.8 $\pm$ 0.2	2.0 $\pm$ 0.7
<b>NaF (250 ppm)</b>	5.0 $\pm$ 0.7	2.4 $\pm$ 0.8	1.0 $\pm$ 0.8	0.0 $\pm$ 0.0

*Enamel (E); Dental slight (Ds); Dental moderate (Dm); Dental extensive (Dx)*

**Table 3.2:** Effect of **HEBI** treatment on *S. mutans* UA159 induced sulcal caries.

Treatment Group	Sulcal Mean Caries Scores ( $\pm$ SEM)			
	E	Ds	Dm	Dx
<b>UA159 untreated</b>	25.6 $\pm$ 0.2	17.8 $\pm$ 0.2	10.4 $\pm$ 0.2	4.2 $\pm$ 0.2
<b>Hydrogel (no drug)</b>	27.0 $\pm$ 0.5	19.6 $\pm$ 0.4	12.4 $\pm$ 0.9	6.8 $\pm$ 0.5
<b>HEBI (100 <math>\mu</math>M)</b>	16.0 $\pm$ 0.6	12.6 $\pm$ 0.2	6.8 $\pm$ 0.7	4.0 $\pm$ 0.0
<b>HA5 (100 <math>\mu</math>M)</b>	22.0 $\pm$ 0.6	16.2 $\pm$ 0.4	8.8 $\pm$ 0.9	4.4 $\pm$ 0.9
<b>NaF (250 ppm)</b>	14.2 $\pm$ 0.7	11.2 $\pm$ 0.4	4.6 $\pm$ 0.2	1.0 $\pm$ 0.3

*Enamel (E); Dental slight (Ds); Dental moderate (Dm); Dental extensive (Dx)*

**Table 3.3:** Effect of **HEBI** treatment on *S. mutans* UA159 induced proximal caries.

Treatment Group	Proximal Mean Caries Scores ( $\pm$ SEM)	
	E	Ds
<b>UA159 untreated</b>	6.0 $\pm$ 0.0	4.0 $\pm$ 0.0
<b>Hydrogel (no drug)</b>	6.8 $\pm$ 0.5	4.4 $\pm$ 0.4
<b>HEBI (100 <math>\mu</math>M)</b>	3.6 $\pm$ 0.4	0.0 $\pm$ 0.0
<b>HA5 (100 <math>\mu</math>M)</b>	4.0 $\pm$ 0.0	3.8 $\pm$ 0.2
<b>NaF (250 ppm)</b>	1.2 $\pm$ 0.8	0.0 $\pm$ 0.0

*Enamel (E); Dentinal slight (Ds); Dentinal moderate (Dm) and Dentinal extensive (Dx) scores are not included as there were no significant proximal dentinal lesions for the control and treated groups in this study*

**Table 3.4:** Effect of **HEBI** treatment on *S. mutans* UA159 CFU and the body weight of the animals.

Treatment Group	CFU/mL (x 10 <sup>6</sup> )		Animals	
	MS	BAP	Weight (g)	Number
<b>UA159 untreated</b>	4.2 $\pm$ 1.4	5.6 $\pm$ 1.6	141 $\pm$ 13	5
<b>Hydrogel (no drug)</b>	1.6 $\pm$ 0.5	2.4 $\pm$ 0.7	130 $\pm$ 9	5
<b>HEBI (100 <math>\mu</math>M)</b>	5.2 $\pm$ 1.4	5.5 $\pm$ 1.4	145 $\pm$ 12	5
<b>HA5 (100 <math>\mu</math>M)</b>	2.5 $\pm$ 0.8	3.0 $\pm$ 1.0	137 $\pm$ 13	5
<b>NaF (250 ppm)</b>	3.4 $\pm$ 0.5	4.0 $\pm$ 0.9	161 $\pm$ 13	5

*Colony Forming Unit (CFU); Mitis Salivarius agar (MS); Blood Agar Plates (BAP).*

## CONCLUSIONS

Based on better solubility, biofilm inhibitory property, lack of effect on oral commensal species, and ability to preserve oral microbiome, the lead biofilm inhibitor **HA5** was selected for encapsulation studies. **HA5** was synthesized in larger scale and characterized by spectroscopic techniques to meet the purity requirements for the *in vivo* study. **HA5** was then encapsulated into pH-responsive hydrogel to generate hydrogel

encapsulated biofilm inhibitor, **HEBI**. The selective biofilm inhibitory effects vs bacterial growth by **HEBI** have been demonstrated. The anticariogenic activity of **HEBI** has been demonstrated *in vivo*. A 4 week treatment of *S. mutans* UA159 infected gnotobiotic rats with 100  $\mu$ M of **HEBI** resulted in significant reduction in buccal, sulcal, and proximal dental caries scores compared to untreated control groups. Our data suggests that **HEBI** can release **HA5** in the oral cavity under the acidic conditions of dental caries infection and the reduction in caries scores produced by this material are comparable to what was observed for **HA5** treatment alone. Taken together, our data suggests that the biofilm-specific therapy using **HEBI** reported here is a viable approach for prevention and treatment of dental caries while preserving the oral microbiome.

## EXPERIMENTAL SECTION

### General considerations

Poly(ethyleneimine) (PEI, average MW 25000), ethylenediamine (EDA), manganese sulfate monohydrate, ammonium bicarbonate and 1-Ethyl-3-(3-(dimethylamino)propyl)-carbodiimide hydrochloride were purchased from Sigma-Aldrich. Poly(methacrylic acid) (PMAA, average Mw 22000 g mol<sup>-1</sup>,  $\bar{D}$  = 1.3) were purchased from Fisher Scientific. Ultrapure de-ionized (DI) water with a resistivity of 18.2 M $\Omega$ -cm at 25 °C was used in all experiments. Monobasic and dibasic sodium phosphate (Fisher Scientific) were used for preparation of polymer and buffer solutions. Poly(N-vinylpyrrolidone) (PVPON, Mw 10000 g mol<sup>-1</sup>) was purchased from MilliporeSigma.

The bacterial strains, *S. mutans* UA159, *S. gordonii* DL1, and *S. sanguinis* SK36 were inoculated statically at 37 °C under 5 % CO<sub>2</sub> in Todd Hewitt Broth (THB) for 24 h.



The cultures were then diluted with fresh THB (1:5) and reinoculated until optical density at 470 nm (OD<sub>470</sub>) reached 1. The optical density was read using BioTtek 800TS microplate reader at 470 nm for bacterial growth and 562 nm for biofilm stained with crystal violet. Data was plotted in Graphpad Prism 9.5.1.

The <sup>1</sup>H-NMR and <sup>13</sup>C-NMR spectra were recorded using Bruker Avance Neo 400 and Avance II 700 spectrometers, with TMS or appropriate solvent signals as internal standards for referencing the chemical shifts (reported in ppm) and coupling constants (measured in Hz). High-resolution mass spectra (HRMS) were obtained using a Waters AutoSpec-Ultima™ NT magnetic sector mass spectrometer with Electron Impact (EI) Ionization source. The mass analyzer employed was an electric-magnetic-electric (EBE) sector, specifically a double focusing sector, ensuring accurate mass measurements. Anhydrous solvents were purchased from MilliporeSigma in Sure-Seal™ bottles, and other chemical reagents were sourced from MilliporeSigma or Fisher and used without purification. The progress of reactions was monitored using thin-layer chromatography (TLC) on silica gel plates with a fluorescent indicator (Silicycle, silica gel, UV254, 25 μm plates). TLC spots were observed under UV light at wavelengths of 254 nm and 365 nm. For purification, column chromatography was employed using Si gel (32-63 μm) from Dynamic Absorbent, Inc., allowing separation based on compound polarity and physical properties. Melting points of compounds were determined using an uncorrected Mel-Temp II melting point apparatus. Final compound had a minimum purity of 95 % as determined by high-performance liquid chromatography (HPLC). HPLC traces were obtained using a Shimadzu SPD-M20A system. The HPLC column used was Kinetex 5 μm C18 100 Å, with dimensions of 150 x 4.6 mm. The compound concentration was 3 mM, and a 20 μL

injection was made. The isocratic mobile phase buffer consisted of 60 % acetonitrile (MeCN), 40 % water (H<sub>2</sub>O), and 0.1 % formic acid. The HPLC analysis was conducted for 0-10 minutes, and signals were detected using a UV detector at 254 nm. A chromatogram of the mobile phase buffer (20  $\mu$ L) was obtained separately for comparison.

### **Synthesis of 1-(2-Hydroxyphenyl)-3-(2',4',5'-trimethoxyphenyl)prop-2-en-1-one (3e)**

To a solution of the 2-hydroxyacetophenone (7.34 mmol) and benzaldehyde 2a (11.01 mmol) in EtOH (20 mL), KOH (18.35 mmol) was added, and the reaction mixture was stirred at room temperature for 48 h. TLC examination (30 % EtOAc in hexanes) indicated the completion of the reaction. The reaction mixture was then poured over crushed ice and acidified the pH to 2 using 1.0 N HCl. The precipitate formed was filtered, washed with copious amounts of water, and dried to obtain the crude product, which was purified on column chromatography over Si gel using 10 % EtOAc in hexanes as eluent to afford clean chalcones **3a** in 87.0 % yield as orange solid; mp. 135-137 °C; <sup>1</sup>H NMR (700 MHz, CDCl<sub>3</sub>)  $\delta$ : 13.08 (s, 1H), 8.21 (d, 1H, J = 15.4 Hz), 7.91 (dd, 1H, J = 7.7, 7.0 Hz), 7.60 (d, 1H, J = 15.4 Hz), 7.46 (dd, 1H, J = 8.4, 7.0 Hz), 6.99 (d, 1H, J = 8.3 Hz), 6.92 (t, 1H, J = 7.9 Hz), 6.5 (s, 1H), 3.94 (s, 3H), 3.92 (s, 3H), 3.90 (s, 3H); <sup>13</sup>C NMR (700 MHz, CDCl<sub>3</sub>)  $\delta$ : 194.0, 163.5, 155.1, 152.9, 143.2, 140.9, 135.8, 129.5, 120.2, 118.6, 118.4, 117.7, 115.1, 111.7, 96.6, 56.5, 56.2, 56.0; HRMS calculated for C<sub>18</sub>H<sub>18</sub>O<sub>5</sub> 314.1154, found 314.1151.

### **Synthesis of 2-[(2',4',5'-Trimethoxyphenyl)methylidene]-2,3-dihydro-1-benzofuran-3-one (MA5)**

Chalcone **3a** (3.18 mmol) was added to a homogeneous solution of Hg(OAc)<sub>2</sub> (1.1 g, 3.50 mmol) in anhydrous pyridine (50 mL) and the reaction mixture was heated at 110

°C for 12 h. The completion of reaction was marked by consumption of starting material and formation of a single product as visualized by TLC (50 % EtOAc in hexanes). The reaction mixture was then quenched with ice and acidified to the pH of 2 by adding 1.0 N HCl. It was extracted in EtOAc (4 × 50 mL), and the combined extract was washed with water (2 × 50 mL), brine (1 × 50 mL), and dried over anhydrous Na<sub>2</sub>SO<sub>4</sub>. The drying agent was filtered off and the filtrate was concentrated *in vacuo* to obtain pure solid product **MA5** in 99 % yield as yellow solid; mp. 240-242 °C; <sup>1</sup>H NMR (700 MHz, CDCl<sub>3</sub>) δ: 7.91 (s, 1H), 7.80 (dd, 1H, J = 7.6, 7.0 Hz), 7.63-7.61 (m, 1H), 7.46 (s, 1H), 7.28 (d, 1H, J = 8.2 Hz), 7.20 (t, 1H, J = 7.6 Hz), 6.51 (s, 1H), 3.96 (s, 3H), 3.95 (s, 3H), 3.90 (s, 3H); <sup>13</sup>C NMR (700 MHz, CDCl<sub>3</sub>) δ: 184.3, 165.4, 155.3, 152.4, 145.7, 143.2, 136.2, 124.5, 123.2, 122.2, 114.5, 113.1, 112.8, 108.0, 96.3, 56.6, 56.4, 56.0; HRMS calculated for C<sub>18</sub>H<sub>16</sub>O<sub>5</sub> 312.0998, found 312.0998.

#### Synthesis of 2-[(2',4',5'-Trihydroxyphenyl)methylidene]-2,3-dihydro-1-benzofuran-3-one (**HA5**)

The methoxy aurone **MA5** (2.24 mmol, 1.0 eq) was dissolved in anhydrous CH<sub>2</sub>Cl<sub>2</sub> (30 mL) and cooled down to 0 °C. BBr<sub>3</sub> (30 mmol, 13.4 eq) was added slowly to the reaction mixture under N<sub>2</sub> atmosphere and while stirring. The reaction mixture was allowed to attain room temperature and stirring continued for 12 h. TLC examination (50 % EtOAc in hexanes) revealed the completion of the reaction. The reaction mixture was then cooled to 0 °C and carefully quenched with slow drop-wise addition of water until the excess BBr<sub>3</sub> reacted completely. The precipitated solid product was filtered, washed with water, and dried over CaCl<sub>2</sub> in a vacuum desiccator. The crude product thus obtained was purified by column chromatography over Si gel using 10 % MeOH in CH<sub>2</sub>Cl<sub>2</sub> to afford pure hydroxy

aurones **HA5** in 74.0 % yield, orange-red solid; mp. 191-193 °C; <sup>1</sup>H NMR (400 MHz, Acetone-d<sub>6</sub>) δ: 8.94 (s, 1H), 8.71 (s, 1H), 7.97 (s, 1H), 7.85 (s, 1H), 7.71-7.76 (m, 2H), 7.43 (d, 1H, *J* = 8.2 Hz), 7.40 (s, 1H), 7.28 (t, 1H, *J* = 7.4 Hz), 6.57 (s, 1H); <sup>13</sup>C NMR (400 MHz, Acetone-d<sub>6</sub>) δ: 183.9, 166.1, 153.8, 150.7, 145.6, 139.7, 137.2, 124.7, 124.1, 123.0, 117.7, 113.7, 111.6, 108.9, 103.7; HRMS calculated for C<sub>15</sub>H<sub>10</sub>O<sub>5</sub> 270.0528, found 270.0529.

### ***S. mutans* and commensal species planktonic growth assays**

Effects of compounds on *S. mutans* and commensal bacterial growth were evaluated using the growth assay as described.<sup>51</sup> *S. mutans* UA159, *S. gordonii*, *S. sanguinis*, cultures were grown for 24 h under 5 % CO<sub>2</sub> at 37 °C. These cultures were then reinoculated with fresh THB (1:5) until OD<sub>470</sub> = 1 when the bacteria were ready to be used. Different concentrations of the inhibitor were assayed in chemically defined media (CDM) with 1 % of the bacteria, 1 % sucrose and 1 % DMSO in 96 well plates. The 96 well plates were incubated under 5 % CO<sub>2</sub> at 37 °C for 16 h. Growth of the bacteria was read after 16 h at OD<sub>470</sub>. Each assay was carried out at least in triplicate.

### **Hydroxyapatite disc assay**

Biofilm inhibition assays were performed in polystyrene microtiter 96 well plates with hydroxyapatite disks suspended in the wells. Stock solutions were prepared in chemically defined medium (CDM, JRH Biosciences, Lenexa, KS) with 1 % sucrose, 1 % bacteria cultures and various concentrations of the small molecule inhibitors to examine their activity against biofilm formation as described.<sup>52 51, 53</sup> These stocks were assayed in 96 well plates and then hydroxyapatite discs were suspended in the media in wells. The plates were incubated at 37 °C and 5 % CO<sub>2</sub> for 16 h. After 16 h, the discs were taken out,

gently washed with water, dried, and stained with crystal violet, and then gently rinsed again with deionized water leaving the stained biofilm on the surface of hydroxyapatite discs. Biofilms were dissolved in 200  $\mu$ L of 30 % acetic acid and absorbance at 562 nm was used read to determine biofilm biomass. Each assay was carried out at least in triplicate.

### **Synthesis of porous cubic manganese oxide microparticle templates**

Porous  $\text{Mn}_2\text{O}_3$  microparticle templates of 3  $\mu\text{m}$  in size were synthesized as described previously.<sup>44, 46</sup> Briefly, a nano-seed solution was prepared by mixing 0.04 g of  $\text{NH}_4\text{HCO}_3$  and 0.02 g of  $\text{MnSO}_4$  in DI water (200 mL). Then, the nano-seed solution (80 mL) was added to a 6 mM of  $\text{MnSO}_4$  (1000 mL) followed by 6 mM solution of  $\text{NH}_4\text{HCO}_3$  (1000 mL) both containing 2-propanol (0.5 % vol) was added to the nano-seed solution and was heated at 60  $^\circ\text{C}$  for 30 minutes to produce 3  $\mu\text{m}$  cubic manganese carbonate particles. Once collected and dried via filtration, the  $\text{Mn}_2\text{CO}_3$  microparticles were heated at 650 $^\circ\text{C}$  for 3.5 h in the muffled oven to produce porous  $\text{Mn}_2\text{O}_3$  microparticles.

### **Synthesis of cubical hydrogel microparticles**

pH-Responsive cubic hydrogel cubic microparticles were synthesized by depositing hydrogen-bonded  $[\text{PMAA/PVPON}]_n$  (the subscript denotes the number of polymer bilayers) multilayers at the surfaces of  $\text{Mn}_2\text{O}_3$  microparticle templates. The porous templates were first exposed to an aqueous poly(ethyleneimine) (PEI) solution in deionized (DI) water (1.5 mg/mL) for 1 h to enhance the adsorption of the following (PMAA/PVPON) layers to the particle surfaces followed by deposition of the polymers from aqueous polymeric solutions (1.5 mg/mL) at pH 2 for 45 min each. The polymer deposition was achieved through sonication (15 min) and shaking (30 min) of the

manganese oxide porous templates in polymer solutions. After the deposition of each layer, the template particles were centrifuged for 10 min at 4,900 rpm and re-suspended in phosphate buffer solution (0.01 M, pH 2) twice to rinse away excess polymer before the next deposition cycle. Following the deposition of a 5-bilayer (PMAA/PVPON)<sub>5</sub> coating, the PMAA layers were cross-linked with ethylenediamine by, first, activating the PMAA carboxylic groups with a carbodiimide solution (5 mg/mL, pH 5, 0.01 M phosphate) for 30 min, then exposing the particles to ethylenediamine (12  $\mu$ L/mL in 0.01 M phosphate, pH = 5.8) for 16 h. Afterwards, PVPON was removed from the PMAA network by exposing the core-shell particles to 0.01 M phosphate buffer solution (pH 8.5) for 24 h while shaking. Cubic PMAA hydrogel microparticles were obtained after dissolving the manganese oxide core in hydrochloric acid solution (8M HCl) for 24 h. The hydrogel microparticles were treated with ethylenediamine tetraacetic acid disodium salt solution (EDTA, 0.1 M) at pH 7 overnight by shaking to remove any residual manganese ions in the hydrogel network. The PMAA hydrogel microparticles were then purified by dialysis in DI water for 3 days using a Float-a-Lyzer (Fisher; MWCO 20 kDa).

### **Rat model of dental caries used in the evaluation of HEBI**

*In vivo* studies of colonization and virulence of *S. mutans* were evaluated using a previously reported rat model of dental caries<sup>54, 55</sup>. Offsprings of gnotobiotic Fischer 344 rats used in this experiment were bred and maintained in trexler isolators. Male and female rat pups were removed from isolators at 20 days of age and randomly assigned into 5 treatment groups of 5 rats/group in cages with filter tops. Rats were then infected with *S. mutans* UA159 strain by oral swabbing daily for four consecutive days with a fresh overnight culture of *S. mutans* UA159. Rats were provided with caries promoting Teklad

Diet 305 containing 5 % sucrose (Harlan Laboratories, Inc., Indianapolis, IN) and sterile drinking water *ad libitum*. Oral swabs were taken 5 days post-infection and plated on Todd Hewitt (TH) agar plates and incubated at 37 °C in an environment of 5 % CO<sub>2</sub> in the air to confirm colonization. Rats were weighed at weaning and at the termination of the experiment. One-week post-infection, the molars of the rats were treated topically twice daily for 4 weeks with the test compounds using camel-hair brushes. The five treatment groups used in this study were: 1) **HEBI** (100 µM); 2) **HA5** (100 µM); 3) hydrogel encapsulated PBS (no drug) containing 0.1 % DMSO (negative control), 4) 250 ppm NaF (positive control) and 5) infected untreated group (negative control). Drinking water was withheld for 60 min following each treatment with the compound. Animals were weighed at weaning and at the termination of the experiment. On day 60, the rats were sacrificed using CO<sub>2</sub> followed by cervical dislocation or bilateral thoracotomy. The mandibles were surgically removed and cleaned of excess tissue to assess the level of bacteria present and the extent of caries formation. The right mandibles from each rat were placed in a tube containing phosphate buffer (3 mL), placed on ice and sonicated (10 sec) to release bacteria from the molars. Each sample was serially diluted, plated on blood agar plates (BAP) and mitis-salivarius (MS) agar plates and incubated in an environment of 5 % CO<sub>2</sub> at 37 °C to quantify the level of total bacteria and *S. mutans* present in the plaque. The right and left mandibles from each rat were then placed in 95 % ethanol for 24 h. The mandibles were cleaned and stained overnight with murexide solution. After drying, the mandibles were sectioned and scored for caries activity using the Keyes method.<sup>56</sup> Caries scores were recorded for the buccal, sulcal and proximal molar surfaces individually so that differences among the surfaces could be distinguished. Statistical significance in the mean caries

scores, colony-forming units (CFUs)/mandible and body weights between groups of rats were determined by one-way analysis of variance (ANOVA) with the Tukey-Kramer multiple comparison test using the InStat program (Graphpad Software, San Diego, CA). When determining the statistical significance between the two groups, an unpaired t-test was applied. Differences between groups were considered significant at a  $P$ -value  $< 0.05$ .

### **ACKNOWLEDGEMENTS**

The contents described in this chapter were supported by the NIH grants R21CA22649 (Velu), R21DE028349 (Velu), R03DE025058 (Velu), and University of Alabama at Birmingham Microbiome Center Pilot Grant (Velu). We acknowledge Drs. Suzanne M. Michalek and Gregory Harber from the department of Microbiology for the *in vivo* rat model studies presented in this chapter. We also acknowledge Dr. Nathaniel Lawson of the UAB School of Dentistry for the freshly extracted, intact third molars used in the hydrogel adhesion studies. Graduate student Teaching Assistantship (Ahirwar) from the Department of Chemistry, University of Alabama at Birmingham is greatly appreciated.

### **IRB AND IACUC APPROVALS**

All *in vivo* experimental protocols were approved by the University of Alabama at Birmingham Institutional Animal Care and Use Committee (Protocol No: IACUC-20047). Slices of human teeth used in this study were provided by Dr. Nathaniel Lawson from the UAB School of Dentistry (IRB-300001291).



## REFERENCES

- (1) Kolenbrander, P. E. Oral microbial communities: biofilms, interactions, and genetic systems. *Annu. Rev. Microbiol.* **2000**, *54*, 413-437.
- (2) Hamada, S.; Slade, H. D. Biology, immunology, and cariogenicity of *Streptococcus mutans*. *Microbiological reviews* **1980**, *44* (2), 331-384.
- (3) Loesche, W. J. Role of *Streptococcus mutans* in human dental decay. *Microbiological reviews* **1986**, *50* (4), 353-380.
- (4) Jenkinson, H. F.; Lamont, R. J. Oral microbial communities in sickness and in health. *Trends in microbiology* **2005**, *13* (12), 589-595.
- (5) Kolenbrander, P. E.; Andersen, R. N.; Blehert, D. S.; Egland, P. G.; Foster, J. S.; Palmer, R. J., Jr. Communication among oral bacteria. *Microbiology and molecular biology reviews : MMBR* **2002**, *66* (3), 486-505.
- (6) Kuramitsu, H. K.; He, X.; Lux, R.; Anderson, M. H.; Shi, W. Interspecies interactions within oral microbial communities. *Microbiology and molecular biology reviews : MMBR* **2007**, *71* (4), 653-670.
- (7) Bowden, G. H.; Hamilton, I. R. Survival of oral bacteria. *Critical reviews in oral biology and medicine : an official publication of the American Association of Oral Biologists* **1998**, *9* (1), 54-85.
- (8) Quivey, R. G., Jr.; Kuhnert, W. L.; Hahn, K. Adaptation of oral streptococci to low pH. *Advances in microbial physiology* **2000**, *42*, 239-274.
- (9) Matsumoto-Nakano, M. Role of *Streptococcus mutans* surface proteins for biofilm formation. *Jpn. Dent. Sci. Rev.* **2018**, *54* (1), 22-29.
- (10) Yamashita, Y.; Bowen, W. H.; Burne, R. A.; Kuramitsu, H. K. Role of the *Streptococcus mutans* gtf genes in caries induction in the specific-pathogen-free rat model. *Infection and immunity* **1993**, *61* (9), 3811-3817.
- (11) Aoki, H.; Shiroza, T.; Hayakawa, M.; Sato, S.; Kuramitsu, H. K. Cloning of a *Streptococcus mutans* glucosyltransferase gene coding for insoluble glucan synthesis. *Infection and immunity* **1986**, *53* (3), 587-594.
- (12) Hanada, N.; Kuramitsu, H. K. Isolation and characterization of the *Streptococcus mutans* gtfC gene, coding for synthesis of both soluble and insoluble glucans. *Infection and immunity* **1988**, *56* (8), 1999-2005.
- (13) Hanada, N.; Kuramitsu, H. K. Isolation and characterization of the *Streptococcus mutans* gtfD gene, coding for primer-dependent soluble glucan synthesis. *Infection and immunity* **1989**, *57* (7), 2079-2085.

- (14) Monchois, V.; Willemot, R. M.; Monsan, P. Glucansucrases: mechanism of action and structure-function relationships. *FEMS microbiology reviews* **1999**, *23* (2), 131-151.
- (15) Hanada, N.; Kuramitsu, H. K. Isolation and characterization of the *Streptococcus mutans* gtfD gene, coding for primer-dependent soluble glucan synthesis. *Infection and immunity* **1989**, *57* (7), 2079-2085.
- (16) Wang, Z.; Zhou, Y.; Han, Q.; Ye, X.; Chen, Y.; Sun, Y.; Liu, Y.; Zou, J.; Qi, G.; Zhou, X.; Cheng, L.; Ren, B. Synonymous point mutation of gtfB gene caused by therapeutic X-rays exposure reduced the biofilm formation and cariogenic abilities of *Streptococcus mutans*. *Cell Biosci.* **2021**, *11* (1), 91.
- (17) Nijampatnam, B.; Ahirwar, P.; Pukkanasut, P.; Womack, H.; Casals, L.; Zhang, H.; Cai, X.; Michalek, S. M.; Wu, H.; Velu, S. E. Discovery of Potent Inhibitors of *Streptococcus mutans* Biofilm with Antivirulence Activity. *ACS Med. Chem. Lett.* **2021**, *12* (1), 48-55.
- (18) Nijampatnam, B.; Casals, L.; Zheng, R.; Wu, H.; Velu, S. E. Hydroxychalcone inhibitors of *Streptococcus mutans* glucosyl transferases and biofilms as potential anticaries agents. *Bioorg. Med. Chem. Lett.* **2016**, *26* (15), 3508-3513.
- (19) Nijampatnam, B.; Zhang, H.; Cai, X.; Michalek, S. M.; Wu, H.; Velu, S. E. Inhibition of *Streptococcus mutans* Biofilms by the Natural Stilbene Piceatannol Through the Inhibition of Glucosyltransferases. *ACS Omega* **2018**, *3* (7), 8378-8385.
- (20) Zhang, Q.; Nijampatnam, B.; Hua, Z.; Nguyen, T.; Zou, J.; Cai, X.; Michalek, S. M.; Velu, S. E.; Wu, H. Structure-Based Discovery of Small Molecule Inhibitors of Cariogenic Virulence. *Sci. Rep.* **2017**, *7* (1), 5974.
- (21) Benoit, D. S. W.; Sims, K. R., Jr.; Fraser, D. Nanoparticles for Oral Biofilm Treatments. *ACS Nano* **2019**, *13* (5), 4869-4875.
- (22) Butron Téllez Giron, C.; Hernandez Sierra, J. F.; DeAlba-Montero, I.; Urbano Pena, M. L. A.; Ruiz, F. Therapeutic Use of Silver Nanoparticles in the Prevention and Arrest of Dental Caries. *Bioinorg. Chem. Appl.* **2020**, *2020*, 8882930.
- (23) Sims, K. R.; Maceren, J. P.; Liu, Y.; Rocha, G. R.; Koo, H.; Benoit, D. S. W. Dual antibacterial drug-loaded nanoparticles synergistically improve treatment of *Streptococcus mutans* biofilms. *Acta Biomater.* **2020**, *115*, 418-431.
- (24) Horev, B.; Klein, M. I.; Hwang, G.; Li, Y.; Kim, D.; Koo, H.; Benoit, D. S. pH-activated nanoparticles for controlled topical delivery of farnesol to disrupt oral biofilm virulence. *ACS Nano* **2015**, *9* (3), 2390-2404.
- (25) Yi, Y.; Wang, L.; Chen, L.; Lin, Y.; Luo, Z.; Chen, Z.; Li, T.; Wu, J.; Zhong, Z. Farnesal-loaded pH-sensitive polymeric micelles provided effective prevention and treatment on dental caries. *J. Nanobiotech.* **2020**, *18* (1), 89.
- (26) Jailani, A.; Kalimuthu, S.; Rajasekar, V.; Ghosh, S.; Collart-Dutilleul, P. Y.; Fatima, N.; Koo, H.; Solomon, A. P.; Cuisinier, F.; Neelakantan, P. Trans-Cinnamaldehyde

Eluting Porous Silicon Microparticles Mitigate Cariogenic Biofilms. *Pharm.* **2022**, *14* (7), 1428.

- (27) Liu, Y.; Huang, Y.; Kim, D.; Ren, Z.; Oh, M. J.; Cormode, D. P.; Hara, A. T.; Zero, D. T.; Koo, H. Ferumoxytol Nanoparticles Target Biofilms Causing Tooth Decay in the Human Mouth. *Nano Lett.* **2021**, *21* (22), 9442-9449.
- (28) Liu, Y.; Naha, P. C.; Hwang, G.; Kim, D.; Huang, Y.; Simon-Soro, A.; Jung, H. I.; Ren, Z.; Li, Y.; Gubara, S.; Alawi, F.; Zero, D.; Hara, A. T.; Cormode, D. P.; Koo, H. Topical ferumoxytol nanoparticles disrupt biofilms and prevent tooth decay in vivo via intrinsic catalytic activity. *Nat. Commun.* **2018**, *9* (1), 2920.
- (29) Melo, M. A.; Guedes, S. F.; Xu, H. H.; Rodrigues, L. K. Nanotechnology-based restorative materials for dental caries management. *Trends in biotechnology* **2013**, *31* (8), 459-467.
- (30) Mohire, N. C.; Yadav, A. V. Chitosan-based polyherbal toothpaste: as novel oral hygiene product. *Indian journal of dental research : official publication of Indian Society for Dental Research* **2010**, *21* (3), 380-384.
- (31) Seneviratne, C. J.; Leung, K. C.-F.; Wong, C.-H.; Lee, S.-F.; Li, X.; Leung, P. C.; Lau, C. B. S.; Wat, E.; Jin, L. Nanoparticle-Encapsulated Chlorhexidine against Oral Bacterial Biofilms. *Plos One* **2014**, *9* (8), e103234.
- (32) Zhang, J. F.; Wu, R.; Fan, Y.; Liao, S.; Wang, Y.; Wen, Z. T.; Xu, X. Antibacterial Dental Composites with Chlorhexidine and Mesoporous Silica. *J. Dent. Res.* **2014**, *93* (12), 1283-1289.
- (33) Nguyen, S.; Hiorth, M.; Rykke, M.; Smistad, G. Polymer coated liposomes for dental drug delivery – Interactions with parotid saliva and dental enamel. *Eur. J. Pharm. Sci.* **2013**, *50* (1), 78-85.
- (34) Feitosa, S. A.; Palasuk, J.; Kamocki, K.; Geraldeli, S.; Gregory, R. L.; Platt, J. A.; Windsor, L. J.; Bottino, M. C. Doxycycline-encapsulated nanotube-modified dentin adhesives. *J. Dent. Res.* **2014**, *93* (12), 1270-1276.
- (35) Zhou, Y.; Yang, J.; Lin, Z.; Li, J.; Liang, K.; Yuan, H.; Li, S.; Li, J. Triclosan-loaded poly(amido amine) dendrimer for simultaneous treatment and remineralization of human dentine. *Colloids Surf. B.* **2014**, *115*, 237-243.
- (36) Naha, P. C.; Liu, Y.; Hwang, G.; Huang, Y.; Gubara, S.; Jonnakuti, V.; Simon-Soro, A.; Kim, D.; Gao, L.; Koo, H.; Cormode, D. P. Dextran-Coated Iron Oxide Nanoparticles as Biomimetic Catalysts for Localized and pH-Activated Biofilm Disruption. *ACS Nano* **2019**, *13* (5), 4960-4971.
- (37) Aframian, D. J.; Davidowitz, T.; Benoliel, R. The distribution of oral mucosal pH values in healthy saliva secretors. *Oral diseases* **2006**, *12* (4), 420-423.
- (38) Baliga, S.; Muglikar, S.; Kale, R. Salivary pH: A diagnostic biomarker. *J. Indian Soc. Periodont.* **2013**, *17* (4), 461-465.

- (39) Bardow, A.; Pederson, A. M. L.; Nauntofte, B. Saliva. In: Miles TS, Nauntofte B, Svensson P eds. *Clin. Oral Physiol.* **2004**, 17-33.
- (40) Lazarchik, D. A.; Filler, S. J. Effects of Gastroesophageal Reflux on the Oral Cavity. *Am. J. Med.* **1997**, *103* (5), 107S-113S.
- (41) Markitziu, A.; Aframian, D. Gastro-intestinal disorders. *Br. Dent. J.* **1997**, *182* (6), 207.
- (42) Robb, N. D.; Smith, B. G.; Geidrys-Leeper, E. The distribution of erosion in the dentitions of patients with eating disorders. *Br. Dent. J.* **1995**, *178* (5), 171-175.
- (43) Meyer, F.; Enax, J.; Epple, M.; Amaechi, B. T.; Simader, B. Cariogenic Biofilms: Development, Properties, and Biomimetic Preventive Agents. *Dent. J.* **2021**, *9* (8), 88.
- (44) Kozlovskaya, V.; Chen, J.; Tedjo, C.; Liang, X.; Campos-Gomez, J.; Oh, J.; Saeed, M.; Lungu, C. T.; Kharlampieva, E. pH-responsive hydrogel cubes for release of doxorubicin in cancer cells. *J. Mater. Chem. B.* **2014**, *2* (17), 2494-2507.
- (45) Xue, B.; Kozlovskaya, V.; Liu, F.; Chen, J.; Williams, J. F.; Campos-Gomez, J.; Saeed, M.; Kharlampieva, E. Intracellular Degradable Hydrogel Cubes and Spheres for Anti-Cancer Drug Delivery. *ACS Appl. Mater. Interfac.* **2015**, *7* (24), 13633-13644.
- (46) Xue, B.; Wang, W.; Qin, J. J.; Nijampatnam, B.; Murugesan, S.; Kozlovskaya, V.; Zhang, R.; Velu, S. E.; Kharlampieva, E. Highly efficient delivery of potent anticancer iminoquinone derivative by multilayer hydrogel cubes. *Acta Biomater.* **2017**, *58*, 386-398.
- (47) Liu, P.; Luo, Q.; Guan, Y.; Zhang, Y. Drug release kinetics from monolayer films of glucose-sensitive microgel. *Polymer* **2010**, *51* (12), 2668-2675.
- (48) Sun, S.; Wu, P. A one-step strategy for thermal- and pH-responsive graphene oxide interpenetrating polymer hydrogel networks. *J. Mater. Chem. B.* **2011**, *21* (12), 4095-4097.
- (49) Hazlett, K. R.; Michalek, S. M.; Banas, J. A. Inactivation of the gbpA gene of *Streptococcus mutans* increases virulence and promotes in vivo accumulation of recombinations between the glucosyltransferase B and C genes. *Infection and immunity* **1998**, *66* (5), 2180-2185.
- (50) Michalek, S. M.; McGhee, J. R.; Shiota, T.; Devenyns, D. Virulence of *Streptococcus mutans*: cariogenicity of *S. mutans* in adult gnotobiotic rats. *Infection and immunity* **1977**, *15* (2), 466-471.
- (51) Liu, C.; Worthington, R. J.; Melander, C.; Wu, H. A new small molecule specifically inhibits the cariogenic bacterium *Streptococcus mutans* in multispecies biofilms. *Antimicrobial agents and chemotherapy* **2011**, *55* (6), 2679-2687.

- (52) Banas, J. A.; Lynch, D. J.; Michalek, S. M.; Zhu, M.; Drake, D.; Qian, F. Cariogenicity of Streptococcus mutans Glucan-Binding Protein Deletion Mutants. *Oral Health Dent. Manag.* **2013**, *12* (4), 191-199.
- (53) Zhang, Q.; Nguyen, T.; McMichael, M.; Velu, S. E.; Zou, J.; Zhou, X.; Wu, H. New small-molecule inhibitors of dihydrofolate reductase inhibit Streptococcus mutans. *Int. J. Antimicrob. Agents* **2015**, *46* (2), 174-182.
- (54) Lynch, D. J.; Michalek, S. M.; Zhu, M.; Drake, D.; Qian, F.; Banas, J. A. Cariogenicity of Streptococcus mutans glucan-binding protein deletion mutants. *Oral Health Dent. Manag.* **2013**, *12* (4), 191-199.
- (55) Peng, X.; Zhang, Y.; Bai, G.; Zhou, X.; Wu, H. Cyclic di-AMP mediates biofilm formation. *Mol. Microbiol.* **2016**, *99* (5), 945-959.
- (56) Keyes, P. H. Dental caries in the molar teeth of rats. II. A method for diagnosing and scoring several types of lesions simultaneously. *J. Dent. Res.* **1958**, *37* (6), 1088-1099.

## CONCLUSIONS

Dental caries or tooth decay is a common oral disease characterized by the demineralization and destruction of tooth structures.<sup>1</sup> It is a global concern with high prevalence,<sup>2, 3</sup> and if left untreated, it can lead to tooth loss and other complications.<sup>4</sup> <sup>5</sup>Advancements in science and technology have contributed to better understanding and management of this condition. However, there are still limitations to the current methods used in the prevention and treatment of dental caries. The oral cavity is home to a diverse range of microbial species, with over 700 bacterial species identified in the oral microbiota. These species belong to various phyla, including Firmicutes, Fusobacteria, Proteobacteria, Actinobacteria, Bacteroidetes, and others.<sup>9</sup> Gram-positive bacteria, such as Streptococcus and Actinomyces, are the initial colonizers of teeth and play a crucial role in the formation of dental biofilms. These biofilms, also known as plaque, consist of a complex community of bacteria surrounded by their extracellular matrix.<sup>18</sup> The biofilm structure and composition contribute to its pathogenicity and resistance to antibiotics.<sup>18, 21</sup> Extracellular polysaccharides (EPS) of bacteria are a key component of the biofilm matrix, providing structural integrity and protection against harmful attacks. EPS also serve as a reservoir for essential ions that support bacterial growth and survival within biofilm. Understanding the

dynamics of the extracellular matrix is important for studying biofilm formation and developing strategies to target oral biofilms.<sup>18, 21</sup>

Certain bacterial species in the oral cavity have a beneficial role in preventing caries. *S. oralis*, *S. sanguinis*, and *S. gordonii* are commonly found on healthy tooth surfaces and may exert antagonistic effects against cariogenic bacteria such as *S. mutans*. These beneficial bacteria contribute to pH homeostasis by producing alkali, helping to prevent tooth erosion caused by acidic conditions in the oral environment.<sup>26</sup> *S. mutans*, the main cause of dental caries, utilize exopolysaccharides to form protective biofilms, exhibits high acidogenicity by producing lactic acid, and thrives in acidic conditions. It adheres to tooth surfaces through both sucrose-dependent and sucrose-independent mechanisms, involving surface proteins and glucans. Understanding these factors is crucial for developing strategies to prevent and treat dental caries.<sup>36-40</sup>

Glucosyltransferases (Gtfs) produced by *S. mutans* are responsible for synthesizing extracellular glucan polysaccharides, promoting bacterial adhesion and biofilm formation.<sup>31</sup> Gtfs have distinct functional domains, including a glucan-binding domain and a catalytic domain. The catalytic domain contains active sites crucial for sucrase activity.<sup>62</sup> *S. mutans* possesses multiple *gtf* genes that encode different Gtfs, leading to the production of both soluble and insoluble glucans. Insoluble glucans contribute to bacterial colonization and cariogenesis.<sup>54, 63-65</sup> Therefore, inhibiting *S. mutans* Gtfs has emerged as a potential strategy for preventing dental caries. The mechanism of glucan formation involves specific residues within Gtfs, facilitating the oligomerization process and the synthesis of glucans.

70, 71

Oral hygiene practices such as regular brushing, flossing, and cleaning are crucial for maintaining oral health. Brushing helps remove bacteria and food particles from the teeth, while flossing cleans hard-to-reach areas. While these practices are essential, they need to be repeated frequently as bacteria can quickly re-colonize tooth surfaces.<sup>89, 90</sup> Mouthwashes containing ingredients like chlorhexidine, cetylpyridinium chloride, fluoride, zinc, and herbal extracts (e.g., licorice and curcumin) are used for oral hygiene. Chlorhexidine is an effective antiseptic agent with bactericidal properties, but long-term use may cause taste alteration and tooth pigmentation. Cetylpyridinium chloride also kills bacteria and reduces plaque and inflammation when used alongside toothbrushing. Herbal extracts like licorice and curcumin exhibit antimicrobial and anti-inflammatory effects and show promise in preventing plaque accumulation and gingivitis.<sup>100</sup>

Fluoride is widely used in drinking water and oral hygiene products to promote oral health. It aids in the remineralization and the formation of caries-resistant fluorapatite. However, prolonged exposure to high levels of fluoride can lead to dental and skeletal fluorosis, and excessive doses have been associated with neurotoxicity.<sup>103, 104, 109, 110</sup> Inhibitors of glucosyltransferases (Gtfs), such as polyphenols from teas, flavonoids, inorganic salts, and small molecules, have shown potential in preventing caries by inhibiting the synthesis of glucans.<sup>125, 144</sup> However, their activities are generally limited, and their *in vivo* anticariogenic activities are either unreported or unclear. Structure-based drug design of inhibitors using the available crystal structure of Gtfs can aid in developing synthetic small molecule biofilm inhibitors with both *in vitro* and *in vivo* efficacy.



## Chapter 1: Design and synthesis of a small molecule library aurones to inhibit *Streptococcus mutans* glucosyltransferases and biofilm.

The challenges encountered in encapsulating our lead compounds **G43** and **IIIC5** prompted us to explore a different class of Gtf inhibitors that possessed improved solubility and were more amenable to encapsulation in hydrogels for pH-responsive release. Considering this, we designed and synthesized a library of methoxyaurones and hydroxyaurones as potential candidates. To assess the potential of these aurone derivatives as Gtf inhibitors, *in-silico* studies were conducted to examine their docking poses against GtfB, as well as to predict their solubilities. All methoxyaurones and hydroxyaurones were found to occupy same binding pocket with similar orientation as that of **G43** crystallized with Gtf-B. Moreover, their calculated physicochemical properties put them well within Lipinski's criteria for drug-likeness. Following the *in-silico* evaluations, a library of aurone compounds was synthesized to experimentally validate their properties. To gauge their solubility, a UV-Vis spectroscopy method was employed, which allowed us to determine the solubility values of each compound. Among the aurones tested, **HA5** and **HA6** emerged as the most promising candidates, exhibiting solubility values of 120.09 µg/mL and 90.77 µg/mL, respectively. The enhanced solubility of **HA5** and **HA6** in comparison to our previous lead compounds **G43** and **IIIC5** suggested that these aurone derivatives possessed more favorable characteristics for encapsulation in hydrogels. This finding encouraged us to further explore their potential as pH-responsive biofilm inhibitors for targeted drug delivery.

## Chapter 2: Evaluation of aurones for their inhibitory activities against *S. mutans* biofilm and glucosyltransferases *in vitro* and anticariogenic activity *in vivo*.

In Chapter 2, our research has yielded novel small-molecule inhibitors of *S. mutans* glucosyltransferases that exhibit selective biofilm inhibition without affecting the growth of oral commensal bacteria. Among these inhibitors, **HA5** and **HA6** were the most potent with biofilm IC<sub>50</sub> values 6.42  $\mu$ M and 18.92  $\mu$ M respectively, whereas **HA5** emerged as the optimized lead compound, demonstrating potent inhibition of *S. mutans* biofilm formation with an IC<sub>50</sub> value of 6.42  $\mu$ M, while showing no adverse effects on the bacterial growth at their biofilm inhibiting doses. Notably, **HA5** and **HA6** exhibited no growth inhibitory activities against *S. sanguinis* and *S. gordonii*, two important oral commensal bacterial species, even at a concentration 14 times higher than their biofilm IC<sub>50</sub> values. To gain insights into the molecular interactions underlying the activity of **HA5**, we resolved a high-resolution X-ray co-crystal structure of **HA5** bound to the catalytic domain of Gtf-B. Furthermore, in a Gtf inhibition assay, inhibitors **HA5** and **HA6** demonstrated effective inhibition of *S. mutans* Gtfs and glucan production, with an IC<sub>50</sub> values of 10.56  $\mu$ M and 8.90  $\mu$ M, respectively. To assess the *in vivo* efficacy of **HA5** and **HA6**, a 4-week treatment study was conducted in a *S. mutans* induced experimental rat model of dental caries. . Remarkably, treatment with 100  $\mu$ M **HA5** or **HA6** resulted in a significant reduction in buccal, sulcal, and proximal dental caries scores compared to control groups, showcasing their anticaries activities in a relevant animal model. Importantly, throughout the study period, rats treated with **HA5** and **HA6** did not experience any weight loss, indicating the non-toxic nature of the compounds and their suitability for therapeutic applications.

In conclusion, our findings in this chapter demonstrate that **HA5** and **HA6** selectively targets *S. mutans* glucosyltransferases and effectively inhibits Gtf-mediated biofilm formation, rather than a simple bacterial growth inhibition. These results highlight the potential of inhibitors **HA5** and **HA6** to be used as novel treatments for dental caries and provide a foundation for further development and optimization of **HA5** and **HA6** based therapies. By specifically targeting the mechanisms underlying biofilm formation, biofilm inhibitors **HA5** and **HA6** represent a promising approach in the pursuit of innovative strategies to combat dental caries.

### **Chapter 3: pH-responsive delivery of biofilm inhibitors to abrogate *S. mutans* cariogenic biofilms.**

The development of pH-responsive encapsulated biofilm inhibitors represents an exciting advancement in the field of anti-caries research. In this study, the lead compound **HA5**, established in previous chapters for its selective biofilm inhibitory activity against *S. mutans*, was successfully encapsulated in pH-responsive hydrogels to generate a hydrogel encapsulated biofilm inhibitors called **HEBI**. This encapsulation strategy aimed at delivery and release of **HA5** in a controlled manner, specifically targeting the biofilm environment with low pH associated with caries formation. To evaluate the performance of the encapsulated materials, extensive *in vitro* assessments were conducted. These investigations involved subjecting **HEBI** to biofilm conditions and examining the release profile of **HA5**. Encouragingly, **HEBI** effectively released **HA5** under the acidic conditions of the biofilm formation and effectively inhibited biofilm comparable to **HA5**. The observed biofilm inhibitory activity was selective to *S. mutans* biofilm as it did not

inhibit the commensal biofilm from *S. gordonii* and *S. sanguinis* at the same doses. In addition, **HEBI** did not affect the viability of *S. mutans* or the commensal species at its biofilm inhibiting dose.

With these promising *in vitro* results, the study progressed to *in vivo* experiments using *S. mutans* induced experimental rat caries models. A 4 week treatment of *S. mutans* infected rats with 100  $\mu$ M **HEBI** significant reduction in caries scores compared to the control, providing evidence of the efficacy of **HEBI** in preventing caries formation. This finding holds substantial clinical significance, as it suggests the potential of pH-responsive encapsulated biofilm inhibitors as a preventive or therapeutic approach for dental caries. By specifically targeting the cariogenic biofilms without disturbing the balance of the oral microbiota, **HEBI** offers a promising avenue for effective caries management. The findings in this chapter highlight the potential of pH-responsive encapsulated biofilm inhibitors as a viable approach for combating dental caries.

Overall, the finding of this thesis represents a significant step forward in the development of novel anti-caries treatment strategies. The combination of pH-responsive encapsulation and selective biofilm inhibition offers a promising platform for the prevention and treatment of dental caries, potentially revolutionizing oral healthcare practices in the future. Further research and optimization of the encapsulated biofilm inhibitors are warranted to fully realize their clinical potential and facilitate their translation into practical applications.

## FUTURE DIRECTIONS

The analyses of crystal structures involving **HA5**, **G43**, and the GtfC inhibitor acarbose has revealed intriguing insights that can greatly impact the future development of potent Gtf inhibitors. Through the overlay of these structures, several notable observations have emerged, each offering valuable clues for the design of novel compounds with enhanced binding efficiency and improved therapeutic potential.

The first observation of particular interest is the convergence of **G43**, **HA5**, and acarbose within the same binding pocket of the GtfB protein. This convergence indicates that these compounds share a common mode of binding, suggesting similar interactions and orientations within the active site. This finding underscores the possibility of leveraging the structural similarities among these compounds to guide the design of future Gtf inhibitors. Second, acarbose, a well-known GtfC inhibitor, displayed an extended structure featuring an additional ‘valienamine’ ring that occupies a deeper region within the binding pocket. This extension enables acarbose to establish multiple hydrophilic interactions with key residues of the protein, including Asp883, His561, Asp562, Asp451, Asn455, and Glu589. Consequently, this observation suggests that the incorporation of an extended structure, potentially containing a valienamine sugar unit, may enhance the binding efficiency of future Gtf inhibitors by facilitating a greater number of beneficial

interactions. Another intriguing finding arose from the independent crystallization of **HA5** and **G43** with GtfB. Interestingly, both crystal structures revealed the presence of a bis-tris buffer molecule occupying the same deep region that the ‘valienamine’ ring of acarbose occupies when overlaid. This shared positioning suggests the existence of multiple hydrophilic interactions between the bis-tris molecule and surrounding residues. Leveraging this observation, it becomes possible to explore the introduction of a bis-tris unit or a similar moiety attached to one of the hydroxy groups of **HA5**. A one-carbon linker, such as an amide or ester bond, could facilitate the attachment of the bis-tris or valienamine unit, enabling it to occupy the deeper binding pocket. This strategic modification aims to maximize favorable interactions with the protein and further improve the binding efficiency and potency of the inhibitors.

Overall, these findings collectively provide a roadmap for future investigations into the design and development of more effective Gtf inhibitors. By capitalizing on the structural insights gained from the crystal structures of **HA5**, **G43**, and acarbose, researchers can now embark on a targeted approach to create novel small-molecule derivatives of **HA5**. These derivatives can incorporate extended structures containing valienamine sugar units or bis-tris moieties, strategically positioned within the binding pocket to maximize interactions with key residues. This approach holds great promise in advancing the field of Gtf inhibition, with the goal of developing innovative targeted strategies for prevention of dental caries.

## GENERAL REFERENCES

- (1) Lingström, P.; van Houte, J.; Kashket, S. Food starches and dental caries. *Crit. Rev. Oral Biol. Med.* **2000**, *11* (3), 366-380
- (2) Vos, T.; Lim, S. S.; Abbafati, C.; Abbas, K. M.; Abbasi, M.; Abbasifard, M.; Abbasi-Kangevari, M.; Abbastabar, H.; Abd-Allah, F.; Abdelalim, A.; et al. Global burden of 369 diseases and injuries in 204 countries and territories, 1990–2019: a systematic analysis for the Global Burden of Disease Study 2019. *Lancet* **2020**, *396* (10258), 1204-1222
- (3) Dye, B.; Thornton-Evans, G.; Li, X.; Iafolla, T. Dental caries and tooth loss in adults in the United States, 2011-2012. *NCHS Data Brief* **2015**, (197), 197
- (4) Hamada, S.; Slade, H. D. Biology, immunology, and cariogenicity of *Streptococcus mutans*. *Microbiol. Rev.* **1980**, *44* (2), 331-384
- (5) Kim, J. K.; Baker, L. A.; Davarian, S.; Crimmins, E. Oral health problems and mortality. *J. Dent. Sci.* **2013**, *8* (2), 115-120
- (6) Zero, D. T. DENTAL CARIES PROCESS. *Dent. Clin. N. Am.* **1999**, *43* (4), 635-664
- (7) Pitts, N. B.; Zero, D. T.; Marsh, P. D.; Ekstrand, K.; Weintraub, J. A.; Ramos-Gomez, F.; Tagami, J.; Twetman, S.; Tsakos, G.; Ismail, A. Dental caries. *Nat. Rev. Dis. Primers* **2017**, *3* (1), 17030
- (8) Oxilia, G.; Peresani, M.; Romandini, M.; Matteucci, C.; Spiteri, C. D.; Henry, A. G.; Schulz, D.; Archer, W.; Crezzini, J.; Boschini, F.; et al. Earliest evidence of dental caries manipulation in the Late Upper Palaeolithic. *Sci. Reports.* **2015**, *5* (1), 12150
- (9) Deo, P. N.; Deshmukh, R. Oral microbiome: Unveiling the fundamentals. *J. Oral. Maxillofac. Pathol.* **2019**, *23* (1), 122-128
- (10) Nelson-Filho, P.; Borba, I. G.; Mesquita, K. S.; Silva, R. A.; Queiroz, A. M.; Silva, L. A. Dynamics of microbial colonization of the oral cavity in newborns. *Braz. Dent. J.* **2013**, *24* (4), 415-419
- (11) Aas, J. A.; Paster, B. J.; Stokes, L. N.; Olsen, I.; Dewhirst, F. E. Defining the normal bacterial flora of the oral cavity. *J. Clin. Microbiol.* **2005**, *43* (11), 5721-5732

- (12) Jiao, Y.; Hasegawa, M.; Inohara, N. The Role of Oral Pathobionts in Dysbiosis during Periodontitis Development. *J. Dent. Res.* **2014**, *93* (6), 539-546
- (13) Okahashi, N.; Nakata, M.; Terao, Y.; Isoda, R.; Sakurai, A.; Sumitomo, T.; Yamaguchi, M.; Kimura, R. K.; Oiki, E.; Kawabata, S.; et al. Pili of oral *Streptococcus sanguinis* bind to salivary amylase and promote the biofilm formation. *Microb. Pathog.* **2011**, *50* (3-4), 148-154
- (14) Wescombe, P. A.; Hale, J. D. F.; Heng, N. C. K.; Tagg, J. R. Developing oral probiotics from *Streptococcus salivarius*. *Future Microbiol.* **2012**, *7* (12), 1355-1371
- (15) He, L.; Yang, H.; Chen, Z.; Ouyang, X. The Effect of *Streptococcus salivarius* K12 on Halitosis: a Double-Blind, Randomized, Placebo-Controlled Trial. *Probiotics Antimicrob.* **2020**, *12* (4), 1321-1329
- (16) Burton, J. P.; Wescombe, P. A.; Macklaim, J. M.; Chai, M. H. C.; MacDonald, K.; Hale, J. D. F.; Tagg, J.; Reid, G.; Gloor, G. B.; Cadieux, P. A. Persistence of the Oral Probiotic *Streptococcus salivarius* M18 Is Dose Dependent and Megaplasmid Transfer Can Augment Their Bacteriocin Production and Adhesion Characteristics. *Plos One* **2013**, *8* (6),
- (17) Kolenbrander, P. E. Oral microbial communities: biofilms, interactions, and genetic systems. *Annu. Rev. Microbiol.* **2000**, *54*, 413-437
- (18) Socransky, S. S.; Haffajee, A. D. Dental biofilms: difficult therapeutic targets. *Periodontol.* **2002**, *28*, 12-55
- (19) Scheie, A. A.; Petersen, F. C. The biofilm concept: consequences for future prophylaxis of oral diseases? *Crit. Rev. Oral Biol. Med.* **2004**, *15* (1), 4-12
- (20) Frias, J.; Olle, E.; Alsina, M. Periodontal pathogens produce quorum sensing signal molecules. *Infect. Immun.* **2001**, *69* (5), 3431-3434
- (21) Saini, R.; Saini, S.; Sharma, S. Biofilm: A dental microbial infection. *J. Nat. Sci. Biol. Med.* **2011**, *2* (1), 71-75
- (22) Marchant, S.; Brailsford, S. R.; Twomey, A. C.; Roberts, G. J.; Beighton, D. The predominant microflora of nursing caries lesions. *Caries Res.* **2001**, *35* (6), 397-406
- (23) Becker, M. R.; Paster, B. J.; Leys, E. J.; Moeschberger, M. L.; Kenyon, S. G.; Galvin, J. L.; Boches, S. K.; Dewhirst, F. E.; Griffen, A. L. Molecular analysis of bacterial species associated with childhood caries. *J. Clin. Microbiol.* **2002**, *40* (3), 1001-1009
- (24) Loesche, W. J.; Eklund, S.; Earnest, R.; Burt, B. Longitudinal investigation of bacteriology of human fissure decay: epidemiological studies in molars shortly after eruption. *Infect. Immun.* **1984**, *46* (3), 765-772
- (25) Caufield, P. W.; Dasanayake, A. P.; Li, Y.; Pan, Y.; Hsu, J.; Hardin, J. M. Natural history of *Streptococcus sanguinis* in the oral cavity of infants: evidence for a discrete window of infectivity. *Infect. Immun.* **2000**, *68* (7), 4018-4023



- (26) Burne, R. A.; Marquis, R. E. Alkali production by oral bacteria and protection against dental caries. *FEMS Microbiol. Lett.* **2000**, *193* (1), 1-6
- (27) Clarke, J. K. On the Bacterial Factor in the Ætiology of Dental Caries. *Br. J. Exp. Pathol.* **1924**, *5* (3), 141-147
- (28) Selwitz, R. H.; Ismail, A. I.; Pitts, N. B. Dental caries. *Lancet* **2007**, *369* (9555), 51-59
- (29) Featherstone, J. D. B. The Science and Practice of Caries Prevention. *J. Am. Dent. Assoc.* **2000**, *131* (7), 887-899
- (30) Zeng, L.; Burne, R. A. Comprehensive mutational analysis of sucrose-metabolizing pathways in *Streptococcus mutans* reveals novel roles for the sucrose phosphotransferase system permease. *J. Bacteriol.* **2013**, *195* (4), 833-843
- (31) Bowen, W. H.; Koo, H. Biology of *Streptococcus mutans*-derived glucosyltransferases: role in extracellular matrix formation of cariogenic biofilms. *Caries Res.* **2011**, *45* (1), 69-86
- (32) Xiao, J.; Klein, M. I.; Falsetta, M. L.; Lu, B.; Delahunty, C. M.; Yates, J. R., 3rd; Heydorn, A.; Koo, H. The exopolysaccharide matrix modulates the interaction between 3D architecture and virulence of a mixed-species oral biofilm. *PLoS Pathog.* **2012**, *8* (4), e1002623
- (33) Lemos, J. A.; Palmer, S. R.; Zeng, L.; Wen, Z. T.; Kajfasz, J. K.; Freires, I. A.; Abranches, J.; Brady, L. J. The Biology of *Streptococcus mutans*. *Microbiol. Spectr.* **2019**, *7* (1),
- (34) Baker, J. L.; Faustoferri, R. C.; Quivey, R. G., Jr. Acid-adaptive mechanisms of *Streptococcus mutans*-the more we know, the more we don't. *Mol. Oral. Microbiol.* **2017**, *32* (2), 107-117
- (35) Matsui, R.; Cvitkovitch, D. Acid tolerance mechanisms utilized by *Streptococcus mutans*. *Future Microbiol.* **2010**, *5* (3), 403-417
- (36) Brady, L. J.; Maddocks, S. E.; Larson, M. R.; Forsgren, N.; Persson, K.; Deivanayagam, C. C.; Jenkinson, H. F. The changing faces of *Streptococcus* antigen I/II polypeptide family adhesins. *Mol. Microbiol.* **2010**, *77* (2), 276-286
- (37) Jakubovics, N. S.; Strömberg, N.; van Dolleweerd, C. J.; Kelly, C. G.; Jenkinson, H. F. Differential binding specificities of oral streptococcal antigen I/II family adhesins for human or bacterial ligands. *Mol. Microbiol.* **2005**, *55* (5), 1591-1605
- (38) Larson, M. R.; Rajashankar, K. R.; Crowley, P. J.; Kelly, C.; Mitchell, T. J.; Brady, L. J.; Deivanayagam, C. Crystal structure of the C-terminal region of *Streptococcus mutans* antigen I/II and characterization of salivary agglutinin adherence domains. *J. Biol. Chem.* **2011**, *286* (24), 21657-21666

- (39) Tamesada, M.; Kawabata, S.; Fujiwara, T.; Hamada, S. Synergistic effects of streptococcal glucosyltransferases on adhesive biofilm formation. *J. Dent. Res.* **2004**, *83* (11), 874-879
- (40) Matsumoto-Nakano, M. Role of Streptococcus mutans surface proteins for biofilm formation. *Jpn. Dent. Sci. Rev.* **2018**, *54* (1), 22-29
- (41) Koo, H.; Xiao, J.; Klein, M.; Jeon, J. Exopolysaccharides produced by Streptococcus mutans glucosyltransferases modulate the establishment of microcolonies within multispecies biofilms. *Am. Soc. Microbiol.*: 2010.
- (42) Xiao, J.; Koo, H. Structural organization and dynamics of exopolysaccharide matrix and microcolonies formation by Streptococcus mutans in biofilms. *J. Appl. Microbiol.* **2010**, *108* (6), 2103-2113
- (43) Nemoto, H.; Nakano, K.; Nomura, R.; Ooshima, T. Molecular characterization of Streptococcus mutans strains isolated from the heart valve of an infective endocarditis patient. *J. Med. Microbiol.* **2008**, *57* (Pt 7), 891-895
- (44) Nakano, K.; Nomura, R.; Matsumoto, M.; Ooshima, T. Roles of Oral Bacteria in Cardiovascular Diseases — From Molecular Mechanisms to Clinical Cases: Cell-Surface Structures of Novel Serotype k Streptococcus mutans Strains and Their Correlation to Virulence. *J. Pharmacol. Sci.* **2010**, *113* (2), 120-125
- (45) Vollmer, T.; Hinse, D.; Kleesiek, K.; Dreier, J. Interactions between endocarditis-derived Streptococcus gallolyticus subsp. gallolyticus isolates and human endothelial cells. *BMC Microbiol.* **2010**, *10* (1), 78
- (46) Slipczuk, L.; Codolosa, J. N.; Davila, C. D.; Romero-Corral, A.; Yun, J.; Pressman, G. S.; Figueredo, V. M. Infective endocarditis epidemiology over five decades: a systematic review. *PLoS One* **2013**, *8* (12), e82665
- (47) Bor, D. H.; Woolhandler, S.; Nardin, R.; Brusch, J.; Himmelstein, D. U. Infective endocarditis in the U.S., 1998-2009: a nationwide study. *PLoS One* **2013**, *8* (3), e60033
- (48) Bedran, T. B.; Azelmat, J.; Spolidorio, D. P.; Grenier, D. Fibrinogen-induced streptococcus mutans biofilm formation and adherence to endothelial cells. *Biomed. Res. Int.* **2013**, *2013*, 431465
- (49) Yeh, C. Y.; Chen, J. Y.; Chia, J. S. Glucosyltransferases of viridans group streptococci modulate interleukin-6 and adhesion molecule expression in endothelial cells and augment monocytic cell adherence. *Infect. Immun.* **2006**, *74* (2), 1273-1283
- (50) Shun, C. T.; Lu, S. Y.; Yeh, C. Y.; Chiang, C. P.; Chia, J. S.; Chen, J. Y. Glucosyltransferases of viridans streptococci are modulins of interleukin-6 induction in infective endocarditis. *Infect. Immun.* **2005**, *73* (6), 3261-3270

- (51) Pang, P. Y.; Sin, Y. K.; Lim, C. H.; Tan, T. E.; Lim, S. L.; Chao, V. T.; Chua, Y. L. Surgical management of infective endocarditis: an analysis of early and late outcomes. *Eur. J. Cardiothorac. Surg.* **2015**, *47* (5), 826-832
- (52) Sabe, M. A.; Shrestha, N. K.; Menon, V. Contemporary drug treatment of infective endocarditis. *Am. J. Cardiovasc. Drugs.* **2013**, *13* (4), 251-258
- (53) Kralj, S.; van Geel-Schutten, G. H.; Dondorff, M. M. G.; Kirsanovs, S.; van der Maarel, M.; Dijkhuizen, L. Glucan synthesis in the genus *Lactobacillus*: isolation and characterization of glucansucrase genes, enzymes and glucan products from six different strains. *Microbiol.* **2004**, *150* (Pt 11), 3681-3690
- (54) Monchois, V.; Willemot, R. M.; Monsan, P. Glucansucrases: mechanism of action and structure-function relationships. *FEMS Microbiol. Rev.* **1999**, *23* (2), 131-151
- (55) Tsai, Y.-W.; Chia, J.-S.; Shiau, Y.-Y.; Chou, H.-C.; Liaw, Y.-C.; Lou, K.-L. Three-dimensional modelling of the catalytic domain of *Streptococcus mutans* glucosyltransferase GtfB. *FEMS Microbiol. Lett.* **2000**, *188* (1), 75-79
- (56) Lis, M.; Shiroza, T.; Kuramitsu, H. K. Role of C-terminal direct repeating units of the *Streptococcus mutans* glucosyltransferase-S in glucan binding. *Appl. Environ. Microbiol.* **1995**, *61* (5), 2040-2042
- (57) Nakano, Y. J.; Kuramitsu, H. K. Mechanism of *Streptococcus mutans* glucosyltransferases: hybrid-enzyme analysis. *J. Bacteriol.* **1992**, *174* (17), 5639-5646
- (58) Mooser, G.; Hefta, S.; Paxton, R.; Shively, J.; Lee, T. Isolation and sequence of an active-site peptide containing a catalytic aspartic acid from two *Streptococcus sobrinus* alpha-glucosyltransferases. *J. Biol. Chem.* **1991**, *266* (14), 8916-8922
- (59) Kato, C.; Nakano, Y.; Lis, M.; Kuramitsu, H. Molecular genetic analysis of the catalytic site of *Streptococcus mutans* glucosyltransferases. *Biochem. Biophys. Res. Commun.* **1992**, *189* (2), 1184-1188
- (60) Funane, K.; Shiraiwa, M.; Hashimoto, K.; Ichishima, E.; Kobayashi, M. An active-site peptide containing the second essential carboxyl group of dextranucrase from *Leuconostoc mesenteroides* by chemical modifications. *Biochem.* **1993**, *32* (49), 13696-13702
- (61) Chia, J.-S.; Lin, S.-W.; Yang, C.-S.; Chen, J.-Y. Antigenicity of a synthetic peptide from glucosyltransferases of *Streptococcus mutans* in humans. *Infect. Immun.* **1997**, *65* (3), 1126-1130
- (62) Chia, J.-S.; Yang, C.-S.; Chen, J.-Y. Functional analyses of a conserved region in glucosyltransferases of *Streptococcus mutans*. *Infect. Immun.* **1998**, *66* (10), 4797-4803
- (63) Aoki, H.; Shiroza, T.; Hayakawa, M.; Sato, S.; Kuramitsu, H. K. Cloning of a *Streptococcus mutans* glucosyltransferase gene coding for insoluble glucan synthesis. *Infect. Immun.* **1986**, *53* (3), 587-594

- (64) Hanada, N.; Kuramitsu, H. K. Isolation and characterization of the *Streptococcus mutans* gtfC gene, coding for synthesis of both soluble and insoluble glucans. *Infect. Immun.* **1988**, *56* (8), 1999-2005
- (65) Hanada, N.; Kuramitsu, H. K. Isolation and characterization of the *Streptococcus mutans* gtfD gene, coding for primer-dependent soluble glucan synthesis. *Infect. Immun.* **1989**, *57* (7), 2079-2085
- (66) Nijampatnam, B.; Ahirwar, P.; Pukkanasut, P.; Womack, H.; Casals, L.; Zhang, H.; Cai, X.; Michalek, S. M.; Wu, H.; Velu, S. E. Discovery of Potent Inhibitors of *Streptococcus mutans* Biofilm with Antivirulence Activity. *ACS Med. Chem. Lett.* **2021**, *12* (1), 48-55
- (67) Nijampatnam, B.; Casals, L.; Zheng, R.; Wu, H.; Velu, S. E. Hydroxychalcone inhibitors of *Streptococcus mutans* glucosyl transferases and biofilms as potential anticaries agents. *Bioorg. Med. Chem. Lett.* **2016**, *26* (15), 3508-3513
- (68) Nijampatnam, B.; Zhang, H.; Cai, X.; Michalek, S. M.; Wu, H.; Velu, S. E. Inhibition of *Streptococcus mutans* Biofilms by the Natural Stilbene Piceatannol Through the Inhibition of Glucosyltransferases. *ACS Omega* **2018**, *3* (7), 8378-8385
- (69) Zhang, Q.; Nijampatnam, B.; Hua, Z.; Nguyen, T.; Zou, J.; Cai, X.; Michalek, S. M.; Velu, S. E.; Wu, H. Structure-Based Discovery of Small Molecule Inhibitors of Cariogenic Virulence. *Sci. Rep.* **2017**, *7* (1), 5974
- (70) Ito, K.; Ito, S.; Shimamura, T.; Weyand, S.; Kawarasaki, Y.; Misaka, T.; Abe, K.; Kobayashi, T.; Cameron, A. D.; Iwata, S. Crystal structure of glucansucrase from the dental caries pathogen *Streptococcus mutans*. *J. Mol. Biol.* **2011**, *408* (2), 177-186
- (71) Monchois, V.; Willemot, R.-M.; Monsan, P. Glucansucrases: mechanism of action and structure–function relationships. *FEMS Microbiol. Rev.* **1999**, *23* (2), 131-151
- (72) Abou Neel, E. A.; Aljabo, A.; Strange, A.; Ibrahim, S.; Coathup, M.; Young, A. M.; Bozec, L.; Mudera, V. Demineralization-remineralization dynamics in teeth and bone. *Int. J. Nanomedicine* **2016**, *11*, 4743-4763
- (73) Arola, D. D.; Gao, S.; Zhang, H.; Masri, R. The Tooth: Its Structure and Properties. *Dent. Clin. North. Am.* **2017**, *61* (4), 651-668
- (74) Koussoulakou, D. S.; Margaritis, L. H.; Koussoulakos, S. L. A curriculum vitae of teeth: evolution, generation, regeneration. *Int. J. Biol. Sci.* **2009**, *5* (3), 226-243
- (75) Chen, L.; Al-Bayatee, S.; Khurshid, Z.; Shavandi, A.; Brunton, P.; Ratnayake, J. Hydroxyapatite in Oral Care Products-A Review. *Materials (Basel)* **2021**, *14* (17),
- (76) Ratnayake, J. T. B.; Mucalo, M.; Dias, G. J. Substituted hydroxyapatites for bone regeneration: A review of current trends. *J. Biomed. Mater. Res. - B Appl. Biomater.* **2017**, *105* (5), 1285-1299

- (77) Goldberg, M.; Kulkarni, A. B.; Young, M.; Boskey, A. Dentin: structure, composition and mineralization. *Front. Biosci. (Elite Ed.)* **2011**, 3 (2), 711-735
- (78) Demarco, F. F.; Conde, M. C.; Cavalcanti, B. N.; Casagrande, L.; Sakai, V. T.; Nör, J. E. Dental pulp tissue engineering. *Braz. Dent. J.* **2011**, 22 (1), 3-13
- (79) Stephan, R. M. Intra-oral hydrogen-ion concentrations associated with dental caries activity. *J. Dent. Res.* **1944**, 23 (4), 257-266
- (80) Mandel, I. The functions of saliva. *J. Dent. Res.* **1987**, 66 (1\_suppl), 623-627
- (81) Bowen, W. H. The Stephan Curve revisited. *Odontology* **2013**, 101 (1), 2-8
- (82) Tabak, L. A. Structure And Function of Human Salivary Mucins. *Crit. Rev. Oral Biol. Med.* **1990**, 1 (4), 229-234
- (83) Slomiany, B. L.; Murty, V. L. N.; Piotrowski, J.; Slomiany, A. Salivary mucins in oral mucosal defense. *Gen. Pharmacol. Vasc. Syst.* **1996**, 27 (5), 761-771
- (84) Mandel, I. D. Impact of saliva on dental caries. *Compendium* **1989**, (13), S476-S481
- (85) Mandel, I. D. The role of saliva in maintaining oral homeostasis. *J. Am. Dent. Assoc.* **1989**, 119 (2), 298-304
- (86) Edgar, W. M. Saliva and dental health. Clinical implications of saliva: report of a consensus meeting. *Br. Dent. J.* **1990**, 169 (4), 96-98
- (87) McNabb, P. C.; Tomasi, T. Host defense mechanisms at mucosal surfaces. *Annu. Rev. Microbiol.* **1981**, 35 (1), 477-496
- (88) Humphrey, S. P.; Williamson, R. T. A review of saliva: Normal composition, flow, and function. *J. Prosthet.* **2001**, 85 (2), 162-169
- (89) K, P. M.; N, K. P.; G, S. M. Anti cariogenic efficacy of herbal and conventional tooth pastes - a comparative in-vitro study. *J. Int. Oral Health* **2013**, 5 (2), 8-13
- (90) Schmidt, J. C.; Zaugg, C.; Weiger, R.; Walter, C. Brushing without brushing?--a review of the efficacy of powered toothbrushes in noncontact biofilm removal. *Clin. Oral Investig.* **2013**, 17 (3), 687-709
- (91) Davies, A. The mode of action of chlorhexidine. *J. Periodontal Res. Suppl.* **1973**, 12, 68-75
- (92) Jenkins, S.; Addy, M.; Wade, W. The mechanism of action of chlorhexidine. A study of plaque growth on enamel inserts in vivo. *J. Clin. Periodontol.* **1988**, 15 (7), 415-424
- (93) Loe, H.; Rindom Schiøtt, C. The effect of mouthrinses and topical application of chlorhexidine on the development of dental plaque and gingivitis in man. *J. Periodontal Res.* **1970**, 5 (2), 79-83
- (94) Marinone, M. G.; Savoldi, E. Chlorhexidine and taste. Influence of mouthwashes concentration and of rinsing time. *Minerva. Stomatol.* **2000**, 49 (5), 221-226

- (95) Eriksen, H. M.; Nordbø, H.; Kantanen, H.; Ellingsen, J. E. Chemical plaque control and extrinsic tooth discoloration. A review of possible mechanisms. *J. Clin. Periodontol.* **1985**, *12* (5), 345-350
- (96) Li, X.; Wong, C. H.; Ng, T. W.; Zhang, C. F.; Leung, K. C.; Jin, L. The spherical nanoparticle-encapsulated chlorhexidine enhances anti-biofilm efficiency through an effective releasing mode and close microbial interactions. *Int. J. Nanomedicine* **2016**, *11*, 2471-2480
- (97) Bescos, R.; Ashworth, A.; Cutler, C.; Brookes, Z. L.; Belfield, L.; Rodiles, A.; Casas-Agustench, P.; Farnham, G.; Liddle, L.; Burleigh, M.; et al. Effects of Chlorhexidine mouthwash on the oral microbiome. *Sci. Rep.* **2020**, *10* (1), 5254
- (98) Cieplik, F.; Jakubovics, N. S.; Buchalla, W.; Maisch, T.; Hellwig, E.; Al-Ahmad, A. Resistance Toward Chlorhexidine in Oral Bacteria - Is There Cause for Concern? *Front. Microbiol.* **2019**, *10*, 587
- (99) Witt, J.; Bsoul, S.; He, T.; Gibb, R.; Dunavent, J.; Hamilton, A. The effect of toothbrushing regimens on the plaque inhibitory properties of an experimental cetylpyridinium chloride mouthrinse. *J. Clin. Periodontol.* **2006**, *33* (10), 737-742
- (100) Rajendiran, M.; Trivedi, H. M.; Chen, D.; Gajendrareddy, P.; Chen, L. Recent Development of Active Ingredients in Mouthwashes and Toothpastes for Periodontal Diseases. *Molecules* **2021**, *26* (7),
- (101) Messier, C.; Epifano, F.; Genovese, S.; Grenier, D. Licorice and its potential beneficial effects in common oro-dental diseases. *Oral Dis.* **2012**, *18* (1), 32-39
- (102) Nagpal, M.; Sood, S. Role of curcumin in systemic and oral health: An overview. *J. Nat. Sci. Biol. Med.* **2013**, *4* (1), 3-7
- (103) Ayoob, S.; Gupta, A. K. Fluoride in Drinking Water: A Review on the Status and Stress Effects. *Crit. Rev. Environ. Sci. Technol.* **2006**, *36* (6), 433-487
- (104) Marinho, V. C. C.; Higgins, J.; Logan, S.; Sheiham, A. Fluoride toothpastes for preventing dental caries in children and adolescents. *Cochrane Database Syst. Rev.* **2003**, (1),
- (105) Buzalaf, M. A. R.; Pessan, J. P.; Honório, H. M.; Ten Cate, J. M. Mechanisms of action of fluoride for caries control. *Monogr Oral Sci* **2011**, *22*, 97-114
- (106) Featherstone, J. D. Fluoride, remineralization and root caries. *Am. J. Dent.* **1994**, *7* (5), 271-274
- (107) Iheozor-Ejiofor, Z.; Worthington, H. V.; Walsh, T.; O'Malley, L.; Clarkson, J. E.; Macey, R.; Alam, R.; Tugwell, P.; Welch, V.; Glenny, A. M. Water fluoridation for the prevention of dental caries. *Cochrane Database Syst. Rev.* **2015**, *2015* (6), Cd010856
- (108) Carey, C. M. Focus on fluorides: update on the use of fluoride for the prevention of dental caries. *J. Evid. Based Dent. Pract.* **2014**, *14 Suppl*, 95-102

- (109) O'Mullane, D. M.; Baez, R. J.; Jones, S.; Lennon, M. A.; Petersen, P. E.; Rugg-Gunn, A. J.; Whelton, H.; Whitford, G. M. Fluoride and Oral Health. *Community Dent. Health* **2016**, *33* (2), 69-99
- (110) Grandjean, P. Developmental fluoride neurotoxicity: an updated review. *Environ. Health* **2019**, *18* (1), 110
- (111) Nakahara, K.; Kawabata, S.; Ono, H.; Ogura, K.; Tanaka, T.; Ooshima, T.; Hamada, S. Inhibitory effect of oolong tea polyphenols on glycosyltransferases of mutans Streptococci. *Appl. Environ. Microbiol.* **1993**, *59* (4), 968-973
- (112) Hirasawa, M.; Takada, K.; Otake, S. Inhibition of acid production in dental plaque bacteria by green tea catechins. *Caries Res.* **2006**, *40* (3), 265-270
- (113) Otake, S.; Makimura, M.; Kuroki, T.; Nishihara, Y.; Hirasawa, M. Anticaries effects of polyphenolic compounds from Japanese green tea. *Caries Res.* **1991**, *25* (6), 438-443
- (114) Yanagida, A.; Kanda, T.; Tanabe, M.; Matsudaira, F.; Oliveira Cordeiro, J. G. Inhibitory effects of apple polyphenols and related compounds on cariogenic factors of mutans streptococci. *J. Agric. Food. Chem.* **2000**, *48* (11), 5666-5671
- (115) Koo, H.; Duarte, S.; Murata, R. M.; Scott-Anne, K.; Gregoire, S.; Watson, G. E.; Singh, A. P.; Vorsa, N. Influence of cranberry proanthocyanidins on formation of biofilms by Streptococcus mutans on saliva-coated apatitic surface and on dental caries development in vivo. *Caries Res.* **2010**, *44* (2), 116-126
- (116) Leitão, D. P.; Polizello, A. C.; Ito, I. Y.; Spadaro, A. C. Antibacterial screening of anthocyanic and proanthocyanic fractions from cranberry juice. *J. Med. Food* **2005**, *8* (1), 36-40
- (117) Feng, G.; Klein, M. I.; Gregoire, S.; Singh, A. P.; Vorsa, N.; Koo, H. The specific degree-of-polymerization of A-type proanthocyanidin oligomers impacts Streptococcus mutans glucan-mediated adhesion and transcriptome responses within biofilms. *Biofouling* **2013**, *29* (6), 629-640
- (118) Koo, H.; Seils, J.; Abranches, J.; Burne, R. A.; Bowen, W. H.; Quivey, R. G., Jr. Influence of apigenin on gtf gene expression in Streptococcus mutans UA159. *Antimicrob. Agents Chemother.* **2006**, *50* (2), 542-546
- (119) Koo, H.; Jeon, J. G. Naturally occurring molecules as alternative therapeutic agents against cariogenic biofilms. *Adv. Dent. Res.* **2009**, *21* (1), 63-68
- (120) Gregoire, S.; Singh, A. P.; Vorsa, N.; Koo, H. Influence of cranberry phenolics on glucan synthesis by glucosyltransferases and Streptococcus mutans acidogenicity. *J. Appl. Microbiol.* **2007**, *103* (5), 1960-1968
- (121) Hegde, K. S.; Bhat, S. S.; Rao, A.; Sain, S. Effect of Propolis on Streptococcus mutans Counts: An in vivo Study. *Int. J. Clin. Pediatr. Dent.* **2013**, *6* (1), 22-25

- (122) Koo, H.; Pearson, S. K.; Scott-Anne, K.; Abranches, J.; Cury, J. A.; Rosalen, P. L.; Park, Y. K.; Marquis, R. E.; Bowen, W. H. Effects of apigenin and tt-farnesol on glucosyltransferase activity, biofilm viability and caries development in rats. *Oral Microbiol. Immunol.* **2002**, *17* (6), 337-343
- (123) Koo, H.; Rosalen, P. L.; Cury, J. A.; Ambrosano, G. M.; Murata, R. M.; Yatsuda, R.; Ikegaki, M.; Alencar, S. M.; Park, Y. K. Effect of a new variety of *Apis mellifera* propolis on mutans Streptococci. *Curr. Microbiol.* **2000**, *41* (3), 192-196
- (124) Devulapalle, K. S.; Mooser, G. Glucosyltransferase inactivation reduces dental caries. *J. Dent. Res.* **2001**, *80* (2), 466-469
- (125) Newbrun, E.; Hoover, C. I.; Walker, G. J. Inhibition by acarbose, nojirimycin and 1-deoxynojirimycin of glucosyltransferase produced by oral streptococci. *Arch. Oral Biol.* **1983**, *28* (6), 531-536
- (126) Chen, L.; Ren, Z.; Zhou, X.; Zeng, J.; Zou, J.; Li, Y. Inhibition of *Streptococcus mutans* biofilm formation, extracellular polysaccharide production, and virulence by an oxazole derivative. *Appl. Microbiol. Biotechnol.* **2016**, *100* (2), 857-867
- (127) Hartman, A. M.; Jumde, V. R.; Elgaher, W. A. M.; Te Poele, E. M.; Dijkhuizen, L.; Hirsch, A. K. H. Potential Dental Biofilm Inhibitors: Dynamic Combinatorial Chemistry Affords Sugar-Based Molecules that Target Bacterial Glucosyltransferase. *Chem. Med. Chem.* **2021**, *16* (1), 113-123
- (128) Oda, M.; Kurosawa, M.; Yamamoto, H.; Domon, H.; Takenaka, S.; Ohsumi, T.; Maekawa, T.; Yamasaki, N.; Furue, Y.; Terao, Y. Sulfated vizantin inhibits biofilm maturation by *Streptococcus mutans*. *Microbiol Immunol* **2020**, *64* (7), 493-501
- (129) Butron Téllez Giron, C.; Hernandez Sierra, J. F.; DeAlba-Montero, I.; Urbano Pena, M. L. A.; Ruiz, F. Therapeutic Use of Silver Nanoparticles in the Prevention and Arrest of Dental Caries. *Bioinorg. Chem. Appl.* **2020**, *2020*, 8882930
- (130) Sims, K. R.; Maceren, J. P.; Liu, Y.; Rocha, G. R.; Koo, H.; Benoit, D. S. W. Dual antibacterial drug-loaded nanoparticles synergistically improve treatment of *Streptococcus mutans* biofilms. *Acta Biomater.* **2020**, *115*, 418-431
- (131) Horev, B.; Klein, M. I.; Hwang, G.; Li, Y.; Kim, D.; Koo, H.; Benoit, D. S. pH-activated nanoparticles for controlled topical delivery of farnesol to disrupt oral biofilm virulence. *ACS Nano* **2015**, *9* (3), 2390-2404
- (132) Yi, Y.; Wang, L.; Chen, L.; Lin, Y.; Luo, Z.; Chen, Z.; Li, T.; Wu, J.; Zhong, Z. Farnesol-loaded pH-sensitive polymeric micelles provided effective prevention and treatment on dental caries. *J. Nanobiotech.* **2020**, *18* (1), 89
- (133) Jailani, A.; Kalimuthu, S.; Rajasekar, V.; Ghosh, S.; Collart-Dutilleul, P. Y.; Fatima, N.; Koo, H.; Solomon, A. P.; Cuisinier, F.; Neelakantan, P. Trans-Cinnamaldehyde Eluting Porous Silicon Microparticles Mitigate Cariogenic Biofilms. *Pharm.* **2022**, *14* (7), 1428



- (134) Liu, Y.; Huang, Y.; Kim, D.; Ren, Z.; Oh, M. J.; Cormode, D. P.; Hara, A. T.; Zero, D. T.; Koo, H. Ferumoxytol Nanoparticles Target Biofilms Causing Tooth Decay in the Human Mouth. *Nano Lett.* **2021**, *21* (22), 9442-9449
- (135) Liu, Y.; Naha, P. C.; Hwang, G.; Kim, D.; Huang, Y.; Simon-Soro, A.; Jung, H. I.; Ren, Z.; Li, Y.; Gubara, S.; et al. Topical ferumoxytol nanoparticles disrupt biofilms and prevent tooth decay in vivo via intrinsic catalytic activity. *Nat. Commun.* **2018**, *9* (1), 2920
- (136) Melo, M. A.; Guedes, S. F.; Xu, H. H.; Rodrigues, L. K. Nanotechnology-based restorative materials for dental caries management. *Trends Biotechnol.* **2013**, *31* (8), 459-467
- (137) Mohire, N. C.; Yadav, A. V. Chitosan-based polyherbal toothpaste: as novel oral hygiene product. *Indian J. Dent. Res.* **2010**, *21* (3), 380-384
- (138) Seneviratne, C. J.; Leung, K. C.-F.; Wong, C.-H.; Lee, S.-F.; Li, X.; Leung, P. C.; Lau, C. B. S.; Wat, E.; Jin, L. Nanoparticle-Encapsulated Chlorhexidine against Oral Bacterial Biofilms. *Plos One* **2014**, *9* (8), e103234
- (139) Zhang, J. F.; Wu, R.; Fan, Y.; Liao, S.; Wang, Y.; Wen, Z. T.; Xu, X. Antibacterial Dental Composites with Chlorhexidine and Mesoporous Silica. *J. Dent. Res.* **2014**, *93* (12), 1283-1289
- (140) Nguyen, S.; Hiorth, M.; Rykke, M.; Smistad, G. Polymer coated liposomes for dental drug delivery – Interactions with parotid saliva and dental enamel. *Eur. J. Pharm. Sci.* **2013**, *50* (1), 78-85
- (141) Feitosa, S. A.; Palasuk, J.; Kamocki, K.; Geraldini, S.; Gregory, R. L.; Platt, J. A.; Windsor, L. J.; Bottino, M. C. Doxycycline-encapsulated nanotube-modified dentin adhesives. *J. Dent. Res.* **2014**, *93* (12), 1270-1276
- (142) Zhou, Y.; Yang, J.; Lin, Z.; Li, J.; Liang, K.; Yuan, H.; Li, S.; Li, J. Triclosan-loaded poly(amido amine) dendrimer for simultaneous treatment and remineralization of human dentine. *Colloids Surf. B.* **2014**, *115*, 237-243
- (143) Naha, P. C.; Liu, Y.; Hwang, G.; Huang, Y.; Gubara, S.; Jonnakuti, V.; Simon-Soro, A.; Kim, D.; Gao, L.; Koo, H.; et al. Dextran-Coated Iron Oxide Nanoparticles as Biomimetic Catalysts for Localized and pH-Activated Biofilm Disruption. *ACS Nano* **2019**, *13* (5), 4960-4971
- (144) Chen, L.; Ren, Z.; Zhou, X.; Zeng, J.; Zou, J.; Li, Y. Inhibition of *Streptococcus mutans* biofilm formation, extracellular polysaccharide production, and virulence by an oxazole derivative. *Appl Microbiol Biotechnol* **2016**, *100* (2), 857-867

## APPENDIX

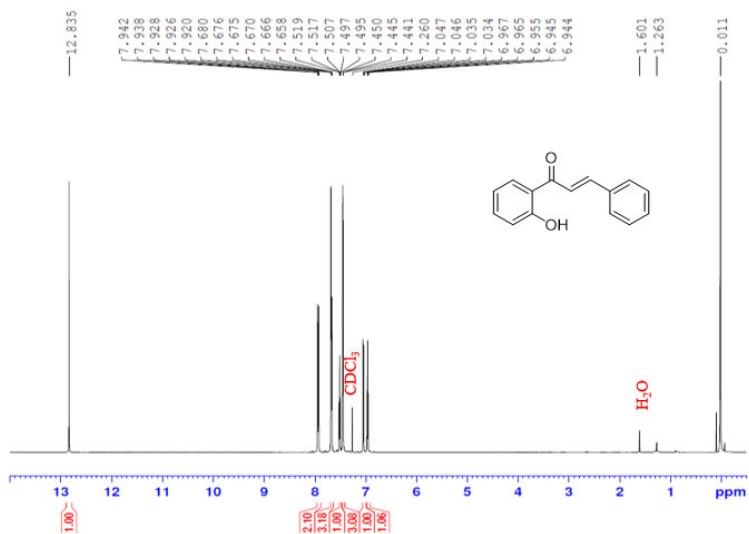
### <sup>1</sup>H AND <sup>13</sup>C SPECTRA, AND HPLC TRACES OF CHALCONES, METHOXYAURONES AND HYDROXYAURONES

**APPENDIX:  $^1\text{H}$  AND  $^{13}\text{C}$  SPECTRA, AND HPLC TRACES OF CHALCONES, METHOXYAURONES AND HYDROXYAURONES**

**$^1\text{H}$ -NMR and  $^{13}\text{C}$ -NMR spectra of compounds**

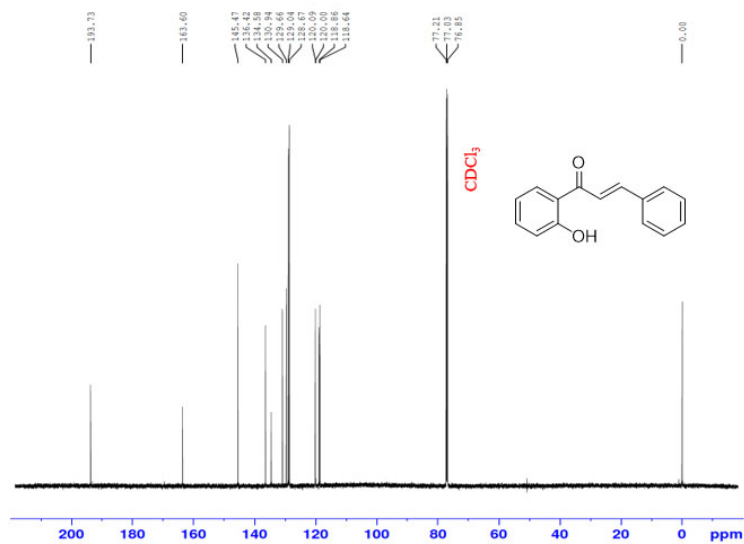
**1-(2-Hydroxyphenyl)-3-phenyl-2-propen-1-one (3a)**

$^1\text{H}$  NMR (700 MHz,  $\text{CDCl}_3$ )



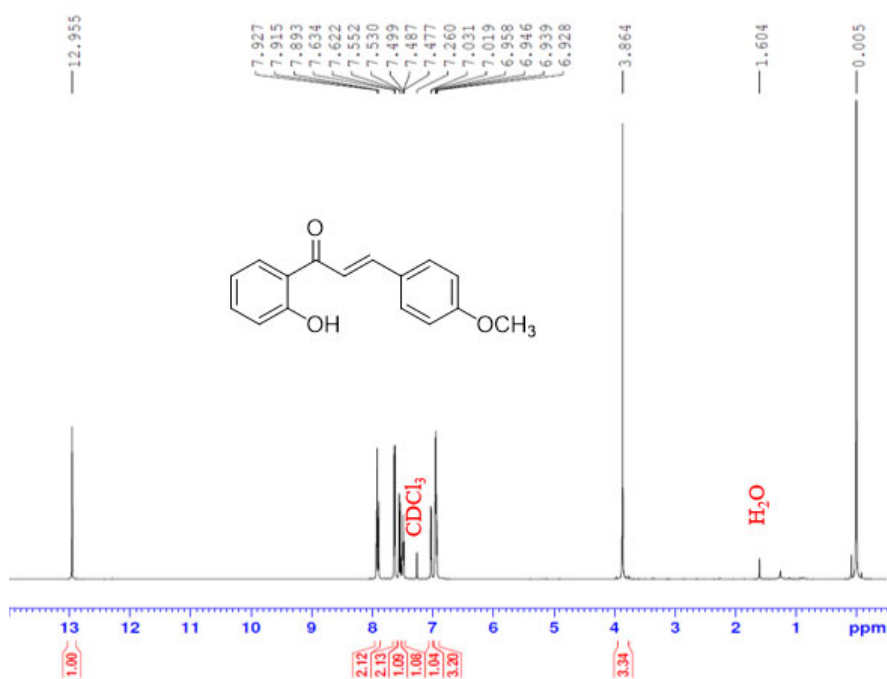
**1-(2-Hydroxyphenyl)-3-phenyl-2-propen-1-one (3a)**

$^{13}\text{C}$  NMR (700 MHz,  $\text{CDCl}_3$ )



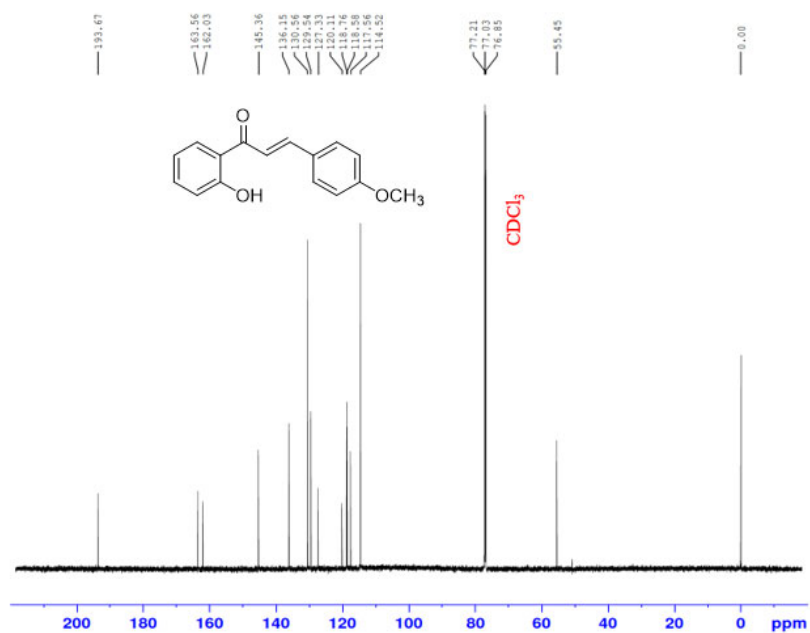
1-(2-Hydroxyphenyl)-3-(4-methoxyphenyl)-2-propen-1-one (**3b**)

$^1\text{H}$  NMR (700 MHz,  $\text{CDCl}_3$ )

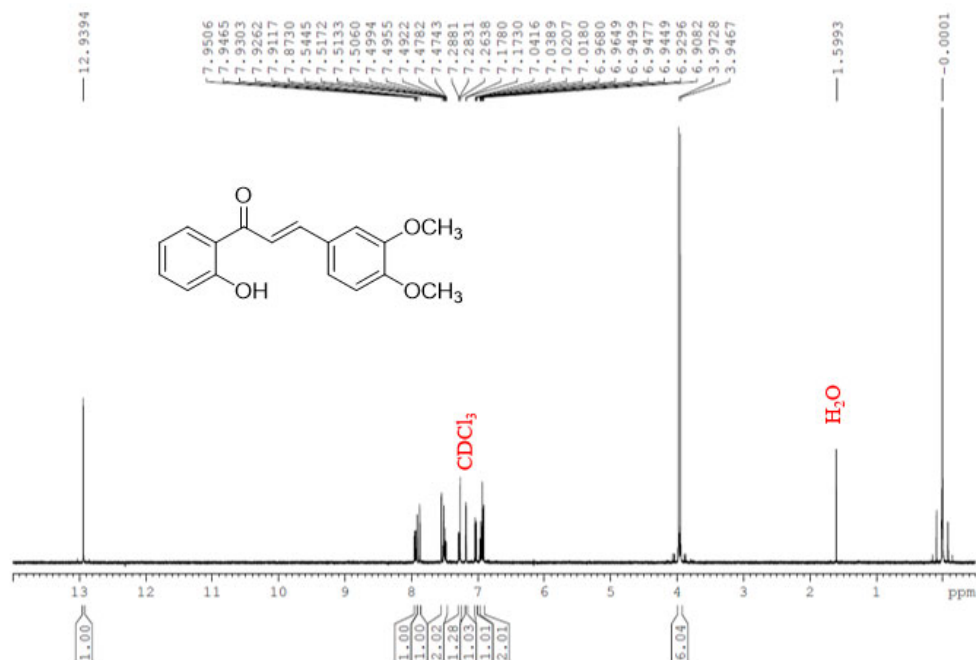


1-(2-Hydroxyphenyl)-3-(4-methoxyphenyl)-2-propen-1-one (**3b**)

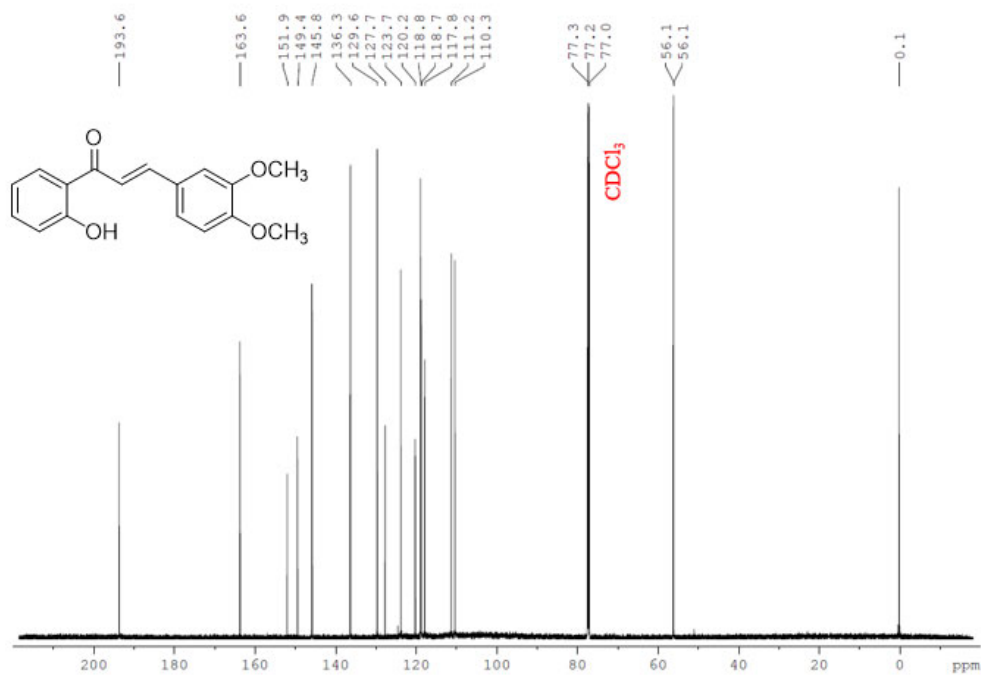
$^{13}\text{C}$  NMR (700 MHz,  $\text{CDCl}_3$ )



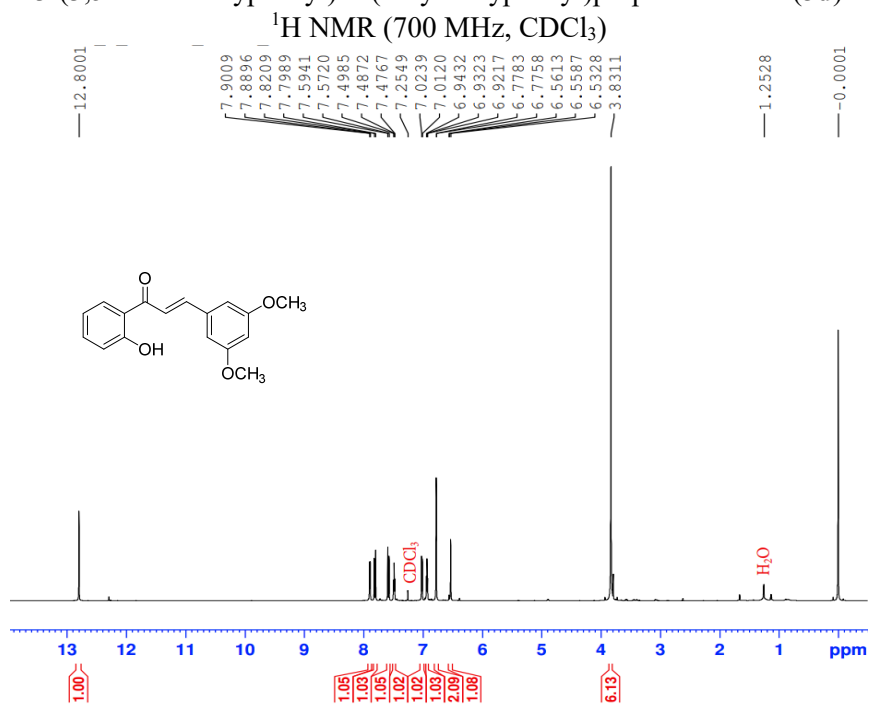
3-(3,4-Dimethoxyphenyl)-1-(2-hydroxyphenyl)prop-2-en-1-one (**3c**)  
<sup>1</sup>H NMR (400 MHz, CDCl<sub>3</sub>)



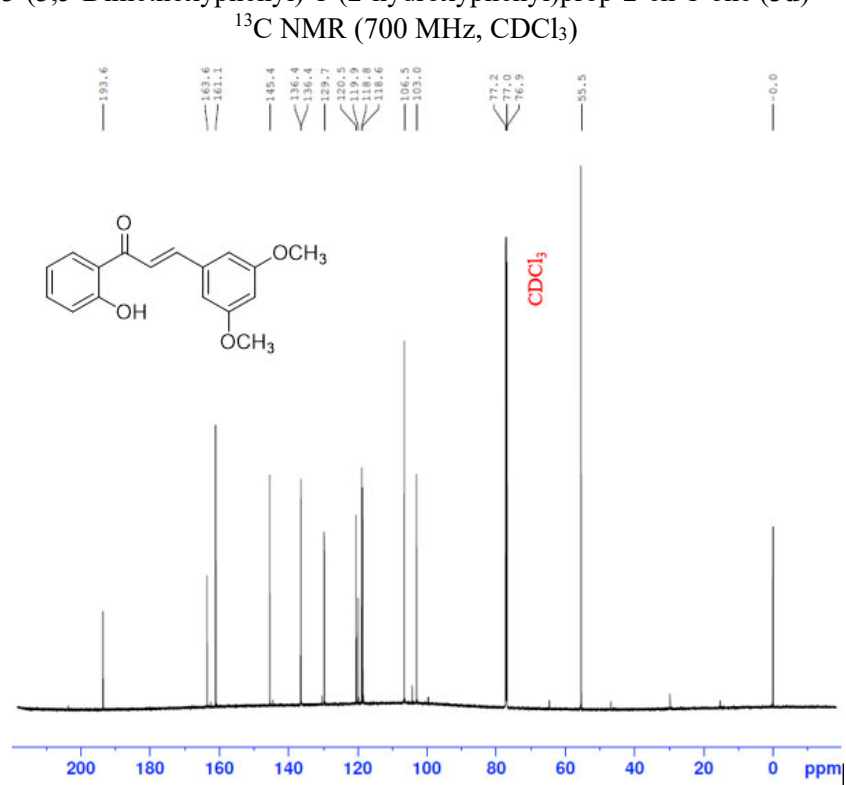
3-(3,4-Dimethoxyphenyl)-1-(2-hydroxyphenyl)prop-2-en-1-one (**3c**)  
<sup>13</sup>C NMR (700 MHz, CDCl<sub>3</sub>)



3-(3,5-Dimethoxyphenyl)-1-(2-hydroxyphenyl)prop-2-en-1-one (**3d**)

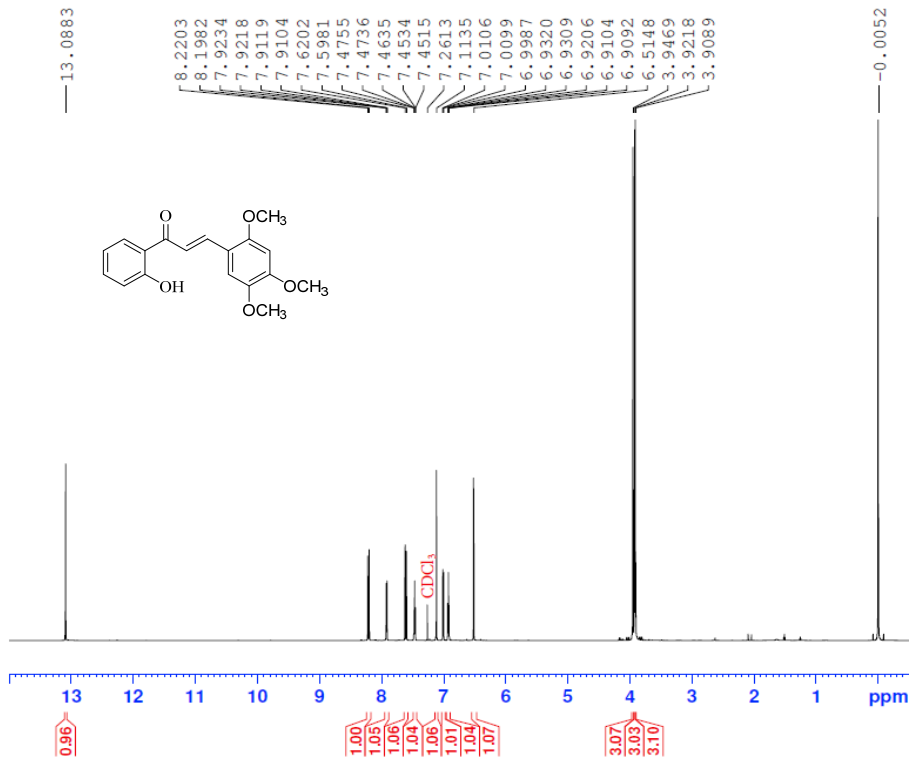


3-(3,5-Dimethoxyphenyl)-1-(2-hydroxyphenyl)prop-2-en-1-one (**3d**)



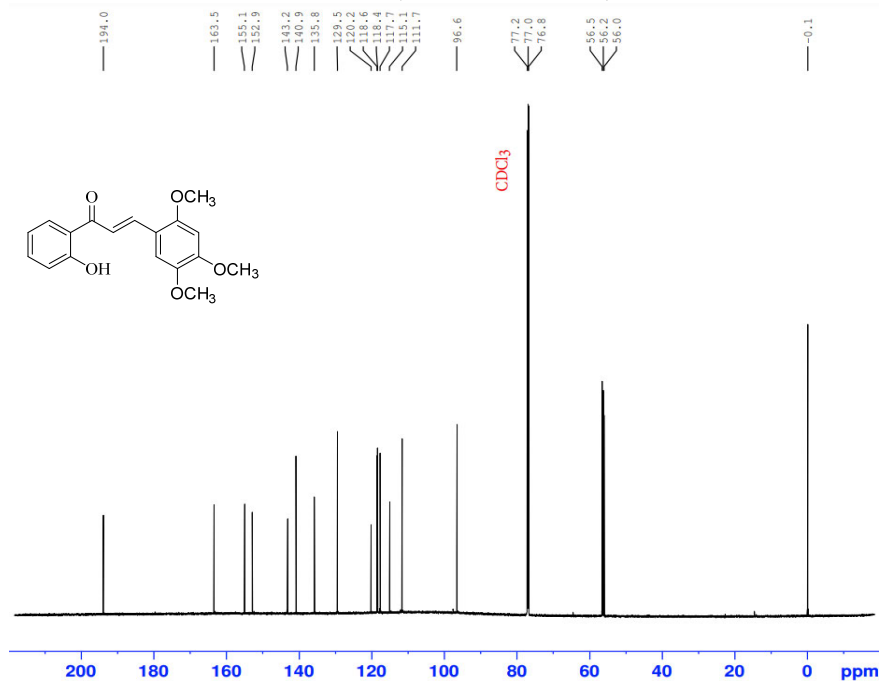
1-(2-Hydroxyphenyl)-3-(2,4,5-trimethoxyphenyl)prop-2-en-1-one (**3e**)

$^1\text{H}$  NMR (700 MHz,  $\text{CDCl}_3$ )



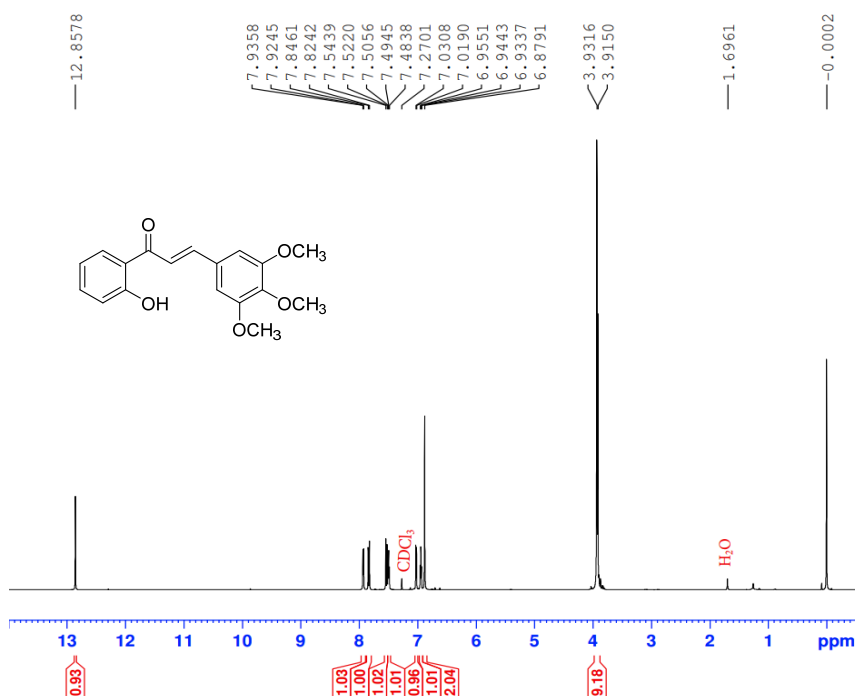
1-(2-Hydroxyphenyl)-3-(2,4,5-trimethoxyphenyl)prop-2-en-1-one (**3e**)

$^{13}\text{C}$  NMR (700 MHz,  $\text{CDCl}_3$ )



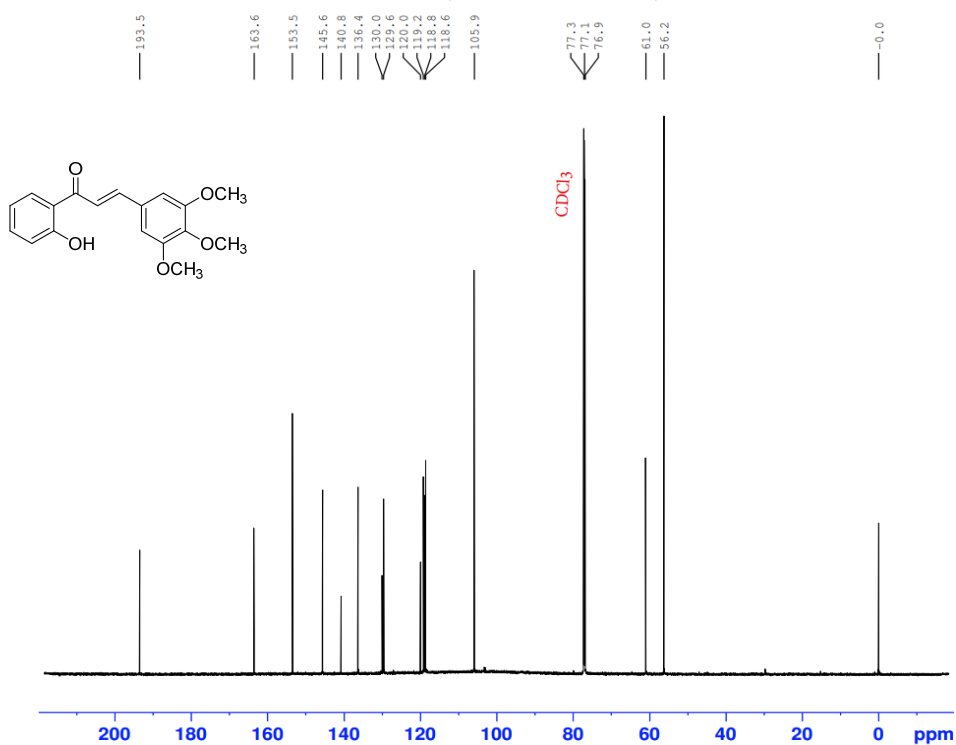
1-(2-Hydroxyphenyl)-3-(3,4,5-trimethoxyphenyl)prop-2-en-1-one (**3f**)

$^1\text{H}$  NMR (700 MHz,  $\text{CDCl}_3$ )



1-(2-Hydroxyphenyl)-3-(3,4,5-trimethoxyphenyl)prop-2-en-1-one (**3f**)

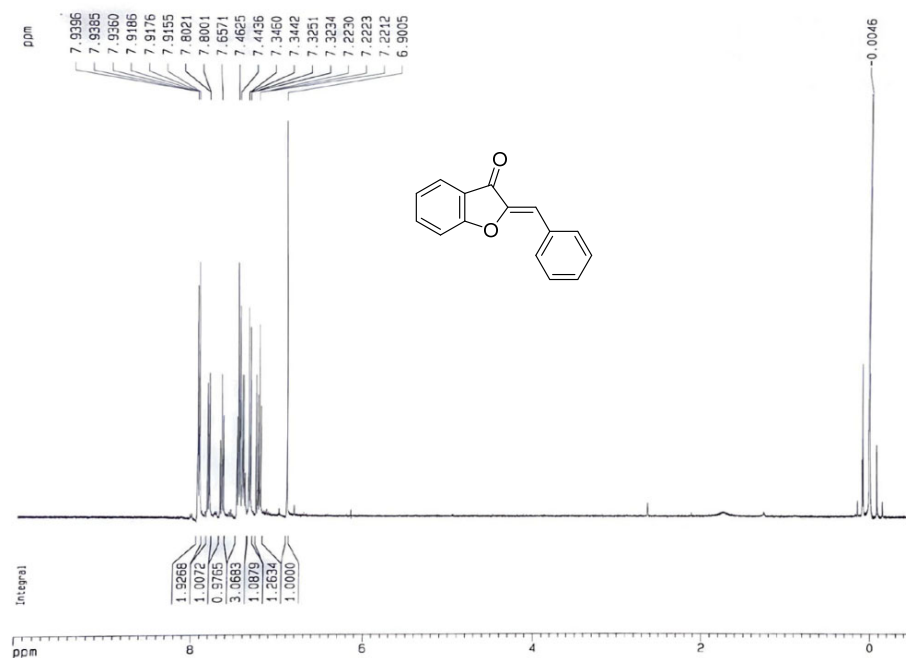
$^{13}\text{C}$  NMR (700 MHz,  $\text{CDCl}_3$ )





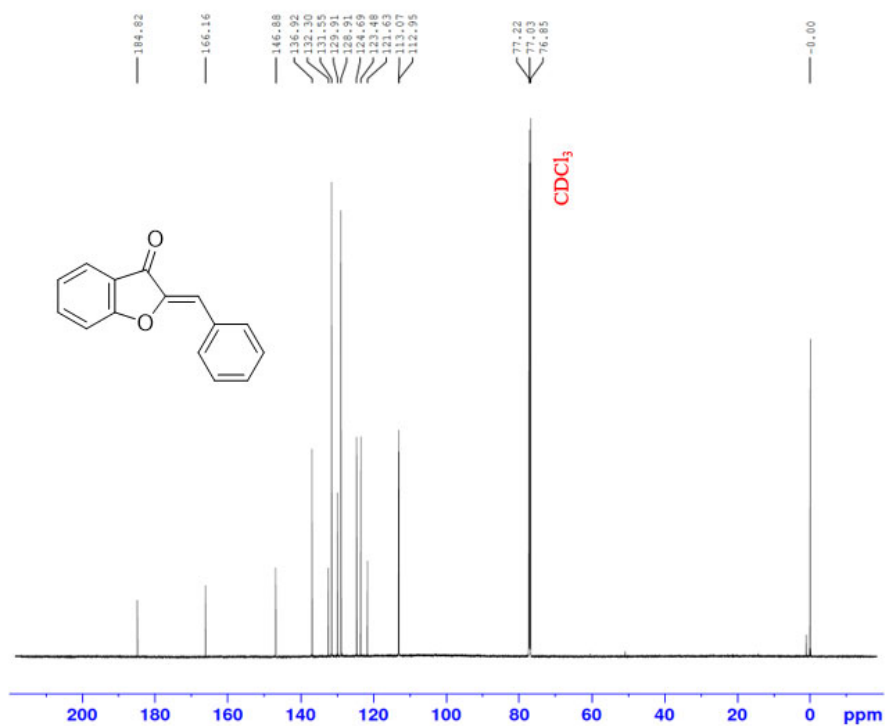
2-(Phenylmethyldene)-2,3-dihydro-1-benzofuran-3-one (MA1)

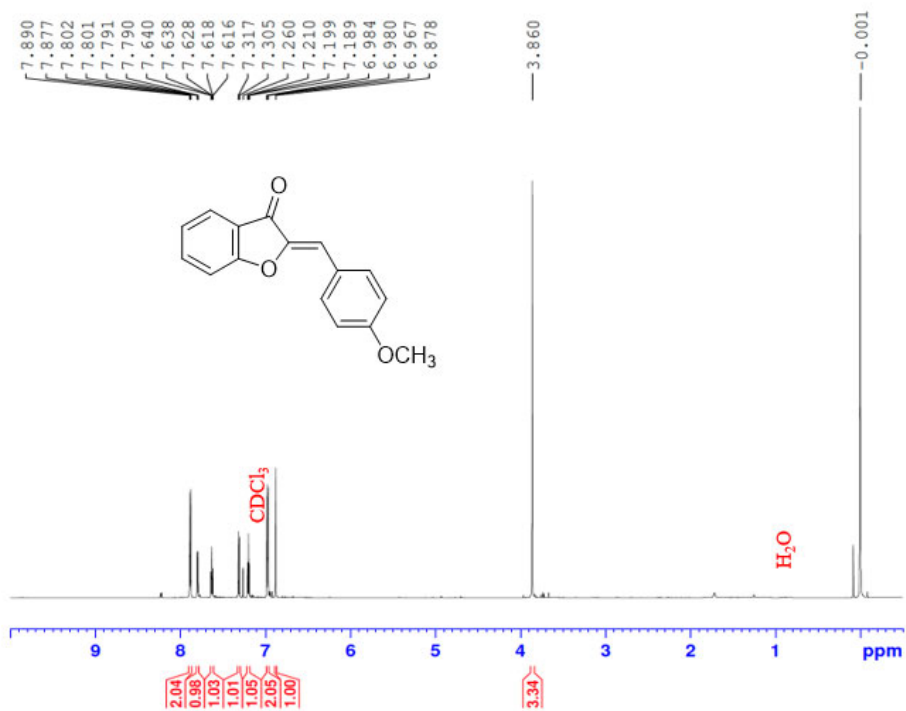
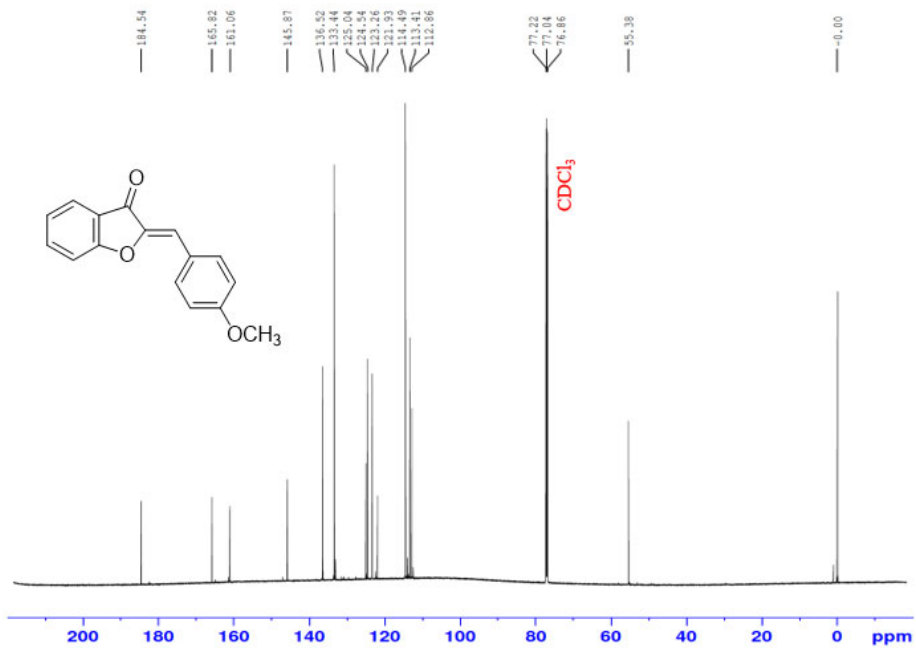
$^1\text{H}$  NMR (400 MHz,  $\text{CDCl}_3$ )



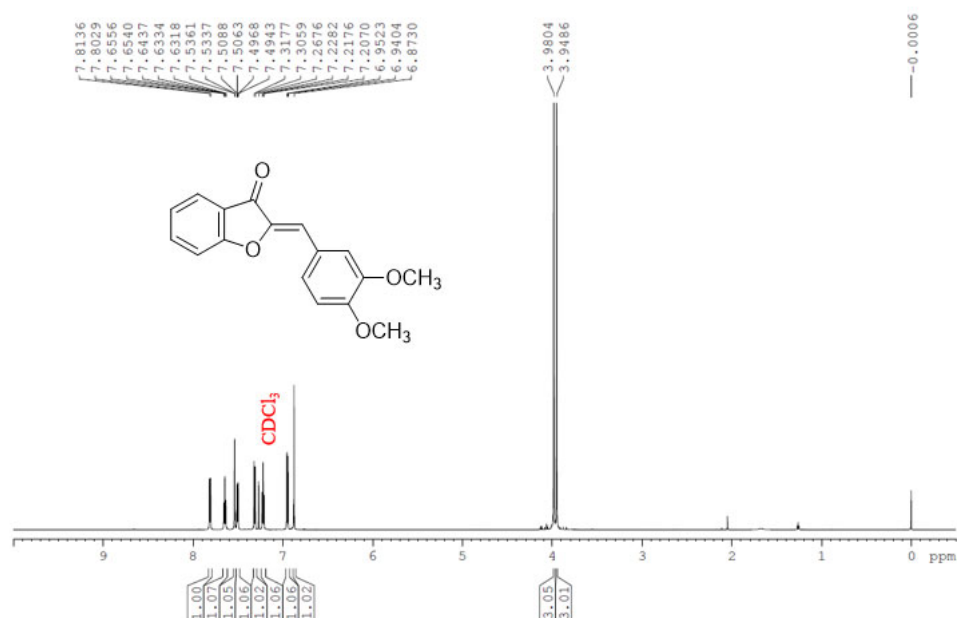
2-(Phenylmethyldene)-2,3-dihydro-1-benzofuran-3-one (MA1)

$^{13}\text{C}$  NMR (700 MHz,  $\text{CDCl}_3$ )

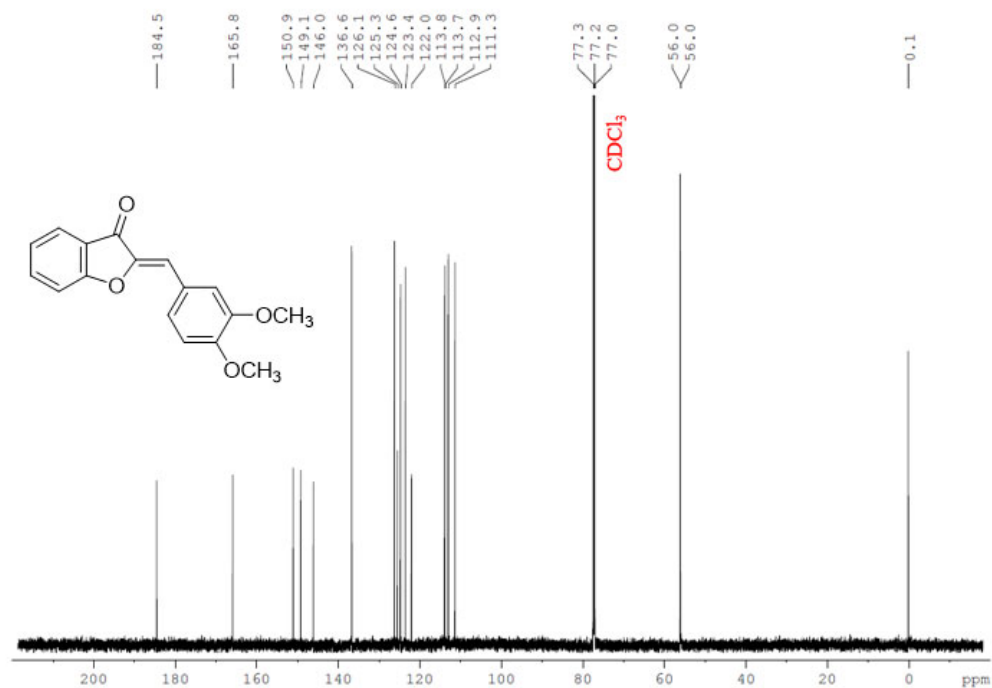


2-[(4-Methoxyphenyl)methylidene]-2,3-dihydro-1-benzofuran-3-one (**MA2**)<sup>1</sup>H NMR (700 MHz, CDCl<sub>3</sub>)2-[(4-Methoxyphenyl)methylidene]-2,3-dihydro-1-benzofuran-3-one (**MA2**) $^{13}\text{C}$  NMR (700 MHz,  $\text{CDCl}_3$ )

2-[(3,4-Dimethoxyphenyl)methylidene]-2,3-dihydro-1-benzofuran-3-one (**MA3**)  
<sup>1</sup>H NMR (700 MHz, CDCl<sub>3</sub>)

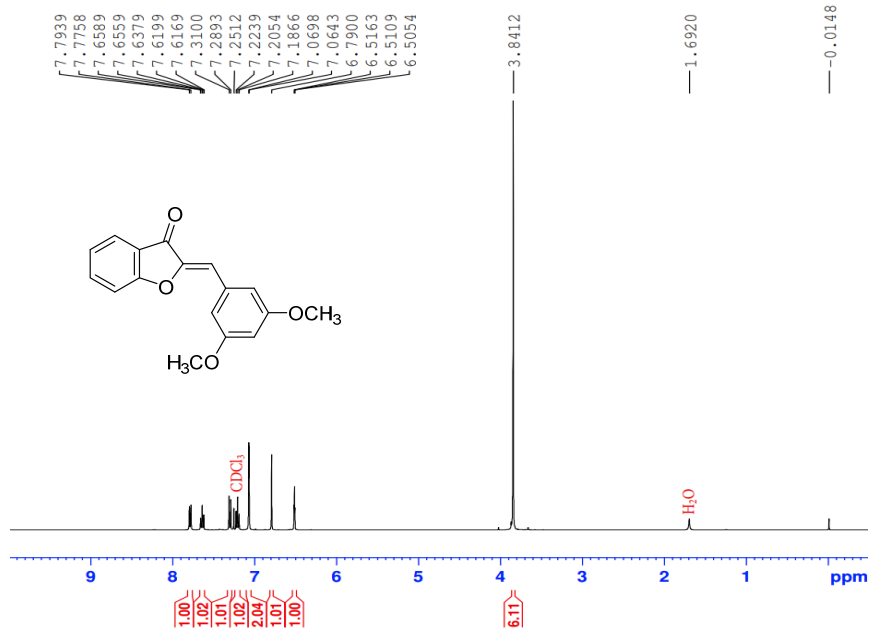


2-[(3,4-Dimethoxyphenyl)methylidene]-2,3-dihydro-1-benzofuran-3-one (**MA3**)  
<sup>13</sup>C NMR (700 MHz, CDCl<sub>3</sub>)



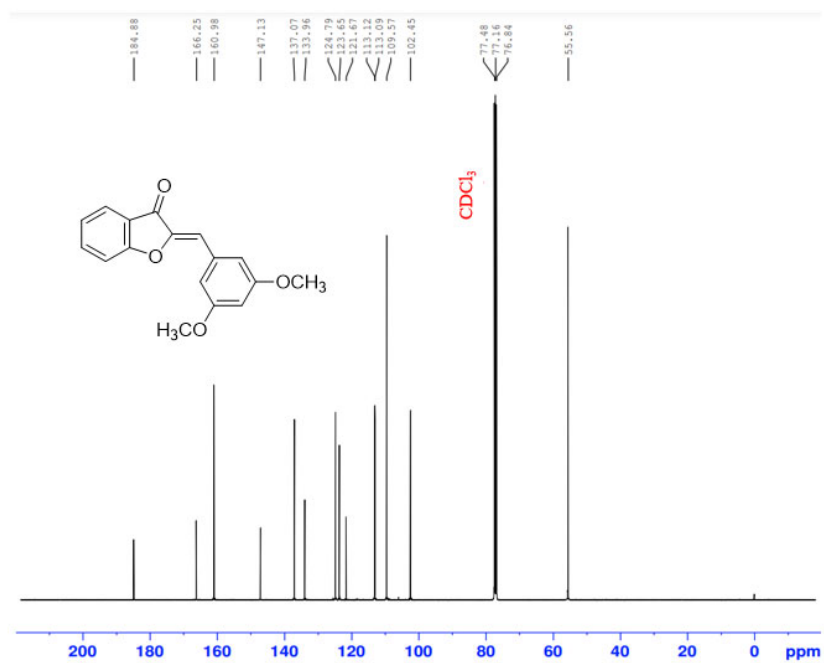
2-[(3,5-Dimethoxyphenyl)methylidene]-2,3-dihydro-1-benzofuran-3-one (MA4)

$^1\text{H}$  NMR (400 MHz,  $\text{CDCl}_3$ )



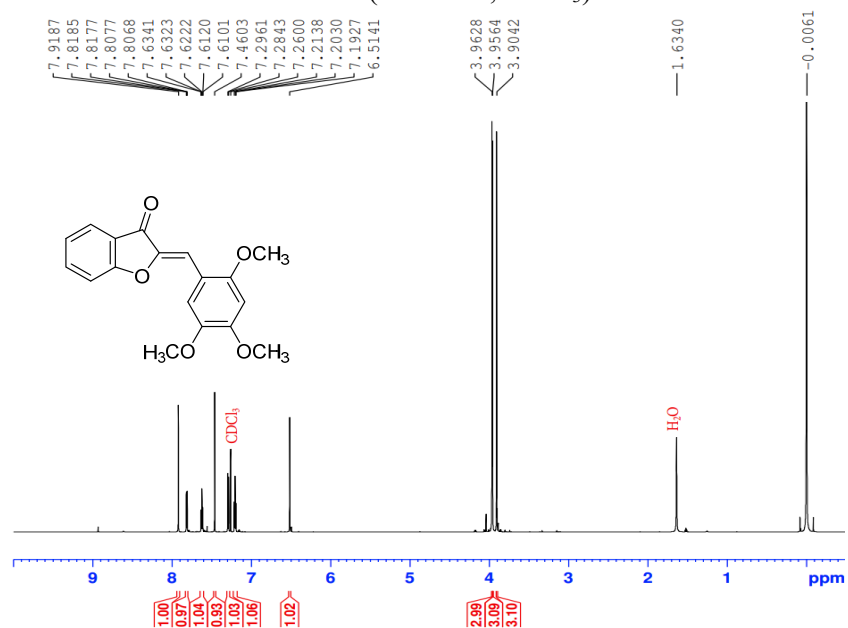
2-[(3,5-Dimethoxyphenyl)methylidene]-2,3-dihydro-1-benzofuran-3-one (MA4)

$^{13}\text{C}$  NMR (400 MHz,  $\text{CDCl}_3$ )



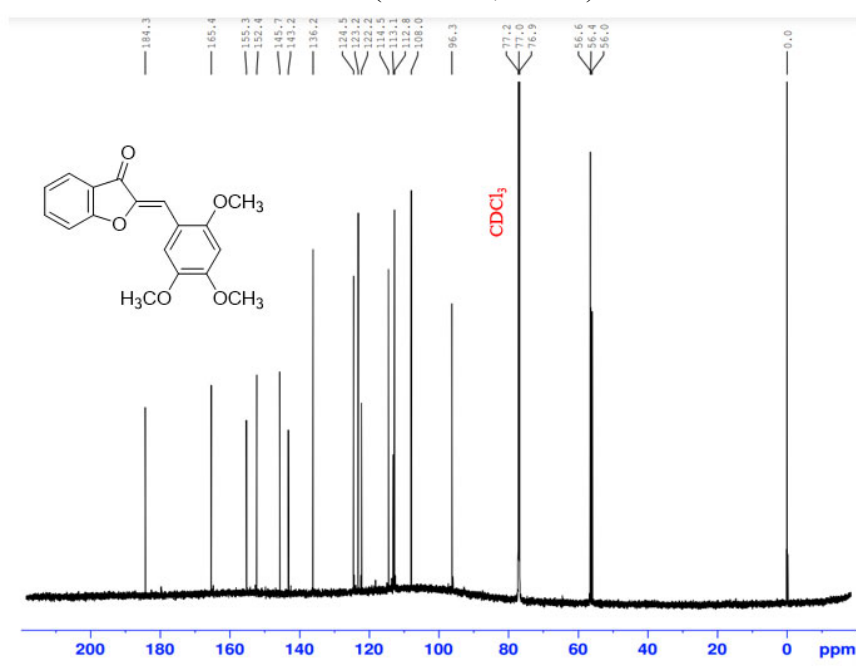
2-[(2,4,5-Trimethoxyphenyl)methylidene]-2,3-dihydro-1-benzofuran-3-one (**MA5**)

$^1\text{H}$  NMR (700 MHz,  $\text{CDCl}_3$ )



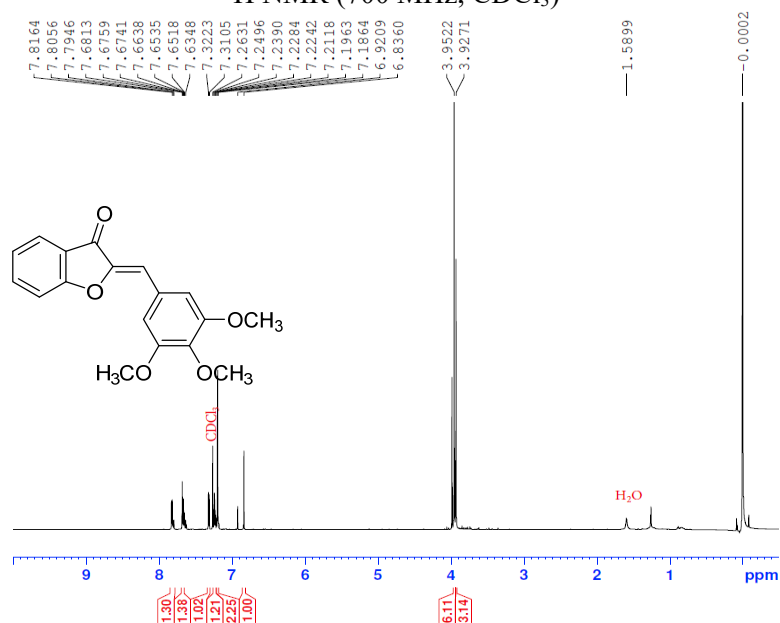
2-[(2,4,5-Trimethoxyphenyl)methylidene]-2,3-dihydro-1-benzofuran-3-one (**MA5**)

$^{13}\text{C}$  NMR (700 MHz,  $\text{CDCl}_3$ )



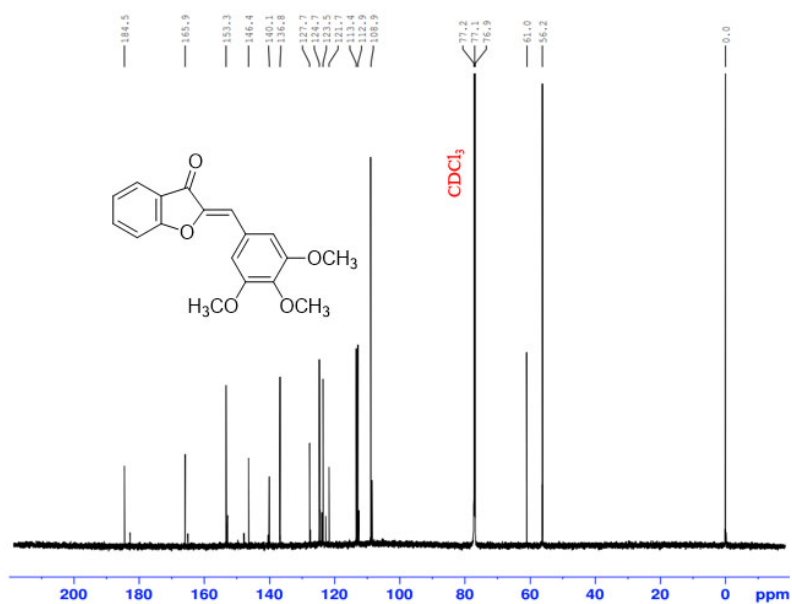
2-[(3,4,5-Trimethoxyphenyl)methylidene]-2,3-dihydro-1-benzofuran-3-one (**MA6**)

$^1\text{H}$  NMR (700 MHz,  $\text{CDCl}_3$ )

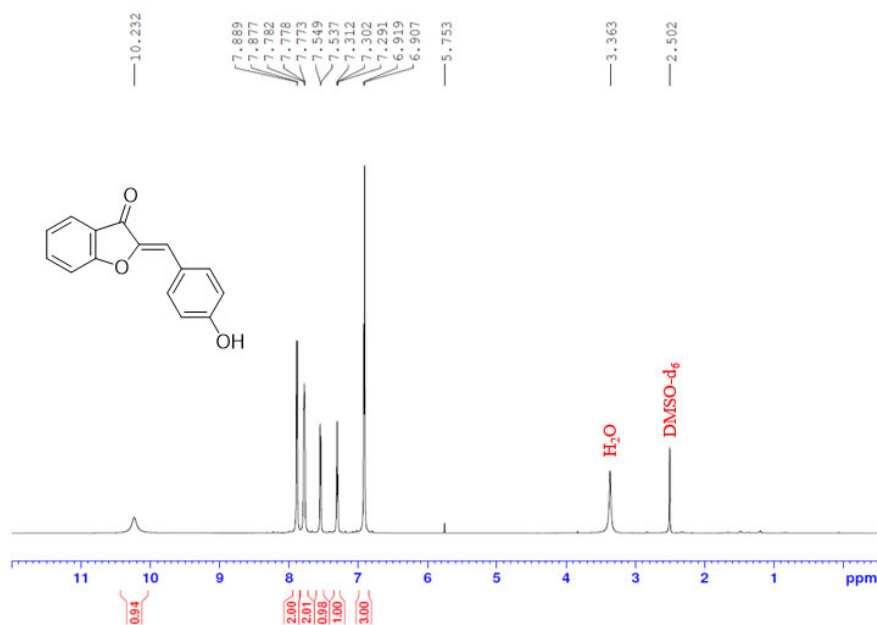


2-[(3,4,5-Trimethoxyphenyl)methylidene]-2,3-dihydro-1-benzofuran-3-one (**MA6**)

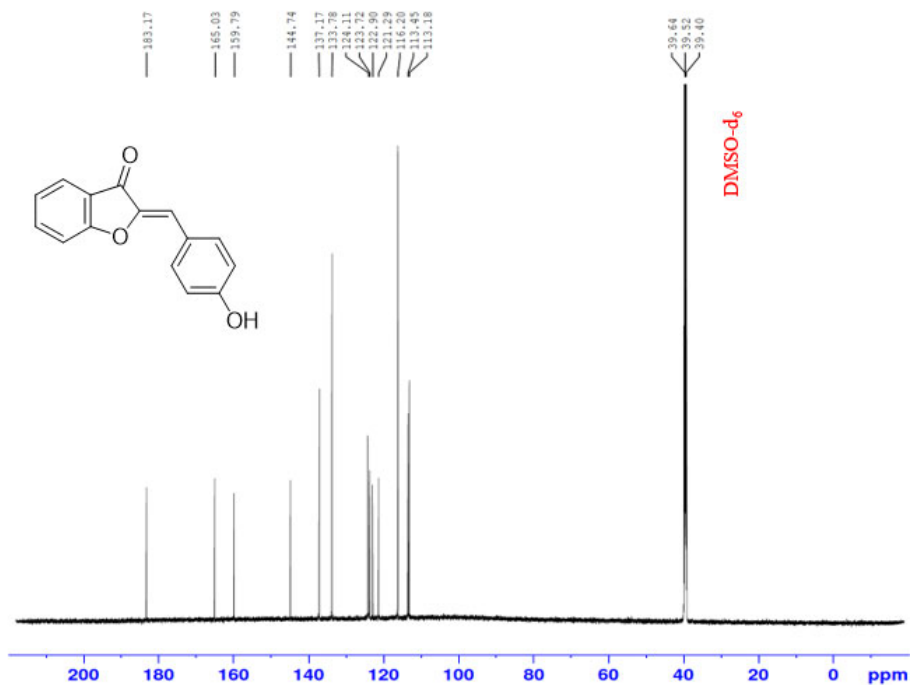
$^{13}\text{C}$  NMR (700 MHz,  $\text{CDCl}_3$ )



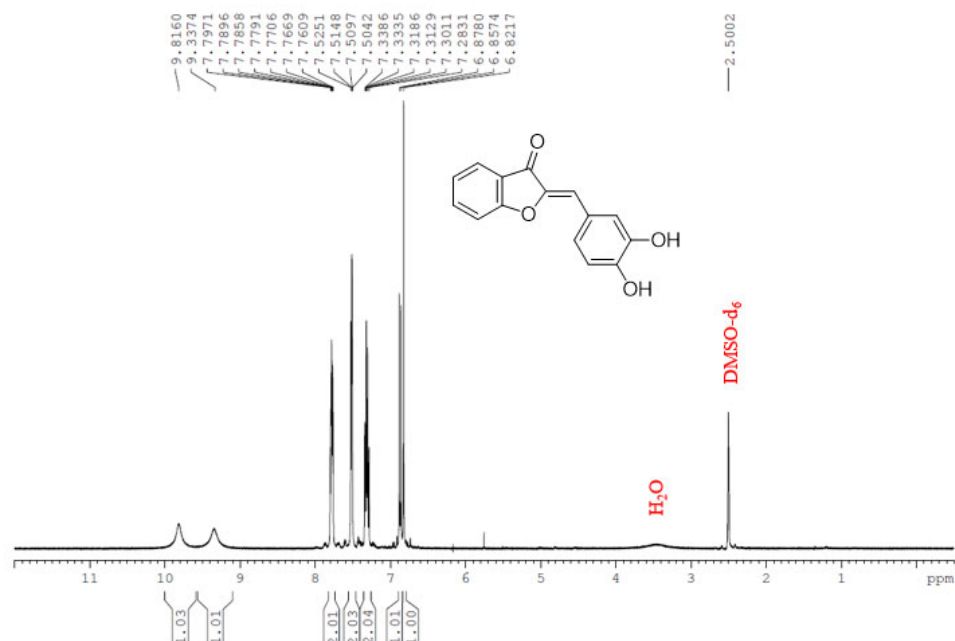
2-[(4-Hydroxyphenyl)methylidene]-2,3-dihydro-1-benzofuran-3-one (**HA2**)  
<sup>1</sup>H NMR (700 MHz, DMSO-d<sub>6</sub>)



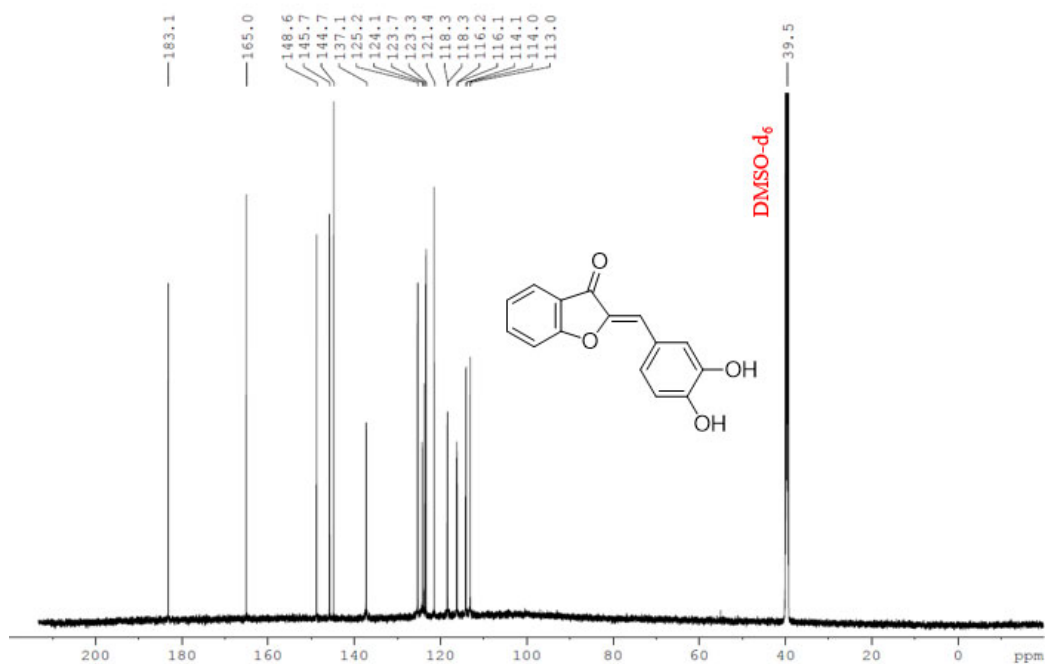
2-[(4-Hydroxyphenyl)methylidene]-2,3-dihydro-1-benzofuran-3-one (**HA2**)  
<sup>13</sup>C NMR (700 MHz, DMSO-d<sub>6</sub>)



2-[(3,4-Dihydroxyphenyl)methylidene]-2,3-dihydro-1-benzofuran-3-one (**HA3**)  
 $^1\text{H}$  NMR (400 MHz, DMSO- $\text{d}_6$ )

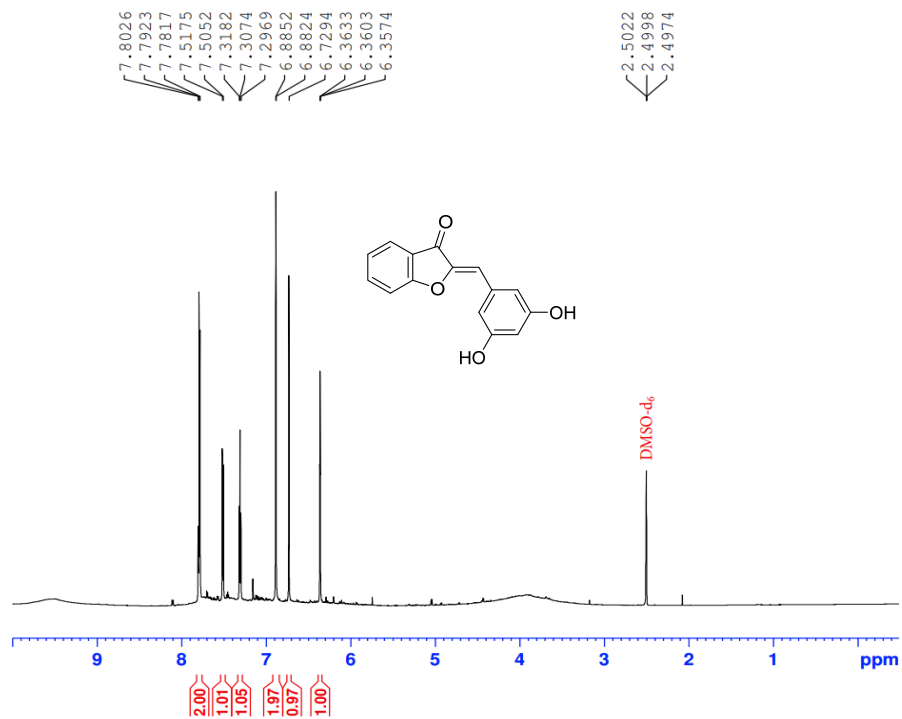


2-[(3,4-Dihydroxyphenyl)methylidene]-2,3-dihydro-1-benzofuran-3-one (**HA3**)  
 $^{13}\text{C}$  NMR (700 MHz, DMSO- $\text{d}_6$ )

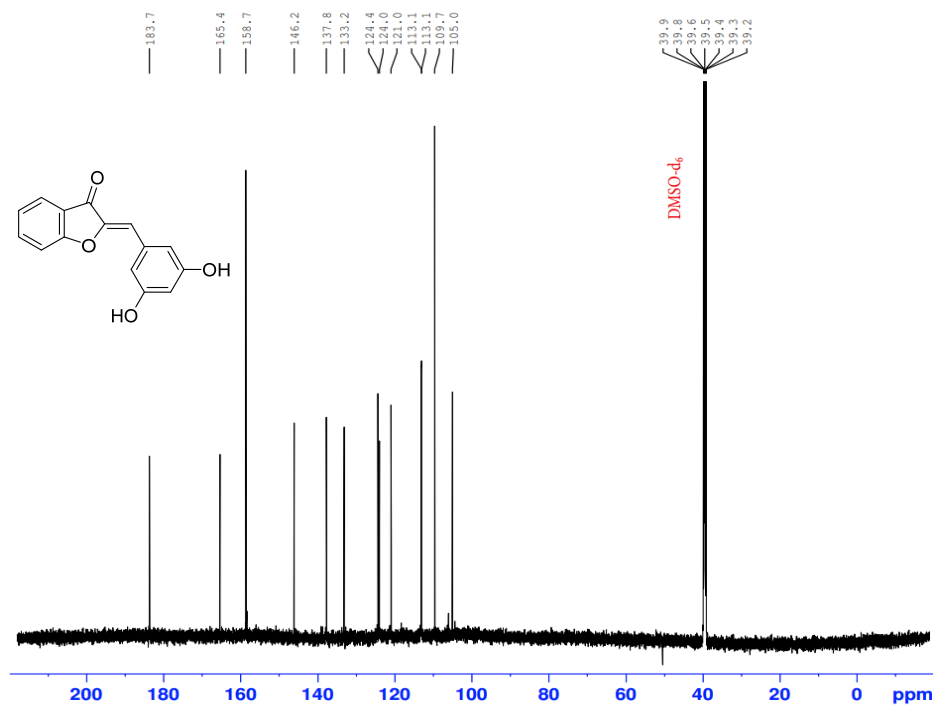


2-[(3,5-Dihydroxyphenyl)methylidene]-2,3-dihydro-1-benzofuran-3-one (**HA4**)  
 $^1\text{H}$  NMR (700 MHz, DMSO-  $\text{d}_6$ )



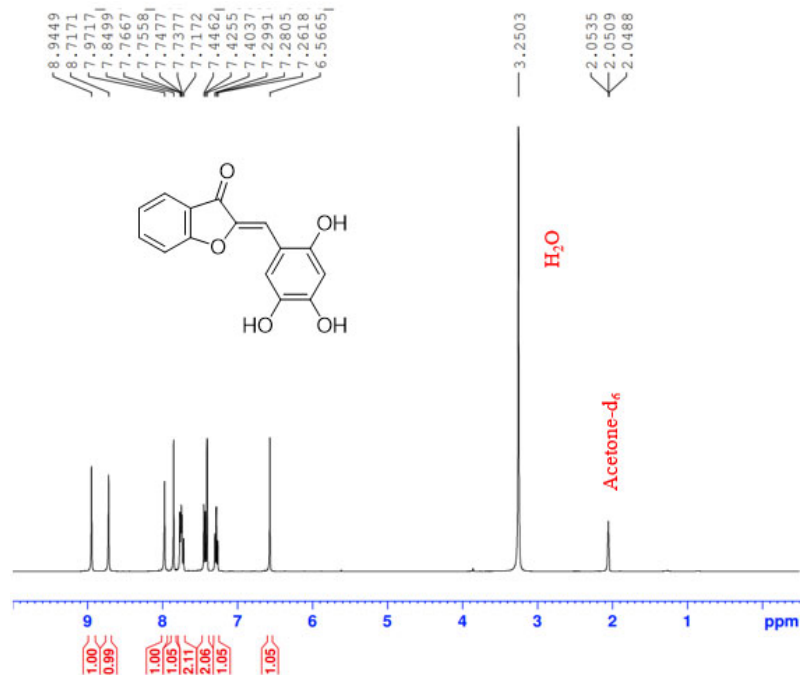


2-[(3,5-Dihydroxyphenyl)methylidene]-2,3-dihydro-1-benzofuran-3-one (**HA4**)  
<sup>13</sup>C NMR (700 MHz, DMSO-*d*<sub>6</sub>)



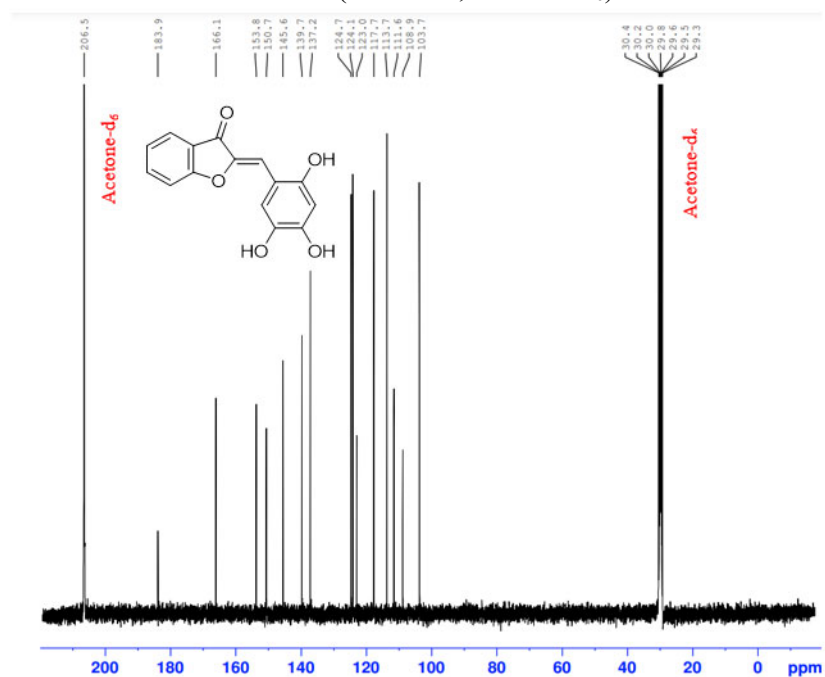
2-[(2,4,5-Trihydroxyphenyl)methylidene]-2,3-dihydro-1-benzofuran-3-one (**HA5**)

$^1\text{H}$  NMR (400 MHz, Acetone- $\text{d}_6$ )

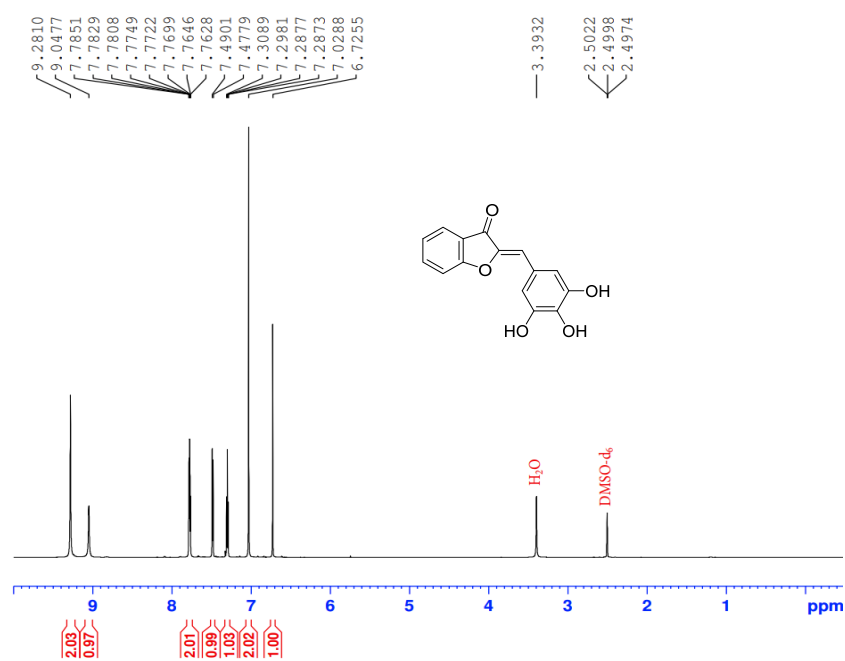


2-[(2,4,5-Trihydroxyphenyl)methylidene]-2,3-dihydro-1-benzofuran-3-one (**HA5**)

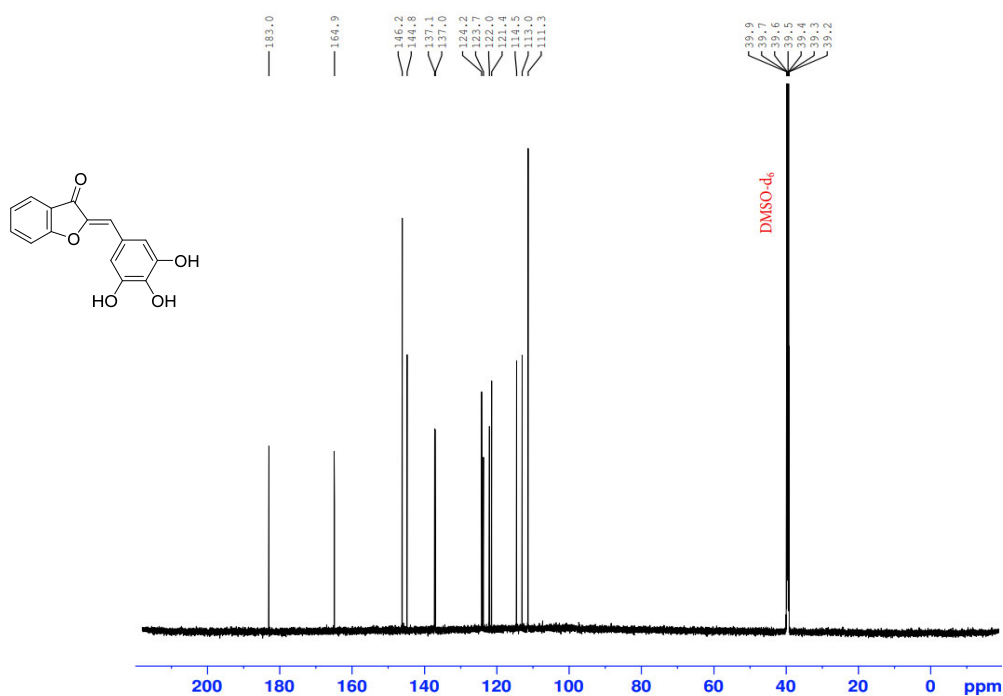
$^{13}\text{C}$  NMR (400 MHz, Acetone- $\text{d}_6$ )



2-[(3,4,5-Trihydroxyphenyl)methylidene]-2,3-dihydro-1-benzofuran-3-one (**HA6**)  
<sup>1</sup>H NMR (700 MHz, DMSO-d<sub>6</sub>)

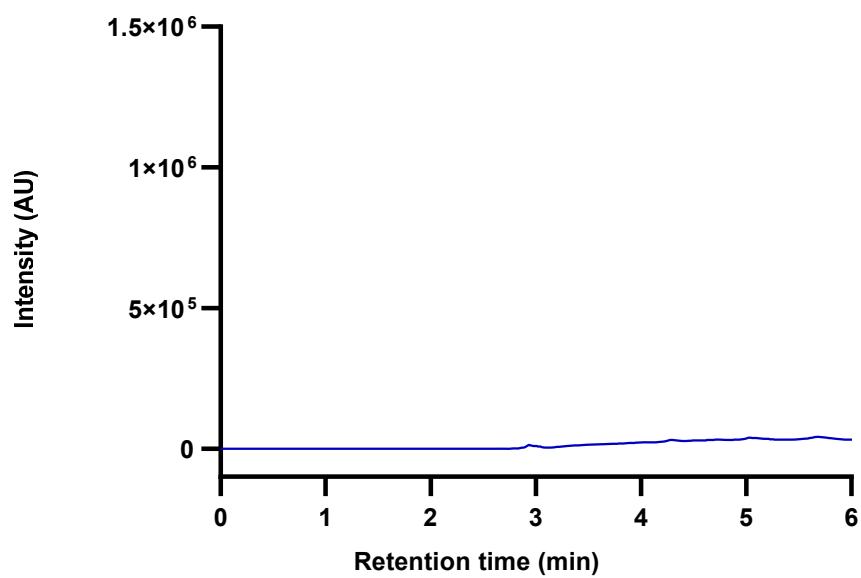


2-[(3,4,5-Trihydroxyphenyl)methylidene]-2,3-dihydro-1-benzofuran-3-one (**HA6**)  
<sup>13</sup>C NMR (700 MHz, DMSO-d<sub>6</sub>)

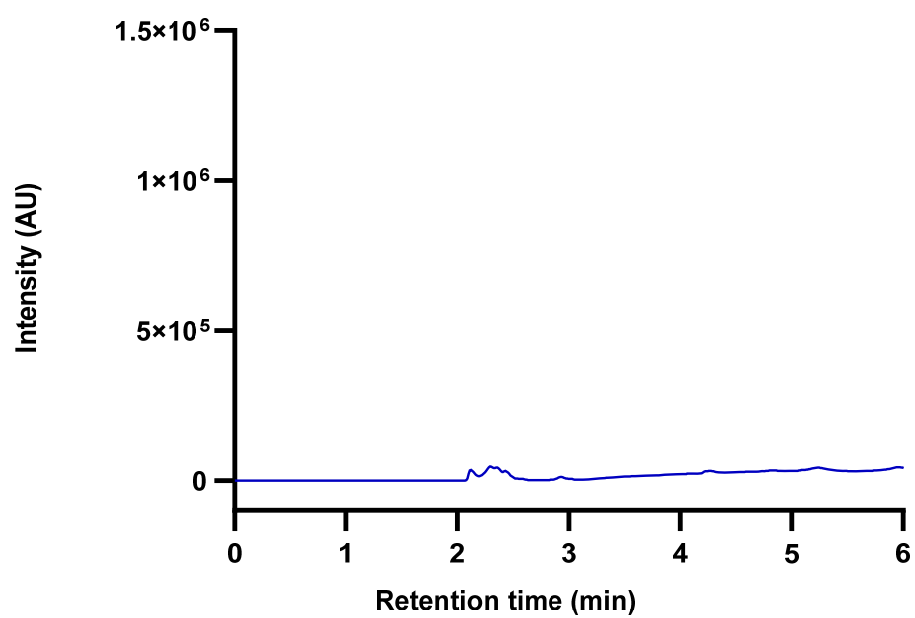


## HPLC Chromatograms

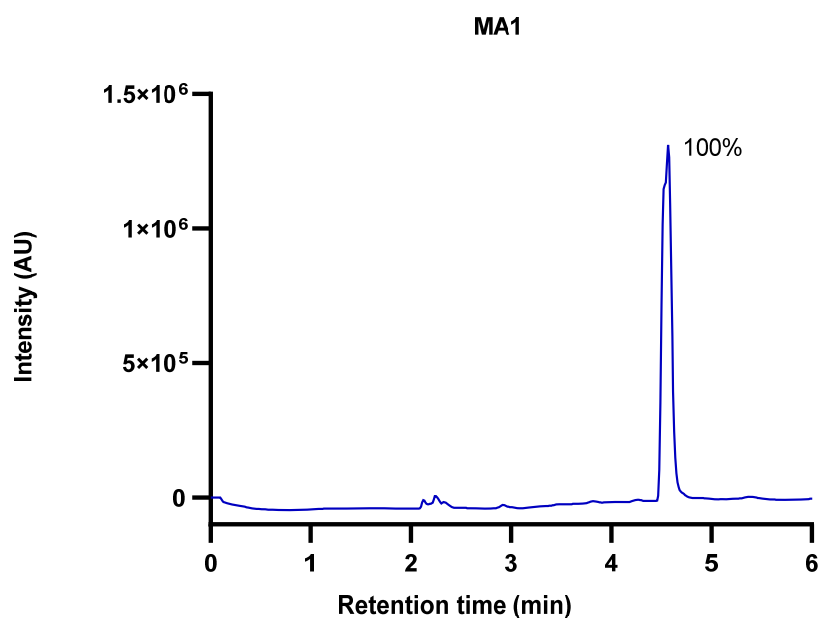
Null



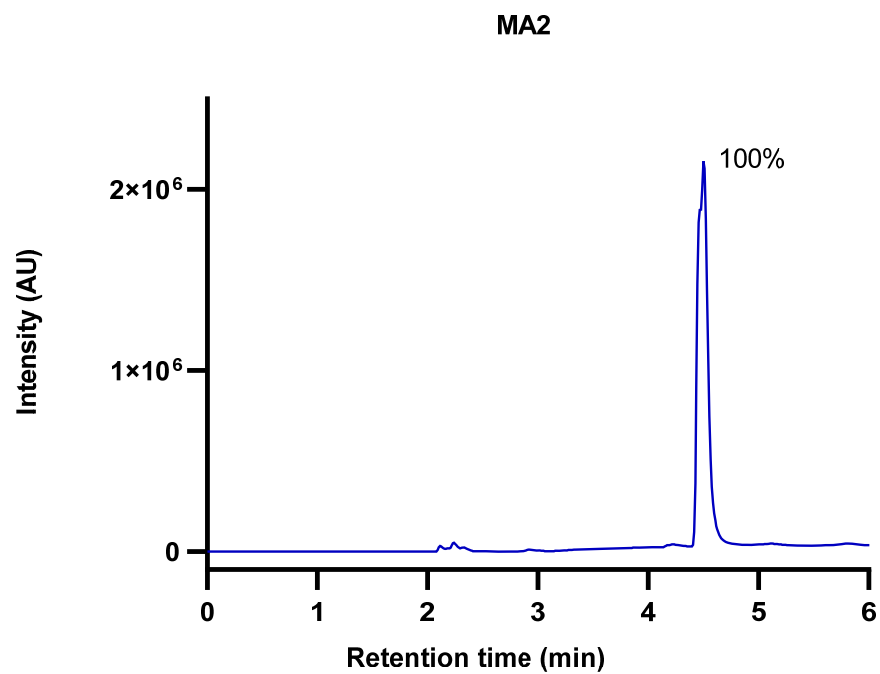
DMSO



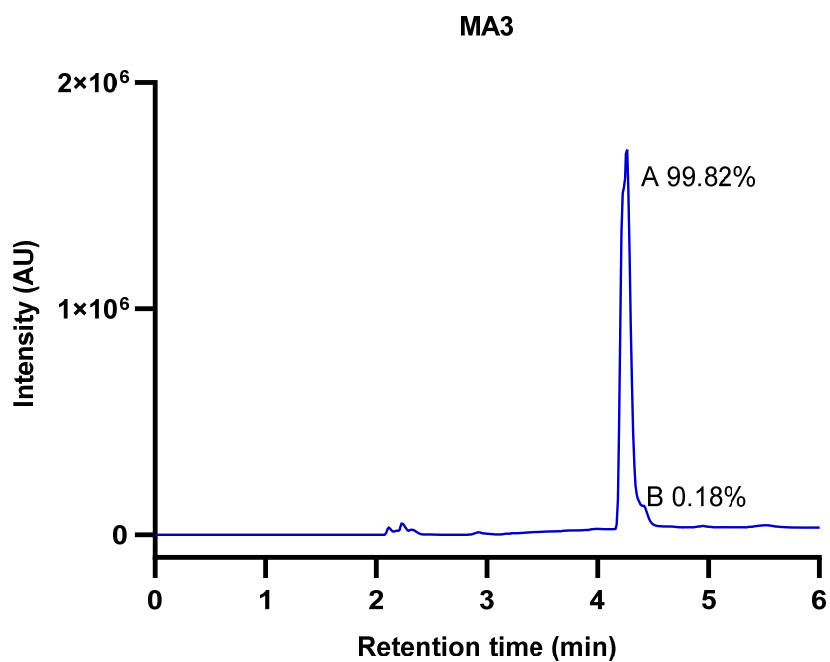
2-(Phenylmethylidene)-2,3-dihydro-1-benzofuran-3-one (**MA1**)



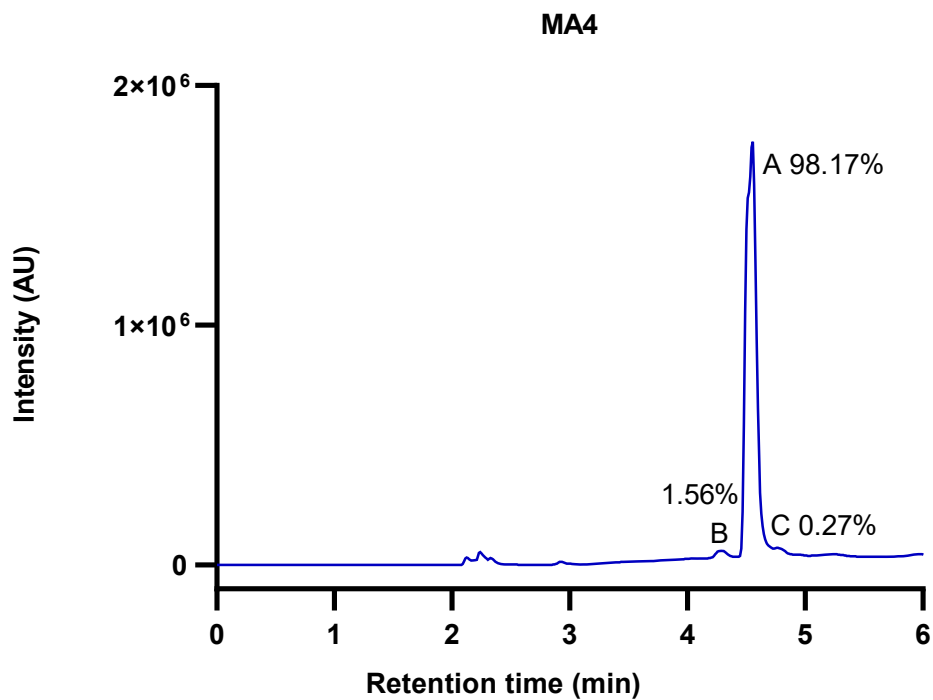
2-[(4'-Methoxyphenyl)methylidene]-2,3-dihydro-1-benzofuran-3-one (**MA2**)



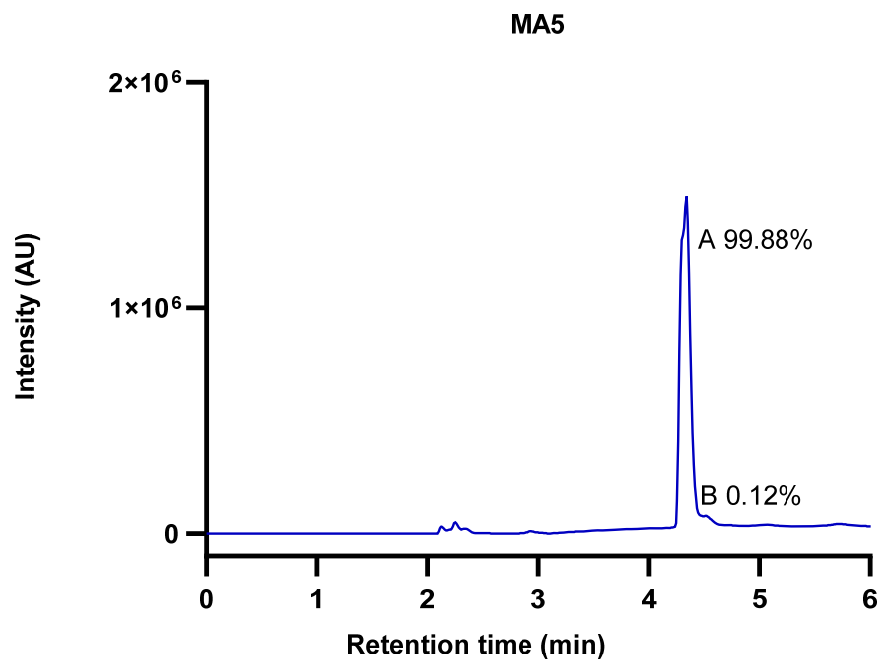
2-[(3',4'-Dimethoxyphenyl)methylidene]-2,3-dihydro-1-benzofuran-3-one (**MA3**)



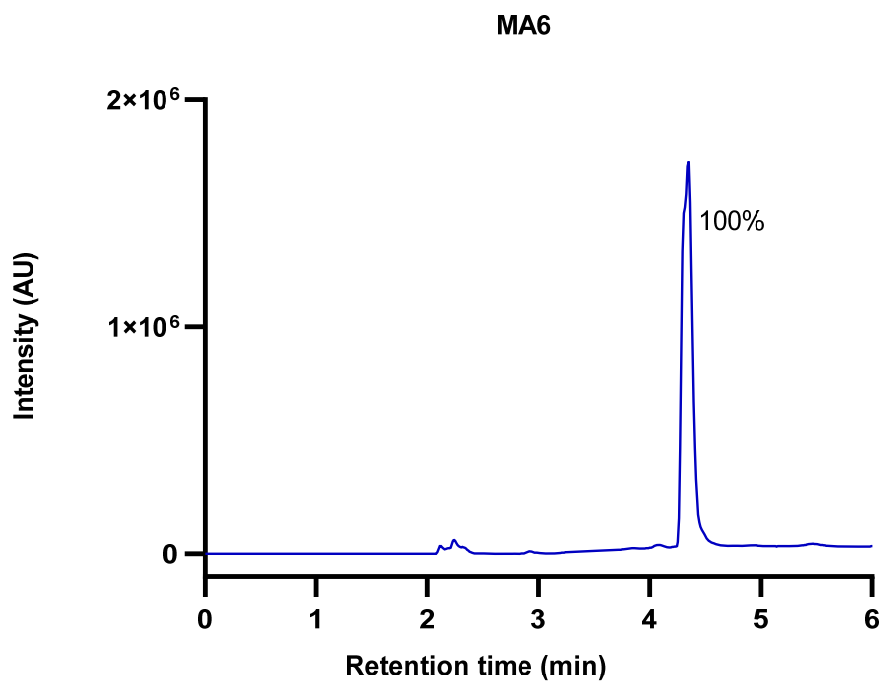
2-[(3',5'-Dimethoxyphenyl)methylidene]-2,3-dihydro-1-benzofuran-3-one (**MA4**)



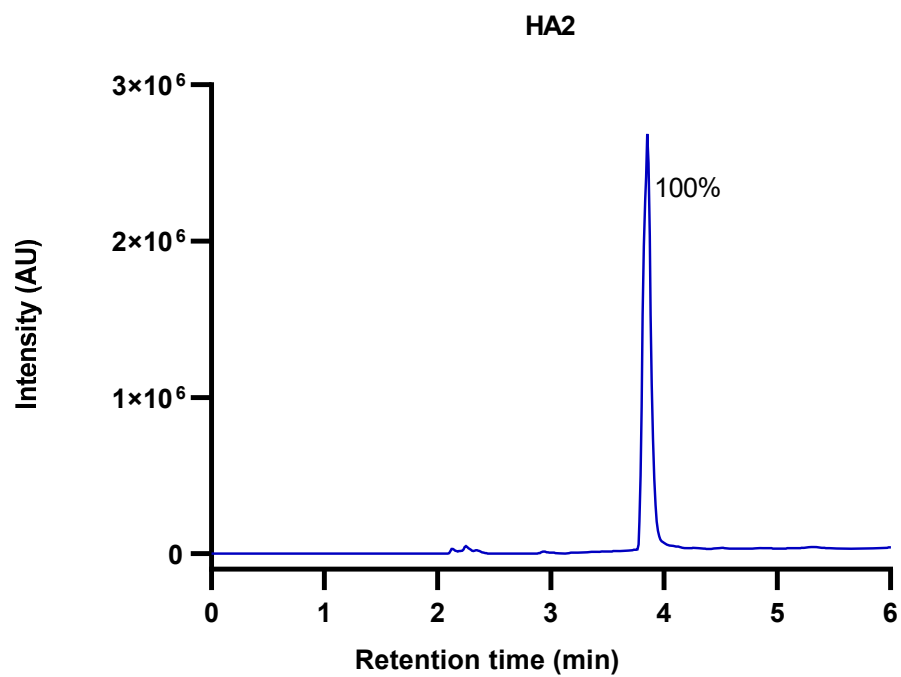
2-[(2',4',5'-Trimethoxyphenyl)methylidene]-2,3-dihydro-1-benzofuran-3-one (**MA5**)



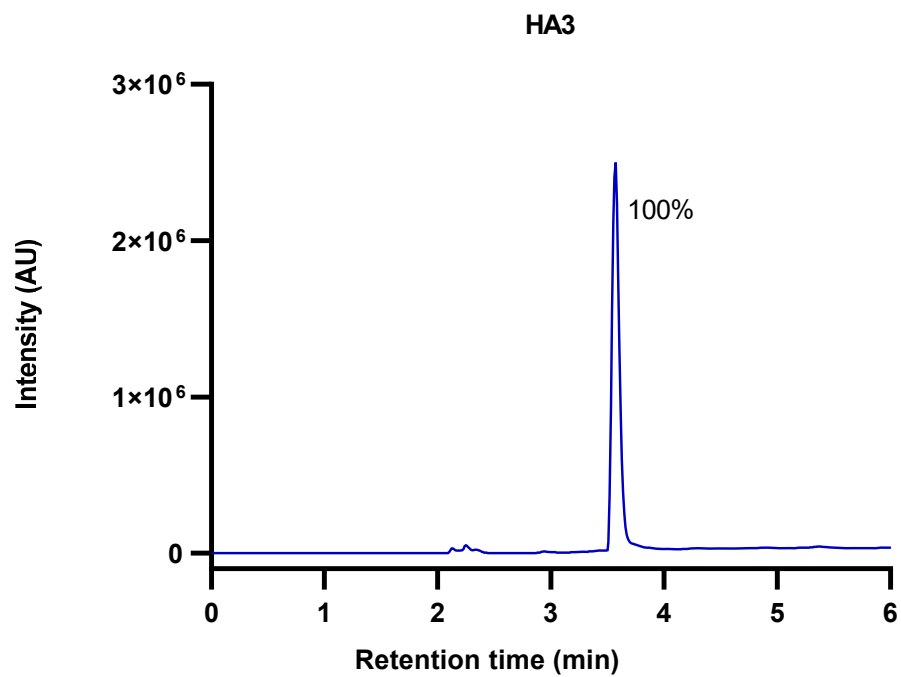
2-[(3',4',5'-Trimethoxyphenyl)methylidene]-2,3-dihydro-1-benzofuran-3-one (**MA6**)



2-[(4'-Hydroxyphenyl)methylidene]-2,3-dihydro-1-benzofuran-3-one (**HA2**)

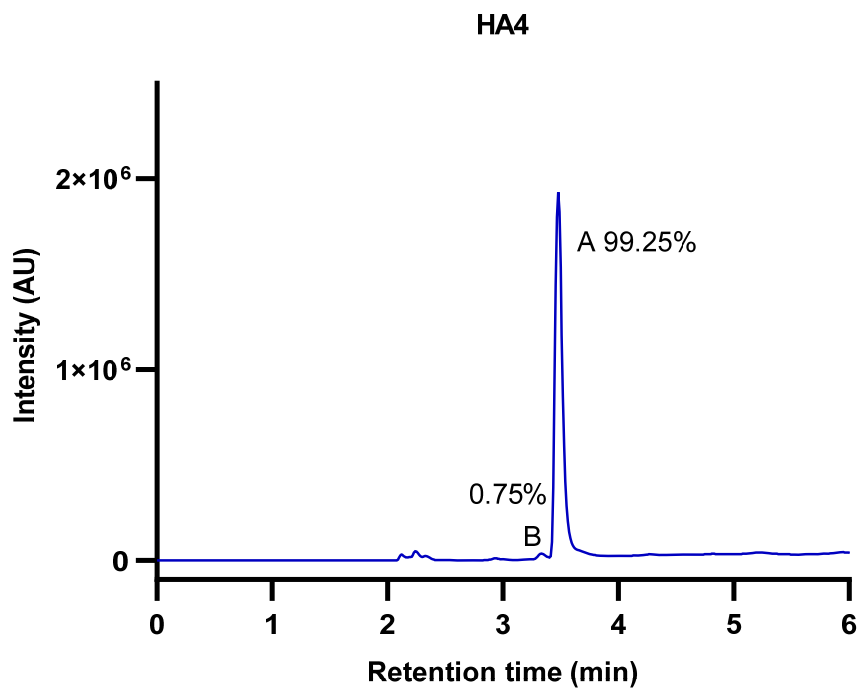


2-[(3',4'-Dihydroxyphenyl)methylidene]-2,3-dihydro-1-benzofuran-3-one (**HA3**)

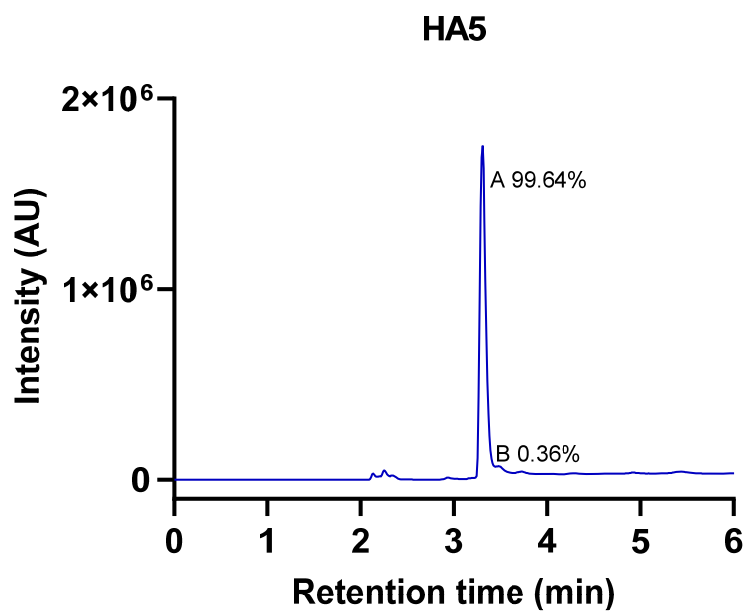




2-[(3',5'-Dihydroxyphenyl)methylidene]-2,3-dihydro-1-benzofuran-3-one (**HA4**)



2-[(2',4',5'-Trihydroxyphenyl)methylidene]-2,3-dihydro-1-benzofuran-3-one (**HA5**)



2-[(3',4',5'-Trihydroxyphenyl)methylidene]-2,3-dihydro-1-benzofuran-3-one (**HA6**)

